AN IN-VITRO MODEL FOR THE DEVELOPMENT OF MATURE BONE CONTAINING AN OSTEOCYTE NETWORK

By ALEXANDRA IORDACHESCU, MSc BSc (Hons)

A THESIS SUBMITTED TO THE UNIVERSITY OF BIRMINGHAM FOR THE TITLE

OF

DOCTOR OF PHILOSOPHY

SCHOOL OF CHEMICAL ENGINEERING

EDGBASTON, B15 2TT

UNITED KINGDOM

2017

ABSTRACT

Bone is a tissue that continuously adapts to changes in mechanical load. This process can also result in maladaptive ectopic bone in response to injury and extreme mechanical insult, in a group of conditions known as heterotopic ossification.

Despite recent advancements, pathological differences at the molecular and structural levels are poorly understood. A number of *in vivo* models exist but can often be unreliable or too complex to allow isolation of factors which may stimulate progression of ossification.

This thesis presents the development of a biologically self-structuring model of mature bone formation using a fibrin gel which self-organises between two calcium phosphate ceramic anchors when seeded with cells. These bioinspired early wound analogues are seeded with primary femoral periosteal cells - key players in bone repair and a range of pathologies- and develop longitudinally over significant culture periods, allowing to study the temporal evolution of bone mineral and microstructure in excess of a year. This work demonstrates the production of a mature, bone-like morphology and chemistry, with differentiation of mature, mineral phase osteocytes.

Raman spectroscopy and XRD revealed that the mineral was non-stoichiometric and poorly crystalline hydroxyapatite and associated with collagen. Second harmonic imaging demonstrated that collagen was organized similarly to mature mouse femora. The initial stem cell population differentiated to the terminal osteocytic phase, was integrated into longitudinal networks similar to the canaliculi in mature bone (as demonstrated with nanoCT) and remained viable over the full year of culture. Using this

model, this work demonstrated that pharmacological compounds can prevent the progress of ossification, displaying promise for applications in drug screening. Pilot work also showed that it is possible to initiate angiogenesis in these constructs, with endothelial tubes also aligned with the mechanical axis, a step closer to mimicking *in vivo* bone.

SIGNIFICANCE STATEMENT

The work performed here is unique since it allows the growth of tissue that not only shares the biochemical composition of bone, but also exhibits a similar structure. The tissues that were produced contain populations of mature cells, osteocytes, which are linked by canalicular networks as encountered *in vivo*. The system developed here allows the maintenance of the osteocytic phenotype for one year in culture, a major advance on the current state of the art, which allows the culture of these cells for less than one month. The biological relevance and utility of this system was demonstrated by blocking bone formation with a retinoic acid receptor (RAR) inhibitor that prevents ossification at the early chondrogenic stage. This model will be an excellent tool for studying both aberrant and normal processes of bone formation.

ACKNOWLEDGEMENTS

The results presented in this thesis were achieved with the continuous support of my two advisors, to whom I would like to express my warmest thanks and appreciation, Professor Liam Michael Grover (University of Birmingham) and Associate Professor Philippa Anne Hulley (University of Oxford) for their valuable scientific advice throughout my doctoral research.

The work has been supported by the National Centre for the Replacement, Refinement and Reduction of animals in research (NC3Rs) (grant (NC/L001403/1), to whom I would like to express my gratitude for making this research possible.

I would like to acknowledge my collaborators for their technical assistance and expertise, Dr Harsh Amin and Professor Sara Rankin (Imperial College London) for sharing their expertise on heterotopic ossification and for providing the methodology for extraction of periosteal cells; Dr Clarence Yapp (Harvard Medical School - University of Oxford) for training me in multi-photon microscopy imaging; Dr Alexandra Pacureanu (The European Synchrotron Radiation Facility, Grenoble, France) for providing support with nano-scale data acquisition on osteocyte morphology, Professor Owen Addison (School of Dentistry, University of Birmingham) for his support with processing the samples for synchrotron radiation nanoCT and Dr Jason Zhang (University of Birmingham) and his lab members for providing support with some of the final work on AFM mechanical characterisation of mature bone samples.

I would like to thank Mr Bill Edwards and my former University, King's College London for allowing the acquisition of original photographs of pathological bone conditions; the Natural History Museum, London and the Lapworth Museum of Geology, University of Birmingham for allowing the acquisition of images of many vertebrate specimens.

I would also like to thank my colleague, Dr Richard Williams for his valuable support at the busiest times of my research and to my colleagues from TRAILab for providing such a joyful working environment during the past 3 years.

Finally, there are a few special people to whom I would like to thank for their support, which has been indispensable. Firstly, my mom Carmen, for her constant encouragement and support along the road, as well as Marion and Alastair Martin. Finally, I would like to end by thanking Dr Donald Ward (University of Manchester) for his continuous scientific support throughout my career.

Alexandra Iordachescu

CONTENTS

LIST OF FIGURES

ACRONYMS

Ab	Antibody
AB	Alcian Blue
ACP	Amorphous Calcium Phosphate
APC	Adenomatous Polyposis Coli
ADP	Adenosine Diphosphate
AFM	Atomic Force Microscopy
ALP	Alkaline Phosphatase
ALPL	*see* TNAP
AS	Ankylosing Spondylitis
ATCC	American Type Culture Collection
ATP	Adenosine Triphosphate
BMC	Bone Mineral Content
BMSC	Bone Marrow Stromal Cell
BMP	Bone Morphogenic Protein
BSA	Bovine Serum Albumin
BSP	Bone Sialoprotein
AM	(Calcein) Acetoxymethyl
Ca	Calcium
CaM	Calmodulin
CaP	Calcium Phosphate
Cbfa1	*see* RUNX2

CCD	Cleidocranial Dysplasia
CK1	Casein Kinase 1
CKD	Chronic Kidney Disease
CNS	Central Nervous System
Col I	Collagen Type I
Col II	Collagen Type II
CSA	Cross-Sectional Area
CT	Computed Tomography
CTC	Chlortetracycline
CTF	Chick Tendon Fibroblasts
CX43	Connexin 43
DAPI	4′,6-diamidino-2-phenylindole
dH_2O	Deionised Water
DLS	Dynamic Light Scattering
DMEM	Dulbecco's Modified Eagle Medium
DMP1	Dental Matrix Acidic Phosphoprotein 1
DMSO	Dimethyl Sulfoxide
DNA	Deoxyribonucleic Acid
ECAAC	European Collection of Authenticated Cell Cultures
ECF	Extracellular Fluid
ECM	Extracellular Matrix
EtOH	Ethanol
FBS	Foetal Bovine Serum
FCS	Foetal Calf Serum

FGF23	Fibroblast Growth Factor 23
FOP	*Fibrodysplasia Ossificans Progressiva*
GA	Gentamicin Sulphate – Amphotericin-B
GAGs	Glycosaminoglycans
GAPDH	Glyceraldehyde 3-Phosphate Dehydrogenase
GSK3	Glycogen Synthase Kinase 3
H&E	Haematoxylin and Eosin
HA	Hydroxyapatite
HIF- 1α	Hypoxia-Inducible Factor 1 alpha
HO	Heterotopic Ossification
HUVEC	Human Umbilical Endothelial Cells
IED	Improvised Explosive Device
IHC	Immunohistochemistry
Ihh	Indian Hedgehog
IL	Interleukin
ITS+	Insulin Transferrin Selenium
MC3T3-E1	Mouse Calvarial Osteoblasts
MEM α	Minimum Essential Medium, alpha modification
MB	Magnetic Bead
MMP	Matrix Metalloproteinase
MRI	Magnetic Resonance Imaging
mRNA	Messenger RNA
MV	Matrix Vesicle
NanoCT	*see* srCT

NTA	Nanoparticle Tracking Analysis
OC	Osteocalcin
OCP	Octacalcium Phosphate
OPN	Osteopontin
Osx	Osterix
OTC	Oxytetracycline
P	Phosphorus
PBS	Phosphate Buffered Saline
PCR	Polymerase Chain Reaction
PDPN	Podoplanin
PHEX	Phosphate-Regulating Endopeptidase, X-linked
PLD	Phospholipase D
PPi	Inorganic Pyrophosphate
P/S	Penicillin/Streptomycin
PTH	Parathyroid Hormone
PTH1r	Parathyroid Hormone 1 Receptor
qPCR	Quantitative Polymerase Chain Reaction
RA	Rheumatoid Arthritis
rhEGF	Recombinant Human Epidermal Growth Factor
rhFGF-B	Recombinant Human Fibroblast Growth Factor – B
R^3- IGF-1	Recombinant Long R Insulin – Like Growth Factor – 1
RUNX2	Runt-Related Transcription Factor 2
TBS	Tris-Buffered Saline
TCP	Tri-Calcium Phosphate

TGF-β3	Transforming Growth Factor β3
THA	Total Hip Arthroplasty
TNAP	Tissue Non-Specific Alkaline Phosphatase
TNF α	Tumour Necrosis Factor α
TPEF	Two-Photon Excited Fluorescence
SCI	Spinal Cord Injury
SDS-PAGE	Sodium Dodecyl Sulphate – Polyacrylamide-Gel Electrophoresis
SEM	Scanning Electron Microscopy
SHG	Second Harmonic Generation
SOST	Sclerostin
srCT	Synchrotron Radiation Computed Tomography
TEM	Transmission Electron Microscopy
UV	Ultraviolet Light
VEGF	Vascular Endothelial Growth Factor
XRD	X-Ray Diffraction
XRF	X-Ray Fluorescence

CHAPTER I

INTRODUCTION TO BONE FORMATION

1.1 BIOMECHANICAL EVOLUTION OF THE SKELETON

Bones have evolved in an environment where gravity represented a factor of physical restriction, which led to the generation of skeletal adaptations in all aquatic, amphibious, terrestrial and volant organisms. The continuously changing mechanical conditions experienced by the ancestors of all living creatures led to molecular and structural adaptations designed to manage this force of gravity. In humans, the skeletal system evolved to counteract the gravitational force during walking and standing on two legs, with the line of gravity passing through the base of the spine so that the body is well balanced when upright, whilst the centre of gravity is located front of the ankles to prevent falling (Buckey 2006, Le Huec, Saddiki et al. 2011). The development of such superior biomechanics was allowed by a continuously changing anatomical design, seen in modifications of long-bones, the verticalization and broadening of the pelvis and the lordotic curvature of the spine in the lumbar and cervical regions and the kyphosis in the thoracic and sacral regions, features that did not develop in primates (Figure 1.1),

which use their upper limbs to reduce the anterior imbalance caused by propulsive forces from the lower limbs (Berge 1998, Le Huec, Saddiki et al. 2011).

Secondly, these traits were allowed by the concomitant evolution of a well-orchestrated biochemical signalling system, which could constantly feedback on the quality and functionality of bones. These events include the processes of bone tissue formation and remodelling and will be discussed in detail in the following sections.

It is therefore not surprising that when alterations in environmental forces take place, such as decreased loading experienced in microgravity during space exploration (Barratt and Pool 2008), extended buoyancy (Gray, Kainec et al. 2007) or immobilisation due to injury (Houde, Schulz et al. 1995, del Puente, Pappone et al. 1996, Demirbag, Ozdemir et al. 2005), dramatic losses in bone content and macrostructure can be observed immediately. These alterations increase the susceptibility of bone to breakage and compromise the ability to perform intense physical tasks.

At the opposite end of the spectrum, increased mechanical forces due to limb exposure to overpressure, CNS or SC injury, or mechanical trauma due to surgical procedures of the knee, hips or spine lead to enhanced bone formation in the tissues surrounding the affected areas (Ahrengart 1991, Pape, Lehmann et al. 2001, Board, Karva et al. 2007, Potter, Burns et al. 2007, Potter, Forsberg et al. 2010, Alfieri, Forsberg et al. 2012, Sullivan, Torres et al. 2013). These ectopic bone formations are very debilitating, especially when forming adjacent to major arteries, veins or nerves (Spencer and Missen 1989, Board, Karva et al. 2007, Baird and Kang 2009, Cullen and Perera 2009, Isaacson, Stinstra et al. 2010).

At the molecular level, bone formation and breakdown are finely controlled by the muscular, endocrine and nervous systems. Dysregulations in these systems or their interactions also have a profound effect on bone composition and architecture.

The following sections of this chapter will expand on these aspects. This review, which continues with the results chapters, is not written as an exhaustive account of information on bone, but as a selection of our current understanding of the biomechanical, physiological and pathological processes which trigger bone tissue formation, that allowed the production of the focused conclusions presented at the end of this thesis. The following sections will focus on the effectors of the skeletal system, the bone cells and the physiological and pathological events underlying normal and abnormal bone formation which lead to the translation of the biomechanical forces into organised, structured bone. Finally, this chapter will discuss the gaps in our understanding of the bone formation process, the current models available in research to study ossification in normal and abnormal states and also the advantages and flaws of these models.

Figure 1.1 | Evolution of the skeletal system to bipedal walking. a, Common chimpanzee (*Pan troglodytes*, Cameroon, West Africa). This specimen is a male showing very strong arms and wrists for knuckle walking. Several other features including the straight spine, small hip size, weak knee joints and flat feet with expansive toes show that this primate is not normally bipedal but uses the arms for balance. **b**, *Australopithecus sediba*, hominin skeleton. This species of primate, originating from South Africa (1.95 million years old) shows an upright posture which indicates its hominin nature. Compared to the specimen in *a*, this primate shows a smaller body and skull and longer lower limbs. **c**, *Homo sapiens*, female skeleton (France, 150 years old). The only extant human species, which developed skeletal adaptations for upright walking, including several curvatures on the spine for balance and absorbing the mechanical shocks, arched feet, and similarly to the specimen in *b*, inward directed femurs used to transfer the weight of the trunk to the knees and lower bones. *Note: image scales are not related, and have been enlarged to allow visualisation of skeletal parts. Original images. The author would like to thank the Natural History Museum, South Kensington, London.*

1.1.1 EARLY BONES

The evolution of a skeleton containing a vertebral spine was one of the major transformations which separated the animal kingdom. The skeletal system was one of the most dramatically changing physiological systems across the millions of years of evolution. Life is thought to have originated in water around 3.5 billion years ago and so the abundance of features that evolved over this substantial period, in bacteria, invertebrates and ultimately vertebrates was for a significant time specialised to the aquatic environment. Therefore, the skeletal systems of marine vertebrates became compositionally and structurally adapted to life under buoyancy conditions (Gray, Kainec et al. 2007), something that will be discussed in detail in the next section.

As the transition from water to land started to take place around 380 million years ago in mid-Devonian, and continued for millions of years, the first terrestrial-suited bones appeared in elpistostegalians, which were tetrapods evolved from fish predecessors (Shubin, Daeschler et al. 2014) that developed physiological features adapted to both life on water and at the surface. The dramatic change in the mechanics of the environment required the development of bone structures with anatomical features suitable for terrestrial walking, a transition which was poorly understood until recently. This aspect was clarified recently (2004) with the extraordinary discovery of the fossil of *Tiktaalik roseae*, a late Devonian tetrapod, in Ellesmere Island in the Canadian Arctic, which provided the missing link in the evolutionary history of modern land vertebrates (Daeschler, Shubin et al. 2006). Tiktaalik contained many musculo-skeletal structures providing support for posture and locomotion on land, including endochondral bones, pelvic girdle and appendices and an articulated skeleton from head to toe similarly to modern tetrapods (Daeschler, Shubin et al. 2006, Shubin, Daeschler et al. 2006).

1.1.2 ADAPTATION OF BONES TO DIFFERENT ENVIRONMENTS

The diversification of the skeletons within the vertebrate subphylum over millions of years of evolution was achieved by changes in cartilaginous and osseous tissue, which developed to provide locomotion based on the environmental constraints present. Figure 1.2 illustrates a selection of skeletons of species from mechanically-distinct ecosystems, highlighting the differences in bones used in locomotion.

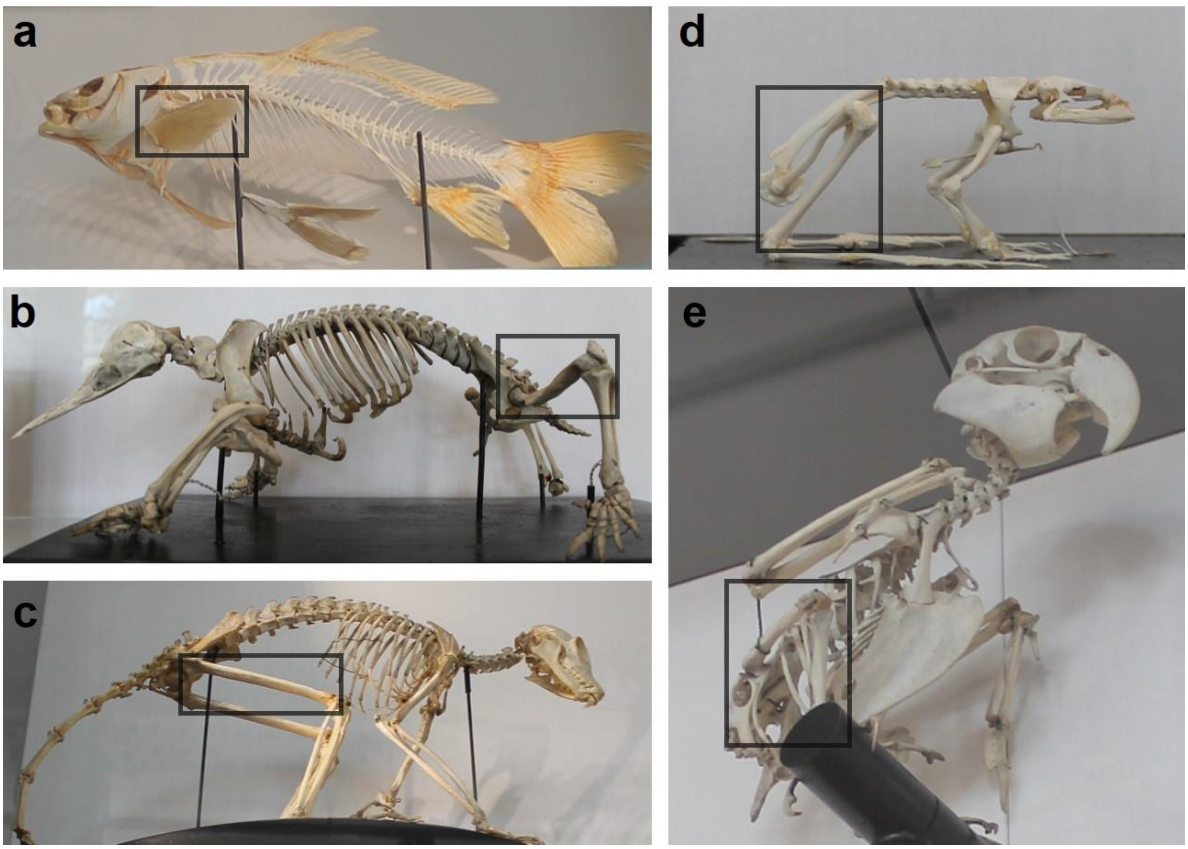

Figure 1.2 | Skeletal systems and limb bones from different orders and classes of animals have evolved to meet the mechanical demands of their environments. a, Fish; **b**, Monotremes; **c**, Primates; **d**, Amphibians; **e**, Birds. The common bones used to translate the mechanical forces from the trunk to the lower parts of the limbs for locomotion are shown in black boxes. *Original images. Author would like to thank the Lapworth Museum of Geology, University of Birmingham.*

As expected, there are evolutionarily-driven skeletal differences across different species. Some of the most striking adaptations include the skeletal pneumatisation of bones in birds (hollow air-filled bones), which have a high density and stiffness but a low mass and volume, an adaptation intended to reduce the metabolic costs of powered flight (*see* Figure 1.3a) (Dumont 2010, Gutzwiller, Su et al. 2013). Additionally, other adaptations in anatomical design have evolved, which include fusions of many skeletal structures and a relatively small body skeleton compared to wing size (Figure 1.4a), a common feature of flying vertebrates, including bats (Figure 1.4b), which has been preserved since their avian pterosaurian predecessors (c) (Swartz, Bennett et al. 1992, Maina 2000, Dumont 2010).

In fish and other aquatic and semi-aquatic animals, the weight is mainly supported by buoyancy and as such, skeletal micro-structure and bone density has adapted to support alternations between powered locomotion and gliding motion to minimise the energetic costs (Sato, Aoki et al. 2013), a feature also present in gliding animals during horizontal flight (Rayner, Viscardi et al. 2001).

At the other end of the spectrum, in land tetrapods which have secondarily invaded aquatic niches, such as sloths, several osteological modifications took place as a result of the increased mechanical constraints caused by locomotion in water, including densification of bones and an increase in volume (Gray, Kainec et al. 2007, Amson, de Muizon et al. 2014). Interestingly, this complex adaptive plasticity of the skeletal bones in response to their environment was also demonstrated by the historical transition of many other species such as archaeocetes (ancient aquatic mammals, ancestors of modern whales and dolphins, 55-20 million years ago) from terrestrial animals. The skeletal microstructure of these animals initially adapted to shallow or semi-aquatic

environments by increasing in density to provide static buoyancy control and stability and was then followed by a process of osteoporosis, meant to provide a dynamic buoyancy control as the animals adapted to a fully oceanic and deep-water life (Taylor 2000, Gray, Kainec et al. 2007).

The processes of increased cortical bone density and volume are known as osteopetrosis and pachyosteosclerosis and in the context of mechanical adaptation, they are recognised as a variable strategy for adapting to buoyancy (Taylor 2000). However, the process of osteopetrosis is also encountered in pathological conditions in humans, where excessive bone mass is caused by genetic mutations in genes responsible for osteoclast formation and function (bone cells involved in resorption) and will be discussed later in this chapter (*see Section 1.6.3 Formation of Osteoclasts*) (Sobacchi, Schulz et al. 2013).

The evolution of other mineralised tissues such as teeth and beaks allowed the development of defence mechanisms, hunting and eating. Indeed, the remarkable diversity in bird beak morphology, specifically adapted to very narrow niches (and illustrated in Figure 1.3), was one of the most significant biological evidences on the basis of which Charles Darwin postulated the theory of evolution of natural selection following his voyage to the Galapagos (Figure 1.4 a-b), the work which was later published as 'On the Origin of Species by Means of Natural Selection'. These skeletal adaptations, based on the nature and accessibility of the food sources (Figure 1.3c-g) allowed to demonstrate important aspects of the evolutionary theory, such as the concepts of speciation, natural selection and niche partitioning (Abzhanov 2010). This diversification process is under the direct control of several bone signalling pathways, some which will be discussed in further detail in section *1.4 Cellular Composition of*

Bone. Specifically, the formation of the pre-nasal cartilage forms under the control of BMP-4 and Calmodulin signalling pathways, whereas the premaxillary bone forms under the action of TGF-βIIr, β-catenin and Dkk3 signalling pathways, as well as the Indian Hedgehog (Ihh) pathway (Mallarino, Campàs et al. 2012). These distinct signalling pathways can exclusively or in combination, generate beak shapes of similar or different morphology in various species of birds (Figure 1.3b) (Grant and Grant 1997, Mallarino, Campàs et al. 2012).

Figure 1.3 | The adaptation of bird skulls to different niches and environments, showing dramatic differences in the osseous structures of the beaks. a, Cross-section through the skull of a Rhinoceros Hornbill (*Buceros rhinoceros*), showing hollow air-filled pockets in its skeletal structure, a feature evolved to meet energetic costs during flying. **b**, Skull of a Silvery-Cheeked Hornbill, a bird related to the specimen in *a* but showing a distinct anatomical beak structure, a feature which is under tight genetic regulation. **c-g**, The adaptation of the osseous structures of the beaks according to different living environments and thus food sources. **c**, Magellanic penguin – fish diet**; d**, Hyacinth macaw – diet of nuts from palm trees**; e**, Common toucan – fruit diet**; f**, Roseate spoonbill – diet of insects; **g**, Scarlet ibis -diet of shrimps and other crustaceans; This dietary specialisation was one of the observations which led to the development of Darwin's theory of natural selection. *Original images. Author would like to thank the Lapworth Museum of Geology, University of Birmingham and the Natural History Museum, South Kensington, London.*

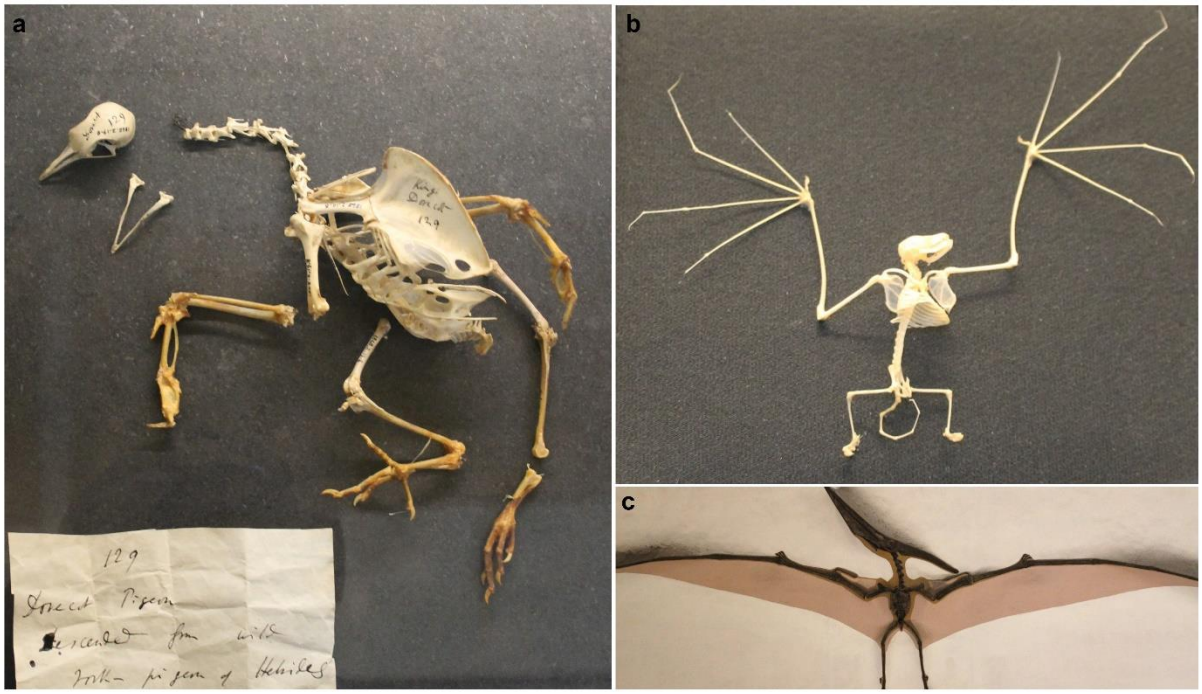

Figure 1.4 | The anatomical adaptation of the skeletons of flying vertebrates. a, Skeleton of a pigeon used by Charles Darwin as part of his research and development of the theory of evolutionary adaptation, later described in the *Origin of Species*. Specimens demonstrates a large wing bone size compared to the body size, a skeletal adaptation to powered flight. This feature can also be seen in other species which have evolved from a different lineage, such as the common pipistrelle bat skeleton (*Pipistrellus pipistrellus*) (**b**); and in the avian ancestors such as Pteranodon, a flying reptile from late Cretaceous (approx. 86-83 million years old) (**c**). *Original images. Author would like to thank the Natural History Museum, South Kensington, London.*

In humans, identical physiological and pathological adaptations take place in bone mass and density as a result of age, immobilisation, unloading, vigorous exercise and trauma and these will be discussed in detail in the following sections.

From an evolutionary perspective, the development of longer leg bones in humans, starting with more recent hominin species such as in *Homo heidelbergensis* compared to the first bipedal humans such as *Homo erectus* was due to an adaptation to tropical conditions, as they could provide a larger surface for cooling the body. This skeletal adaptation did not take place in other species such as *Homo neanderthalensis*, which lived in colder climates, and as such had shorter limb legs and a lower body size (Elton 2008). CT analysis of trabecular bone density from these different hominid species revealed that high trabecular bone density was a feature of earlier hominin species compared to more recent ones including *Homo sapiens* (Chirchir, Kivell et al. 2015), which was probably due to the intense physical activity undertaken by these species during hunting of large animals, which placed considerable stress on the bones and hence resulted in a higher bone density.

1.2 FUNCTIONS OF BONE

Despite their inert appearance, bones are responsible for more than shaping the human skeleton, and fulfil a whole range of vital functions (Figure 1.5).

1.2.1 MECHANICAL SUPPORT

As discussed in the previous sections of this chapter, bones provide a framework for mechanical support. The lower limbs provide support to the trunk during standing and walking, while other structures, such as the rib cage, support the thorax. In addition, bones provide suspension of the soft, internal organs of the abdomen and cavities for sensory organs of the head (Marieb and Hoehn 2010) (Figure 1.5a-c).

1.2.2 PROTECTIVE FUNCTION

Several bones offer protection to the vital organs, including the fused cranio-facial bones, which enclose and protect the brain, the ribcage which protects the heart and lungs; and the vertebra of the spine which protect the spinal cord (Marieb and Hoehn 2010) (Figure 1.5a-c).

1.2.3 LOCOMOTION

Bones provide a source of attachment to all muscles, tendons and ligaments, acting as levers during body movement. This has implications for many vital functions, especially breathing. Moreover, the biomechanical design of bone joints directly influences

different types of movement, including flexion, extension, gliding, retraction and protraction, elevation and depression (Marieb and Hoehn 2010) (Figure 1.5a,c).

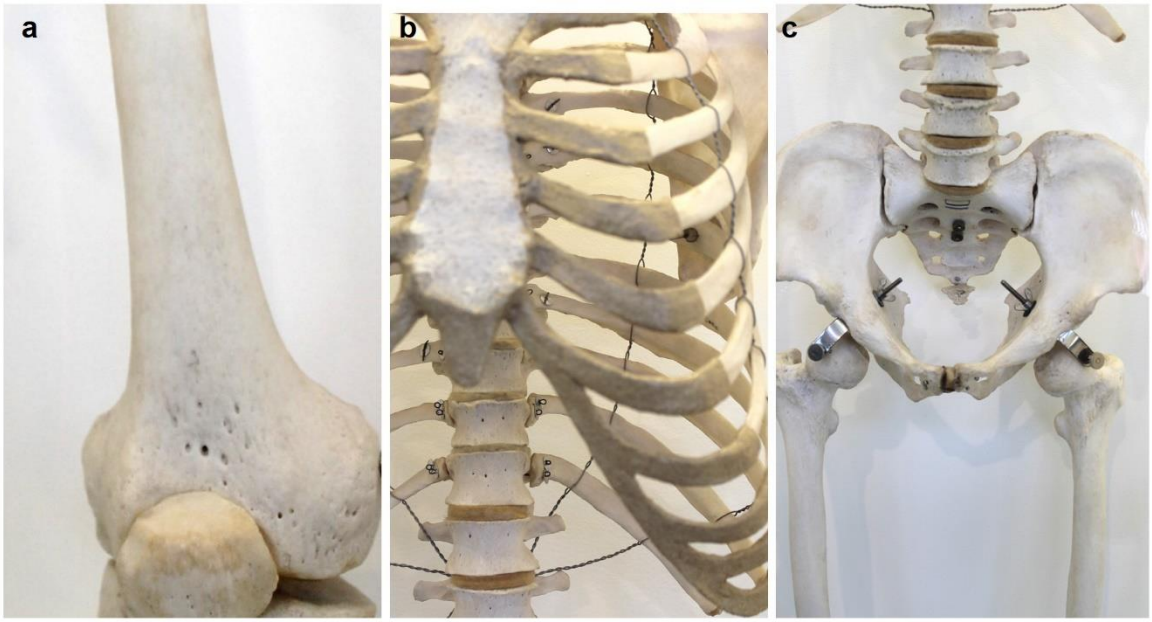

Figure 1.5 | Functions of bones. Bones perform numerous functions including supporting the body during movement, providing levers for moving the limbs (**a**); protecting the fragile internal organs (ribcage) (**b**) and the spine (**b-c**); as well as supporting the weight of the trunk during walking (**c**). *Original images acquired from a skeletal specimen at the Natural History Museum, South Kensington, London.*

1.2.4 STORAGE OF MINERALS

In addition to their mechanical functions**,** bones provide a source of calcium and phosphate to the rest of the body (Boden and Kaplan 1990). The maintenance of constant levels of these minerals in the bloodstream is essential not only for the skeletal system, but also for the function of other body systems, including the nervous system (Braet, Cabooter et al. 2004), where Ca^{2+} signalling is essential for the operation and integration of chemical and electrical signals by neurons and glial cells at the synapse; and muscular system (Szent-Györgyi 1975) where the same element directly regulates muscle contraction through binding to regulatory proteins such as troponin. As such, Calcium and Phosphorus are continuously deposited and released into the bloodstream under the action of regulatory hormones including PTH, which also aid in maintaining Ca and P homeostasis by acting on other organs as well, including the kidneys and the intestines.

The simultaneous physiological processes undertaken by bones make it very difficult to maintain their health and restore their normal composition. This is because both mechanical loading and the hormone-controlled release of ions to the body continuously require these elements. Therefore, the ionic balance can be quickly disrupted, as seen in numerous pathological states (Boden and Kaplan 1990, del Puente, Pappone et al. 1996, Lau and Guo 2011). The chemical properties of the calcium and phosphate content of bone will be discussed in detail in section *1.4 Chemical Composition of Bone*.

Bone matrix also provides a supply of growth factors, including insulin-like growth factors (Kawai and Rosen 2012, Mohan and Kesavan 2012), transforming growth

factors (Baylink, Finkelman et al. 1993)and bone morphogenic proteins (BMPs) (Shore, Xu et al. 2006, Katagiri, Osawa et al. 2015) essential for cellular communication.

1.2.5 SOURCE OF BLOOD CELLS

The inner cavities of bones contain the red bone marrow, which is the body's source of hematopoietic and stem cells (Taichman 2005), essential for differentiating into all the different types of blood cells, including erythrocytes and lymphocytes. Hematopoietic tissue (red marrow) is found between the trabeculae of spongy bone, whereas in flat bones such as the sternum or skull is found in the spongy tissue known as diploë. The red marrow of flat bones and in some irregular bones (such as the hip) have a higher level of haematopoiesis and for this reason, are regularly used clinically for sampling marrow tissue. Despite a high hematopoietic activity at birth, red marrow in the medullary cavities of long bones become gradually converted with age into a less metabolically-active, yellow (fatty) bone marrow, a process which concludes in adulthood (25-30 years). However, yellow bone marrow can dynamically revert to red marrow in certain pathologic conditions (e.g. anaemia, obesity) that require an enhanced red blood cell supply and a higher tissue oxygenation (Bigelow and Tavassoli 1984, Guillerman 2013).

1.2.6 STORAGE OF TRIGLYCERIDES

Bones also contain triglycerides as a source of stored energy (Mularchuk and Boskey 1990). Although lipids only constitute less than 2% of the dry weight of bone tissue, they appear to have an influential role in the development of mechanical functionality of bones (Goldberg and Boskey 1996), as phospholipase D is involved in the initial stages of ossification during embryogenesis, and it has been found to be expressed in the extracellular matrix of the developing mouse skeleton (Gregory, Kraemer et al. 2005).

1.2.7 STORAGE OF TOXIC COMPOUNDS

In addition to storing essential minerals ions, bone tissue can temporarily house dangerous compounds in the systemic circulation, including radioactive compounds, lead (Pounds, Long et al. 1991), aluminium (Ballanti, Wedard et al. 1996) and tetracyclines from diet, including oxytetracycline (OTC) and chlortetracycline (CTC) (Honikel, Schmidt et al. 1978).

1.3 STRUCTURE OF BONE

Bones are composed of two structurally distinct textures, compact bone on the exterior and spongy bone, also known as trabecular or cancellous bone, internally (Figure 1.6).

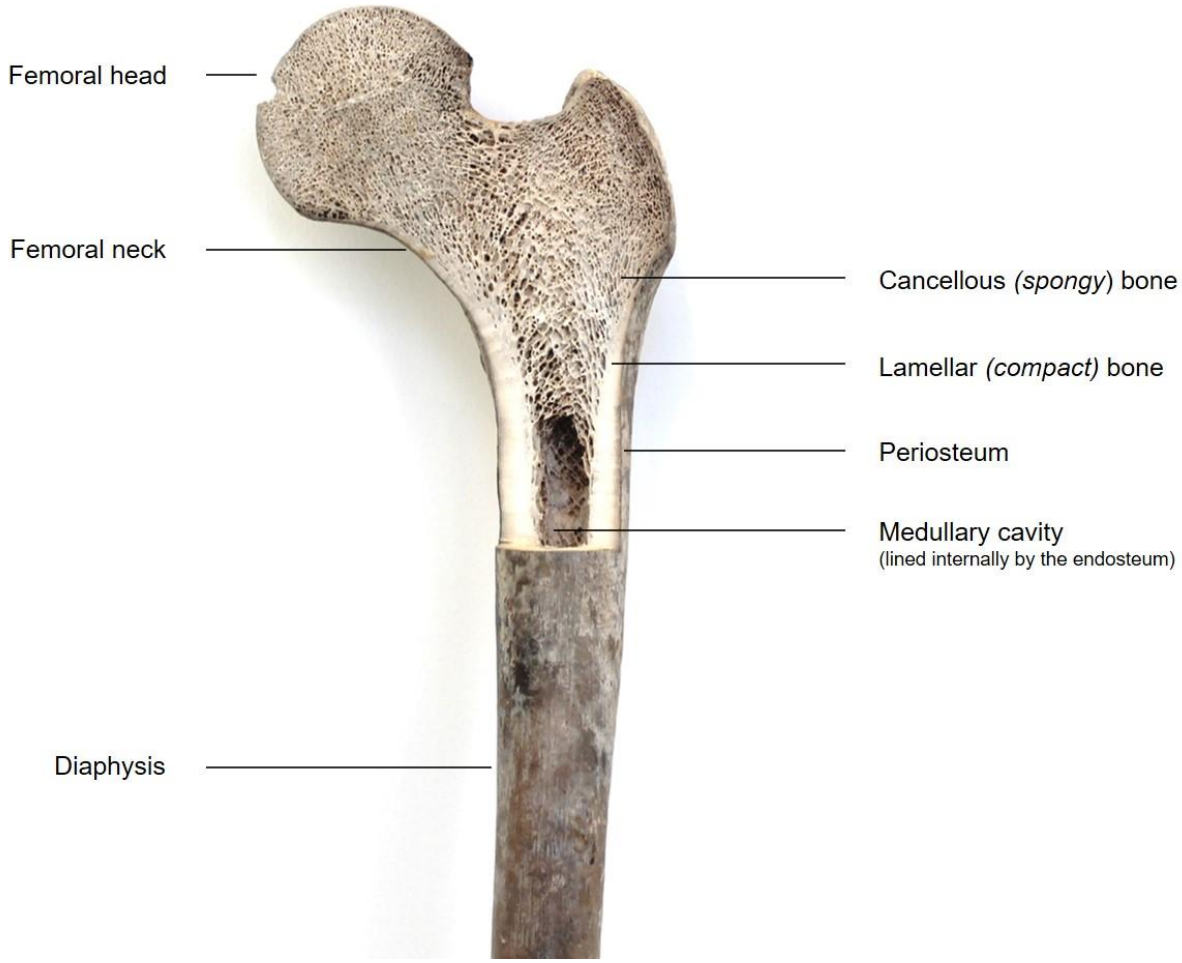

Figure 1.6 | Bone textures: spongy and compact bone in the femur. Long bones are composed of two texturally different types of tissue, compact bone and spongy bone, adapted for providing support during different types of mechanical load. The outer cortical layer is lined externally by the periosteum and internally by the endosteum. The internal cavities of bones contain the red and yellow marrow. *Original image. Image of the femoral section acquired from a skeletal specimen at the Natural History Museum, South Kensington, London.*

1.3.1 COMPACT BONE

Compact bone is composed of highly organised units named osteons, which are long, cylindrical structures arranged parallel to the long axis of the bone. These structures provide canals through which blood and lymphatic vessels and nerves can supply the surrounding bone tissue. Each osteon is composed of concentric, hollow tubes (lamellae), which are made of mineralised collagenous matrix. Each lamella contains collagen fibres running in the same direction but in a different direction from fibres in other lamellae, a reinforced design meant to withstand torsion forces (Figure 1.7). This arrangement of lamellar collagen directly affects the mechanical properties of individual lamella. Mechanical studies by Pidaparti and colleagues (Pidaparti and Burr 1992) and later by Ascenzi and colleagues (Ascenzi, Baschieri et al. 1994) showed that in combined loading situations (torsion and bending), collagen fibres with a geometrical orientation ranging between 15°-30° of the long axis are the best suited for maximizing the overall mechanical properties of bone tissue.

The central portion of osteons contains the Haversian canals, which contain the small blood vessels and nerves that supply the cells inside osteons. These central canals communicate with the blood supply and innervation of the periosteum using Volkmann's canals, which run perpendicular to the long axis of the bones. The interior lining of these canals consists of the endosteum.

There are additional lamellae in compact bone which are not part of osteons. These are interstitial lamellae which fill the spaces between osteons. Additionally, there are circumferential lamellae just underneath the periosteum and above the endosteum which play a role in mechanical resistance against stress. A study by Liu and colleagues (2000) comparing the mechanical properties of circumferential and osteonal lamellar

bone in a primate model showed that the mechanical behaviour of the two types of lamellar bone under bending tests were similar for the same orientations relative to the bone axis, suggesting that the complex arrangement of mineralised collagen fibrils itself is reposible for stress resiliance. However, the authors found that osteonal and circumferential lamellar bones exhibit different behaviours during induced fractures, with osteonal lamellar bones tending to remain connected after the main fracture event, whereas circumferential lamellar bones separated following fracture. This implied that osteonal fractures have higher chances of repair and the chances of fracture non-unions are lower compared to circumferential fractures (Liu, Wagner et al. 2000).

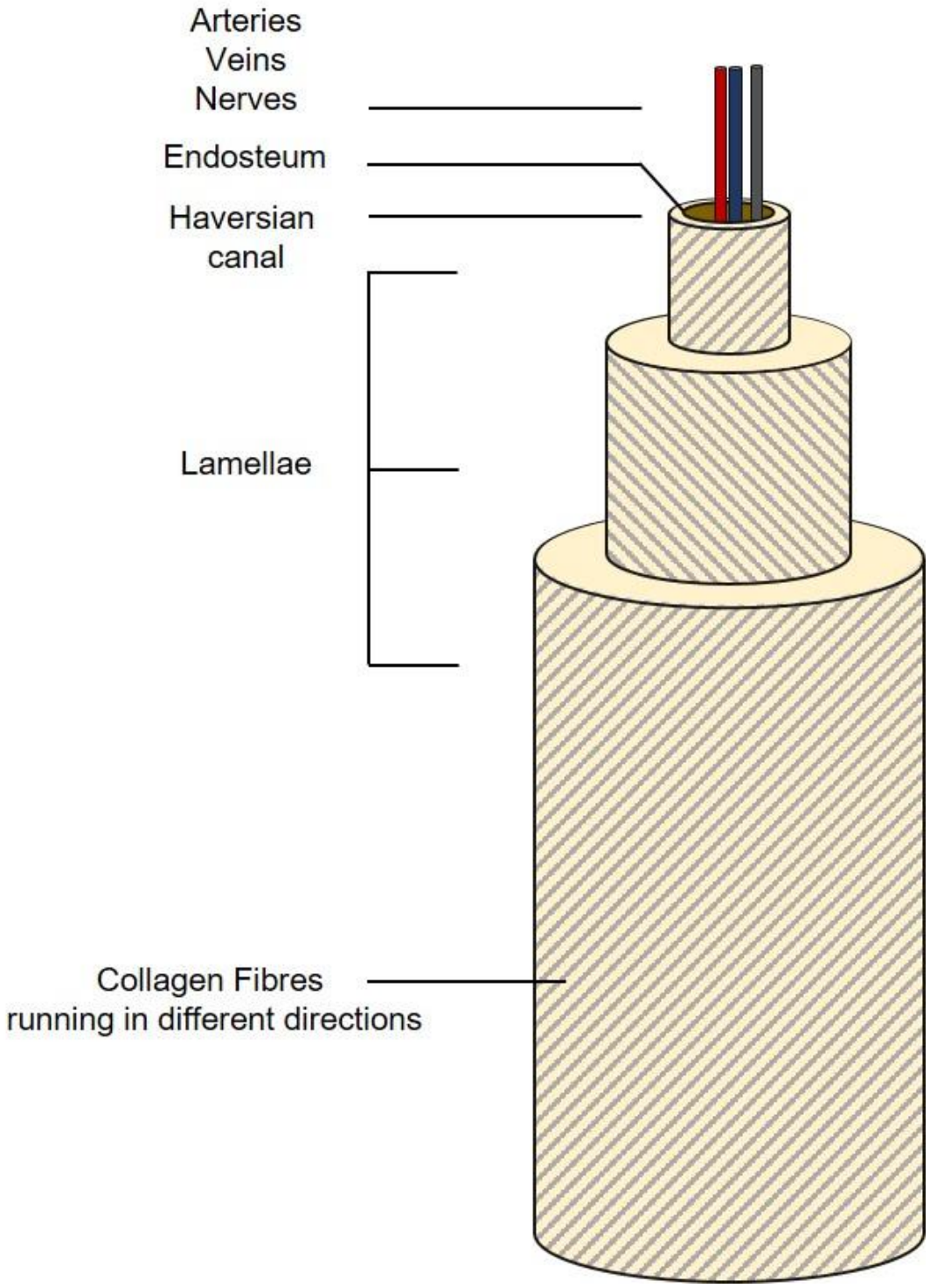

Figure 1.7 | Structure of an osteon. Individual lamellae are arranged concentrically and are composed of mineralised collagenous fibres arranged in different directions in each lamellar unit to provide maximal resistance to stress. Centrally, osteons act as passageways for blood vessels (arteries and veins) and nerve fibres and are lined internally by the endosteum.

The mature bone cells, osteocytes, are located concentrically at the lamellar junctions (Figure 1.8). These cells are embedded in lacunar spaces and contain numerous projections which are contained within canalicular structures. These canaliculi allow inter-cellular communication, the flux of waste and nutrients, as well as connecting osteocytes to the endosteum (Dallas and Bonewald 2010, Bonewald 2011). The formation of osteocytes and their complex function is described in further detail in section *1.5 Cellular Composition of bone*.

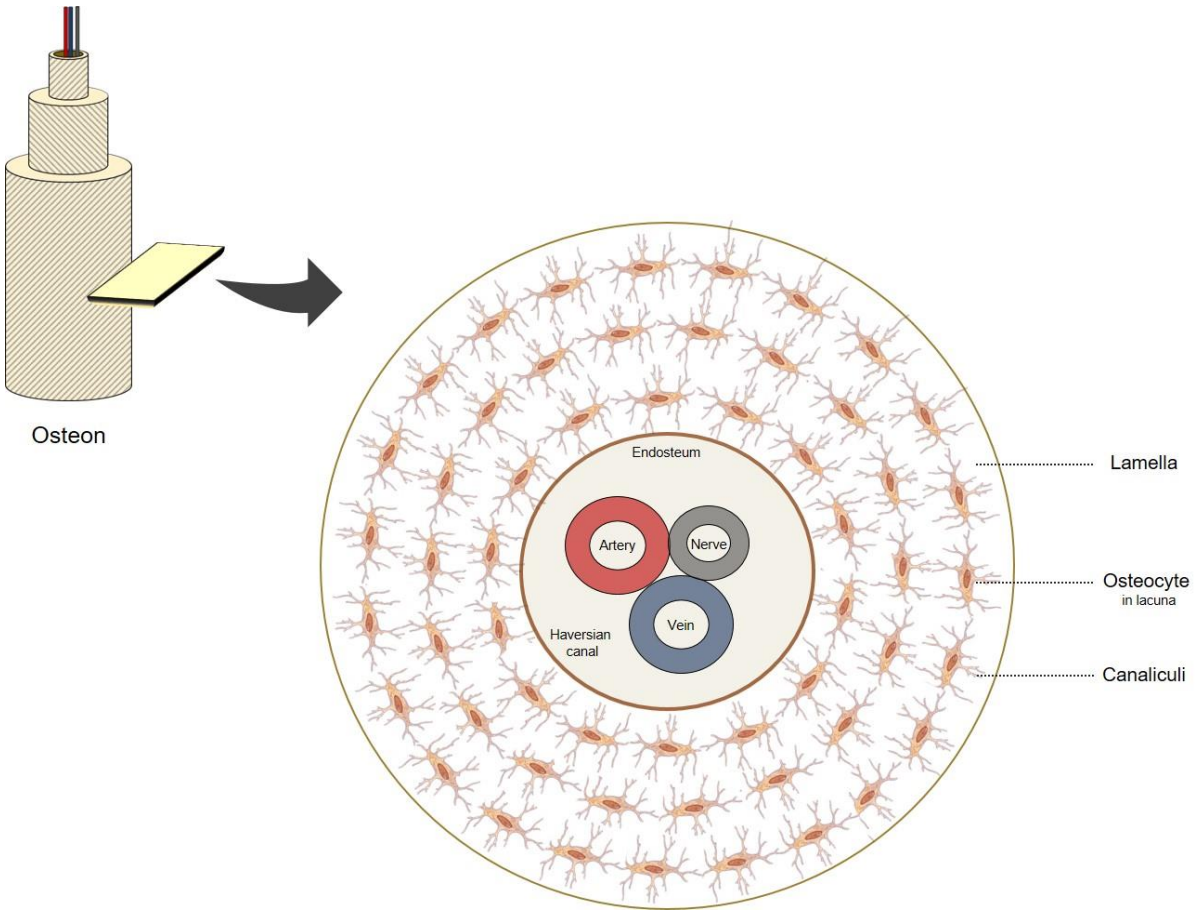

Figure 1.8 | Horizontal section through an osteon. Osteocytes, the mature bone cells, are arranged concentrically at the junctions between lamellae. They are embedded in lacunae and linked by canaliculi, which allow cell-to-cell communication and connect to the endosteum.

1.3.2 TRABECULAR BONE

Unlike compact bone, spongy bone appears to consist of disorganised bone tissue. However, the trabeculae are actually aligned in a fashion which allows the bones to withstand maximal amounts of stress, and are located at anatomical points where significant amounts of stress are transmitted to the rest of the skeleton (e.g. femoral head – Figure 1.6)(Ryan and Ketcham 2005). The trabeculae contain irregularly arranged lamellae and osteocytes, which communicate with each other through canaliculi, and receive nutrients from capillaries passing these canaliculi emerging from the endosteum surrounding the trabeculae (Lafage-Proust, Roche et al. 2015, Prideaux, Schutz et al. 2016).

1.3.3 THE PERIOSTEAL MEMBRANE

As discussed above, bones also contain an external membrane, the periosteum, which covers the entire surface with the exception of the joint. The periosteum is composed of two thin layers – externally by an outer fibrous layer, composed of dense irregular connective tissue, whereas the internal layer, the cambium, is highly osteogenic, consisting of bone-forming osteoblasts and bone-resorbing osteoclasts as well as a large population of stem cells which can differentiate into osteoblasts (Zhang, Naik A Fau - Xie et al. 2005, Marsell and Einhorn 2011, Chang and Knothe Tate 2012). The periosteum contains a rich supply of nerve fibres, blood vessels and lymphatic vessels, which enter the bone through the nutrient foramina openings. This layer is firmly anchored to the underlying bone tissue through collagen fibres (Sharpey's) fibres. The periosteum serves an additional purpose, which is to provide anchorage to the ligaments and

tendons. These regions are very rich in Sharpey's fibres (Marieb and Hoehn 2010, Chang and Knothe Tate 2012).

1.3.4 THE ENDOSTEUM

Internally, bone is covered by the endosteum, a fragile connective tissue structure which covers the trabeculae of spongy bone and lines the canals in lamellar bone. This layer is similar to the periosteum in terms of cellular composition, containing both osteoblasts and osteoclasts.

1.4 CHEMICAL COMPOSITION OF BONE

1.4.1 THE INORGANIC COMPONENT

The nature of the inorganic component of bone was elucidated many decades ago using X-Ray diffraction. Studies by de Jong in 1926 (de Jong 1926) and later by Roseberry (1931) (Roseberry, Hastings et al. 1931) were the first to show using X-Ray Diffraction that bone samples contained small particles with diffractograms very similar to the crystals of naturally-occurring hydroxyapatite (HA) $Ca_5(PO_4)_3(OH)$ (Figure 1.9), a calcium phosphate mineral with a Ca:P ratio of 1.67. This composition, which was mainly deducted from cortical bone samples due to the ease of preparation for examination, was initially generalised to a variety of calcified tissues. However, over time, it became clear that there were differences in the mineral phases in different tissues, and in the same mineral phase across different phyla and species. The molar ratios of Ca and P can vary considerably in osseous tissues due to variations in vacancies and substitutions (Palmer, Newcomb et al. 2008), which take place due to the ongoing process of homeostasis, where calcium, magnesium and phosphorus ions are continuously removed from the bone reserves in order to supply the rest of the tissues (Boden and Kaplan 1990, Favus and Goltzman 2013).

In both the bones and teeth of mammalian vertebrates, the mineral is mainly carbonated apatite, $Ca_{10}(PO_4,CO_3)(OH)_2$ (Favus and Goltzman 2013), although other minerals have been identified in small proportions, such as whitlockite (Jang, Jin et al. 2014, Jang, Lee et al. 2015) and more recently, intermediate phases such as octacalcium phosphate (OCP) (Ban, Jinde et al. 1992, Crane, Popescu et al. 2006).

Figure 1.9 | Apatite mineral. Apatite is a calcium phosphate mineral that is produced and used by many biological environmental systems. Hydroxyapatite, one of principal types of apatite, is the main inorganic component of bone and dentin. *Original image. Author would like to thank the Lapworth Museum of Geology, University of Birmingham.*

1.4.2 THE ORGANIC COMPONENT

The organic component of bone is composed of cells (osteogenic cells, osteoblasts, osteoclasts and osteocytes) and osteoid. Osteoid comprises approximately 35% of the weight of the matrix and is composed of the ground substance (which includes proteoglycans and glycoproteins) and collagenous tissue, both which are the product of osteoblasts. As discussed in the previous sections, collagen contributes not only to the structure of the matrix, but also to the resistance of bone to tensile and bending forces.

The organic component of bone matrix is composed in a proportion of 90% of collagen type I, with the remaining 10% composed of non-fibrous proteins. Type I collagen is found in both osseous tissue and non-calcifying mesenchymal tissues and is composed of fibrils of approximately 78 nm diameter, showing a very characteristic periodic banding appearance when viewed under the electron microscope (Olsen 1964). Two bands can be identified, which have different densities, of 0.4 D and 0.6 D (Bonucci 2007). Their appearance of these periodic bands depends on the arrangement of the molecules and their amino acid sequence (von der Mark, Wendt et al. 1970). Collagen molecules are 280-300 nm long and are composed of three polypeptide chains which assemble into a left-handed triple helical configuration (Ramachandran 1956, Hulmes 2002, Orgel, Irving et al. 2006). The polypeptide chains are composed of approximately 33% glycine, found in every third position in the conformation gly-x-y, and approximately 22% is composed of proline and hydroxyproline (Martin, Piez et al. 1963, Bonucci 2007). Molecules of collagen type I consist of three chains, out of which two are identical and termed αI(I) and a different, third chain, αI(II) (Bonucci 2007).

The inorganic component, hydroxyapatite, which accounts for approximately 65% of the weight of the bone is associated with collagenous fibres, which offers the bone

tissue great strength and resistance to compression. Although the role of collagen in nucleation of hydroxyapatite crystals has been a subject of great debate, fundamental studies performed since the 1950s on the mineral distribution in avian calcifying tendons suggested that two types of collagen mineralisation take place in vertebrates: intrafibrillar (Jackson 1957, Weiner and Traub 1986, Landis, Moradian-Oldak et al. 1991, McEwen, Song et al. 1991) and interfibrillar (Landis, Hodgens et al. 1996). In the intrafibrillar model of mineralisation, it was proposed that crystals penetrate through the fibrils, suggesting this as a mechanism through which apatitic crystals become orientated parallel to the collagen fibre axis (Jackson 1957). Later studies by Weiner and colleagues (1986) reported that crystals are located within the fibrils at the level of 'grooves' created by adjacent gaps (Weiner and Traub 1986) (Figure 1.10).

Work by McEwen and colleagues showed that 64% of the crystals were located in the collagen gap areas and only 36% in the collagen overlap areas (McEwen, Song et al. 1991). Later work (Landis, Hodgens et al. 1996) demonstrated the presence of mineral crystals on the surface of collagen fibrils (inter-fibrillar mineralisation) along intra-fibrillar mineralisation.

Recent evidence from Wang and colleagues (2012) revealed that collagen type I itself can initiate and orientate the growth of apatite crystals *in vitro* in the absence of any other biochemical components involved in vertebrate skeletal development (Wang, Azaïs et al. 2012). Moreover, the authors showed that collagen type I can control the 3D distribution of the inorganic component from the atomic to the macroscopic scales. Recently (2017), the work of Niu and colleagues demonstrated using a polyanion and polycation-directed mineralisation that that the process of interfibrillar mineralisation is mediated by a balance between osmotic equilibrium and electroneutrality, as the

outward movement of ions and intrafibrillar water through the collagen surface occurred irrespective of the charges of the electrolytes (Niu, Jee et al. 2017).

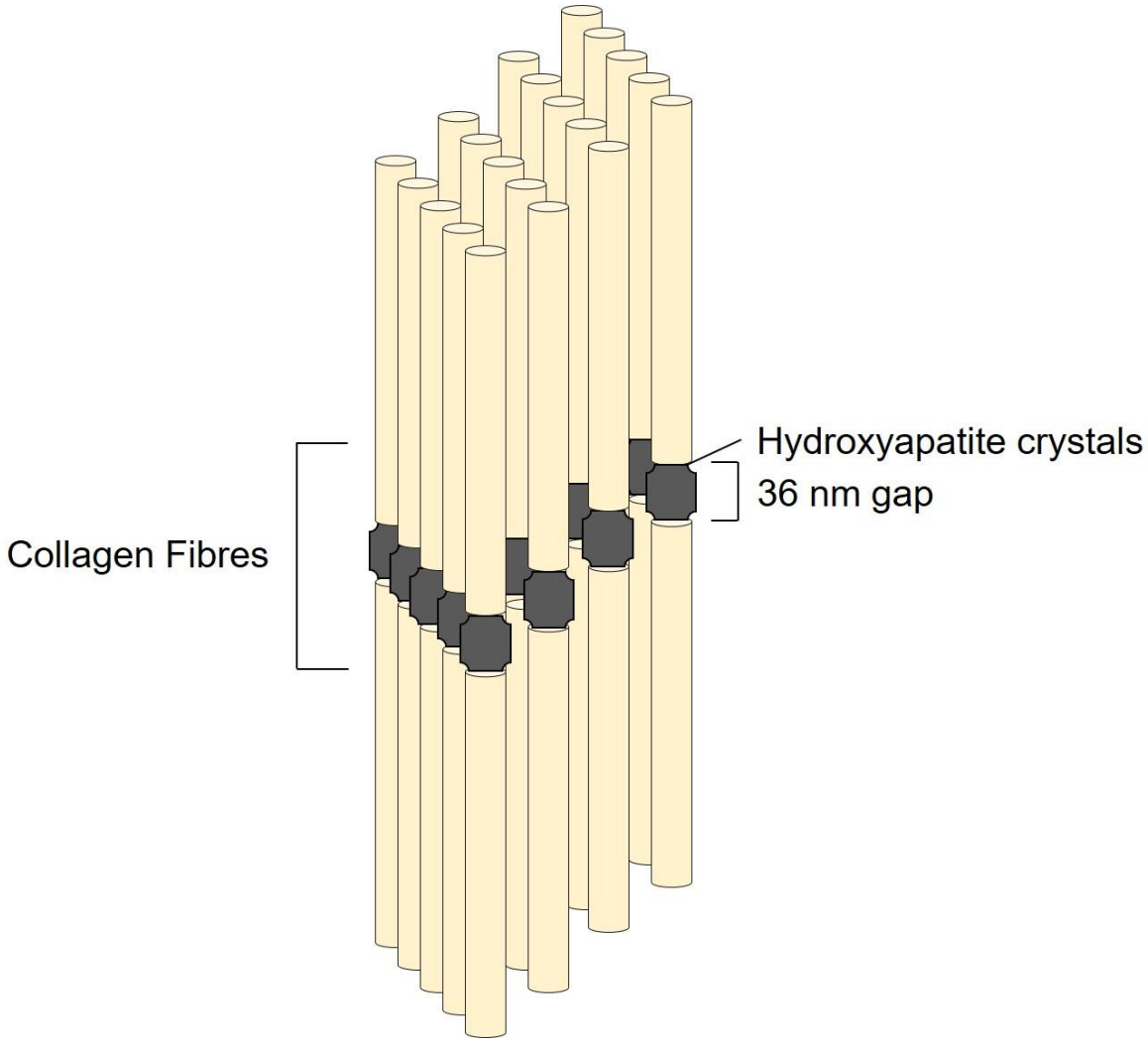

Figure 1.10 | Simplified schematic of the organic-inorganic hierarchical structure in bone tissue. This model was first proposed by (Petruska and Hodge 1964). Collagen molecules (normally triple-helical, simplified here) are arranged end-to-end and parallel to each other. These structures contain spaces of approximately 36 nm between them, which facilitate nucleation by apatitic crystals. The mineral develops in this space in the fibrils. Diagram inspired from (Fang and Holl 2013) and (Alexander, Daulton et al. 2012).

The organic component of bone is sometimes referred to as being completely separate from the inorganic component, a definition that not necessarily correct, as the two components are highly inter-related and defects in cell processes can lead to abnormal matrix production, which in turn gives rise to abnormal mineral deposition (e.g. *osteogenesis imperfecta*, a number of dysplasias and tumours) (Marie 2015). These will be reviewed in detail in *Section 1.11 Pathological Bone Formation*.

1.5 TYPES OF BIOMINERALISATION

The process of deposition of mineral salts in the organic matrix of biological tissues has been referred to using multiple terms such as calcification, biomineralization and ossification. Whilst sometimes they are considered to be synonymous, in many contexts their meanings change. In this thesis, the process of calcification is referred to as the precipitation of calcium phosphate salts on the surface of tissues, whereas the term 'ossification' is used to describe a hierarchical and organised deposition of mineral on collagen and other proteins belonging to the organic matrix of bone. However, it has to be stressed that it is not always possible to distinguish between the two processes, and therefore, in this thesis, the term 'biomineralization' is sometimes used to refer to the process of cell-mediated formation of a stable, crystalline phase of inorganic material. Irrespective of the pathway of mineralisation, this process is indispensable to many organisms, from prokaryotic forms of life to invertebrates and vertebrates.

1.5.1 BIOMINERALISATION IN INVERTEBRATES

Biomineralization in animals of the invertebrate subphylum is a process that is found in many morphologically-distinct structures. These can range from intracellular mineral particles, calcifying bacteria, calcified exoskeletons of arthropods (Figure 1.11a-c), which include extinct marine arachnomorphs as far as the Cambrian period (approx. 500 million years ago) such as trilobites (a) and (b) and the exoskeletons of crustaceans (c); shells of molluscs and gastropods (d-e) and coral skeletons (e). These structures have a very high mineral component composed of calcium phosphates and carbonates, and a very low organic component (e.g. in molluscs, the organic matrix constitutes less

than 5% of the total weight). The mineral in these species can range from calcium carbonate ($CaCO_3$) in mollusc shells (Weiner and Hood 1975) to crystalline fluorapatite in most crustacean mandibular teeth (Bentov, Aflalo et al. 2016).

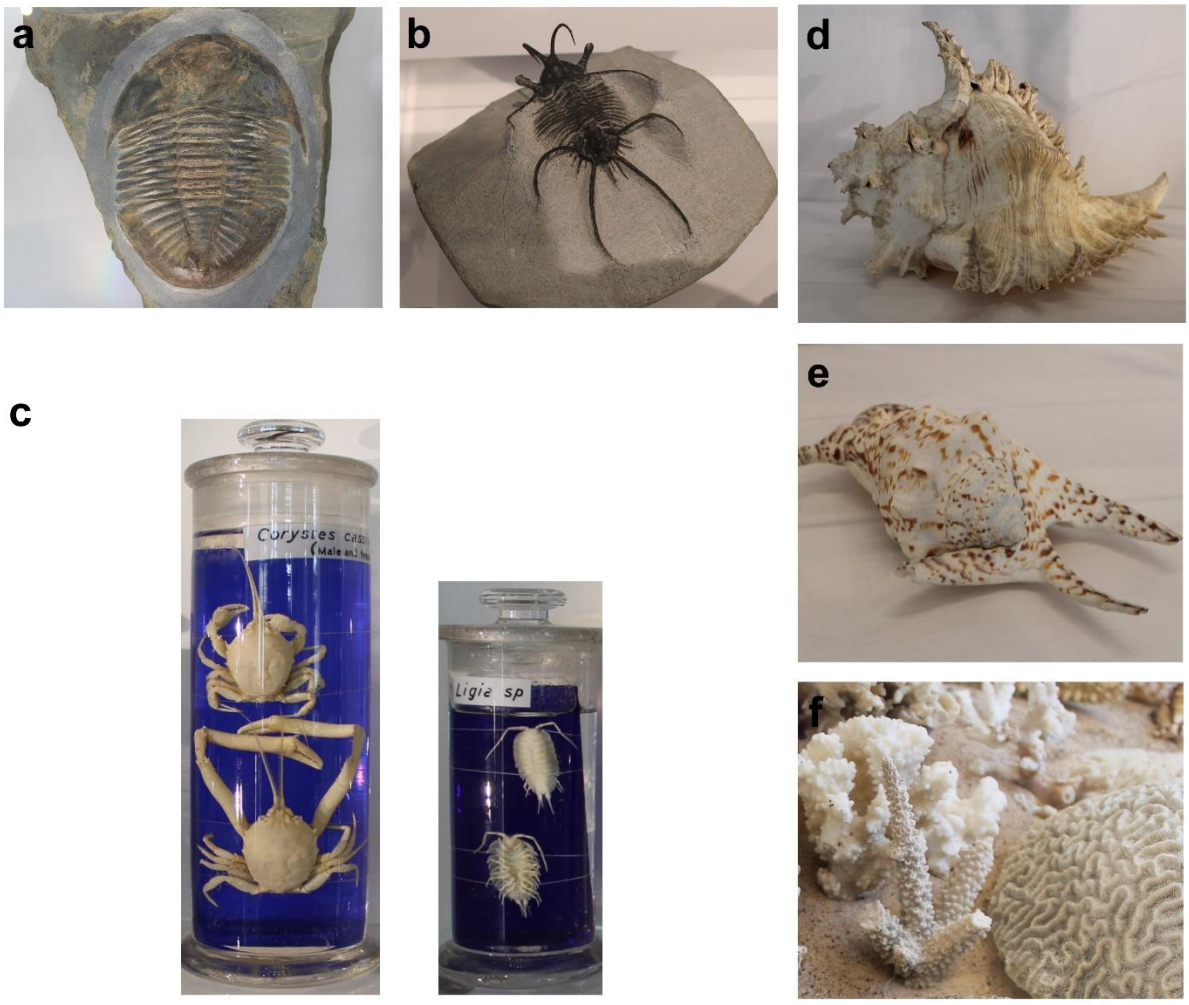

Figure 1.11 | Biomineralization is a process encountered in many orders and in the invertebrate forms of life, such as the exoskeletons of many arthropods, including extinct organisms such trilobites from the Palaeozoic Era (**a**- *Ogyginus Cordensis* trilobite and **b**- *Ceratarges Armatus* trilobite); shells of crustaceans including the *Corystidae* family (including crabs); the marine shells of gastropods (**d-e**) and coral skeletons (**f**). *Original images. Author would like to thank the Lapworth Museum of Geology, University of Birmingham.*

1.5.2 BIOMINERALISATION IN VERTEBRATES

In terrestrial vertebrates, different parts of the skeletal system form through complex ossification pathways, known as endochondral and intramembranous ossification.

1.5.2.1 INTRAMENBRANOUS OSSIFFICATION

In the first type of ossification, known as intramembranous ossification, osteoprogenitor cells directly differentiate into osteoblasts, the bone building cells, to form mature bone. This is the major pathway of ossification in the bones of the skull and one of the main repair pathways during callus-mediated fracture repair, which takes place at the broken ends of a bone, compared to the central portion, which forms through a cartilage intermediate (Gerstenfeld, Cullinane et al. 2003, Claes, Recknagel et al. 2012).

1.5.2.2 ENDCHONDRAL OSSIFFICATION

The second type, known as endochondral ossification, represents the formation of bone through a cartilage intermediate or template. In this type of ossification, osteochondral progenitors differentiate into separate lineages of chondrocytes and osteoblasts to give rise to a cartilage template on top of which the future mature bone will eventually form. This is the major process by which long bones of the limbs form and, as mentioned above, is also involved in bone repair (Einhorn and Gerstenfeld 2015).

The processes of intramembranous and endochondral ossification will be described in more detail in *Section 1.8 – Bone Fracture Repair*. An introduction to the essential cellular events in bone formation is presented in the next section.

1.6 CELLULAR AND CYTOPATHOLOGICAL EVENTS IN BONE FORMATION

The skeletal system in vertebrates is composed of cartilaginous and osseous tissue, which forms during embryogenesis through the action of mesenchymal osteochondral progenitor cells, which differentiate into either chondrocytes or osteoblasts.

1.6.1 FORMATION OF CHONDROCYTES

Chondrocytes form during endochondral ossification, the first step which is the formation of a cartilage template. Chondrocytic cells differentiate from osteochondral precursors and undertake a series of tightly controlled events of proliferation, which take place along the longitudinal axis of the cartilage template (interstitial growth) and continue with appositional growth, where the structure becomes thicker with subsequent matrix deposition. A peripheral cartilage formation takes place as the structure grows in thickness (the perichondrium). This template is subsequently invaded by a mixed population of cells which give rise to a primary ossification centre (located centrally in the diaphysis). The perichondrium becomes the periosteum, containing osteoprogenitor cells which will give rise to osteoblasts and produce bone appositionally (Mackie, Ahmed et al. 2008). Chondrocytes which are located furthest from the ossification centre are actively proliferating and become flattened as they pack into column-like structures. Chondrocytes which are closest or inside the ossification centre become hypertrophic, secreting collagenous matrix (type II and X) which becomes mineralised (Rosen, Bouillon et al. 2013). Secondary ossification centres develop in the epiphyses, in a similar manner, and continue to grow until the cartilage remaining between the two ossification centres forms an epiphyseal plate.

Chondrocytes in this structure continue to produce cartilage which is replaced by bone, which is essential for the longitudinal growth of bones. The bone-resorbing cells, osteoclasts, aid in removing excess cartilage matrix. The transition of chondrocytes is a process controlled by multiple signalling and genetic mechanisms and different stages of endochondral ossification show different gene expression patterns. Chondrocytes in immature stages express the transcription factors Sox 5, Sox 6, Sox 9 (Hardingham, Oldershaw et al. 2006, Leung, Gao et al. 2011). The pre-hypertrophic stage is characterised by parathyroid hormone I receptor (PTH1r) and Indian hedgehog expression, which form a negative feedback loop that controls the chondrocyte's decision to carry on proliferating or become hypertrophic (Yang 2013). $Ihh^{-/-}$ rodents show a lack of endochondral bone due to a 50% reduction in proliferation and increase in hypertrophic progression (St-Jacques, Hammerschmidt et al. 1999, Long, Zhang et al. 2001). Early hypertrophic chondrocytes decrease the expression of Sox 5,6 and 9 and collagen type II and increase the production of collagen type X (Kielty, Kwan et al. 1985). Hypertrophic chondrocytes develop with the expression of vascular endothelial growth factor A (VEGFA)(Zelzer, Mamluk et al. 2004), matrix metalloproteinase 13 (MMP-13) and osteopontin (Gerstenfeld and Shapiro 1996, Pullig, Weseloh et al. 2000), indicating the subsequent invasion of osteoblasts, osteoclasts and endothelial cells which are going to replace the cartilage template with bone (Li and Dong 2016).

It is important to note that cartilage is an avascular tissue which develops under hypoxic conditions, as some of the centrally-located chondrocytes do not have access to vasculature-provided oxygen. As a result, the transcription factor hypoxia-inducible factor 1α (HIF- 1α) is essential, as seen in other hypoxic conditions, in mediating the

hypoxic response in cartilage. Removal of HIF- 1α results in the death of chondrocytes inside the growth plate (Schipani, Ryan et al. 2001).

1.6.2 FORMATION OF OSTEOBLASTS

The osteoblastic differentiation can be classified according to four stages, including division, extracellular matrix deposition, matrix maturation and mineralisation (Stein and Lian 1993). There are several key enzymes and proteins essential in these processes, including alkaline phosphatase (ALP), type I collagen (Col I), bone sialoprotein (BSP), osteopontin (OPN) and osteocalcin (OC). These are also used as differentiation markers which can be detected at different stages in osteogenesis, for which ALP is known to be an early osteoblastic marker, whereas OC is used as a late marker for osteoblast differentiation (de Gorter and ten Dijke 2013). Several signalling pathways control these processes, including RUNX2, BMP, TGF-β, WNT, HEDGEHOG, PTH, IGF-1, FGF and NOTCH (de Gorter and ten Dijke 2013). The pathways which are important for understanding some of the results in this thesis are described in detail below.

1.6.2.1 RUNX2 PATHWAY

This pathway is a critical event in osteoblastic differentiation. The activation of transcription factor RUNX2 is indispensable for the mineralisation step and formation of a skeleton. Homozygous mutants for RUNX2 (also known as Cbfa1) are not able to survive at birth due to respiratory failure and show a lack of osteoblasts and of both intramembranous and endochondral bone (Otto, Thornell et al. 1997). Heterozygous

mutants develop skeletal abnormalities which appear to be similar to pathological conditions such as cleidocranial dysplasia (CCD), a condition characterised by abnormal development of the cranial bones and marked absences in parts of the collar bone (Mundlos 1999). RUNX2 is able to interact with gene promoters to increase or downregulate the expression of Col I, ALP, OPN, OC and ON and osterix (Osx)(Harada, Tagashira et al. 1999, Kern, Shen et al. 2001).

1.6.2.2 BMP PATHWAY

Experiments conducted by Urist in 1965 originally identified bone morphogenic proteins (BMPs) as active components in bone extracts which are able to promote ossification when implanted subcutaneously, giving rise to ectopic bone (Urist 1965). Since then, the role of BMPs in bone formation has become well known. They are present in skeletal tissue and are involved in bone homeostasis and fracture repair (Gazzerro and Canalis 2006) and as such, several types such as BMP-2 and 7 have recently been applied in clinical practice to accelerate bone healing and treat fracture non-unions (Gautschi, Frey et al. 2007, Schmidmaier and Wildemann 2009). Their abnormal activity caused by genetic mutations which trigger overactivation in conditions such as *Fibrodysplasia ossificans progressiva* leads to large amounts of ectopic bone formation and will be discussed later in this chapter.

BMPs are part of the TGF-β superfamily of proteins and bind to type I and II serine/threonine receptor kinases, forming an oligomeric complex (de Gorter and ten Dijke 2013), which leads to the phosphorylation and hence activation of type I receptors by the constitutively active type II receptors. This in turn, activates intracellular

signalling mediators Smad 1, 5 and 8, which then associate with co-Smad 4, and together they translocate to the nucleus, where they act as transcription factors, stimulating alkaline phosphatase activity and ultimately bone formation (Feng and Derynck 2005, Massague, Seoane et al. 2005, de Gorter and ten Dijke 2013).

1.6.2.3 TGF-β PATHWAY

TGF-β signalling is involved in the proliferation and differentiation of numerous cell types, including chondrocytes and osteoblasts. The signalling mechanism is similar to BMPs, but is mediated by Smad 2 and 3 factors (Feng and Derynck 2005, Massague, Seoane et al. 2005). Smad3 is able to greatly increase ALP activity in osteoblastic cells (MC3T3) *in vitro*, as well as type I procollagen and OPN (Sowa, Kaji et al. 2002).

1.6.2.4 WNT PATHWAY

The WNT pathway regulates bone mass and influences osteoblast differentiation (Wang, Li et al. 2014). WNTs are glycoproteins which signal via membrane receptors to β-catenin. In normal conditions, β-catenin forms a complex with adenomatous polyposis coli (APC), axin, glycogen synthase kinase 3 (GSK3) and casein kinase 1 (CK1). The presence of WNT causes dissociation of this complex, which releases β-catenin into the cytoplasm and translocates to the nucleus, where it affects expression of proteins such as ALP. This pathway is essential for the transition of mesenchymal cells to an osteoblastic phenotype and thus, bone formation (de Gorter and ten Dijke 2013). Disruption of WNT signalling is linked to osteoporosis (Canalis 2013) and deletion of β-catenin causes osteochondral progenitors to differentiate into a chondrocytic lineage as

opposed to osteoblastic (Day, Guo et al. 2005). Moreover, ectopic WNT signalling enhances osteoblastic differentiation and suppresses chondrocyte formation (Day, Guo et al. 2005). Importantly, the WNT signalling pathway plays an essential role in osteocytes (Bonewald and Johnson 2008), where it is believed to allow osteocytes to signal information on mechanical loading to the cells on the bone surface. Osteocyte-deficient β-catenin deficient mice show progressive bone loss in the appendicular and axial skeleton (Kramer, Halleux et al. 2010) and mutations in *SOST*, the gene encoding sclerostin, which is produced by osteocytes and acts as an antagonist of WNT, lead to the rare Van Buchem disease and sclerosteosis (Semenov, Tamai et al. 2005, ten Dijke, Krause et al. 2008), which are characterised by abnormally high bone mass.

1.6.2.5 PTH PATHWAY

The parathyroid hormone (PTH) can have both anabolic and catabolic effects on bone formation and appear to vary with the mode of administration. For example, intermittent parathyroid hormone therapy leads to increased bone mass by conversion of the quiescent lining cells to active osteoblasts (Kim, Pajevic et al. 2012), and by reducing sclerostin levels, thereby allowing WNT-driven bone formation (Keller and Kneissel 2005); whereas continuous PTH administration leads to greater bone resorption (Tam, Heersche et al. 1982, Neer, Arnaud et al. 2001). Homozygous inactivating mutations in the PTH or PTH related peptide receptor lead to the lethal genetic disorder known as Blomstrand chondrodysplasia (Zhang, Jobert et al. 1998).

1.7 FORMATION OF OSTEOCLASTS

Osteoclasts are exclusively bone-resorptive cells, which derive from bone macrophage lineages (Suda, Takahashi et al. 1999). Osteoclastogenesis take place under the action of two important cytokines, the receptor activator of nuclear factor kB ligand (RANKL), a member of the tumour necrosis factor (TNF) superfamily, which is crucial for osteoclast formation (Boyle, Simonet et al. 2003); and the macrophage-colony stimulating factor (M-CSF/CSF-1), which influences proliferation and differentiation (Pixley and Stanley 2004). These cytokines exist as membrane bound, secreted by T cells, and soluble forms, secreted by bone marrow stromal cells and osteoblasts and therefore, the initiation of osteoclastogenesis requires the presence and activity of bone residing cells (Ross 2013). However, it has been recently shown that the mature bone cells, osteocytes are the major producers of RANKL *in vivo*, as mice with osteocytes deficient for RANKL show an osteopetrotic phenotype (Nakashima, Hayashi et al. 2011) (*see 1.1.2 Adaptation of Bones to Different Environments* and *1.65 Osteocyte control of bone remodelling*).

Mutations in the genes responsible for proper osteoclast formation (genes *TNFSF11* and *TNFRSF11A*) and proper resorptive function of these cells (defects in the chloride channels that modulate osteoclast acid secretion) (*TCIRG1*, *CLCN7*, *OSTM1*, *SNX10*, *PLEKHM1*) (Sobacchi, Schulz et al. 2013) have also been linked to osteopetrosis. At the opposite end of the spectrum, RANKL overactivation leads to osteolytic bone disease (Wittrant, Théoleyre et al. 2004) and RANKL production by osteocytes and B lymphocytes is required for bone loss caused by estrogen decline at menopause (Fujiwara, Piemontese et al. 2016).

1.7.1 OSTEOCYTES

Aside from the osteoblasts which constitute around 4-6% of the cells in bone, and the osteoclasts, which represent 1-2% of the total cell population, 90-95% of the cells in bone are actually osteocytes, the mature bone cells, which are terminally differentiated osteoblasts that play an essential role in mechano-sensing and orchestrating the bone remodelling process. They are also the longest-living bone cells, with a life span of around 25 years (Franz-Odendaal, Hall et al. 2006), where they live entrapped within 15-20 μm lacunae, in a highly mineralised matrix. For a long time, due to their localisation and the inability to isolate them, they were considered passive cells and their functions were poorly defined. Over the recent years, we have become more aware of the essential role they play in many physiological processes (Bonewald 2011).

As mentioned above, evidence has recently emerged which shows that osteocytes are essential in regulating phosphate homeostasis, by secreting into the circulation the fibroblast growth factor 23 (FGF23), acting as mini 'endocrine glands' (Dallas, Prideaux et al. 2013). Therefore, abnormalities in these cells may contribute towards several bone diseases, including bone fragility induced by corticoids and osteoporosis (Bonewald 2011, Bonewald 2013).

They also perform a mechanical sensing function, which is permitted by their strategic, regular arrangement in the lacuno-canalicular system (*see* Figure 8), containing dendritic processes which extend to the bone surface and to the marrow. These events are still not fully characterised, and this section will summarise the current state of knowledge.

Osteocytes form from the terminal differentiation of osteoblastic cells derived from a bone marrow lineage. Following ossification, osteoblasts can become embedded in their

own osteoid, becoming osteocytes, they can become quiescent bone lining cells or can undergo apoptosis (Jilka, Weinstein et al. 1998). The genetic mechanisms controlling the fate of these cells is still unknown. Several recent studies in osteocyte-like cell lines (IDG-SW3 and MLO-Y4) indicated changes in gene expression involving the hedgehog signalling pathway and a desensitisation to the vitamin D3 hormone (St John, Bishop et al. 2014) and a role in vitamin K in promoting differentiation (Atkins, Welldon et al. 2009).

The mechanism by which osteocytes become entrapped in the matrix is also unknown, although several authors (Franz-Odendaal, Hall et al. 2006) suggested a progressive embedding mechanism in which a population of osteoblasts on the surface of bone slow down the production of matrix relative to adjacent cells, which become buried in the matrix (Dallas and Bonewald 2010). Although some authors consider this event a passive matrix embedding process (Nefussi, Sautier et al. 1991), other researchers believe this is an active and invasive process that requires matrix degradation and cleavage of collagen under the action of MT1-MMP for the formation of lacunar and canalicular structures and maintenance of an osteocytic phenotype, as mice deficient for this metalloproteinase develop osteocytes without processes and which are unable to degrade collagen (Holmbeck, Bianco et al. 2005). Moreover, mice resistant to collagen I degradation show osteocytic and osteoblastic death and an increase in bone mass in a similar way caused by PTH in wild type mice (Zhao, Byrne et al. 2000).

Osteoid osteocytes actively produce and calcify their matrix (Bonewald 2013) and shrink in size by 30% from the osteoblastic phase during the formation of projections and by 70% when they have become fully mature (Bonewald 2013).

Their characteristic genetic markers have been identified rather recently, with low alkaline phosphatase (ALP) expression, high CD44 linked to E11 (Hughes, Salter et al. 1994), E11/GP38/Podoplanin involved in early embedding and dendrite formation and increases with mechanical load (Zhang, Barragan-Adjemian et al. 2006); dentin matrix protein 1 (DMP 1) (Toyosawa, Shintani et al. 2001) and phosphate-regulating neutral endopeptidase on chromosome X (PHEX) (Westbroek, De Rooij et al. 2002, Plotkin and Bellido 2016), expressed in both early and late osteocytes, and support phosphate metabolism and mineralisation; elevated FGF23 in early and mature osteocytes induces hypophosphatemia (Bonewald and Wacker 2013); and sclerostin (SOST) and ORP150, expressed in mature osteocytes inhibit bone formation and protect from hypoxia, respectively (Poole, van Bezooijen et al. 2005, Guo, Keightley et al. 2010).

1.7.2 OSTEOCYTE CONTROL OF BONE REMODELLING

The mature skeleton of mammals, although appearing mechanically inert, is continuously maintained through the well-synchronised activity of osteoblasts and osteoclasts, termed *remodelling units* and with the input of the mature bone cells, osteocytes. These processes are temporally and spatially coupled and so when dysregulation in these functions take place, abnormal changes in bone mass take place.

In the adult skeleton, bone remodelling takes place at the surface of both the periosteum and endosteum (the thin connective tissue lining of the internal part of bones). The mass of forming bone is maintained constant, an indication that the rates of bone production and removal are approximately equal. However, there are regional differences, for example in the femur, where the distal part is remodelled every 5-6 months, whereas the shaft is processed much less frequently (Marieb and Hoehn 2010).

Evidence has accumulated over the past years which indicated that osteocytes play a major role in bone deposition and resorption. Growth medium from the osteocytic line MLO-Y4 can promote proliferation of MSCs and increase the expression of ALP and OC (Heino, Hentunen et al. 2004) as well as inhibiting resorption by osteoclasts (Heino, Hentunen et al. 2002). Moreover, these cells are able to support osteoclast formation in the absence of any exogenous osteotropic factors and express RANKL on their surface (Zhao, Zhang et al. 2002). The viability of osteocytes is necessary to prevent the loss of bone mass, as shown in a study in mice where osteocyte necrosis was induced by DMP1-directed diphtheria infection, causing osteoclast activation, osteoporosis-like effects and a decrease in mechanotransduction, indicating that the osteocyte control of osteoblasts and osteoclasts is mechanically-induced (Tatsumi, Ishii et al. 2007), something that will be discussed in section *1.7.3 - Mechanotransduction*.

1.8 TRANSLATION OF MECHANICAL FORCES

1.8.1 THE LOWER LIMBS: THE FEMURS

The lower limbs of most species, highlighted in Figure 1.2, are subjected to exceptional forces during locomotion. In humans, they support the weight of the erect body and as such, are much thicker and stronger compared to upper limb bones.

Femoral bones are the single bones comprising the upper parts of the leg in most species of vertebrates. In humans, femurs are the largest, strongest and longest bones in the skeletal system. They are able to resist significant loading stress during intense exercise, reaching up to 280 kg/cm^2. Lengthwise, they average approximately 25% of a person's height (Marieb and Hoehn 2010).

From an anatomical perspective, femurs articulate with the hip bones proximally and continue medially towards the knee. As mentioned at the start of this chapter, this design allows the knee joints to be closer to the body's centre of gravity and as such, the body is better balanced during upright positions. Gender differences exist in the medial course of the femoral bones, this geometry being more pronounced in females due to their wider pelvic area (arch is approximately 30 degrees broader), and this is believed to contribute to a greater incidence in knee problems, particularly in female athletes (Boling, Padua et al. 2010).

As discussed in previous chapters, the force of gravity and muscle pull on the bones represent two stressors which influence bone formation. According to Wolff's law, which was developed by German anatomist and surgeon Julius Wolff in the 19th century, the response of bones to mechanical stress is proportional to the load placed on them and as such, the anatomy of bones directly influences local changes (Wolff, Maquet et al.

1986). This is particularly obvious with the femoral bones, as body weight transmitted to the femoral head bends the bone on one side, causing great compression. The internal trabecular structure functions as an arch, which transfers the compressive load to the femoral shaft (Rudman, Aspden et al. 2006). For this reason, bones are thickest centrally (mid-diaphysis), where compression and tension stresses are the greatest. Compression and tensile forces cancel each other out towards the centre of the bone (Figure 1.12) and hence the stress is minimal internally. Because less bone material is needed, the central portion of bones is hollow and filled with spongy bone to minimise mass (Marieb and Hoehn 2010).

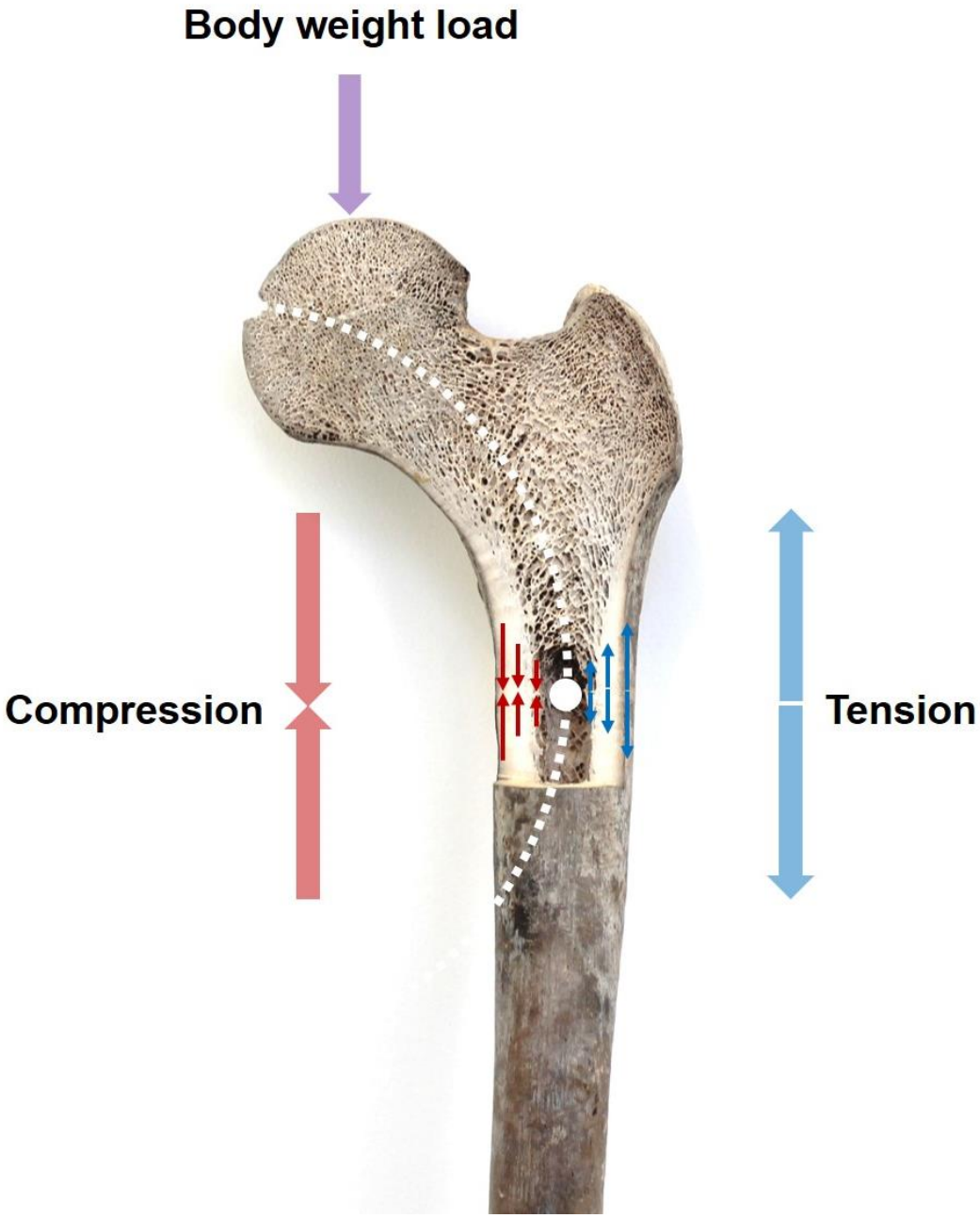

Figure 1.12 | Bending stress in femoral bones is distributed according to anatomical design. The weight of the upper body is transmitted to the femoral head, articulated to the hip. These compression (bending) forces act primarily along the dotted line, creating tensile (stretching) forces on one side (blue arrows) and compression on the other side (red arrows). These forces cancel each other internally, with very little stress being experienced in this region (white dot). Schematic inspired from (Marieb and Hoehn 2010). *Original image. Image of the femoral section acquired from a skeletal specimen at the Natural History Museum, South Kensington, London.*

1.8.2 THE UPPER LIMBS

The set of observations described by Wolff centuries ago are particularly noticeable in handedness (strong right or left-handed individuals) and in sport players who undertake vigorous exercise (Ireland, Degens et al. 2015), who show differences in bone thickness in the dominant arm. For example, in tennis players, the serving arm bones become thicker and show a higher bone mineral content (BMC) (Figure 1.13) (Bass, Saxon et al. 2002, Ireland, Maden-Wilkinson et al. 2013, Ireland, Maden-Wilkinson et al. 2014). Humeral bone cross sectional areas (CSA) have been reported to expand up to 23 ± 12 % (Ireland, Maden-Wilkinson et al. 2014) and this enlargement appears to be a cortical one as opposed to a medullary one (Kontulainen, Sievänen et al. 2003), with cortical areas reported to expand as much as 7-11% (Bass, Saxon et al. 2002) particularly in the distal portions compered to central areas. Multiple tomographic and MRI studies indicated that these differences persist in long-term and take place in a similar fashion irrespective of gender (Bass, Saxon et al. 2002), age (Ireland, Maden-Wilkinson et al. 2014) or starting age (Ireland, Maden-Wilkinson et al. 2014).

As described in sections 1.1.2 and 1.6.3, this type of increase in bone density and volume takes place in other species as well during re-adaptation to a higher-loading regime, but can also happen pathologically, in autosomal dominant and recessive conditions known as osteosclerosis and osteopetrosis, also known as ‘marble bone disease’ (Huang and Ogawa 2010).

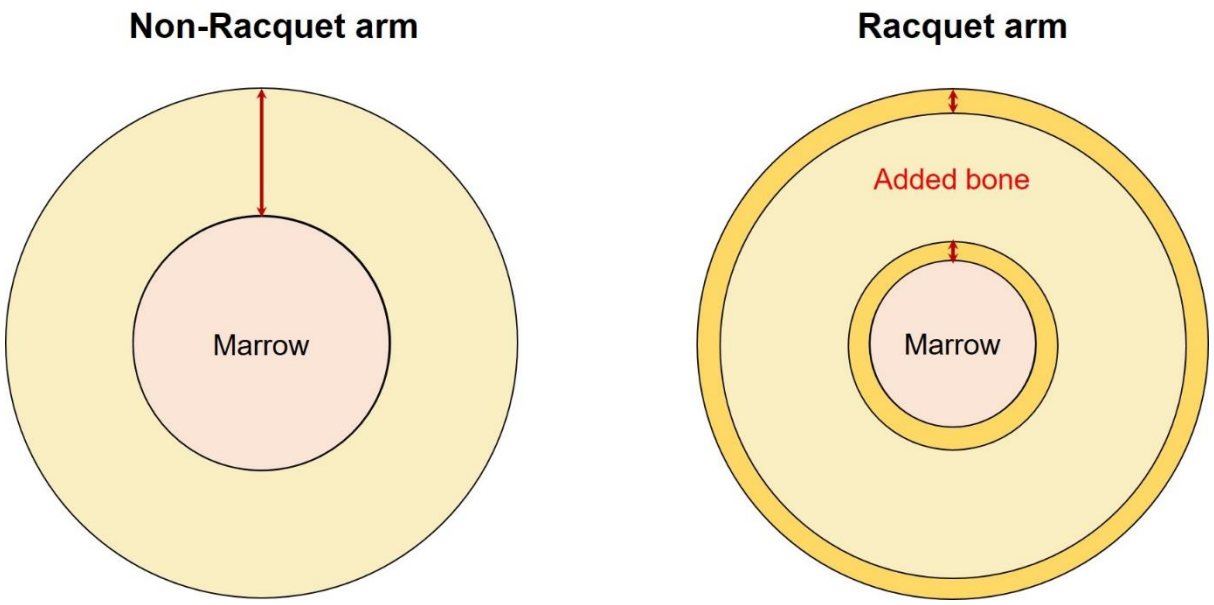

Figure 1.13 | Adaptation of dominant hand to increased loading forces. Cross-sectional differences in the arms of tennis players following prolonged periods of intense exercise. Bones of the racquet arm increase in strength and rigidity and the effect is more pronounced in players who started this type of exercise early in life. Diagram is based on CT/MRI cross-sectional appearance of arm bones and inspired by (Marieb and Hoehn 2010).

1.8.3 MECHANOTRANSDUCTION

Mechanical strain is required for the formation of post-natal bone, but not the pre-natal skeleton. Bone mass depends on peak applied strain (Rubin 1984) and studies in rats showed that the rate of new bone formation is related to the frequency of loading (Robling, Hinant et al. 2002). However, a loading regime containing rest intervals is more beneficial for increasing bone formation and strength is maximised if the applied loading forces are shorter and more frequent (Robling, Hinant et al. 2002).

The mechanism by which these mechanical signals are received and interpreted by cells are still a subject of great debate, although it is widely accepted that a process of sensory transduction is involved, which converts mechanical signals into electro-chemical information and directs remodelling. Moreover, the amplitude of electrical potentials as a result of stress is related to the frequency and scale of bony deformation, while polarity is determined by the direction of bending (Bassett and Becker 1962). In the 1960s, Bassett and colleagues performed a series of experiments on excised and *in vivo* bones and determined that the areas which underwent compression developed negative potentials with respect to other regions. As a result of different charges observed in tensed areas, it is believed that these electrical impulses control the process of remodelling (Marieb and Hoehn 2010) and this is the basis for many electromagnetic therapies designed to accelerate bone repair and fracture healing, representing a 500 million $ market in the US (Mollon, da Silva et al. 2008).

The same group proposed that collagenous matrix-inorganic crystal piezoelectricity was a mechanism through which osteocytic and osteoblastic cells perceive loading forces and areas of greater stress (Bassett and Becker 1962, Ahn and Grodzinsky 2009) and was based on the principle that applied mechanical deformation on femoral bones (and

the apatite-collagen junctions) creates local gradients in electric potential. They proposed that these electrical signals propagate along the collagen fibres and thus provide an osteogenic stimulus locally by affecting differential cellular responses and changing the orientation of the newly forming collagen, ultimately allowing the bone to withstand the greater forces experienced. Interestingly, these effects were absent when the inorganic component of bones was removed (Bassett and Becker 1962, Bassett, Pawluk et al. 1964).

This theory was later substituted by other theories, such as streaming potential and fluid-generated shear stress (Bonewald 2006, Wittkowske, Reilly et al. 2016).

Theoretical and in vitro models show that the flow of bone fluid is dependent upon extravascular pressure and applied cyclic loading of osteocytes (Weinbaum, Cowin et al. 1994). The forces that bones are subjected to during walking or standing cause fluid flow via canaliculi connecting osteocytes, which create waves of shear stress and deform the cell membranes and cilia (flagellar-like structures extending from the body to the ECM) (Malone, Anderson et al. 2007, Temiyasathit and Jacobs 2010). These stresses on *in vivo* membranes have been estimated to be range from 8-30 dynes/cm^3 (Weinbaum, Cowin et al. 1994) and in vitro they have been estimated to be around 5 Pa (Price, Zhou et al. 2011, Bonewald 2013). Indeed, more recent evidence has confirmed the link between osteocyte response to compressive mechanical forces and control of both osteoclasts and bone surface cells (osteoblasts and bone lining cells), to which they are connected through processes containing gap junctions, most importantly Cx43. They are able to communicate with these cells either directly, through these channels, or by releasing short-distance metabolites such as prostaglandin PGE_2, ATP and nitric oxide

into the extracellular fluid (Palazzini, Palumbo et al. 1998, Kamioka, Ishihara et al. 2007, Schaffler, Cheung et al. 2014, Takano-Yamamoto 2014).

1.9 BONE FRACTURE REPAIR

The process of skeletal regeneration is essential to maintain the quality and functionality of bones. There has been a great amount of research involved in understanding bone repair following injury, in both human subjects and animal models, in order to develop more efficient measures to accelerate healing, prevent fracture non-union and many other bone complications.

The final purpose of all developmental events is the formation of a tissue which can provide an adequate morphological structure that can allow it to carry out the physiological function it is designed for. In the case of fracture healing, the regeneration process initiated following injury requires a complex set of processes meant to re-establish not only the initial geometry but also the biomechanical capabilities of the damaged structure (Gerstenfeld, Cullinane et al. 2003).

1.9.1 CELLULAR EVENTS

The bone healing process involves different cell types, including inflammatory cells, osteoprogenitor, chondrocytes and pre-chondrocytes, osteoblasts and osteoclasts.

The healing process is common across different vertebrate groups, but takes place more rapidly in small rodents such as mice and rats (Zuscik 2013). In all cases, the process involves a combination of intramembranous and endochondral ossification (Figure 1.14) (Gerstenfeld, Cullinane et al. 2003, Marsell and Einhorn 2011, Einhorn and Gerstenfeld 2015).

The initial mechanical trauma results in bleeding and the formation of a haematoma, which surrounds the fracture site. Several cytokines are involved in the process,

including tumour necrosis factor-α (TNF-α) and interleukins (IL) IL1, IL6, IL11 and IL18 which control the initiation and modulation of the immune response (Gerstenfeld, Cullinane et al. 2003).

These cytokines are believed to be involved in the generation of secondary responses involving recruitment of mesenchymal stromal cells, which may derive from the marrow space adjacent to the damaged cortical bone (Matsumoto, Mifune et al. 2008, Ueno, Uchida et al. 2011), the surrounding muscular tissue (Glass, Chan et al. 2011, Henrotin 2011), the periosteum (Zhang, Naik A Fau - Xie et al. 2005, Ushiku, Adams et al. 2010) and the systemic circulation (Granero-Moltó, Weis et al. 2009).

1.9.2 THE ROLE OF PERIOSTEAL CELLS IN FRACTURE REPAIR

The primary source of cells that enters the callus is the periosteal population of cells from the cambium layer, which has the ability to differentiate into both chondrocytes and osteoblasts (Fang and Hall 1996, Li, Amizuka et al. 2004). Intramembranous bone formation always takes place close to the bone fracture ends (Figure 1.14d), where vasculature is preserved, whereas the site furthest away from the fracture, where oxygen tension is the lowest due to disrupted blood supply, takes place via an endochondral route, consistent with what is seen during bone formation (Mackie, Ahmed et al. 2008, Zuscik 2013). Cells closest to the fracture site differentiate into osteoblasts, which secrete collagenous matrix and lay down mineral without a cartilage intermediate. The most central cells give rise to cartilage and recapitulate several stages of chondrocyte maturation in the growth plate (Claes, Recknagel et al. 2012). The forming calcified cartilage turns into a template for the new bone formation and terminally differentiated chondrocytes contribute to the mineralisation of the tissue

(Gerstenfeld, Cullinane et al. 2003). Ultimately, they undergo apoptosis and a process of osteoclast-mediated resorption takes place under the action of M-CSF, RANKL and osteoprotegerin (OPG) (Kon, Cho et al. 2001).

The mechanical properties of the forming bone depend on the stability of the fracture, with stabilised fractures showing little evidence for cartilage, whereas non-stabilised fractures produce high amounts of cartilage (Thompson, Miclau et al. 2002).

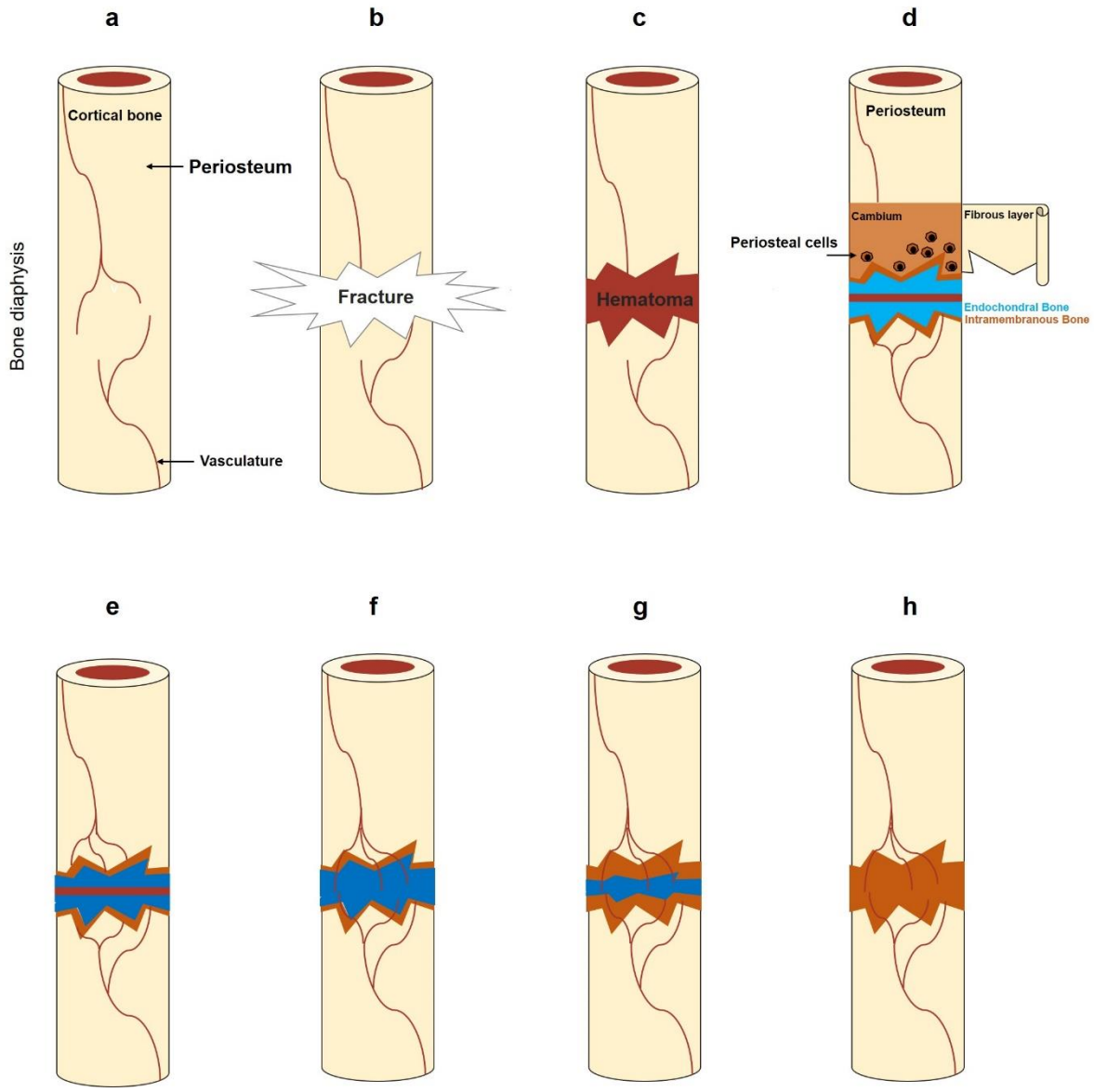

Figure 1.14 | Schematic of the tissue morphogenesis during fracture repair. a, The outside layer of long bones (periosteum) is a well-vascularised tissue. **b**, Trauma during fracture disrupts the blood supply at the site, which leads to the formation of a blood clot, also known as hematoma (**c**). Periosteal cells located inside the deeper, cambium layer, migrate to the site of injury (**d**) where they differentiate into osteoblasts and give rise to intramembranous bone close to the bony ends, where blood supply is still active. The central portion of the hematoma is replaced with endochondral bone, which allows central cells, furthest to the blood supply, to survive the hypoxic conditions. Cartilage formation continues (**e**) and blood vessels invade this structure until the initial hematoma is completely replaced (**f**). Following maturation, the cartilage template becomes progressively replaced with intramembranous bone (**g-h**), which is ultimately conversed under the action of osteoblasts and osteoclasts into lamellar bone and the initial geometric shape and function of the fractured bone is restored.

1.10 THE EFFECT OF UNLOADING ON BONES

The microgravity environment in Space is an excellent model to study the effect of the absence of gravitational forces and muscle pull on the bones. Space exploration during the past 50 years has provided valuable clues into the pathological effects of prolonged periods of unloading on the skeletal system. These consequences are profound and are characterised by a marked bone loss and increased bone resorption, similar to clinical conditions such as osteoporosis, and are accompanied by hypercalcemia and hypercalciuria (Lau and Guo 2011).

These physiological changes, aimed to adapt the skeletal system to the new loading regime, constitute a major barrier for potential interplanetary travel. This is because the major motivation behind sending human crews in planetary explorations compared to robotic probes is their potential to perform complex physical tasks and choose research spots, as well as to handle complex research tools. However, the environment on planets such as Mars is far more challenging than on Earth, requiring a good skeletal health. Whilst the gravity of Mars is approximately one third of that of Earth's, thus providing some degree of loading, the landscape contains geographical structures such as canyons and mountains which are far wider and higher. This would require a potential crew to be of superior physical fitness in order to perform such strenuous exercise (Buckey 2006, Barratt and Pool 2008).

Whilst the technology to return to the Moon and for a journey to Mars has been available for some time, the level of bone loss during such long, strategic missions is still being investigated, as it is directly proportional to the time spent in microgravity. Although the journey to Mars would only last approximately 6 months, to allow for the return journey, astronauts would have to wait for another period of planetary

alignment that would allow for a low-energy transfer between the two planets. This would imply a further 1-1.5 years spent on the planetary surface, and therefore a total journey time of approximately 3 years (Buckey 2006, Clément 2007). The severe bone loss during that period could lead to increased susceptibility to contraction damage and therefore potentially compromise the success of the mission. It could also make the bones too weak to withstand the intense re-entry forces and re-exposure to the Earth gravity, which could potentially have fatal consequences.

1.10.1 THE 'ACCELERATED AGING' EFFECT OF BONE UNLOADING

In space, very little muscular force is required to initiate movement, which is accomplished mainly with the help of the upper part of the body and limbs and for this reason, the muscles and bones of the upper part are less affected than the ones in the hip and legs, which do not receive the powerful muscle contractions that are usually required on Earth during walking or standing and these are mainly used for stability (Clément 2007). Similar effects can be observed on Earth in the elderly and in conditions such as primary and secondary osteoporosis (Lau and Guo 2011), as well as in paraplegic patients following injury of the CNS or peripheral nerves, in disuse osteoporosis (Houde, Schulz et al. 1995, del Puente, Pappone et al. 1996, Demirbag, Ozdemir et al. 2005).

Studies have reported that on average, astronauts lose between 1-1.6% of bone mass per month (Surhone, Timpledon et al. 2010). The most affected bones are those of the vertebra, pelvis and the femoral neck and trochanter, which are essential in counteracting and distributing the force of gravity.

The monthly losses in proximal femur per month are very similar to the yearly bone loss in post-menopausal osteoporotic women (Cavanagh, Licata et al. 2005, Lane 2006).

Initial studies on the MIR space station showed that the rate of bone loss following 6 month missions can reach 4.5% in trabecular bone and 2.94% in cortical bone in the tibia, whereas slight increases in the bones of the arm (radius) were recorded, with a 0.2% increase in trabecular bone and 0.51% increase in cancellous bone (Collet, Uebelhart et al. 1997). Studies by Lang and colleagues (Lang, LeBlanc et al. 2004) showed that the spinal volumetric bone mineral density (vBMD) was reduced at an average rate of 0.9% and 0.7% in trabecular and cortical bone, respectively, during 4-6 months of spaceflight, whereas the hip integral, cortical and trabecular bone density was lost at a rate of 1.2-1.5%/month, 0.4-0.5%/month and 2.2-2.7%/month respectively.

In all studies, bigger losses appear to happen in cancellous bone as opposed to cortical bone, which is a feature also seen in type I (postmenopausal) osteoporosis (Iwamoto, Takeda et al. 2005, Finkelstein, Brockwell et al. 2008).

Calcium supplementation does not affect bone homeostasis, but decreases the abnormally high serum levels (Iwamoto, Takeda et al. 2005). As such, a regime of exercise and frequent loading is performed in microgravity in order to slow down the rate of bone loss (Cavanagh, Licata et al. 2005).

When prolonged bed-rest studies (33 weeks) were performed on healthy individuals, a decrease in bone mineral content ranging between 25% and 44.5% were reported (Donaldson, Hulley et al. 1970).

In simulated microgravity using ground-based rodent models, where hind-limb unloading using tail suspension was used, a preferential decrease in periosteal bone

mineral mass following 90 days of unloading was reported (LeBlanc, Marsh et al. 1985, Sessions, Halloran et al. 1989).

1.10.2 THE EFFECT OF UNLOADING ON BONE CELLS

The weightlessness experienced by bones in space leads to structural and molecular changes meant to stabilise the body to the reduced loading introduced by the micro-G environment. Observations from both spaceflight studies and ground-based analogues have provided significant amounts of evidence on the cellular processes underlying the significant bone loss.

In C5BL/6J mice which were flown for 15 days on the International Space Station, dramatic losses in pelvic bone mass were observed. These changes have been found to occur due to an increase in osteoclast-mediated bone resorption, but also due to a process of osteocytic osteolysis, as well as a cell cycle arrest in osteoblasts. (Vico, Hinsenkamp et al. 2001, Tamma, Colaianni et al. 2009, Blaber, Dvorochkin et al. 2013).

The decrease in bone forming capacity as well as the increased bone breakdown and decrease in osteocytic ability to modulate these processes, resulted in major imbalances in bone tissue formation during unloading.

Recent work from Nabavi and colleagues (Nabavi, Khandani et al. 2011) showed a decrease in cellular integrity in space flown osteoblasts, with fragmented or condensed nuclei, shorter and wavier microtubules, fewer focal adhesions, thinner cortical actin and a high number of stress fibres. These effects on the nucleus and cytoskeleton had been previously observed in space-flown MC3T3-E1 osteoblasts, but a reduced growth activation and glucose consumption were also observed (Hughes-Fulford and Lewis 1996).

1.11 PATHOLOGICAL BONE FORMATION

As described in the sections above, bone is a tissue that has evolved to counteract the changing mechanical and environmental conditions. Different pathways controlled by an accurately synchronised control system allow the deposition and resorption of mineralised tissue to meet the physiological demands. However, maladaptive ectopic ossification can occur in bone and other types of tissues in response to altered genetic expression, injury or extreme mechanical insult. This process is known as heterotopic ossification (HO) and is best defined as an ectopic bone formation in bone and extra-skeletal soft tissues that would not calcify under normal physiological circumstances (Isaacson, Brown et al. , Isaacson, Stinstra et al. 2010). The underlying manifestations vary greatly in every condition and as such the underlying causes are still a subject of debate. *Section 1.6 Cellular and Cytopathological events in bone formation* provided an introduction to the cellular mechanisms underlying the major pathways in bone formation and the clinical consequences that take place following dysregulation of these mechanisms. This section aims to demonstrate the complexity of heterotopic bone formation by providing representative examples of the clinical appearance of these ossifications.

1.11.1 ABNORMAL BONE CONDITIONS

Pathological ossification is a rather frequently encountered condition, which can occur at specific and/or multiple sites in the body, including the subcutaneous tissue, tendons and ligaments, skeletal muscle and the periarticular regions or can extend from bones into the surrounding tissues (Isaacson, Stinstra et al. 2010).

Heterotopic bone can develop in various clinical contexts, most noticeably in genetic, post-traumatic and post-surgical circumstances. Interestingly, it is frequently encountered in individuals who have experienced traumatic brain injury (TBI) or spinal cord injury (SCI) (Cipriano, Pill et al. 2009, Sullivan, Torres et al. 2013). These forms of neurologic injury are typically followed by bone formation in multiple sites, highlighting a strong neurogenic component of the disease (McCarthy and Sundaram 2005, Vanden Bossche and Vanderstraeten 2005). When heterotopic ossification is triggered by neurogenic causes, the most common sites for bone formation are the periarticular sites, mostly affecting the joints of the hip, shoulder and elbow. It appears that ankylosing of the knee area rarely occurs following head injury, but it is the second most common place for HO formation following trauma to the spinal cord (Pape, Lehmann et al. 2001).

The most common site for post-surgical HO formation is the pelvic bone following open-reduction internal fixation surgery for fractures of the acetabulum. The hip is the second most affected area following total hip arthroplasty (THA) (Ahrengart 1991). Figure 1.18 provides a similar example of ectopic bone formation in the acetabulum and surrounding area, as a result of osteoarthritis.

Orthopaedic procedures of the knee, shoulders and elbows can also sometimes result in ectopic bone formation in the surrounding areas (Baird and Kang 2009).

The incidence of HO following surgical interventions like hip arthroplasty ranges between 16-53%, although it is reported that only a rather small number of patients (3-7%) develop clinically significant manifestations. In contrast, the incidence of HO following neurologic trauma has been reported to be as high as 10-30% (Baird and Kang 2009).

The ossification of soft tissues can also be encountered in degenerative conditions such as atherosclerosis, forming along vascular smooth muscle cells, as a secondary effect to other conditions such as diabetes and chronic kidney disease (CKD) (Hayden, Tyagi et al. 2005). It also occurs in other conditions known as *chondrocalcinosis* (Caswell, Guilland-Cumming et al. 1983) forming in hyaline and/or fibrocartilage; in *scoliosis* (Mullaji, Upadhyay et al. 1994, Murphy and Mooney 2016) (Figure 1.15), and *ankylosing spondylitis* (McVeigh and Cairns 2006) (Figure 1.16) where it forms in intervertebral disks and in the sacroiliac joint, in *diffuse idiopathic skeletal hyperostosis*, (Atzeni, Sarzi-Puttini et al. , Nascimento, Gatto et al. 2014) forming along the anterior longitudinal ligament of the spine; in as well as in osteogenic osteosarcomas of the femurs and tibias (Kumar, Barwar et al. 2014, Pan, Chan et al. 2014) (Figure 1.19).

The ossification of soft tissues is a severely debilitating process. The damage associated with its formation in regions such as joints, major arteries and muscles can cause considerable loss of function, with additional manifestations including pain, stiffness and immobility and in some cases premature death (Balboni, Gobezie et al. 2006).

The following sections will provide examples of the clinical manifestations in some of the most severe conditions.

1.11.2 OSSIFICATION OF THE SPINE

Ossification of the spine can occur in various conditions, including scoliosis, ankylosing spondylitis and due to trauma associated with vertebral fracture; and the underlying causes are still poorly understood. Figures 1.15-1.17 present examples of clinical manifestations of these conditions.

Both scoliosis and ankylosing spondylitis (AS) are characterised by a significant transformation of the vertebral disks and in the case of AS, the surrounding ligaments as well into mature bone (Figures 1.15 and 1.16, respectively). In both cases these ectopic ossifications cause severe disability due to deformations of the spine and the attached structures, such as ribs, diminishing the thoracic capacity and causing immobilisation (Figure 1.15 a-c). Interestingly, longitudinal sections through an ankylosed spine (presented in Figure 1.16e) reveal that the new formation of bone connecting the vertebral bodies is mainly composed of trabecular bone, with compact bone surrounding the outer edges of the vertebral discs, as encountered in long bones.

The underlying causes of both AS and scoliosis are still unknown. It is believed that a combination of genetic and environmental factors are involved. Exome sequencing has recently identified a missense variant in the *HSPG2* gene in scoliosis, coding for the heparan sulphate proteoglycan 2 (perlecan), a ubiquitous multifunctional ECM protein (Baschal, Wethey et al. 2014). Buchan and colleagues have recently demonstrated using the same technique that variations in the fibrillin-1 and 2 genes (FBN1 and FBN2) are most commonly associated with adolescent scoliosis (Buchan, Alvarado et al. 2014). In ankylosing spondylitis, several abnormal gene variants have been recently found, including *ERAP1*, *HLA-B27*, *RUNX3* and *ILI213* (Evans, Spencer et al. 2011).

Figure 1.17 presents an example of heterotopic bone forming as a result of fracture and vertebral dislocation in the lumbar area (a), with a major bone growth extending across the vertebra. Similarly, in secondary osteosarcoma of the spine (b-c), a mass of imperfectly ossified bone can be observed on the surface of the vertebral bodies and under the periosteum, again supporting the role of this structure in heterotopic bone formations. The mechanisms of ectopic bone formation following trauma will be discussed later in this chapter.

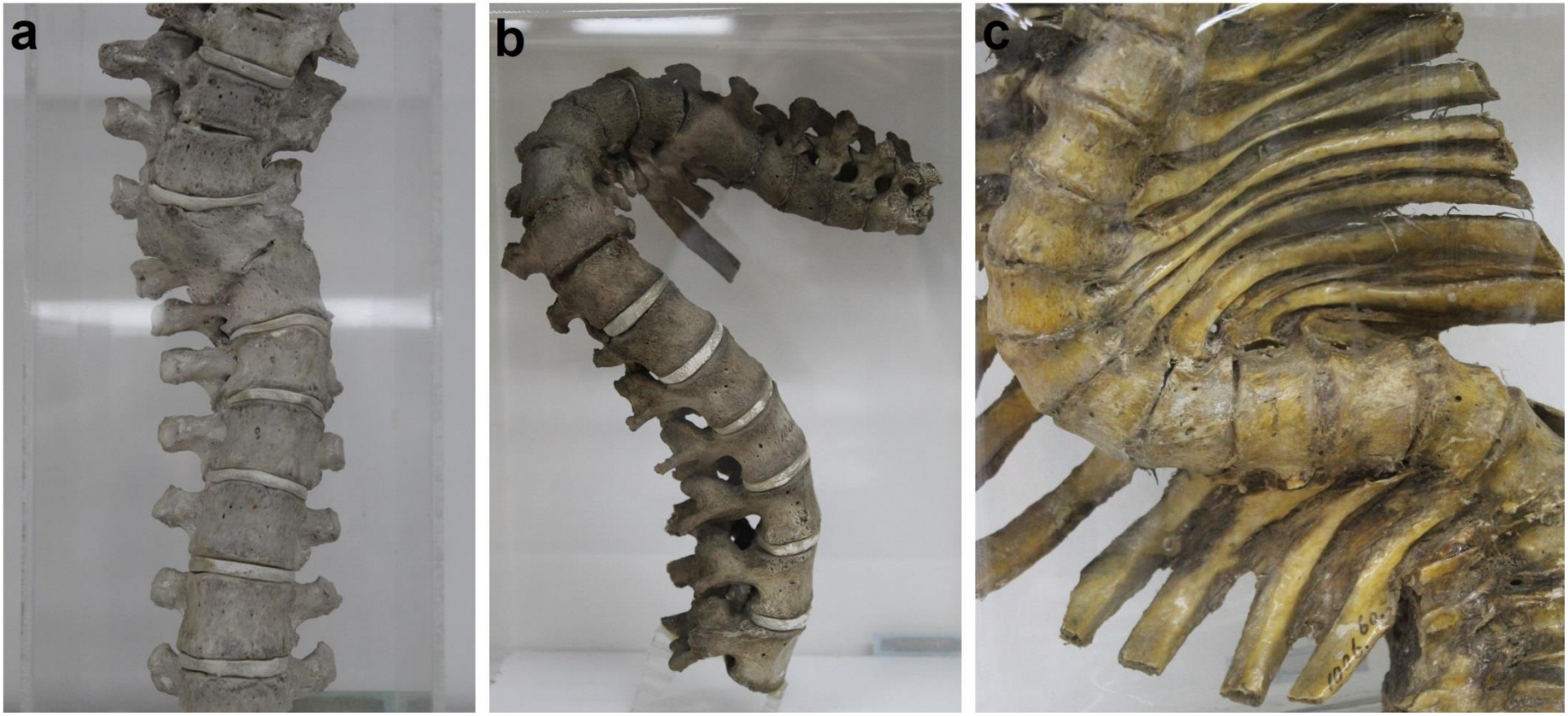

Figure 1.15 | Spinal fusion in Scoliosis. a, A spinal section from a patient with this condition, containing 2 cervical and 10 dorsal vertebrae. The bodies of the 3rd, 4th and 5th vertebra fused as a result of vertebral disk ossification and formed a bone mass, which created a typical S-shaped deformation in the upper dorsal region. At this stage of the disease, there appears to be no alteration in the vertebra located below and above. **b,** A more advanced case of scoliosis where the curvature and deformation caused a significant rotation of the vertebral bodies, which affected the thoracic greatly by reducing its size on the right side. The 4th-11th dorsal vertebra are ankylosed and fused together by a bony mass. **c**, an advanced case of scoliosis, showing multiple curvatures. The first one is caused by the fusion of the upper vertebra, causing a convex curvature to the right, and a fusion of the lower dorsal and lumbar vertebra, which causes a convex curvature to the left. These ectopic bone formations caused the vertebral bodies in the thoracic region to rotate significantly, causing a rib movement towards the back at the junction with vertebral bodies and got carried forward at the other end. As a result, the ribs became crowded together and their shafts became ossified and fused. *Original images. Author would like to thank King's College London.*

Figure 1.16 | Ossification of the spine and the sacro-iliac joint in Ankylosing Spondylitis. a, A section of the spine of a patient with this condition, showing significant ankylosing of 6 cervical and the first dorsal vertebrae, which are firmly united on the anterior side due to ossification of the anterior common ligament; **b**, A specimen containing 4 dorsal vertebrae, which show an advanced degree ossification and ankylosis. The ligaments surrounding the vertebrae have become converted into compact bone, causing the joint cavities to become narrow and fixing them in place, causing immobility. The inter-spinous ligaments are also ossified, and fused to the transverse processes of the vertebra. **c**, This specimen from the lower part of the spine shows osteo-arthritis of the lumbar spine by spondylitis. The 3 lumbar vertebra show prominent osteophytic outgrowths emerging from the margins of the cell bodies, restricting movement, but they do not show signs of ankylosis. The intervertebral space has become narrower due to a partial collapse of the vertebral bodies; **d**, In contrast, this specimen, containing the last 3 lumbar vertebra as well as portions of the sacrum and ilia shows ankylosis caused by ossification of the ligaments connecting the vertebra of the lumbar and sacrum regions. In addition, the sacro-iliac joints are also partially ossified and ankylosed, showing a high degree of osteophytosis and disk space damage; **e**, a spine from a patient with advanced ankylosis. The specimen has been cut longitudinally, showing a striking, complete replacement of all intervertebral disks by trabecular bone, making it very difficult to distinguish between the original bone structure and the newly formed bone, which appear to be continuous with each other. Laterally, the vertebra and disk spaces are surrounded by compact bone, which has formed in the outer part surrounding the trabecular bone and highlights the complexity of the pathological bone formation. *Original images.*

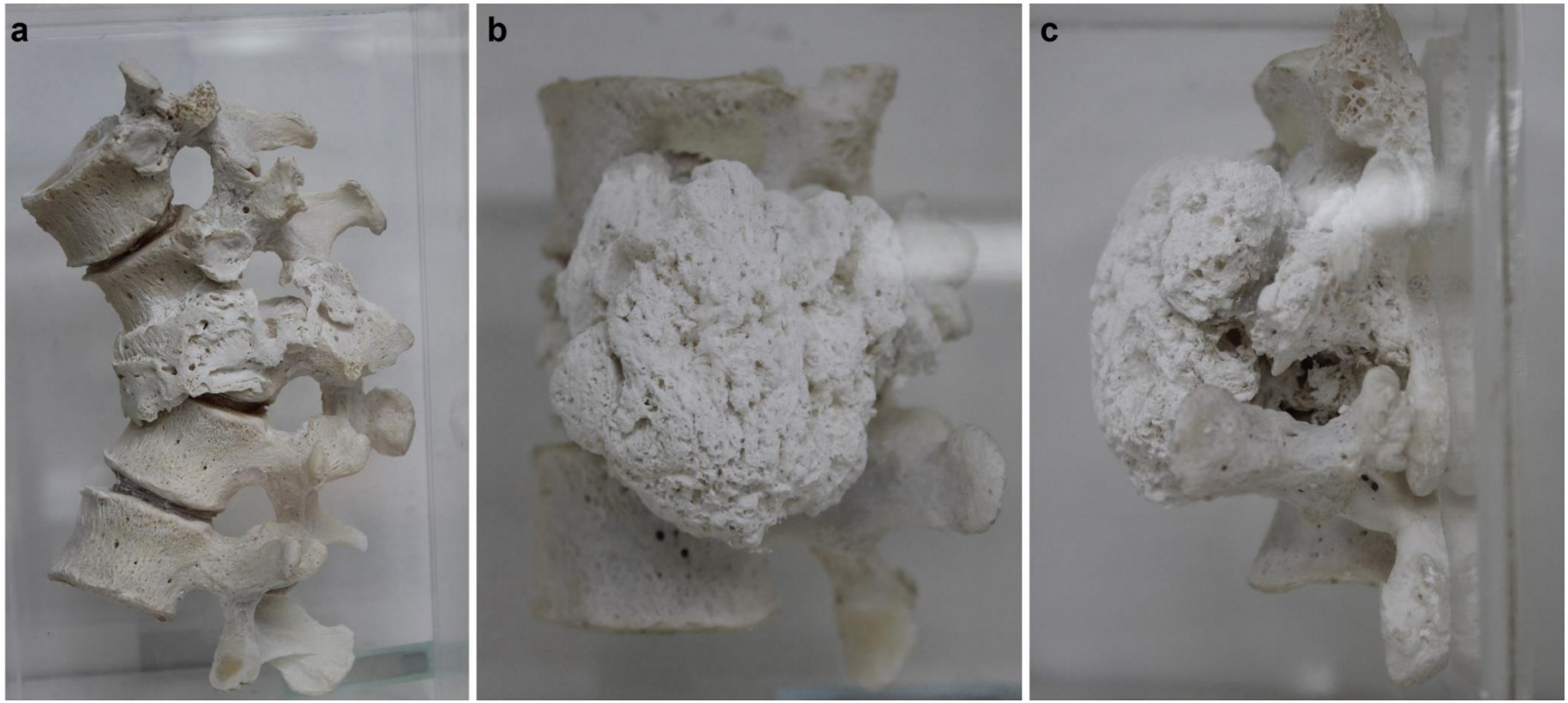

Figure 1.17 | Ectopic bone formation following spinal fractures and osteosarcoma. a, Portion of a spine that underwent trauma causing dislocation of the dorso-lumbar region. A mass of new bone emerges from and connects the last 2 dorsal and first 3 lumbar vertebra. **b-c**, A similar bone formation takes place in secondary sarcoma, in this specimen from the lumbar region showing a mass of imperfectly ossified growth which has been deposited on the surface of the vertebral body under the periosteum. *Original images.*

1.11.3 CONDITIONS WITH ABNORMAL BONE MASS DEPOSITION

Several metabolic and cancerous disorders lead to abnormal ossification, characterised by a diminished or enhanced bone deposition. These include conditions such as Rickets, Paget's disease, osteoarthritis, osteosarcomas, osteomyelitis and malunions of fractures. Figures 1.18-1.22 demonstrate the clinical manifestations of these conditions.

Figure 1.18 presents an example of the hip and proximal femurs where ectopic bone has arisen around the femoral heads and inside the acetabulum as a result of osteoarthritis, massively impairing the hip joints. The underlying causes of this condition are still unknown (Koczy, Stoltny et al. 2009). As that junction is biomechanically essential for transferring the upper body weight to the lower limbs, movement is significantly impaired.

Figure 1.18 | Ectopic ossification of the hip joints in osteoarthritis. Femoral bone heads and hip joints show ossification as a result of osteoarthritis. The femoral heads show thick, osteophytic collars and further ossification can be seen at the point of attachment, where the *ligamentum teres* is located. The acetabulum appeared re-modelled by osteophytic bony outgrowths, causing abnormal grooves in which the abnormal femoral heads fit. *Original images.*

Osteosarcomas of the upper and lower limb bones are the most common primary osseous malignancies (Kundu 2014) characterised by a significant deposition of mature bone, which emerges from the bone shafts and extends into the surrounding tissues (Figure 1.19). These bone masses can manifest as compact, dense bone (a), a mixture of trabecular and compact (b-c) or trabecular bone (d).

Although the causes of these malignancies are still unknown, it is thought that point mutations affecting tumour suppressor genes such as p53 or retinoblastoma susceptibility gene (Rb) play a major role in the formation of the osteosarcomas (Miller, Aslo et al. 1996, Kong and Hansen 2009, Martin, Squire et al. 2012).

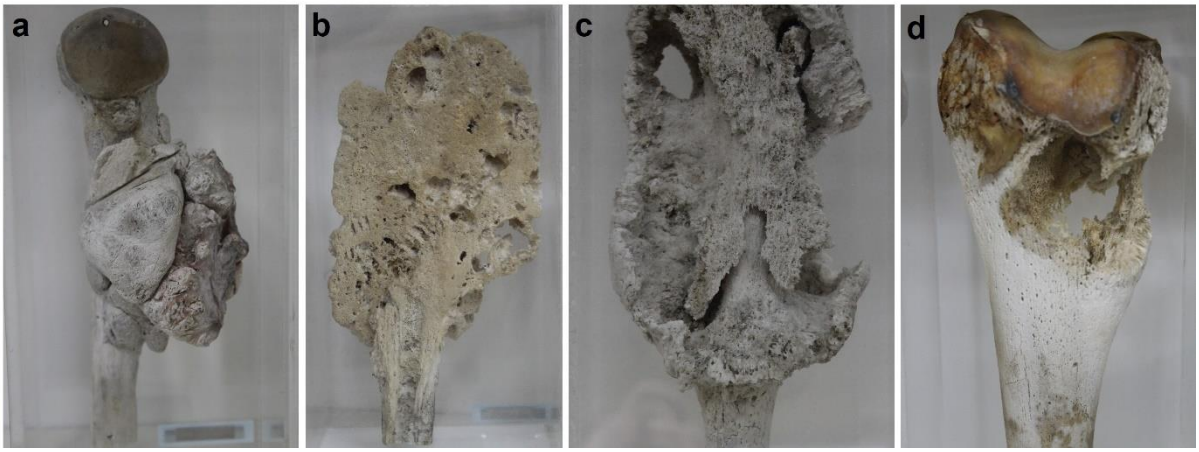

Figure 1.19 | Osteosarcomas of the upper and lower limbs. a-b, Osteomas of the humeral bones. **a**, Presents a lobulated growth of very dense, cortical bone attached to a large part of the upper shaft. **b**, Longitudinal section through the upper part of a humerus, which has been invaded by a large tumour, composed of dense connective tissue. The original structure of the shaft is completely lost in the newly forming bone. **c**, Parosteal osteosarcoma of the tibia, situated between the metaphysis and upper diaphysis. The underlying tibial shaft is preserved. This type of osteosarcoma produces large quantities of mature bone without affecting the medullary cavity. **d**, Osteosarcoma of the lower part of the femur, extending from the articular surface upwards, causing significant destruction of the bone tissue. The cavity left behind shows a growth of spongy bone. *Original images.*

In conditions such as osteomyelitis, considerable bone infections are caused most frequently by *Staphylococcus aureus* (Calhoun, Manring et al. 2009). They affect mainly the long bones of the upper and lower limbs, where significant bone 'collars' grow from the periosteum of the original shaft, causing necrosis or entrapping the original bone (Figure 1.20). Interestingly, these structures always show cavities that are used to communicate with other tissues on the exterior. The condition is thought to arise following the significant bone necrosis and the formation of new bone from surviving fragments of the periosteum (Calhoun, Manring et al. 2009). Some researchers believe that this formation mimics the process of bone tumour formation (Huang, Wu et al. 2013, Anagnostakos, Schmitt et al. 2014).

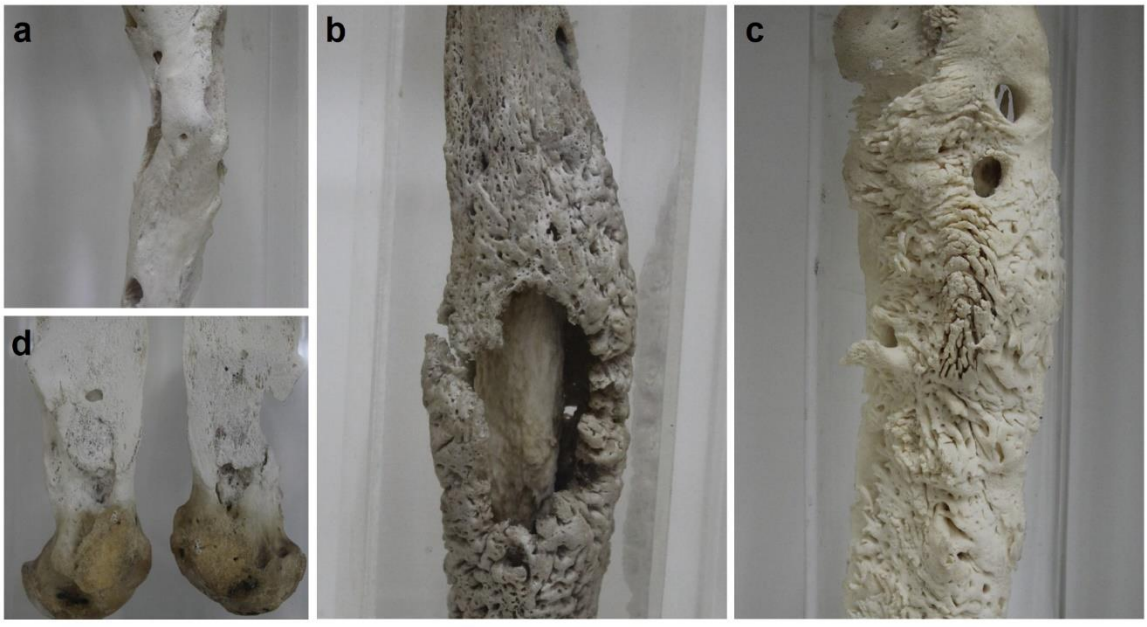

Figure 1.20 | Osteomyelitis of the upper and lower limbs. a, Chronic osteomyelitis of the humerus where the whole shaft has undergone necrosis as a result of acute osteomyelitis and has been replaced by a hollow cylinder of new bone, which is significantly deformed and communicates with the exterior using several openings, or grooves. **b**, Acute osteomyelitis of the right humerus, showing necrosis of a significant part of its shaft, and forms a sequestrum which lies within an involucrum composed of dense bone growing from the periosteum. **c**, Chronic osteomyelitis of the femur, showing great amounts of new bone (involucrum), perforated by 3 large openings. At the top end, a sequestrum can be observed. **d**, Chronic osteomyelitis of the femur which has been divided sagitally. The shaft is greatly thickened, and the marrow cavity has been replaced with dense white bone. *Original images.*

Whilst in many long bone fractures the repair process is slow and may result in non-union based on the severity and location of the injury as well as the degree of immobilisation (De Buren 1962)(Figure 1.21a presents an example of a fracture non-union), in some cases mal-unions form around the broken bone ends to try and reconnect the original bone parts, irrespective of their spatial arrangement following injury. This can occur when considerable rotation or movement of these parts has taken place and no surgical intervention has been performed (Hillen and Eygendaal 2007). These bone masses can be considerable and are composed of both trabecular and cortical bone (Figure 1.21 b-d).

Other conditions in which significant bone deformation takes place due to abnormal ossification are Rickets (Figure 1.22a) and Paget's disease (*Osteitis deformans*) (b), where bones of the femur and tibia and fibula become significantly bent. Both conditions are characterised by abnormal mineralisation, which although triggered by different factors (impairment of Ca, P and Vitamin D metabolism in Rickets compared to excessive bone formation and breakdown and disorganised bone remodelling in Paget's disease)(Roodman and Windle 2005, Holick 2006), the cortical bone tissue at the site of maximal bending becomes thicker in size in both conditions, highlighting the amazing plasticity of this tissue.

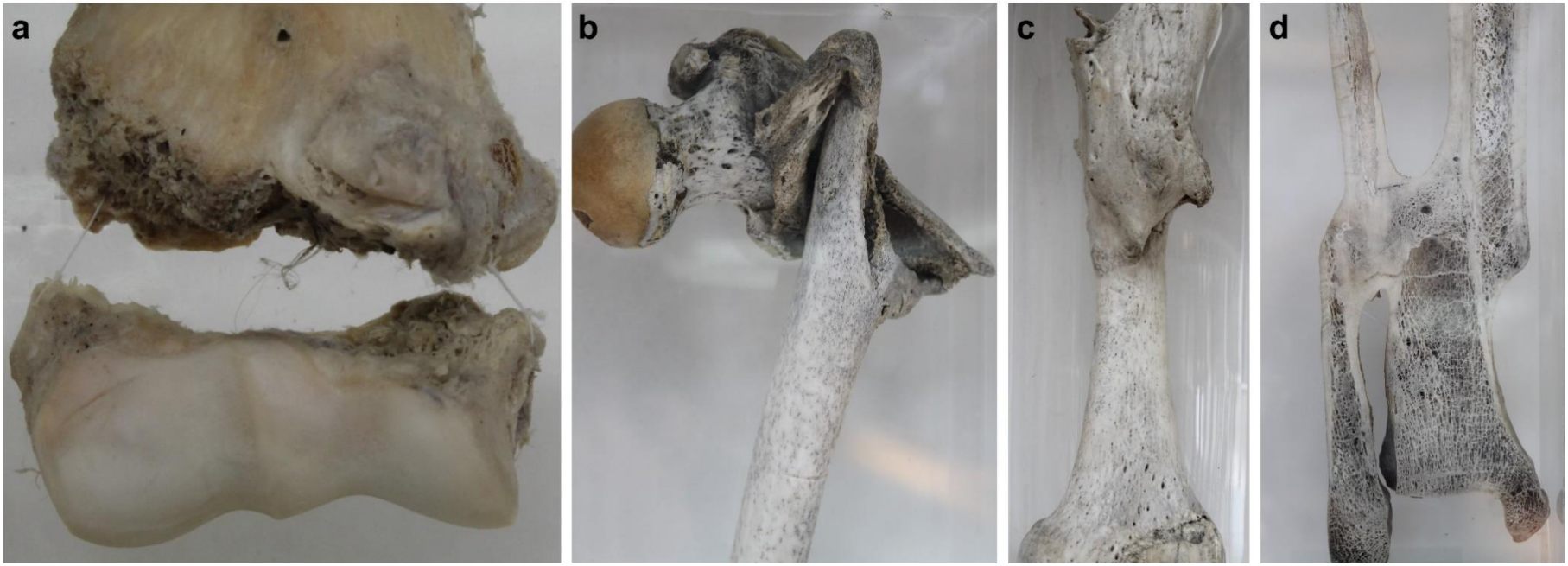

Figure 1.21 | Fracture non-union and ectopic bone deposition in fracture malunion. a, Example of a transversal fracture of the humerus, just above the condyle, resulting in non-union. **b**, An oblique fracture which damaged the upper shaft of a femoral bone, leading to a significant and firm bony mal-union between the two parts, which causes significant deformity. The lower part rotated inwards and at the same time moved upwards, resulting in a disarrangement where the broken end is located at a higher level than the femoral head; **c**, Fracture of the middle third of a femur, where the upper fragment lies in front of the lower one. Despite this arrangement, a firm bony mal-union took place, formed of dense, mature bone. **d**, Coronal section of an oblique fracture through the shafts of both the tibia and fibula. Because of the outward displacement of fractured ends, the upper fragment of the fibula has come into contact with the lower part of the tibia and has become fused to it through a firm, dense mass of bone. *Original images.*

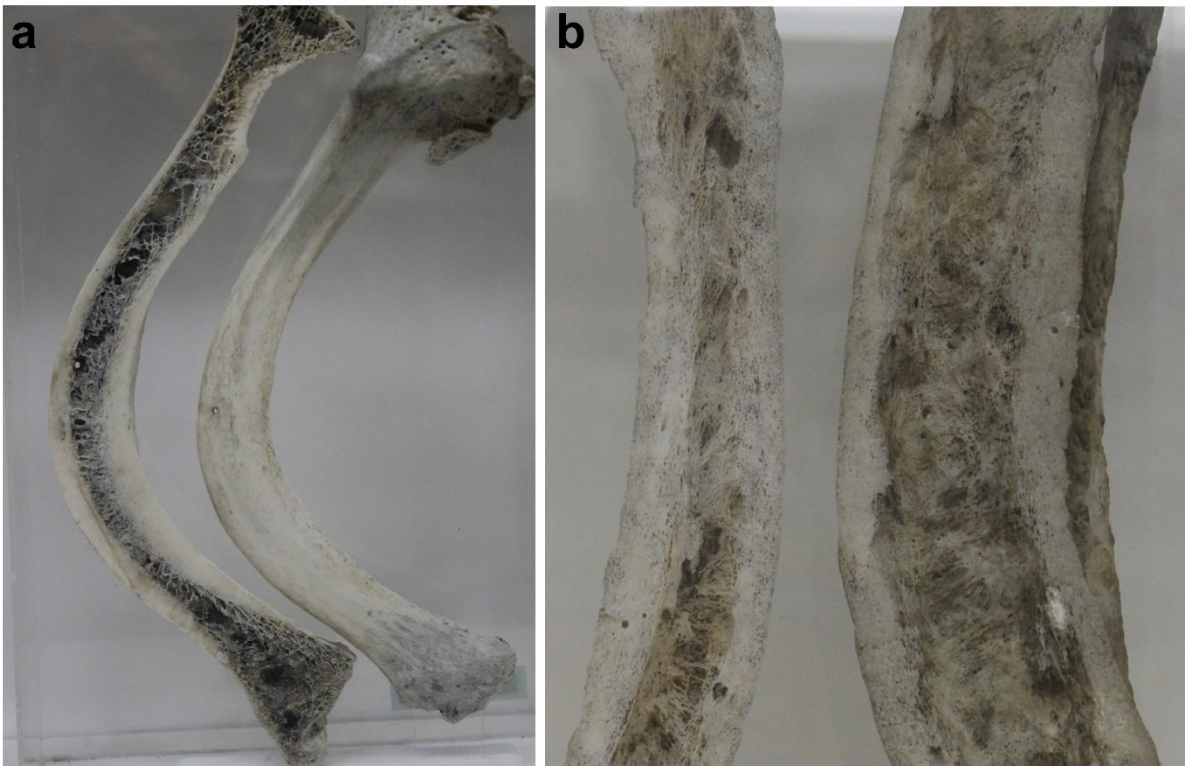

Figure 1.22 | Other conditions of abnormal bone deposition. a, Rickets. Longitudinal section through a tibia of an individual with the condition showing a significant deformation and a thickening of the cortical bone on the concave surface. **b**, Paget's disease (*Osteitis deformans*). Longitudinal sections through the tibia and femoral bone. The femoral bone (right) shows a marked convexity and enlargement and is composed of porous bone, which has been deposited in patches. Compact bone is increased in thickness. Both tibia (left) and fibula show a similar appearance externally and internally to the femur. *Original images.*

1.11.4 CONGENITAL HETEROTOPIC OSSIFICATION

Some of the most severe manifestations of HO are those caused by hereditary disorders such as *Fibrodysplasia ossificans progressiva* (FOP) and *Progressive osseous heteroplasia* (POH), where impaired regulation of bone morphogenic proteins (BMPs) leads to a severely debilitating and progressive post-natal ossification of muscles, tendons, ligaments, cutaneous and sub-cutaneous tissues (Kaplan, Craver et al. 1994, Glaser, Rocke et al. 1998, Vanden Bossche and Vanderstraeten 2005, Kaplan, Le Merrer et al. 2008). Unlike FOP, which has been identified for more than a century ago, POH has only been recognized since 1994, when a new pattern of ossification was observed in a group of patients, which was characterized by ossification of primarily the cutaneous and subcutaneous tissue (Kaplan, Craver et al. 1994). In genetic types of HO, bone formation can occur spontaneously but it is exacerbated by environmental factors such as minor traumas of the soft tissues (Cohen, Hahn et al. 1993).

1.11.5 HO FOLLOWING MILITARY OPERATIONS

Heterotopic ossification is also a condition which has recently emerged as a consequence of exposure to modern wartime combat devices, such as improvised explosive devices (IEDs). Over the recent years, extremity injuries caused by exposure to IEDs have led to very complex and challenging bone formations in the soft tissues surrounding the affected areas (Isaacson, Stinstra et al. 2010). The complications associated with these ectopic bone formations have led towards considerable patient morbidity and loss of function, as well as significantly obstructing the use of prostheses following amputation (Potter, Burns et al. 2007, Potter, Forsberg et al. 2010, Alfieri, Forsberg et al. 2012). Unlike other acquired forms of HO or the rare genetic forms, the

prevalence of HO in combat-related injuries has been reported to be as high as 64%, thus making it one of the most devastating medical complications in the war-wounded population (Potter, Burns et al. 2007, Brown, Dharm-Datta et al. 2010, Potter, Forsberg et al. 2010, Alfieri, Forsberg et al. 2012).

Whilst significant progress has been made recently in understanding the genetic mechanisms underlying the inherited forms of the disease, the aetiology of trauma and blast-induced heterotopic ossification remains largely unknown. These mechanisms will be described later in this chapter.

1.11.6 MANAGEMENT AND PROPHYLAXIS OF HO

Considerable effort has been directed towards understanding the fundamental mechanisms leading to heterotopic bone formation and the most effective ways of managing and preventing the recurrence of the condition. However, the lack of knowledge regarding early events in particular makes treatment and the development of effective compounds very difficult.

Following the development of ectopic bone structures, surgical excision is the most effective intervention that allows the removal of the unwanted formations. However, surgical intervention is not possible in the prophylaxis of the hereditary forms, as the tissue trauma associated with surgery can cause further ossification at the site of operation (Connor and Evans 1982).

Additional systemic therapy with pharmacological compounds such as NSAIDS (naproxen, indomethacin) is used to attenuate the inflammatory response that is thought to play a role in ossification and thus indirectly prevent further tissue mineralization in a wide range of pathologies including ankylosing spondylitis.

Localized radiation (G_y XRT) is used to prevent recurrence following surgery and it believed to interfere with the differentiation of pluripotent mesenchymal stem cells into bone precursor cells (Vanden Bossche and Vanderstraeten 2005, Cullen and Perera 2009, Shore and Kaplan 2010). There are, however, major drawbacks with both drug and radiation therapies. Whilst continuous NSAID therapy causes side effects in the form of gastrointestinal bleeding, XRT radiation cannot be applied effectively in early stages as it requires the physician to predict the area which will undergo ossification (Popovic, Agarwal et al. 2014, Mourad, Packianathan et al. 2015). Radiation administration is also impeded by the open-wound nature of injuries, delaying wound healing and also presenting the risk of post-radiation cancer. These effects limit the group of treatable patients to either those individuals who do not exhibit visible traumatic wounds or an apparent soft tissue compromise, and those who have easily detectable ectopic bone zones.

1.11.7 PHARMACOLOGICAL TARGETING OF HO

Several pharmacological agents are used to manage HO, including bisphosphonates. These are enzyme-resistant analogues of pyrophosphates which are given orally and intravenously in a range of malignancies. Bisphosphonates are however poorly absorbed and they also chemically interact with compounds present in some types of foods, such as dairy products, having a reduced potential. It is thought that approximately 50% of the drugs accumulate at the site of interest, with the remaining free compounds being excreted unchanged by the kidneys. Etidronate is an example of a first-generation bisphosphonate which has been used in the prevention and management of HO (Banovac, Gonzalez et al. 1993, Banovac, Gonzalez et al. 1997,

Banovac 2000). Etidronate has been reported to act by inhibiting calcium phosphate precipitation, thus delaying hydroxyapatite crystal aggregation. It is still debated whether the inhibitory effects of bisphosphonates on HO are limited to the crystallization process or if they have an effect on the matrix formation as well (Vanden Bossche and Vanderstraeten 2005). Other bisphosphonates including pamidronate, neridronate and zoledronate are used to treat conditions such as Paget's disease, osteogenesis imperfecta and ankylosing spondylitis (Filipponi, Cristallini et al. 1998, Merlotti, Gennari et al. 2007, Toussirot and Wendling 2007, Viapiana, Gatti et al. 2014).

Novel compounds have recently emerged and have successfully been used to stop the progression of genetic and acquired HO in animal models by interacting with the cartilage formation pathway that precedes bone deposition, thus removing the template base on which mineral can be deposited and built on. These compounds are known as retinoic acid receptor gamma agonists (RAR-γ) (Kaplan and Shore 2011, Shimono, Tung et al. 2011) and will be discussed further at a later stage in this thesis, in *Chapter IX, Administration of ossification-inhibiting compounds*.

In conclusion, the choices of treatment of HO are of limited efficacy and this is a result of the gap in understanding the fundamental processes occurring in the initial stages of the disease. The development of advanced prophylactic treatments for HO will require a more complete understanding of the cellular mechanisms that contribute to this disease.

1.11.8 MICRO-STRUCTURAL FEATURES OF ECTOPIC BONE

The morphology of HO appears to be rather heterogeneous, as the amount of bone forming in soft tissues has been described to vary from small osteophytes to widespread osseous attachment to the skeleton; and that HO manifests as cancellous bone, cortical bone or woven bone (Isaacson, Stinstra et al. 2010).

Unlike dystrophic calcification, associated with conditions such as renal failure and hyperparathyroidism, heterotopic ossification can be differentiated morphologically and histologically, due to the presence of trabecular features, typically encountered in bone (Balboni, Gobezie et al. 2006, Tannous, Stall et al. 2013).

This is an aspect which was noticed as early as 1980s, when Spencer and Missen noticed areas of progressive maturation in excised ectopic tissue from the femoral area from a patient with *myositis ossificans*, which included a cortical bone shell and an inner core of young, cancellous or woven bone (Spencer and Missen 1989). Isaacson and colleagues (Isaacson, Brown et al.) also found that heterotopic bone forming in wounds from burns and trauma due to accidents, showed only signs of endochondral ossification, with a high proportion of adipose tissue and bone marrow present in the tissue samples obtained from these patients.

It is important to note that the sample size was very limited in many of these studies, which makes it extremely difficult to answer some of the basic questions regarding the processes taking place or any of the further implications. However, in vivo models where rabbits and other rodents were used confirmed an endochondral bone formation pathway (Tannous, Stall et al. 2013). Intramembranous ossification was reported to occur in one of the hereditary forms of HO, POH, where both intramembranous and

endochondral ossification were thought to occur when examining samples from children with this condition (Kaplan, Craver et al. 1994).

1.11.9 CELLULAR PATHOPHYSIOLOGY OF HO

Some of the current views suggest that ectopic bone originates from distant, migrating or local mesenchymal stem cells residing in soft tissues such as muscle in a dormant state (van Kuijk, Geurts et al. 2002, Anthonissen, Ossendorf et al. 2016). Mesenchymal stem cells are pluripotent progenitor cells with the ability to divide as uncommitted cells and to then differentiate to lineages of different tissues, including cartilage, fat, tendon, ligament, bone and muscle (Caplan 1991). It is thought that during the process of ectopic bone formation, these cells can differentiate to osteogenic cells under the right micro-environmental stimuli (Williams, Southerland et al. 1999, van Kuijk, Geurts et al. 2002). This is a generally accepted view, which has been hypothesised as early as the 1970s, which states that that the induction of bone formation following trauma or injury requires three major components (Chalmers, Gray et al. 1975):

1. An inducing biomechanical agent (trauma applied to the tissue);
2. A population of progenitor or mesenchymal cells that are able to undergo osteogenic differentiation in response to this event;
3. A microenvironment that is favourable for osteogenesis.

However, this model is likely to be more complex, as newly emerging data supports the idea of a multi-systemic involvement in this disorder. For instance, in subjects who have experienced TBI and SCI, neurogenic factors could create the favourable conditions for the release of systemic factors which subsequently interact with local factors to

stimulate MSCs to differentiate into osteoblasts and thus give rise to heterotopic ossification (Williams, Southerland et al. 1999, Pape, Lehmann et al. 2001, Sullivan, Torres et al. 2013).

Tissue hypoxia is thought to play a major role in the formation of endochondral bone. A study by Agarwal and colleagues has recently shown that inhibition of HIF- 1α in mice can prevent both the acquired and congenital forms of HO (Agarwal, Loder et al. 2016). In addition, Wang and colleagues have recently demonstrated that early human FOP and murine model lesions are highly hypoxic, and that HIF- 1α increases BMP signalling via the ACVR1 receptor (Wang, Lindborg et al. 2016).

Other authors have demonstrated that tissue hypoxia is also driven by the accumulation of adipocytes in the lesioned areas, which lower the oxygen tension in the tissue, thus favouring the formation of cartilage (Olmsted-Davis, Gannon et al. 2007). Recently, it has been demonstrated using a murine model that excised ectopic tissues, but not normal tissues, express a high level of uncoupling protein 1 (UCP1), a marker for brown adipocytes, which, as thought previously, play a critical role in regulating heterotopic ossification (Salisbury, Dickerson et al. 2017).

In addition, circulating osteoprogenitor cells of hematopoietic origin are thought to migrate from close bone marrow sources. A study by Suda and colleagues (Suda, Billings et al. 2009) showed that a population of type I collagen^{+}/CD45^{+}, mononuclear adherent cells are present in the early, pre-osseous, fibroproliferative lesions of FOP patients and have been shown to nucleate HO in a murine implantation assay. In addition, these authors demonstrated that patients with an active form of FOP have a higher number of these cells in their bloodstream compared to patients with a stable stage of FOP or unaffected individuals.

A separate, underlying mechanism was demonstrated by Medici and colleagues (Medici, Shore et al. 2010, Medici and Olsen 2012), who showed that in both human FOP and mouse lesions, endothelial cells transdifferentiate into mesenchymal stem cells through a mechanism known as endothelial-to-mesenchymal transition (EndMT). This process was shown to be mediated in an ALK2 signalling manner and ultimately contributed to HO formation. Interestingly, the process was inhibited by application of short interfering RNA (siRNA).

1.12 *IN-VIVO* MODELS OF ECTOPIC OSSIFFICATION

As described in the previous sections, bone tissue forms in various physiological circumstances, ranging from normal bone development and callus-mediated fracture repair (Einhorn and Gerstenfeld 2015), to pathological heterotopic bone formation in extra-skeletal tissues, as seen following muscle trauma (Potter, Burns et al. 2007, Potter, Forsberg et al. 2010, Shore and Kaplan 2010, Edwards and Clasper 2014), traumatic brain and spinal cord injury (Wittenberg, Peschke et al. 1992, Sullivan, Torres et al. 2013), surgical procedures of the hip and knee (Thilak, Panakkal et al. , Board, Karva et al. 2007); and in genetic conditions such as *Fibrodysplasia ossificans progressiva* (*FOP*) (Thilak, Panakkal et al. , Shore and Kaplan 2010). These contexts, normal or otherwise, share fundamental characteristics at many levels, including molecular (overexpression of bone morphogenic proteins, BMPs) (Ramirez, Ramirez et al. 2014, Katagiri, Osawa et al. 2015), cellular (a set of progenitor cells that commits to an osteoblastic lineage) (Kan, Liu et al. 2009, Shore and Kaplan 2010, Ramirez, Ramirez et al. 2014) and biomechanical (translation of the mechanical forces into structured and organized bone) (Isaacson, Brown et al. , McCarthy and Sundaram 2005, Lin, Shen et al. 2010). However, there are still significant gaps in our understanding of these events.

There are several modalities to recreate pathological ossifications in animal models, including the overexpression or inhibition of molecular osteoinductive factors (Liu, Kang et al. 2014), trauma induction (Liu, Kang et al. 2014) and heterotopic implantation (Ueno, Kagawa et al. 2003, Lounev, Ramachandran et al. 2009).

1.12.1 ANIMAL MODELS OF INHERITED HO AND GENETIC MANIPULATION

Currently, there are representative animal models for the inherited form of HO, such as FOP, since the genetic mutations underlying this disease have been identified. The genetic fault lies in a mutation consisting of a heterozygous single nucleotide substitution in the gene encoding ACVR1/ALK2, a BMP type I receptor, which causes a dysregulation in the BMP pathway and leads to an over-activation of the signalling process even in the absence of a BMP ligand (Shore, Xu et al. 2006). This process is further enhanced when BMP ligands are present (Shore, Xu et al. 2006). As a result, there are some successful, genetic knock-in murine models which are able to recreate the hereditary form of HO (Chakkalakal, Zhang et al. 2012). Gene targeting in these animals allowed the development of models showing progressive endochondral bone formation. Moreover, it was shown that both wild-type and mutated osteoprogenitor cells exist within the ectopic bone formations, suggesting that whilst the mutations were necessary to induce bone formation, it was not required for the contribution of progenitor cells to cartilage and bone formation (Chakkalakal, Zhang et al. 2012).

In general terms, the effects of abnormal BMP function can be studied in several ways (Kaplan, Shore et al. 2005, Kan and Kessler 2011, Liu, Kang et al. 2014) specifically by:

1. Introducing a hyperactive BMP receptor (Le and Wharton 2012);
2. Knocking-out BMP inhibitors (Zhao 2003);
3. Implanting BMP-releasing Matrigels (Glaser, Economides et al. 2003);
4. Overexpressing specific BMP target genes (Wang, Green et al. 2014);
5. Modifying BMP signalling indirectly by interfering with other molecular factors that play a role in the BMP pathway (e.g. TGF-β, Smads)(Yamazaki, Fukushima et al. 2009).

Genetic manipulation, whilst straightforward and inexpensive, presents numerous disadvantages (Tong, Huang et al. 2011). In the case of target gene overexpression models, constitutive overexpression often leads to non-relevant levels of protein expression, being misleading with regards to the role of the gene and as such, animals with dominant negative variants have to be simultaneously produced. Secondly, overexpression of genes which play a major role in bone formation can lead to lethality, making it hard to establish consistent transgenic lines for investigation (M. Lyons 2013).

With respect to gene targeting, loss of function is very useful in understanding the role of the ablated gene product. There are several issues with this technique, however, which is that knock-outs are not necessarily limited to a particular tissue or system and the deletion of these genes may prevent an adequate analysis of their role in skeletal processes. In addition, many knockout strains do not exhibit obvious phenotypes and as such, multiple-knockouts have to be performed (M. Lyons 2013).

Finally, there are major environmentally-driven differences in phenotype between different populations of rats despite being genetically-identical, making results less reproducible (Nagy, Krzywanski et al. 2002, Champy, Selloum et al. 2004).

In conclusion, care must be taken when extrapolating the results from animal studies to humans, especially as they have different mechanical loading and metabolic activity.

1.12.2 ANIMAL MODELS OF ACQUIRED HO

There are also several models available for simulating the acquired form of HO (for a review see (Kan and Kessler 2011)) and they include:

1. The hip arthroplasty model
   (Tannous, Stall et al. 2013, Amar, Sharfman et al. 2015);
2. Immobilisation-manipulation of knee joints (Michelsson model)
   (Michelsson, Granroth et al. 1980);
3. Achilles tenotomy
   (Lin, Shen et al. 2010, Zimmermann, Schwitter et al. 2016);
4. Trauma-induction (limbs and brain)
   (Elder, Dorr et al. 2012, Liu, Kang et al. 2014, Liu, Zhang et al. 2015);
5. Injection of osteogenic agents (BMP-2) into the muscles
   (Olmsted-Davis, Gannon et al. 2007, Liu, Kang et al. 2014);

However, some of these models are not fully representative of the pathological states, requiring the use of a large number of animals (Kan and Kessler 2011). Some results cannot be generalised to other tissues or are too complex to allow the isolation of individual molecular components in early-phase bone formation, which makes it difficult to answer some essential questions on biological ossification objectively. As so, it is hard to develop a single hypothesis that can unify all the clinical and experimental findings into one model.

This lack of knowledge of early pathogenesis has, for a long time, hindered the validation of these animal models or their improvement. The inconsistencies generally noticed with these models and the fairly low reproducibility mean that a high number of

animals is required for consistent results. In addition, some of these models require the application of significant amounts of trauma to animals, which means that some of these animals have to endure suffering during their lifespan.

1.13 IN-VITRO MODELS OF BONE FORMATION

For many years, *in vitro* cell cultures have been used for first-stage analysis of the behaviour of bone cells. These cells can originate either from primary bone sources, being isolated through matrix digestion, or expanded from ex-vivo bone fragments, or used from highly-proliferative engineered populations (e.g. MC3T3-E1, 2T3). They are then cultured and sub-cultured in monolayer (2D) on rigid, flat surfaces, where they can produce osteoid and mineralisation nodules (Bellows, Aubin et al. 1986, Buttery, Bourne et al. 2001, Wang, Liu et al. 2006).

2D cell culture is a valuable tool which is excellent for reproducibility and standardisation. However, it cannot simulate the tissue architecture and cellular interactions found *in vivo* in bone as these cells are organised within the extracellular matrix in a 3D fashion.

Therefore, it is necessary to engineer new biological models that can shed light on both the processes of bone formation and of heterotopic ossification. Intermediate models, more complex than monolayer 2D populations but less complex than *in vivo* rodent models could provide further information regarding the cellular pathophysiology of the condition and the involvement of different molecular factors.

Many biomaterials and methods have been developed over the past years for producing mineralised bone-like cultures in 3D, with closer structural similarities to *in vivo* bone tissue (Edmondson, Broglie et al. 2014, Bouet, Cruel et al. 2015), which will be discussed in the next section.

1.14 3D MINERALISED CULTURES USING BIOMATERIALS

This method for producing bone-like tissue involves applying cells to a variety of biomaterials to create artificial tissues *in vitro*. The materials used for scaffolds are natural or synthetic polymers such as hydrogels or elastomers (Liu, Zeng et al. 2017). Other materials include bioactive ceramics such as calcium phosphates (Wang, Zhao et al. 2014) and bioactive glasses (Rahaman, Day et al. 2011).

Composite systems containing both ceramics and polymers have been used to increase the mechanical properties of the scaffolds and to simulate the biochemical composition of bone (Wahl and Czernuszka 2006, Chesnutt, Viano et al. 2009, Moreau, Weir et al. 2009, Šupová 2009, Maas, Guo et al. 2011, Thein-Han, Liu et al. 2012, Wang, Bongio et al. 2014).

Since the 1990s, a variety of hydrogels have become available for bone and cartilage tissue engineering, due to their structural similarity to the extracellular matrix and their porosity, which enables cell proliferation and exchange of nutrients. Hydrogels are three-dimensional cross-linked networks formed by homopolymers, copolymers and macromeres (Liu, Zeng et al. 2017) which provide cells with an environment similar to the ECM, thus facilitating cell adhesion, proliferation and differentiation of osteoprogenitor cells towards an osteoblastic lineage.

These biomaterials include gelatin, chitosan, alginate, hyaluronic acid, polyethylene glycol, collagen I and fibrin, each with significant advantages and disadvantages (Lee and Mooney 2001, Perka, Stern et al. 2003, Chesnutt, Viano et al. 2009, Wang, Bongio et al. 2014).

For bone tissue engineering, collagen type I gels are the most popular choice due to its chemical and structural similarity to the osteoid of bone (Kikuchi, Itoh et al. 2001, Wahl

and Czernuszka 2006, Moreau, Weir et al. 2009, Matthews, Naot et al. 2014). However, these gels show a low mechanical flexibility and it is hard to separate the new collagen produced by embedded cells from the scaffold collagen. In addition, the presence of a non-cell-derived matrix will most likely have an influence on the differentiation of the embedded cells.

Alternative hydrogels such as fibrin are widely used in tissue engineering and have been used in clinical practice and surgery for many years as a haemostatic agent (Eyrich, Göpferich et al. 2007). In addition, their biodegradability can be controlled using the addition of inhibitions of proteinases, such as aprotinin (Ye, Zund et al. 2000). Whilst they have a more limited mechanical strength (Lee and Mooney 2001), their biodegradability means that as seen during wound healing, they can be replaced over time with endogenous cell-secreted collagenous matrix which can more closely mimic the geometry and composition of *in vivo* bone tissue (Eyrich, Brandl et al. 2007, Eyrich, Göpferich et al. 2007). Fibrin gels can be easily assembled by polymerisation of fibrinogen in the presence of thrombin and can be produced from the patient's own blood components (Lee, Kwan et al. 2008, Ahmed, Ringuette et al. 2015), making them ideal for implantation and minimising the risk for rejection.

Although these cell-scaffold constructs can simulate the biochemical composition of bone tissue, to date, there are no in vitro/3D cell culture systems that are able to continuously produce loading forces similar to what is seen *in vivo* (Weinbaum, Cowin et al. 1994, Boukhechba, Balaguer et al. 2009, Vazquez, Evans et al. 2014). For this reason, animal models have remained the gold standard for evaluating whole tissue response and mechanical function.

CHAPTER II

ENGINEERING A SELF-STRUCTURING BONE SYSTEM

2.1 CONTEXT OF THE PRESENT WORK

Developing novel ways to produce ossified tissue is essential for several scientific reasons. From a biological perspective, new models will help to develop a deeper understanding of the fundamental processes underlying both early bone development and the pathological ossification events following trauma or injury (Potter, Burns et al. 2007, Potter, Forsberg et al. 2010). New approaches to develop bone-like materials are also required for the augmentation of bone defects and ultimately the replacement and surgical transplantation of tissue grafts (Matassi, Nistri et al. 2011, Claes, Recknagel et al. 2012, Einhorn and Gerstenfeld 2015). In this context, the present work focused on developing a new, biological model of bone tissue formation, which would allow for the investigation of individual osteogenic factors in a less complex environment than *in vivo* conditions, and may ultimately be used for skeletal regeneration.

Biological hydrogels provide a 3D microenvironment that is analogous in structure and composition to the extracellular matrix (ECM) of innate tissues, and therefore when used for cell encapsulation, they enable the embedded cells to exhibit phenotypes more representative to those *in vivo* than cells grown in monolayer culture (Abbott 2003). As discussed previously, these materials have been shown to promote cell survival and proliferation both *in vitro* and when implanted *in vivo* (Wahl and Czernuszka 2006).

The first scaffold encountered by many types of cells during wound healing, tissue trauma and repair is a fibrin clot (Janmey, Winer et al. 2009). The clot is a fibrin network which forms when soluble fibrin is cleaved by thrombin into strands which are then cross-linked under the action of factor XIII into a blood clot (Eyrich, Brandl et al. 2007, Eyrich, Göpferich et al. 2007). Fibrin gels exhibit a high bioactivity and specifically their ability to bind cells, growth factors, nutrients and metabolites makes them good substrates for stem cell differentiation and tissue engineering research (Lee and Mooney 2001, Drury and Mooney 2003, Eyrich, Brandl et al. 2007, Eyrich, Göpferich et al. 2007).

The biomechanical behaviour of these matrices can be clinically relevant and their degradability over time means that cells embedded in such a culture system can replace the scaffold over time with endogenous matrix, giving rise to more complex tissues than pre-formed analogous scaffolds (Eyrich, Brandl et al. 2007).

Starting from these principles, the work in this thesis focused on engineering a biological bone system which is seeded with primary cells and monitored longitudinally over significant periods of time, allowing to study the temporal evolution of bone mineral and microstructure.

2.2 AIMS OF THIS THESIS

The aim was to develop a system that could be easily manipulated biochemically and biomechanically to simulate the ossification microenvironment encountered in both normal and pathological environments and that could ultimately be applied to investigate both biological and physical research questions. To develop this system, populations of osteoprogenitor cells that were extracted from the periosteum of rat femoral bones were selected for investigation. As described in Chapter 1, periosteal cells are the main determinants in the reparative phase of bone fracture healing, when they interact with the temporary fracture callus, which serves as a scaffold for the formation of new bone (Einhorn and Gerstenfeld 2015). Furthermore, they have been shown to have the ability to give rise to endochondral bone when implanted in muscle (Ueno, Kagawa et al. 2003), and therefore may be central to traumatic heterotopic ossification. Moreover, their ability to give rise to endochondral bone has been discussed by several groups as being an underlying cause in degenerative conditions such as Ankylosing Spondylitis (*see* Chapter 1).

Following isolation, periosteal cells were seeded into hydrogels formed from fibrin, analogous structurally and biochemically to the microenvironment of the callus formed early in fracture healing or the early-wound microenvironment in HO.

As matrix organization is essential for bone development, the environment of the fracture callus was further emulated by introducing two calcium phosphate anchors composed of a mixture of brushite and β-TCP at the extremities of the culture dish. These anchors exhibit a mineral composition similar to that of the inorganic component of bone and mainly served to enhance retention of the forming matrix and to provide a source of calcium and phosphate ions to aid in triggering the ossification process.

Remarkably, over time, constructs self-structure from a homogenous polymer, in the form of fibrin, into complex, heterogeneous structures (for an overview, see Figure 2.1). Samples were characterized over a period of 1 year in culture in terms of matrix organization, cell behaviour and mineralization using a combination of optical, spectroscopic and chemical techniques.

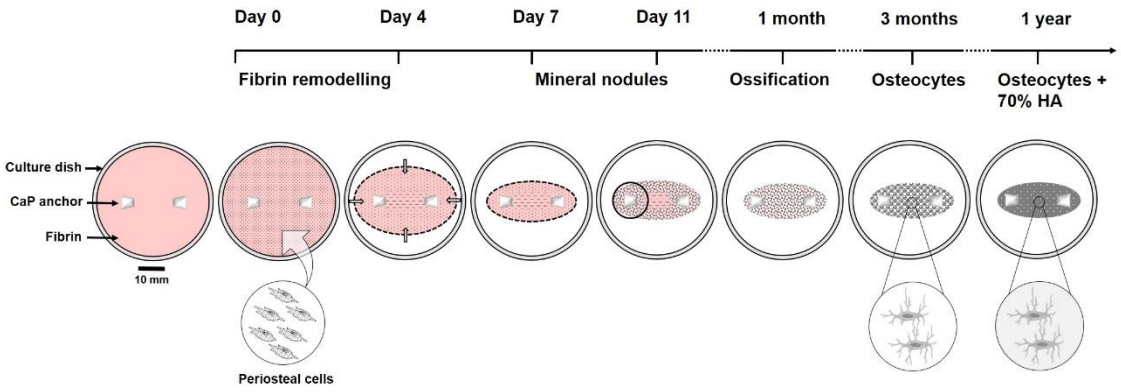

Figure 2.1 | Schematic representation of the development of a construct over time. Contraction and alignment of the matrix occur maximally within the first 7 days. Within the following 2-3 days, the mineralization process becomes apparent, through the creation of nucleation points which aid in the formation of mineralized nodules, most prominently around the two anchors. These nodules increase in size over the first month in culture and ultimately fuse into a fully mineralized matrix. Following 1 month in culture, significant amounts of collagen can be detected around the anchor areas. The mineralized matrix advances from the anchor regions towards the centre of the construct until the previous template is completely substituted with the new, bone-like matrix containing hydroxyapatite-like mineral. Cells differentiate into osteocyte-like cells after 2 months of full osteogenic supplementation and maintain their phenotype over the extended months in culture.

2.3 GENERAL METHODS

2.3.1 ASEPTIC TECHNIQUE AND CONTAMINATION PREVENTION

Cell work was conducted in sterile conditions inside laminar flow cabinets (BSB, Gelaire Laminar Flow, Victoria, Australia). Cabinets were sterilised using UV light, followed by disinfection using Distel High-Level Medical Surface Disinfectant (Tristel, Snailwell, United Kingdom) and in some cases using 70% EtOH. Distel was used to provide enhanced protection against bacteria, fungi and viruses as well as having a tuberculocidal action and providing protection against blood diseases including Hepatitis B. It was also used in some molecular procedures in addition to other reagents such as RNAseZAP (Sigma-Aldrich-Merck, Germany) to destroy DNAse and RNAse enzymes which could interfere with the results. Dissection tools, pipettes and other metallic tools were sterilised using immersion in 70% EtOH. Pipette tips, 1.5 ml tubes and ultra-high-recovery centrifugation tubes (Starlab, Milton Keynes, United Kingdom) were DNAse and RNAse certified, as well as 15 ml and 50 ml tubes (Corning, New York, USA) and culture-treated flasks (Greiner Bio-One, Kremsmünster, Austria). Ethanol of molecular grade certification was chosen (Fisher Scientific, New Hampshire, United States) and was diluted to the required concentrations using sterile water. Where molecular work such as purification was undertaken, molecular grade water was used (Fisher Scientific, New Hampshire, United States) and a PCR Mini-UV-cabinet (Geneflow, Lichfield, United Kingdom) equipped with four 15 Watt UV lights was used to remove potential DNA and RNA contaminants from equipment. A sample sterilisation time of 30 minutes was used.

2.3.2 ISOLATION AND CULTURE OF PRIMARY FEMORAL CELLS

Femurs from left and right limbs of euthanised female Wistar rats (3 weeks old, 50-70 grams weight) were excised and surrounding muscular and connective tissue was removed. Femurs were stored in phosphate buffered saline solution (pH = 7.4; Gibco®, Life Technologies, Thermo Fisher Scientific, UK) until use. Osteoprogenitor cells were extracted from the periosteum via enzymatic digestion using a cocktail containing 2.5 mg/ml collagenase I, 0.7 mg/ml collagenase II and 0.5 units/ml dispase I, in PBS (Gibco®, Life Technologies, Thermo Fisher Scientific, UK). Bones were incubated with this solution at 37°C for 1 hour in a 5% CO_2 atmosphere. Following incubation, tubes containing bones and solution were shaken rigorously for 30 seconds to detach the remaining cells. Solutions were then pooled and filtered using 70μm filters (Falcon, Becton Dickinson, UK). Cells were recovered using centrifugation at 21°C, 1400 rpm for 6 min. The supernatant was discarded and the resulting pellet was resuspended in 10 ml D20 growth medium (DMEM containing 20% serum) to encourage attachment. Approximately 1 million PO cells extracted from each bone were cultured to a level of 70% confluence in D20 medium (Figure 2.2) at 37°C, in a 5% CO_2, humidity-controlled incubator containing copper sulphate water (1 g/L) to prevent fungal contamination (Fisher Scientific, USA). The medium was replaced every 2-3 days.

Where human primary osteoblasts were used, they were derived from tissue obtained from the Oxford Musculoskeletal BioBank and were collected with informed donor consent in full compliance with national and institutional ethical requirements, the United Kingdom Human Tissue Act, and the Declaration of Helsinki.

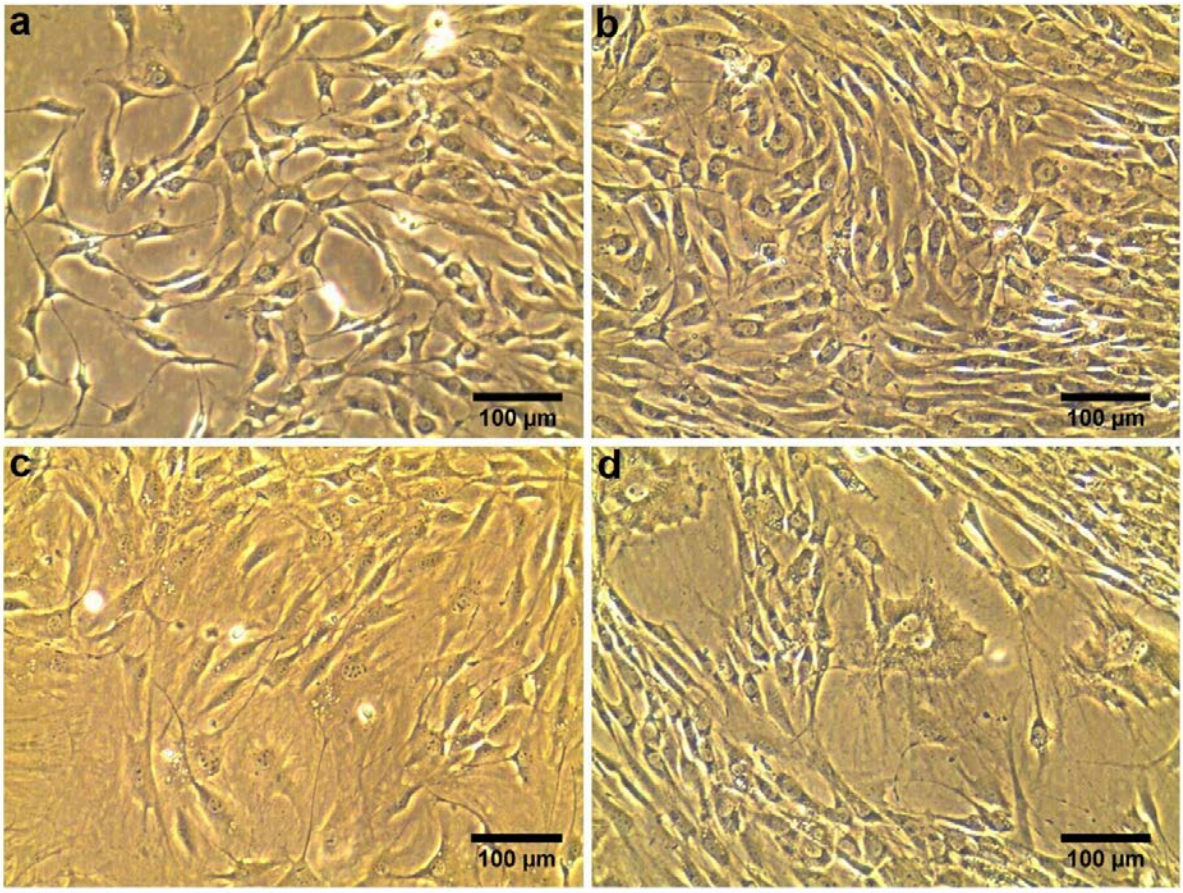

Figure 2.2 | Cell morphologies observed in 2D prior to embedding in fibrin hydrogels. **a**, Femoral periosteal cells cultured in 2D for ten days displayed typical osteoblastic morphology (**a-b**), with some developing long projections (**c**). A few cells appeared hypertrophic, with typical senescent morphology (**d**).

2.3.3 CULTURE OF IMMORTALISED CELL LINES

Cells originating from cell lines MC3T3-E1/2T3 were obtained from the European Collection of Authenticated Cell Cultures (ECACC). MC3T3-E1 cells were C57BL2/6 murine derived calvarial osteoblasts and originated from the Riken Cell Bank in Japan. Cells were cultured according to standard procedures in Minimal Essential Medium Eagle (MEM) Alpha Modification (10% FBS, 1% P/S, 2.4% L-glutamine) (Sigma-Aldrich, Germany).

2.3.4 CRYOPRESERVATION OF CELLS FROM CELL LINES

For long-term storage, cells were frozen at -196^{o}C by immersion in liquid nitrogen inside a vacuum insulated, alarm-connected storage vessel (Thermo Fisher Scientific, USA). The freezing medium was a solution consisting of 60% culture medium, 30% FBS and 10% DMSO (Sigma-Aldrich, Germany) to protect cells from mechanical injury induced by ice crystal formation. Cells were frozen at a density of 1 million cells/ml in 1.5 ml cryovials. The cryopreservation process was performed rapidly, as DMSO is toxic at this concentration in metabolically-active cells, but does not affect frozen cells.

2.3.5 THAWING OF CRYOPRESERVED CELLS

Vials containing cells were quickly removed from liquid nitrogen and tubes were immersed into a 37^{o}C water bath for 30 seconds to partially defrost the contents. The tubes were gently swirled and transferred to a laminar flow cabinet. The tubes were quickly wiped with tissues soaked in 70% EtOH and their contents, whilst still containing small amounts of ice, were dispersed into 50 ml of supplemented medium to dilute the DMSO and reduce immediate toxicity to cells. Cells were pelleted by centrifugation at 1000 RPM for 3 minutes and the supernatant containing residual DMSO was discarded. Cells were then re-suspended in supplemented medium and cultured in T75 or T175 flasks. The success of thawing was assessed based on the level of cellular adherence to culture flasks, the adopted morphology and the rate of population doublings.

2.3.6 CULTURING OF PASSAGED CELLS

Primary femoral periosteal cells were cultured immediately following isolation and were not frozen for long-term storage. Cells originating from cell lines were only passaged for a maximum of 4 times in order to maintain their osteoblastic phenotype.

2.3.7 ISOLATION OF CELLS FROM CULTURE FLASKS

Adherent cells or cell lines were isolated from T75/T175 culture flasks (Greiner Bio-One, Kremsmünster, Austria) upon reaching 70% confluency using a TrypLE Select enzyme (pH 7.0-7.4, 1X), which did not contain phenol red (Gibco, Thermo Fisher Scientific, USA). This enzyme is a non-animal derived, recombinant enzyme which cleaves peptide bonds on the C-terminal of lysine and arginine. This product was chosen instead of traditional dissociation agents such as Trypsin due to its increased purity and hence specificity for cellular bonds, making it less likely to produce cellular damage due to additional enzymes present in these products. In addition to the rProtease, the product also contained 200 mg/L KCl, 200 mg/L KH_2PO_4, 8000 mg/L NaCl, 2160 mg/L Na_2HPO_4-$7H_2O$ and 457.6 mg/L EDTA. Before addition of the enzyme to the cells, the growth medium was removed from the flasks and cells were gently washed with 5 ml of sterile PBS for a few seconds to remove cell debris and remaining medium. The PBS was then discarded and the enzyme was applied at a ratio of 1 ml per 25 cm^2 of growth area (i.e. 1 ml for a T25 culture flask, 3 ml for T75 and 7 ml for a T175 flask). The flasks were placed in an 37^oC incubator for 3 minutes to allow activation of the enzyme and cell detachment. Following the short incubation time, an equal amount of growth medium containing 10% FCS was added to the flasks in order to inactivate the enzyme. The liquid containing detached cells was then recovered from the flasks and added to a 50

cm sterile tube (Corning, New York, USA) which was centrifuged at 1000 RPM for 3 minutes to pellet the cells. Following centrifugation, the supernatant was discarded and cells were re-suspended in 10 ml of fresh growth medium.

2.3.8 DETERMINATION OF CELL NUMBERS

Isolated cells were counted using the Trypan-Blue dye exclusion test, which selectively differentiates viable and dead cells based on the concept that viable cells are not able to take up this impermeable dye, whereas dead cells, which have become permeable, are able to take up this dye. 10 µl of cell suspension was mixed with an equal part of 0.4% Trypan Blue and 10 µl of the mix were inserted into a counting chamber slide (Thermo Fisher Scientific, USA), which was introduced into a Countess automated cell counter (Thermo Fisher Scientific, USA), which automatically generated the total cell count, viable cell count and a distribution of the cell size. Measurements were taken in duplicate and an average cell number was calculated. The viability of cells following isolation always ranged between 85% - 97% and 85% was set as the lower limit for selecting a healthy cell population for embedding into fibrin hydrogels.

2.3.9 PRODUCTION OF THE MINERAL 'BACKBONE'

2.5 g of β-TCP powder (<125 m particle size) were added per 1 ml of Orthophosphoric Acid (3.5 M) to generate a paste, composed of a mixture of brushite and β-TCP. The liquid mixture was poured into individual, pre-shaped wells of moulds, placed on top of a shaking platform, to encourage uniform setting inside the shapes. 1.4 cm stainless steel insect pins (Austerlitz minutiens, Fine Science Tools, USA), with a diameter of 0.20

mm were inserted into the individual wells on the moulds before the mixtures advanced into a solid state. The mixtures containing the pins were allowed to fully harden for 3-4 hours and were sterilized overnight using UV light exposure, as well as with 70% EtOH for 30 minutes on the day of use. The final anchors had a trapezoidal shape and measured approximately 3 mm x4 mm x 4mm in height.

2.3.10 COATING OF CULTURE PLATES

Culture wells were coated with 1.5 ml of a silicone elastomer base (Sylgard184, Dow Corning, USA). This was a colourless polydimethylsiloxane elastomer, which was formed by mixing the Sylgard base to a curing agent at a 10:1 ratio. Plates were placed on a flat surface and allowed to dry at room temperature for 7 days to allow polymerization.

Two anchors per 35 mm culture well were attached to the silicone base using the pins, and were placed at a distance of 1.5 cm from each other. Plates were sterilised using UV radiation overnight before the commencement of the experiment and were sprayed with 70% EtOH on the date of use with 5 hours before use.

2.3.11 CELL EMBEDDING IN FIRBIN HYDROGELS

Constructs were developed by seeding fibrin hydrogels with an osteoprogenitor cell population, either periosteal cells from mice femurs, or from cell lines such as MC3T3-E1 or 2T3. The fibrin scaffolds were produced through the interaction of the normal plasma components thrombin and fibrinogen and were developed on the mineral backbone structure. Bovine-derived thrombin powder (Calbiochem, EDM Chemicals;

1KU) was reconstituted using 0.1% w/v BSA and 5 ml F12K Nutrient Mixture (1X) with Kaighn's Modification (Gibco Life Technologies) to make a final concentration of 200 U/ml. Powdered bovine fibrinogen (Sigma Life Sciences) was reconstituted in F12K Nutrient Mixture (1X) with Kaighn's Modification (Gibco Life Technologies) at a ratio of 20 mg/ml. Thrombin was added to a solution containing the cell culture medium (either DMEM or αMEM) at a ratio of 50 µl/ml solution. The anti-fibrinolytic agents aminohexanoic acid (200 mM) and aprotinin (10 mg/ml) were added to the thrombin solution at a ratio of 2 µl/ml in order to reduce the degradation rate of the fibrin gel, in order for it to match the rate of new matrix formation so that the mechanical integrity of the tissue can be maintained over longer periods of time. Hydrogels were generated by mixing 500 µl thrombin solution with 200 µl fibrinogen. Thrombin cleaves small peptides from the fibrinogen chain, producing soluble fibrin monomers, which then cross-link into an insoluble, polymerized fibrin clot. Gels were allowed to polymerize for 30-40 minutes. Cells were seeded into the fibrin constructs immediately following gel polymerization; at a density of 100K/2ml of cell culture medium.

2.3.12 FULL OSTEOGENIC SUPPLEMENTATION OF CONSTRUCTS

Constructs developed with periosteum cells were supplemented following 1 month of culture with full osteogenic DMEM culture medium containing β- glycerophosphate (10 mM), ascorbic acid (0.1 mM) and dexamethasone (10 nM) (Sigma Aldrich, Germany), to encourage new matrix deposition along the entire length of the constructs.

2.3.13 PRO-COLLAGEN SUPPLEMENTATION OF OTHER CONSTRUCTS

Following 7 days of development, the MC3T3-E1 constructs were supplemented with ascorbic acid (250 μM final concentration) and proline (50 μM final concentration) every 2 days, to stimulate collagen deposition (Sigma Life Sciences, Germany).

CHAPTER III

EARLY EVENTS AND INITIATION OF OSSIFICATION

3.1 INTRODUCTION

Following cellular embedding into the scaffolds, early developmental events were monitored to determine whether the population of osteoprogenitor cells encapsulated was able to adhere to the new 3D environment and to observe how successful the cells were in proliferating and re-modelling the surrounding hematoma-like matrix. Constructs were visually observed in order to determine the extent of contraction, the initiation of mineralisation and the localisation of mineral in constructs.

3.2 AIMS AND OBJECTIVES

The aim of this work was to characterize the early events as well as the development of mineralisation microscopically and macroscopically using a combination of optical and histological techniques.

3.3 CHARACTERISATION METHODS

3.3.1 WHOLE MOUNT STAINING OF MINERAL DEPOSITS

An **Alizarin Red dye** was used to chemically detect the presence of mineralization in constructs. Alizarin Red S powder (Sigma-Aldrich, Germany) was dissolved in distilled H_2O to a concentration of 40 mM. The pH was adjusted to 4.2 with 10% (v/v) ammonium hydroxide (Fisher Scientific, USA). Constructs were fixed with 10% PFA for 30 minutes at room temperature. Following fixation, the constructs were rinsed in phosphate buffered saline solution (Sigma-Aldrich, Germany) to remove the excess PFA, and were inserted into 2 ml of Alizarin Red solution for 30 minutes at room temperature. Constructs were rinsed 3 times with PBS to remove unbound dye.

3.3.2 OPTICAL VISUALISATION OF MINERAL DEPOSITS

Constructs were imaged using a CETI Inverso TC100 brightfield microscope (Medline Scientific, Oxon, United Kingdom) and Alizarin Red-stained constructs were visualised using a Zeiss Axio Lab A1 microscope (Carl Zeiss, Jena, Germany).

3.3.3 PHOTOGRAPHS OF CONSTRUCTS

Constructs were photographed at various time points to illustrate the degree of contraction during the first week in culture. Photographs were acquired using a Canon EOS 1100D camera (Canon, Tokyo, Japan). To illustrate the visually noticeable compositional change in constructs over the first three months of culture, photographs were taken using the Bruker M4 Tornado μXRF built-in camera, equipped with strong

lighting source (Bruker Instruments, Germany). Pictures were taken before chemical mapping of whole constructs, which will be discussed in Chapter V, *Characteristics of the Newly-Formed Matrix*.

3.4 RESULTS AND DISCUSSION

Early developmental events commence with remodelling of the callus-like matrix following cell attachment to the scaffolds. The presence of the two calcium phosphate anchors causes the cells to contract the matrix around the two holding points (Figure 3.1a). Cell-seeded constructs which are not provided with the anchorage points assemble into spherical structures (Figure 3.2a), as demonstrated in previous work (Wudebwe, Bannerman et al. 2015). Over time, this retention results in the formation of tensile forces in the soft tissue between the two anchors, which causes alignment at the cellular and molecular level along the direction of the force (Figure 3.1b and Figure 3.3b). Unanchored constructs do not show this complex organisation (Figure 3.3a).

Early mineralization started adjacent to the bone-like anchors between days 7-10, and progressed over the subsequent days as mineral nodules formed throughout the structure (Figure 3.1b-c). The initial fibrin scaffolds became visibly transformed during the first 3 weeks from the anchors towards the centre, until the structures became completely opaque at 3 months (Figure 3.1d).

The use of cells extracted from the periosteum of rats was advantageous for this system as these animals contain a much higher proportion of cortical bone (72%) compared to humans (12.5%) that is evenly distributed across many regions, compared to humans bones, which can show mm-thick differences between different anatomical portions (Bagi, Wilkie et al. 1997). This feature made the isolation procedure more constant and reproducible. In terms of cell activity, because biomineralization and metabolic processes take place much quicker in rodent cells compared to human ones (bone turnover in rats is several times higher)(Takakura, Takao-Kawabata et al. 2016), they are able to quickly adapt cortical and periosteal thickness via modelling-mediated

periosteal apposition in order to increase inertia and meet mechanical demands (Bagi, Wilkie et al. 1997). As such, the tension-induced biomineralization in this system should be observed more rapidly using rat cells compared to human cells. Indeed, the compatibility of primary, human-derived cells has been tested in this system and these observations are mentioned in *Chapter 10 – Further work*. Results from these quick experiments suggest that human osteoblastic cells can attach to and remodel the matrix in a similar way to rodent cells, however, the rate of contraction is less consistent across construct populations and develops over much longer time scales. Unlike rat cell constructs, human constructs require approximately 3 weeks for full contraction.

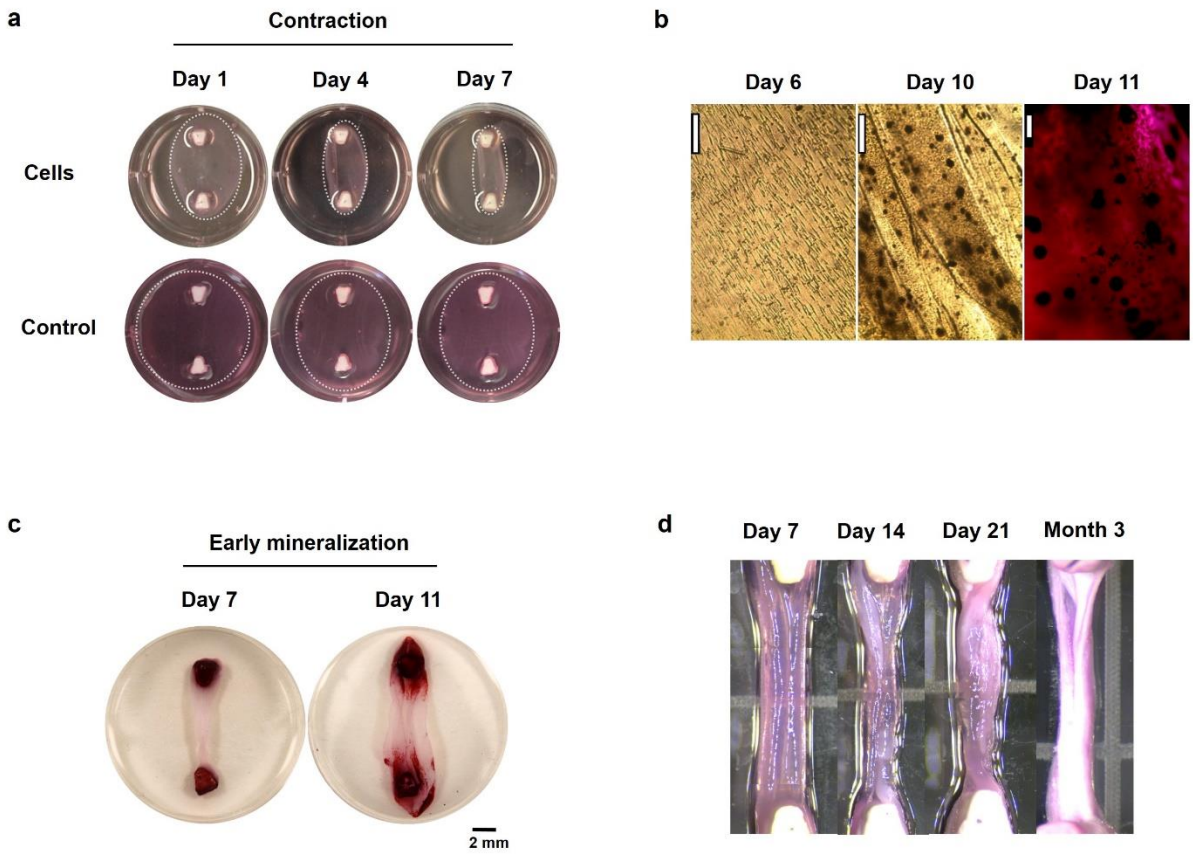

Figure 3.1 | Early construct development. a, Fibrin scaffold is reorganized around the retention points over the first week in culture. Control constructs, developed without cells showed a small degree of contraction over 7 days, but remained as flat gels and did not assemble into 3D structures. **b**, Tensile forces between the two anchor points cause cell alignment before day 6 (**left**). Mineralization nodules are observed throughout the structure after 10 days (**middle**). **c**, Mineral deposits are not noticeable following 7 days but individual mineralization points can be observed 4 days later in the close proximity of the calcium phosphate source. Scale bars **b** = 50 μm (Day 6, 10), 200 μm (Day 11). **d**, Changes in the fibrin template are visually noticeable at 14 days, with a distinct matrix forming from the anchor regions towards the centre, until the constructs appear to be fully covered with the new matrix at 3 months.

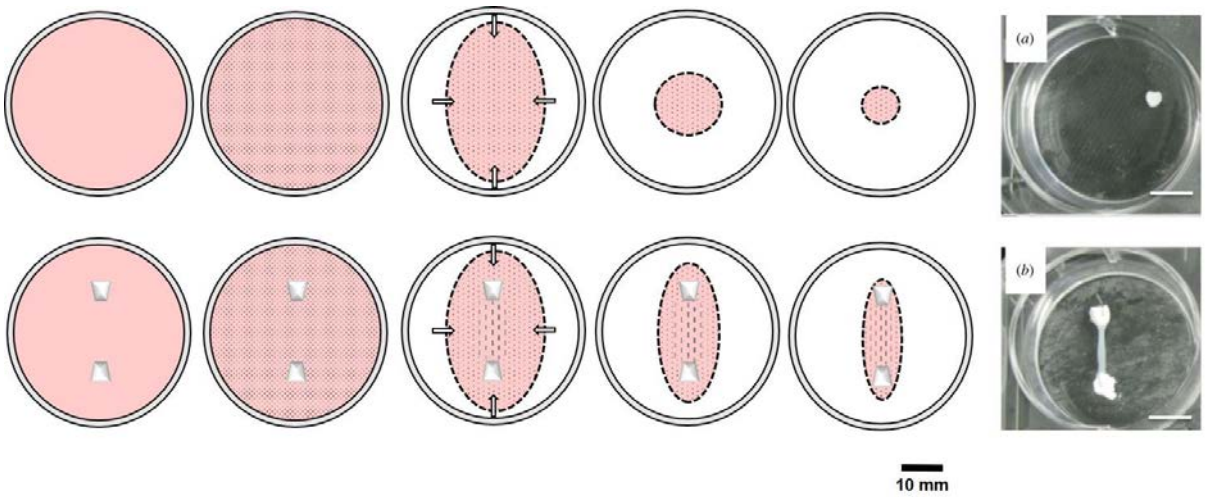

(Wudebwe, Bannerman et al. 2015)

Figure 3.2 | The effect of CaP anchors on matrix contraction and alignment. Previous work has demonstrated that in the absence of anchors (illustrated in the diagram series in the top row), cells contract the fibrin scaffolds over three weeks into spherical structures (a), whereas the provision of the 2 retention points (bottom row) allows the formation of a cylindrical structure in-between the two calcium phosphate structures (b). Scale bars = 10 mm. Images *a* and *b* are taken from (Wudebwe, Bannerman et al. 2015).

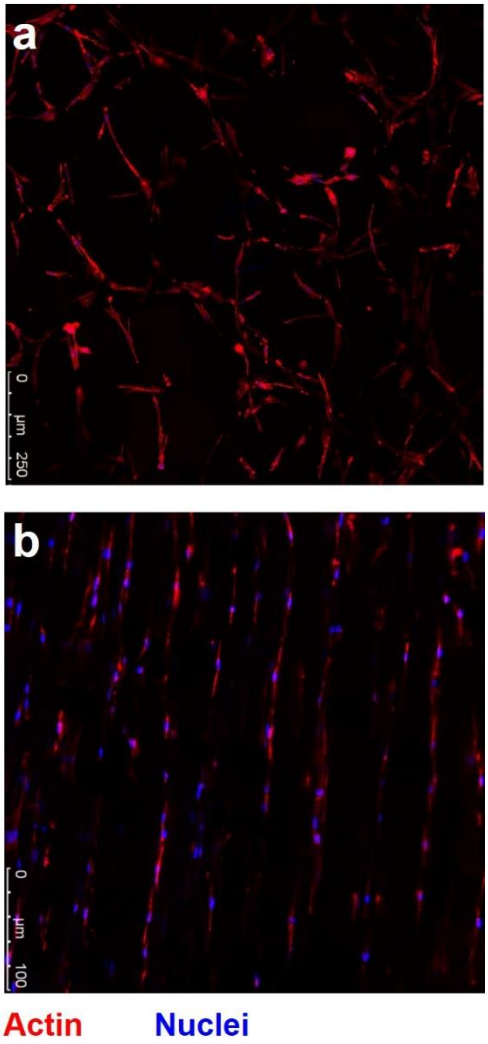

(Iordachescu, Amin et al.)

Figure 3.3 | Anchors are required for cellular alignment in constructs. Previous work has demonstrated using immunofluorescence staining that the formation of tensile forces during contraction causes alignment at a cellular level, with the cytoskeleton and nuclei arranged along the direction of force. Confocal microscopy images of (**a**) disordered cells in unanchored constructs at day 0 and (**b**) elongated, highly aligned cells in anchored constructs at day 18.

Images *a* and *b* are taken from Iordachescu A., Amin D.H., Rankin S.M., Williams R.L., Yapp C., Bannerman A., Pacureanu A., Addison O., Hulley P.A., Grover L.M. *An in-vitro model for the development of mature bone containing an osteocyte network.* Advanced Biosystems (2017).

CHAPTER IV

LONG-TERM STRUCTURAL AND CHEMICAL EVALUATION

4.1 INTRODUCTION

Early results indicated marked changes in the matrix of constructs during the first culture month. To determine whether this visually distinct matrix was composed solely of inorganic components or whether organic matrix was being produced at the same time, the density of the matrix was probed by applying non-destructive X-ray imaging to create 3D density-based reconstructions of whole constructs, at a scale of high resolution, and without interfering with the construct chemical composition, thus keeping constructs intact. Additional non-destructive imaging and spectroscopic techniques were employed to characterise the formation of bone in 3D, in intact constructs. These include micro-X-Ray Fluorescence, Two-Photon Microscopy, but also physico-chemical technologies which have only recently been employed to study disease processes, such as Raman spectroscopy.

4.1.1 MICRO-COMPUTED TOMOGRAPHY

The underlying principle of tomographic analysis (CT) is that the X-rays applied to the sample are attenuated at different rates depending on the density of the tissue they are passing through. As the object is rotated during scanning, thousands of images are acquired from numerous angular views, creating stacks of virtual cross-sections which are then integrated to give the final volume. Thus, internal structure can be analysed and fine scale details are significantly more visible compared to conventional microscopy (Campbell and Sophocleous 2014, Peyrin, Dong et al. 2014), without the need to interfere with the sample during processing. Moreover, morphometric parameters can be quantitatively analysed following reconstruction, something that will be discussed in more detail in *Chapter IX – Administration of ossification-inhibiting compounds*.

4.1.2 RAMAN SPECTROSCOPY

Raman spectroscopy is a technique which can detect specific chemical groups associated with mineral formation and the deposition of matrix components by detecting the vibrational bands associated with bonds between molecules (Morris and Mandair 2011). It has also been recently employed in understanding the molecular mechanisms of heterotopic ossification in wound injuries caused by blast overpressure and bone formation in general (Crane, Popescu et al. 2006, Crane, Polfer et al. 2013).

The technique is based on using monochromatic light (in the case of this work, a near-infrared laser) to exploit the effect of inelastic scattering (Butler, Ashton et al. 2016), which concerns the excitation of photons to virtual energy states. The laser light interacts with the vibration associated with chemical bonds between molecules in the

sample, which causes the energy of the laser photons to fluctuate higher or lower (Figure 4.1). This shift in energy can reveal biochemical information based on the vibrational models of the polarisable molecules (Butler, Ashton et al. 2016).

Because this technique has a high molecular specificity and because different biological materials have a characteristic Raman spectrum, this technique is exceptional for both qualitative and quantitative analysis of biological materials which are different at the molecular scale. Biological samples tend to occupy the 400 – 2000 cm^{-1} region of the Raman spectrum, with proteins appearing between 1500-1700 cm^{-1}, carbohydrates between 470-1200 cm^{-1}, and phosphate groups associated with mineralisation between 950-970 cm^{-1} (Morris and Mandair 2011, Butler, Ashton et al. 2016).

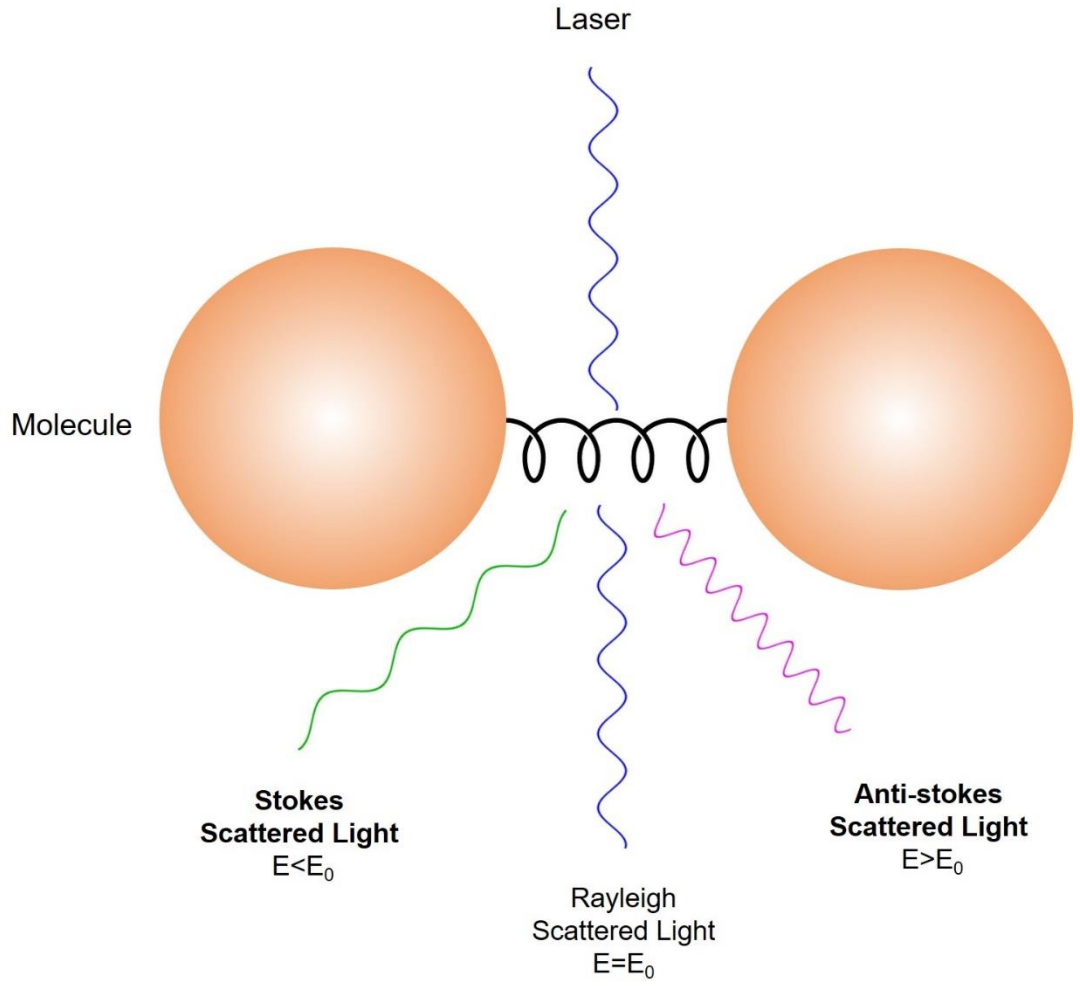

Figure 4.1 | Inelastic scattering in Raman spectroscopy. This technique uses monochromatic light (laser) to excite photons to virtual energy states. When photos are scattered from a molecule most of them are elastically scattered (Rayleigh scattering), having the same energy (frequency and wavelength) as the incident photons. A very small proportion of these photons (1 in 10 million) are scattered inelastically (Raman scattering), which involves the loss (Stokes) or gain (anti-Stokes) of energy due to the interaction of light with vibrations associated with bonds within the sample.

4.1.3 SECOND HARMONIC IMAGING AND TWO-PHOTON EXCITATION FLUORESCENCE

Multi-photon microscopy was employed to image collagen in 3D in live constructs by making use of the non-linear optical effect known as second-harmonic generation (SHG) generated exclusively by collagen when exposed to a laser of an infrared/near-infrared wavelength (Chen, Nadiarynkh et al. 2012). This optical phenomenon in microscopy was first described in 1978 (Gannaway and Sheppard 1978). Generation of a second harmonic takes place when the incident light used has an electrical field of sufficient power to cause molecular deformations (Cox and Kable 2006). If the molecule is not symmetrical (i.e. non-centro-symmetrical), the resulting anisotropy creates an oscillating field at twice the frequency and half the wavelength, the second harmonic (Cox and Kable 2006). Individual non-centro-symmetric molecules of collagen, arranged in a triple helix, are able to generate very strong SHG signals (Figure 4.2).

Where structural information was necessary, such as the spatial dynamics between osteoblasts and their secreted matrix protein, second harmonic imaging was used in combination with an additional high-resolution optical technique, two-photon excited fluorescence (TPEF) (Denk, Strickler et al. 1990, Gauderon, Lukins et al. 2001), which allowed the simultaneous visualization of collagen and viable cells, stained with a cell-permeant fluorescent dye (Calcein AM), at a cellular resolution but over the tissue length scale.

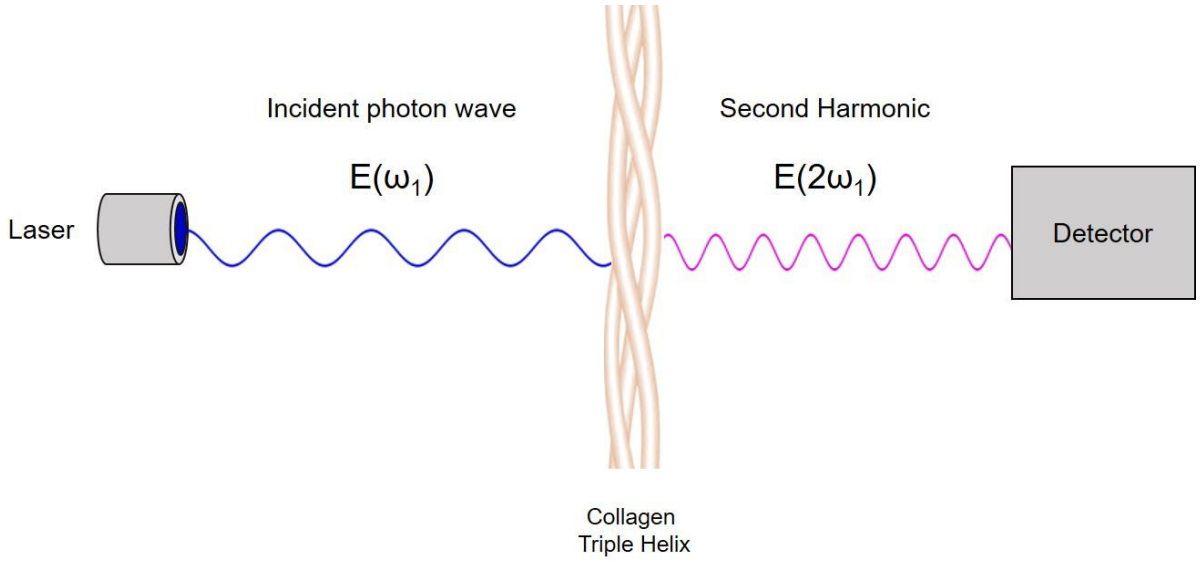

Figure 4.2 | The optical effect of Second Harmonic Generation. Collagen has a molecular structure (triple helix) which is non-centro-symmetrical. The incident monochromatic light emitted by a laser interacts with collagen and creates an oscillating field at twice the frequency and half the wavelength.

4.1.4 MICRO X-RAY FLUORESCENCE MAPPING

Novel techniques such as micro-X-Ray Fluorescence (μ-XRF) spectroscopy have been traditionally used in archaeology for resolving the chemical composition of valuable artefacts (Shackley 2014), and recently for quantitating elements in Leonardo da Vinci's most famous paintings, using specifically designed algorithms (de Viguerie, Sole et al. 2009, de Viguerie, Walter et al. 2010) (Figure 4.3b-d). This is due to the high accuracy of the technique, the ability to work on irregularly-shaped samples and the non-destructive properties. Although this technique can only provide information in the form on individual elements, it is extremely valuable for monitoring the temporal evolution of these elements, thus providing information on compositional changes. This technology was employed in this work to chemically map the inorganic composition of developing constructs over significant periods of time in a non-destructive manner based on the emission lines of calcium (Ca) and Phosphorus (P), the main constituents of calcium phosphates and bone mineral. The increased or decreased presence of these elements can give valuable structural information regarding the local formation of ossified matrix. The principle by which X-Ray fluorescence works is based on the response of atom excitation by high energetic radiation (Figure 4.3a), which generates a vacancy in the affected shell as a photoelectron is ejected. This vacancy is filled by electrons from outer shells, a process that is accompanied by the emission of a characteristic X-Ray photon, otherwise known as X-Ray Fluorescence. This fluorescence is different for each element and the yield depends on the atomic number, that is, a high atomic number generates high fluorescence and low atomic number elements generate low levels of fluorescence. When the transition of an electron takes place from the outer L layer to the K layer, the emission line is known as the K_α emission line, whereas when

electrons from the outer M shell jump to occupy the vacant position the emission line is known as K_{β}.

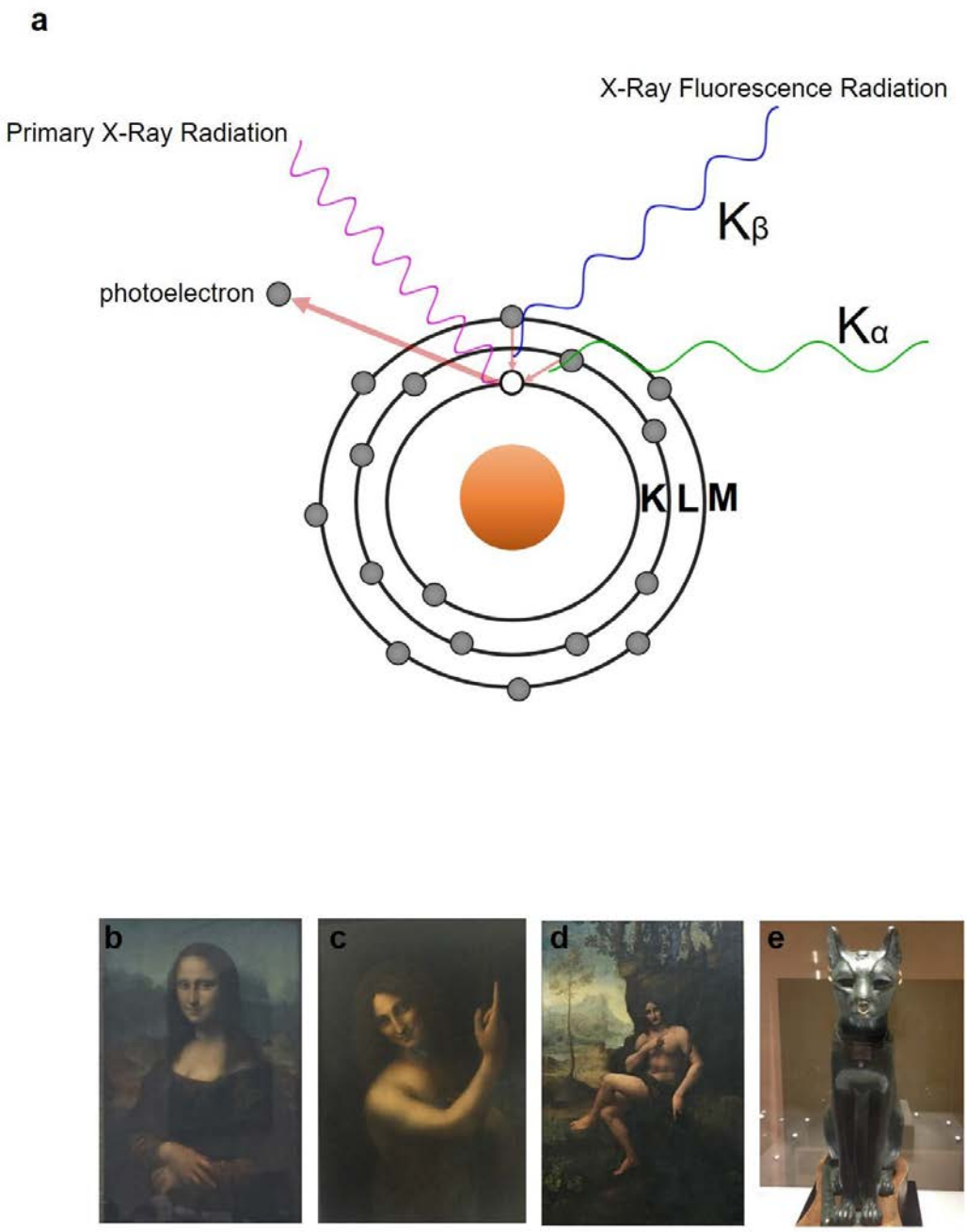

Figure 4.3 | Applications of non-destructive XRF. a, XRF follows a series of processes including a photoelectron ejection from the atomic shell exposed to high-energy primary X-Ray radiation and the subsequent 'jump' of an outer electron from the near shells in order to fill this vacancy. The process is associated with the emission of X-Ray Fluorescence, with different characteristics for each chemical element. When the jump takes place from the L to the K layer, it is known as the Kα emission line. When an electron from the M layer jumps to fill the place, the emission line is known as Kβ. **b-e**, Due to its non-destructive properties and highly accurate detection levels, this technique has been recently applied to some of the most valuable historical artefacts and paintings, including Mona Lisa (**b**), St. John the Baptist (**c**), Bacchus (**d**) and the Gayer-Anderson cat (**e**). *Original images. Author would like to thank the Louvre Museum, Paris and the British Museum, London.*

4.2 AIMS AND OBJECTIVES

The aim of this work was to observe the structural evolution of the cell-seeded fibrin matrix over extended periods of time (1 year) and to monitor the concomitant evolution of the newly forming matrix longitudinally. Micro-computed tomography (μCT) was one of the many techniques used in this work for assessing maturation the cell-produced matrix. Density-based inspections and comparison with the inorganic component (anchors) were used to estimate the temporal maturation of the ossified component. The subsequent goals were to identify the composition, organisation and pattern of deposition of the new matrix in early and mature stages. Preliminary work was conducted in all cases to optimize the system for use with different analytical and imaging techniques, on aspects including sample preparation, determination of suitable sample holders and positioning of sample.

4.3 CHARACTERISATION METHODS

4.3.1 MICRO-TOMOGRAPHIC ANALYSIS

A micro-Computed Tomography (μCT) system (SkyScan 1172, Bruker Instruments, Germany), was used to evaluate mineralization and matrix development in constructs over time. Constructs were removed from the culture medium and were placed vertically inside plastic tubes, on a rotating stage located at 260.650 mm distance from the X-ray source and 347.109 mm from the detector. High-resolution scans were performed at ambient pressure using the cone-beam imaging system, composed of a Hamamatsu X-Ray source with a voltage of 80 kV and a tube current of 100 μA. The X-Ray detector consisted of an 11 Mp X-Ray camera of a 9.01 μm pixel size, generating images of 6.76 μm pixel size. 2D cross-section slices of the constructs were acquired at a rotation step of 0.2 degrees, with 2 frames averaging per step and an exposure time of 1050 ms. Acquired images were 3D reconstructed using the Bruker micro-CT NRecon Software (v. 1.6.10.2). For removal of scanning artefacts, several reconstruction parameters were adjusted during reconstruction. The beam hardening parameter was set to a value of 30 to correct for the surface-to-depth density gradient caused by increased X-Ray attenuation at the surface of the constructs. A ring artefact correction was set to a level of 9. The smoothing parameter was adjusted to a value of 4. These optimized, construct-specific settings were used for all time points investigated.

4.3.2 RAMAN SPECTROSCOPY

Confocal Raman spectroscopy was used to detect and spatially resolve specific chemical groups associated with mineralized collagen deposition through the constructs. Maps and spectra were acquired using a confocal Raman microscope (Alpha 300R, WITec, Ulm, Germany), equipped with an Acton SP2300 Imaging Monochromator/ Spectrograph (Princeton Instruments, MA, USA), fitted with a 300g/mm with 750nm blazing grating, and a 785nm 250mW diode laser (XTRA II, Toptica photonics, Munich, Germany). Spectra were acquired from various points on the constructs, including the anchor; the interface between the anchor and the soft tissue and the central portion, via a 20X (NA = 0.45) objective lens and using an integration time of 3s and 20 accumulations. Data was accumulated and exported using the WITec Control software version 1.6 (WITec, Ulm, Germany).

Raman maps of whole constructs (Large scale image scans) were acquired by rastering the beam over the samples via the 20X (NA = 0.45) objective lens with a 20μm step size and accumulating 3 spectra with in integration time of 0.5 seconds at each point. The laser power was measured at 60mW (standard deviation 0.06mW) at the back aperture of the objective lens. The data was accumulated using the WITec control version 1.6 software (WITec, Ulm, Germany). To prevent sample movement during the long scan times, the slides the samples were mounted on were clamped to the stage with Blu-Tack. In all cases, map data acquisition involved between 3 and 4 days of continuous, uninterrupted scanning. Spectral data cubes were pre-processed to remove cosmic rays using the instrument associated software (Witec Project v2.10., Witec, Ulm, Germany).

4.3.3 SECOND HARMONIC IMAGING AND TWO-PHOTON EXCITATION FLUORESCENCE

A multi-photon microscopy system was used to observe collagenous matrix formation in constructs using the optical effect of second harmonic generation (SHG). To concomitantly visualize collagen and cells, constructs were stained with the fluorescent dye Calcein AM (Sigma-Aldrich, Germany) at a ratio of 2 µl/ml of Opti-MEM culture medium (Gibco, Thermo Fisher Scientific, USA) to assess viability and distribution of cells. The microscopy system consisted of a Zeiss LSM710 NLO (Zeiss Gmbh, Germany) coupled to a Ti:Sapphire mode-locked Coherent Chameleon Vision II laser. Collagen and fluorescent cells were imaged using second harmonic generation (SHG) and two photon excitation fluorescence (TPEF) between 385-475 nm and 480-655 nm respectively. Photons were collected through a 10x Plan Apo 0.45 N.A. and the two-photon laser was tuned at 860 nm. The presence of collagen was confirmed by spectral imaging and collecting the second harmonic signal at 430 nm via a 10x Plan Apo 0.45 N.A. or 40x Plan-Apo 0.95 N.A. objective. Where z-stacks were acquired, a slice interval of 6 µm was used. Images were visualised in ZEN 2009. Cell viability measurements were taken at different time points using Calcein AM, as described above and imaging was performed using either the Zeiss LSM710 NLO or a Leica DM2500/TCS SPE Confocal (Leica Microsystems, Wetzlar, Germany). Where z-stacks were acquired, a step size of 0.50 µm was used and excitation was performed using a 488 nm laser.

4.3.4 ELEMENTAL CHARACTERIZATION USING MICRO X-RAY FLUORESCENCE

A micro X-ray fluorescence (μ-XRF) system (M4 Tornado, Bruker Nano Gmbh, Berlin, Germany) was used to generate spatially-resolved elemental maps of constructs and to investigate mineral and organic matrix distribution using the localization of Ca, P and S in constructs.

The machine contains a Rhodium μ-focus X-Ray tube and a polycapillary lens, used to focus the X-Rays to a spot size of 25 μm. Recordings were taken without sample processing, at room temperature and ambient pressure. The X-Ray tube voltage used was 50 kV and tube current was 400 μA. μXRF spectra and maps from constructs of different ages were acquired using a 50 μm spot distance, 25 μm spot size and 50 ms/pixel exposure time.

Elemental maps were formed in real time by integrating the photon counts around the emission lines of: Calcium ($K\alpha_1$ 3.692 keV), Phosphorus ($K\alpha_1$ 2.010 keV), Sulphur ($K\alpha_1$ 2.309 keV), generating an image where pixel intensity was proportional to the number of X-Ray counts/second per electronvolt (eV) from each measured point on the construct. Thus, pixel intensity increased with X-Ray counts, with maximum pixel intensity normalized to the highest count rate per eV for each element of interest, across the entire construct.

4.3.5 HISTOLOGICAL DETECTION OF COLLAGEN

Sirius Red dye was used to detect collagen synthesis in constructs. Sirius Red dye (Direct Red 80, Sigma- Aldrich, Germany) was dissolved in saturated aqueous picric acid at a concentration of 100 mg/100 ml. Constructs were rinsed with PBS and fixed with 2 ml standard Bouin's fluid for 1 hour at room temperature. The fixation fluid was aspirated and constructs were washed with dH_2O for 15 minutes. 2 ml of dye was added per construct and the recipients were placed on a plate shaker for 1 hour (100 RPM). The excess liquid was removed and the unbound dye was removed by rinsing with 2 ml 0.01 N hydrochloric acid. Collagen deposits were visualized under the microscope.

4.4 RESULTS AND DISCUSSION

The evolution of mineral and matrix in constructs over time is presented in Figure 4.4, which contains microtomographic 3D reconstructions of early (12-15 days) and mature constructs (3 months-1 year) developed with periosteal cells. These high-resolution microtomographies, acquired at sequential time points, also showed, similarly to whole-mount histology, that mineralized matrix started forming in early stages (12-15 days) at the calcium-phosphate extremities in the absence of further osteogenic supplementation (Figure 4.4a-c). This matrix advanced with further osteogenic supplementation throughout the entire length of the constructs, until the structures became fully ossified after approximately 3 months (d-e). The initial fibrin structure became gradually replaced with greater-density matrix (h-j), which after 3 months contained deposits of high density mineral independent of the main bone-like structure (k-l). Thus, a combination of clinically-relevant types of ossification were noticed in this system: the first type - starting from the bone-like ends- resembling fracture repair; as well as an isolated form, distant from the main bone-like structure, resembling mineral deposition in soft tissues as seen in ectopic ossification (Potter, Burns et al. 2007, Potter, Forsberg et al. 2010, Einhorn and Gerstenfeld 2015). During the subsequent culture period up to one year, this new matrix becomes very dense and compact (f-g/m-n), containing a high-proportion of mineral, particularly on the outside surface (g).

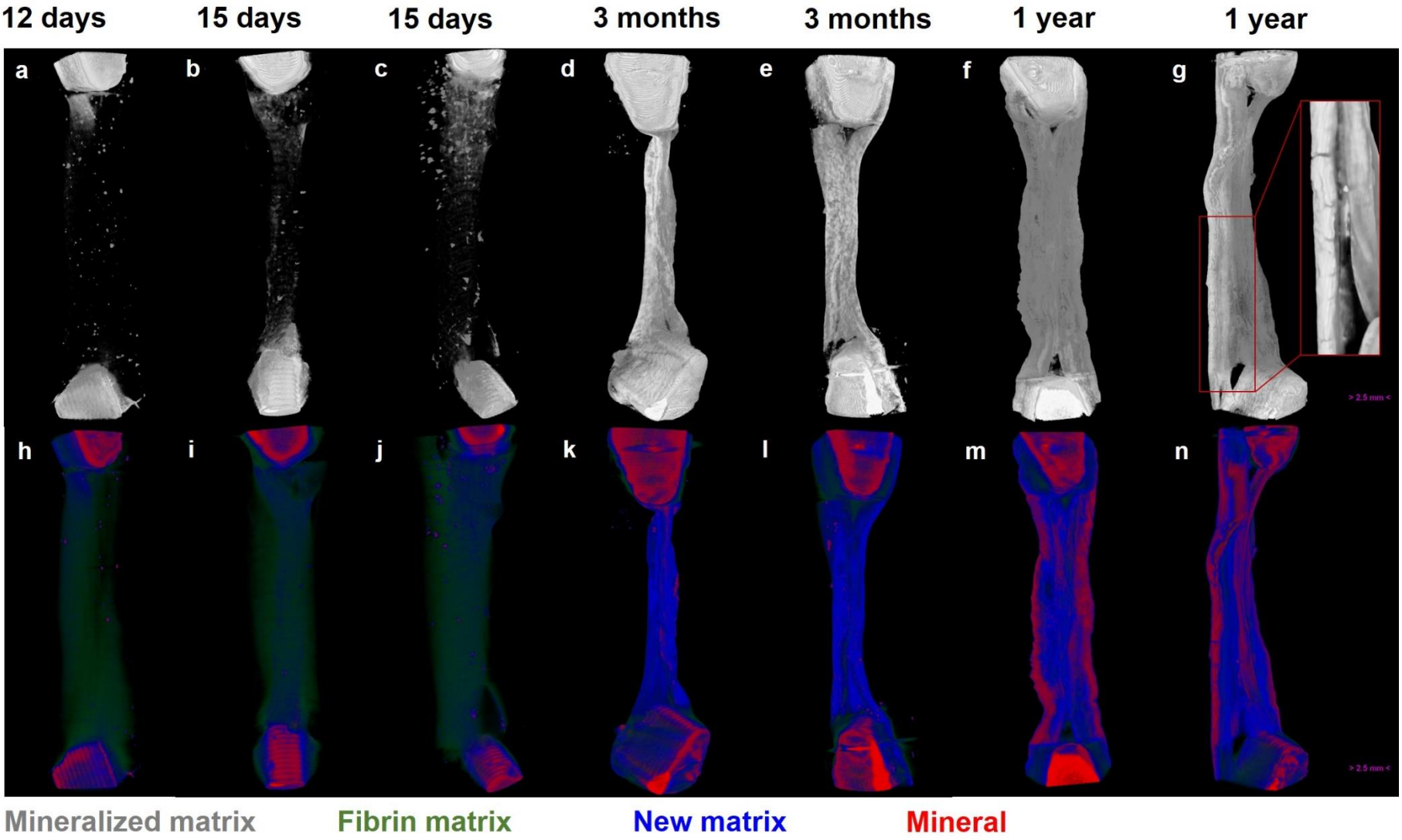

Figure 4.4 | Development of mineralization and matrix over time. a-n, Reconstructed μCT images of early constructs (days 12-15, **a-c/h-j**) and mature constructs (3 months – 1 year, **d-g/k-n**), illustrating the development of ossification over time. **a-e**, Mineralization starts at the anchors (**a**) and progresses over time throughout the entire length of the constructs (**b-c**) until the mineral covers the entire structure of constructs (**d-e**). Bottom panel presents colour-coded versions of the constructs above, illustrating the development of the new matrix over time. The fibrin template (green), which predominates after 15 days (**j**), is progressively replaced over time with new matrix (blue) (**h-j**) until it becomes completely substituted after 3 months with the new, denser matrix, which also contains discrete deposits of high-density mineral (red) (**k-l**). Following a year in culture, the constructs contain considerable amounts of the high-density mineral (**m-n**). Cropped section illustrates the high-density material comprising the outer layer of constructs after a year in culture. Scale bars = 2.5 mm.

As indicated by tomographic analysis, constructs became mineralized through a process that was more complex than a simple calcification, i.e. the precipitation of calcium phosphate compounds on the fibrin matrix. Microtomographies indicated significant amounts of new, greater-density matrix co-localized with mineral deposits, which formed gradually throughout the culture period, indicating that a process of ossification was taking place. The nature and characteristics of these matrix components were analysed through a combination of molecular, spectroscopic and optical methods, which revealed an abundance of structural proteins associated with the extracellular matrix of connective tissues.

Figure 4.5a illustrates a comparison between the novel matrix observed in early stages (15 days) using μCT, and a high-resolution compositional Raman map developed based on the signal corresponding to one of the organic components identified in abundance, CH_2 (1447 cm^{-1}), indicative of collagen. The latter analysis revealed that a higher amount of this compound was distributed in a similar pattern observed with CT, at this equivalent time point. In bone, collagen is produced by osteoblastic cells during the assembly of the extracellular matrix (ECM) and accounts for approximately 90% of the organic component (Boskey 2013). As such, its simultaneous deposition with the early mineral can be used as an indication of early ossification. Spectral analysis of constructs which had just completed undergoing the contraction phase (7 days), revealed that the CH_2 band was accompanied by other bands such as amides I and III (1646 cm^{-1} and 1316 cm^{-1} respectively), proline and hydroxyproline (861 cm^{-1} and 872 cm^{-1}, respectively), major components of collagen, and later, at day 12, by phosphate compounds in the central and interface regions, indicative of mineral formation and co-localised with the organic components (Figure 4.5b). All the mineral detected using

Raman spectroscopy at these early time points was different from the anchor material (Figure 4.6), the majority being octacalcium phosphate (OCP, 954 cm^{-1}). OCP, $Ca_8H_2(PO_4)_6.5H_2O$ is a calcium phosphate with a Ca:P molar ratio of 1.33 and has been suggested a few decades ago to be to be an intermediate crystalline phase in hydroxyapatite formation in bones, enamel and dentin (Johnsson and Nancollas 1992). Fundamental studies by Eanes and colleagues in the 1960s-1970s (Eanes, Gillessen et al. 1965, Eanes and Meyer 1977) did suggest that in aqueous suspensions at physiological pH, the first crystals which form from amorphous calcium phosphate are strikingly different from apatitic crystals, in terms of morphology structure and solubility and molar ratio (1.4). These crystals then undergo a process of maturation to HA by becoming thicker, but smaller laterally and less soluble. The authors suggested OCP as an intermediate phase which subsequently hydrolyses to HA. However, the presence of OCP as an intermediate phase in the formation of bone and dentin mineral has been a subject of great debate over the subsequent decades and it has more recently been confirmed and described as taking place during *in vivo* mineralized tissue formation (Ban, Jinde et al. 1992), and in pathological dental and renal calcifications (Kani, Kani et al. 1983). It has also been identified using similar Raman spectroscopy analysis in cultured calvarial bone tissue explants (Crane, Popescu et al. 2006).

The presence of a novel phosphate phase in our system support a cell-mediated mineralisation, but also indicates an advantage of our system in terms of the ability to simulate the temporal evolution of bone mineral.

At the end of an initial month in culture, a regime of full osteogenic supplementation was commenced, containing additional ascorbate, β-glycerophosphate and dexamethasone. The purpose of this additional supplementation was to encourage

ossification to progress more rapidly towards the centre, at a point when the matrix was robust enough to maintain integrity during the rapid dissolution of the remaining fibrin caused by the new matrix replacement. Raman spectroscopic analysis performed following 2 months of supplementation revealed the presence of the complete set of peaks that have been reported to be present in mature bone, and in all regions investigated, including the centre (Morris and Mandair 2011, Crane, Polfer et al. 2013) (Figure 4.5c). Interestingly, the mineral detected at this time point was the complex bone hydroxyapatite (957-962 cm^{-1}), suggesting a maturation process from the intermediate phases, and was in all cases associated with collagen.

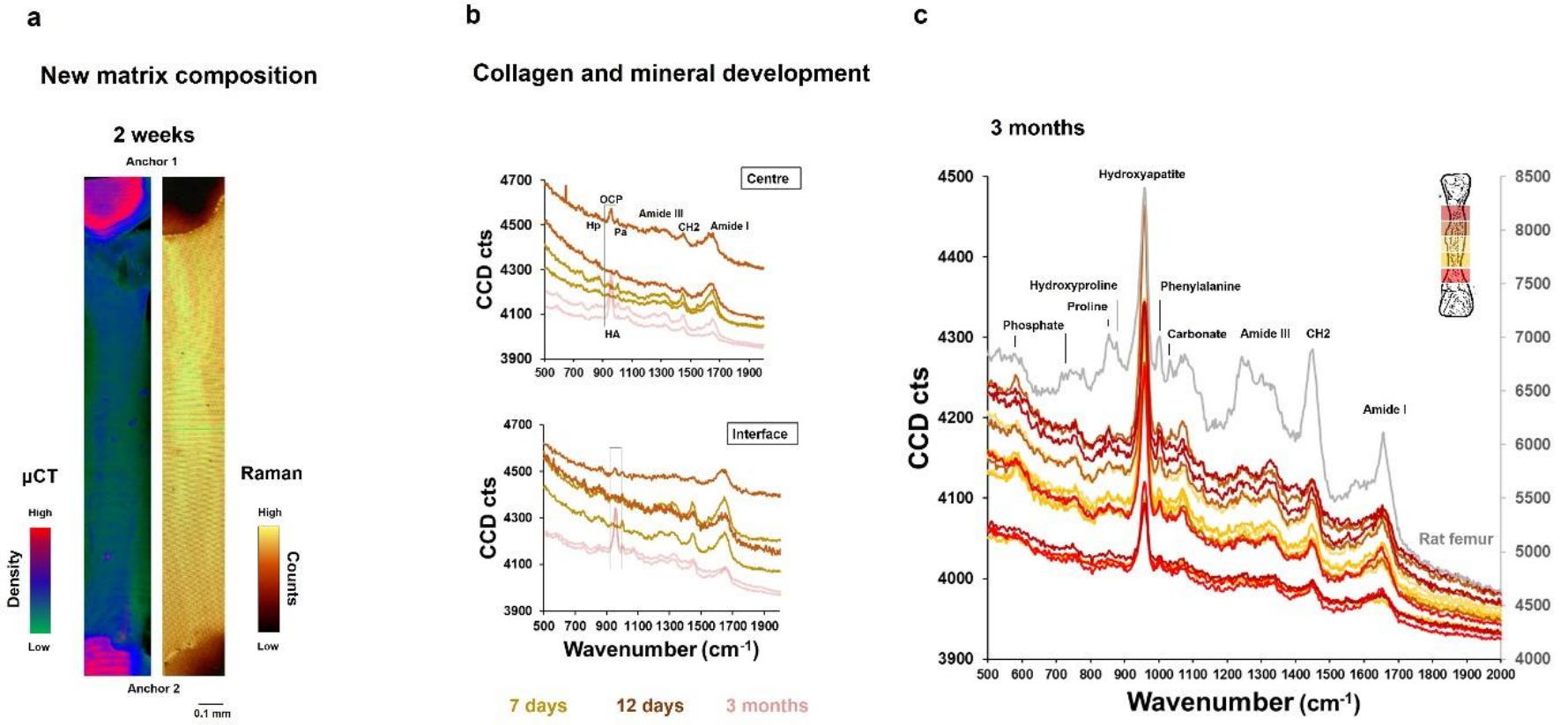

Figure 4.5 | Chemical characteristics of the newly forming matrix. a, Comparison of a microCT reconstruction and a high-resolution Raman map, developed based on the CH_2 peak (1447 cm^{-1}) showing a similar distribution of the denser, newly forming matrix in constructs which are 2 weeks old. **b**, As early as day 7 (yellow), peaks corresponding to collagen can be detected, including amide I, III, CH_2, but also hydroxyproline (Hp) and phenylalanine (Pa). 5 days later (day 12, brown), small phosphate peaks corresponding to OCP start to emerge in the central and interface regions. Spectra from mature (3 month constructs, pink) are provided for comparison**. c**, Spectra from spatially distinct regions from a mature construct (3 months) showing in all cases a strong hydroxyapatite content co-localised with all the components associated with collagen. Spectra contain all peaks detectable in bone using this technique.

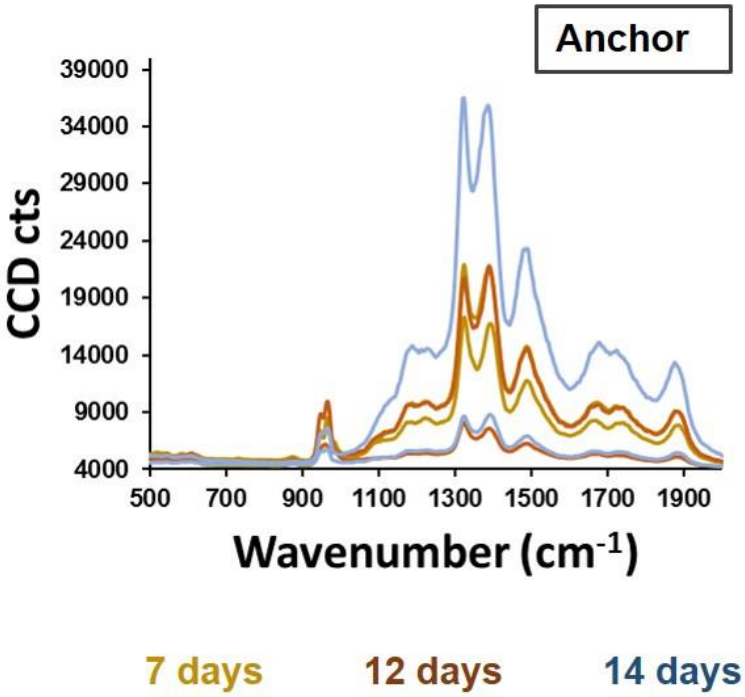

Figure 4.6 | Raman Spectra of the anchors of early constructs. Raman spectra acquired from distinct points on the anchor surface at 3 time points within the first two weeks of development revealed spectral characteristic for the brushite-TCP component, and different in all cases from the new mineral phases forming within the soft tissues.

In terms of localisation and organisation of collagen in constructs, as early as day 7, collagen was detected using whole-mount picrosirius red staining, abundantly around the edges in the vicinity of the two anchors (Figure 4.7a) and adjacent to the anchors, where it appeared to emerge from cell-like structures (Figure 4.7b). As mineral deposits composed of calcium phosphate advance towards the centre during the first month of culture (Figure 4.7c), the organic matrix progresses as well.

Three-dimensional second harmonic imaging of collagen and excitation fluorescence analysis of cells in constructs which were cultured for approximately one month, showed significant deposits of collagen arranged in pocket-like structures in the interface regions, surrounded by cells (Figure 4.7d illustrates an example). Further analysis using second harmonics (Figure 4.7e) revealed that the central region of constructs did not contain detectable deposits of collagen at this time point, indicating that the ossification had not progressed as far up to that time point, but also that the collagen species secreted by cells centrally had not reached the sufficient maturity (i.e. the non-centro-symmetrical, triple-helical structure) required to reflect half the wavelength of the incoming laser and thus to be detected using this technique (Denk, Strickler et al. 1990, Chen, Nadiarynkh et al. 2012).

Throughout the additional osteogenic regime, over the following months, ossification progressed at the mm scale until the two sides met centrally, showing the same pattern of organisation of collagen pockets as observed in murine femoral bones (Figure 4.7e). Together, these results suggest a progressive deposition and maturation of mineralised collagen as seen in bone formation and fracture repair (Phillips 2005).

The visualisation of collagen exclusively in the emission channel corresponding to the 432 nm wavelength (half of that of the incoming laser) for all samples investigated is presented in Figure 4.8 for validation.

Interestingly, over the following culture months up to one year the inorganic component proportion (calcium phosphate) increases to a level similar to that of mature murine femurs (Figure 4.9). This process will be discussed further in the following chapter, *Cellular development in constructs*.

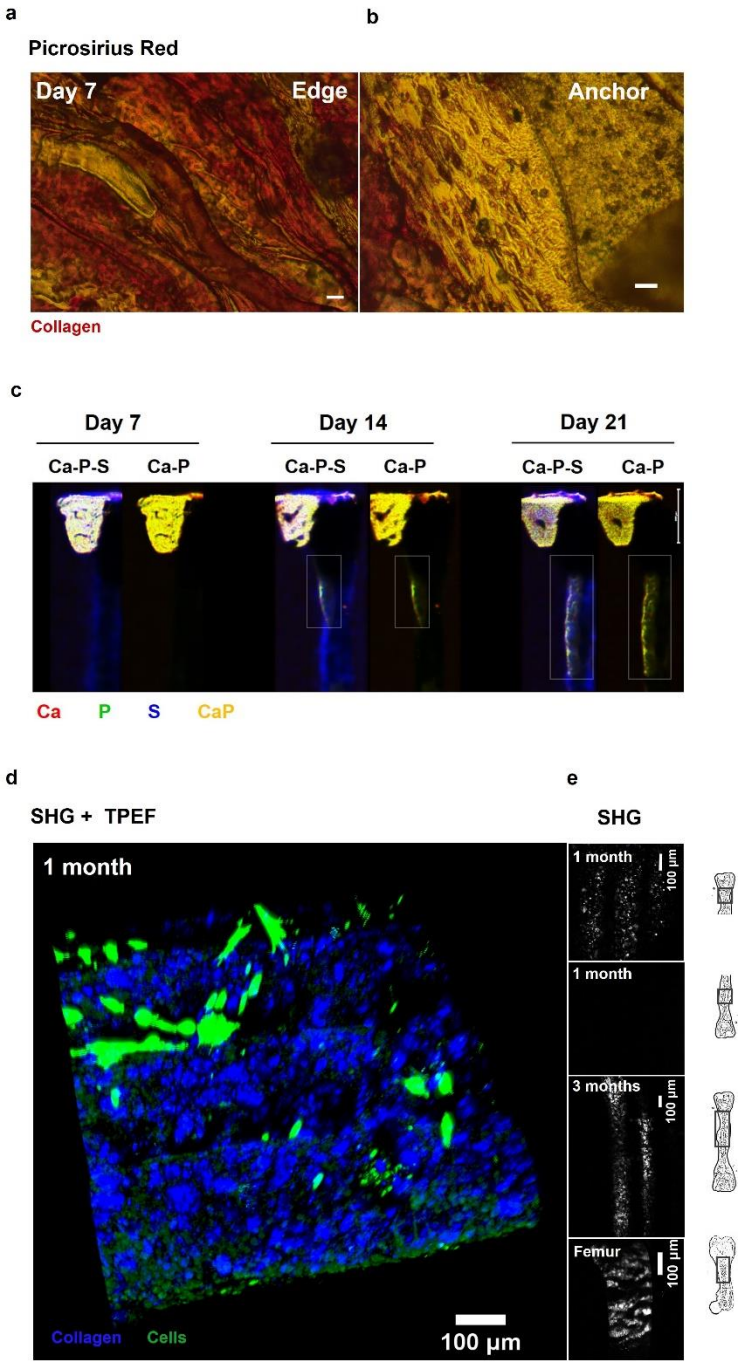

Figure 4.7 | Development of the collagenous matrix in constructs. a, Images of 7 day constructs stained with Sirius Red for collagen. Left image illustrates high amounts of collagen in the marginal region adjacent to the brushite anchor; right image demonstrates collagen emerging from cell-like structures next to the anchor. Scale bars = 200 µm. **b**, Micro-XRF mapping of live constructs over 21 days, based on Ca and P, the inorganic components of bone and S, as an indicator of the organic matrix. Maps show the progression and co-localisation of Ca and P from the anchor towards the centre during this period of development up to one month. Scale bar = 4mm. **c**, Two-photon microscopy 3D reconstruction of cells (TPEF) and collagen (SHG), simultaneously visualised in live constructs. Collagen is present in 'pocket'-like deposits. Scale bars = 100 µm. **d**, SHG visualisation of collagen in distinct regions at different time points. **e**, Collagen is abundant around the anchor areas in early stages, but not detected in the central region at 1 month. Over the subsequent 2 months, the collagenous matrix extends into the tissue at the mm level, displaying a level of organisation similar to murine femora.

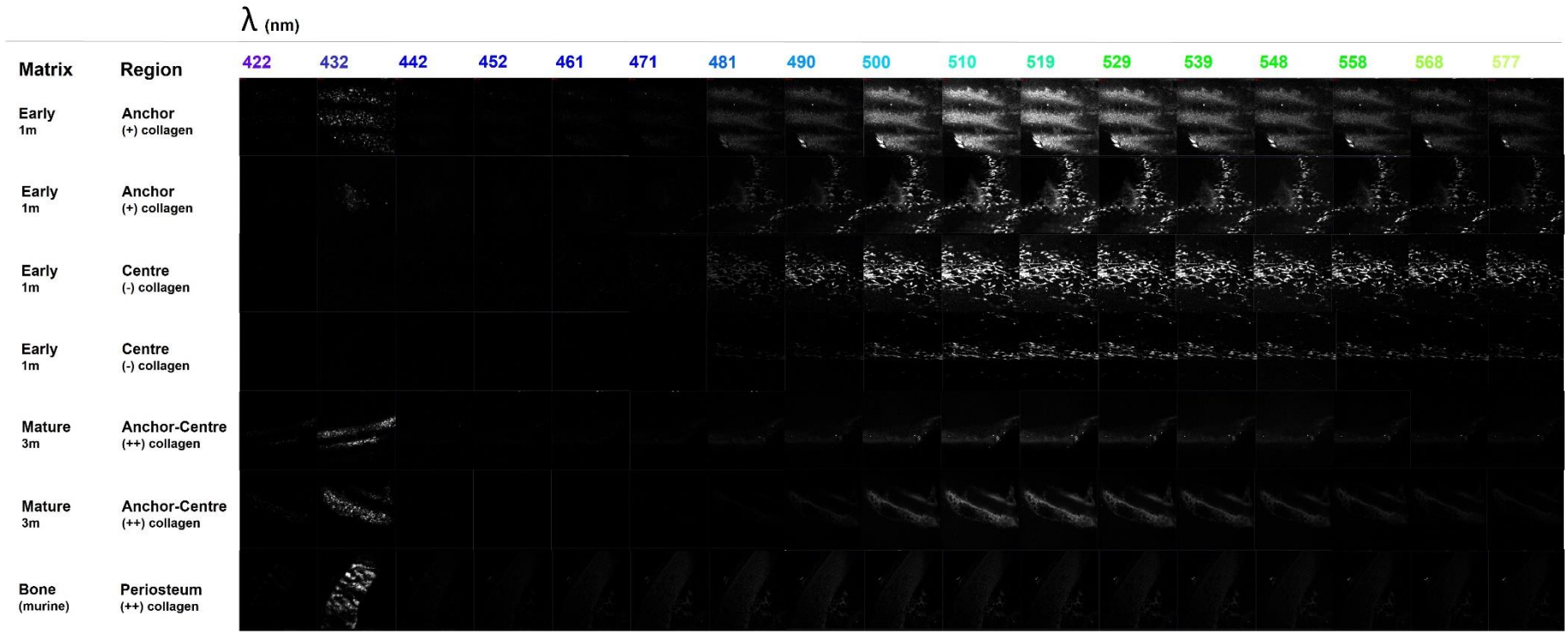

Figure 4.8 | Collagen and cells, observed using SHG/TPEF. Emission spectra of early and mature constructs in different regions, illustrating the second harmonic linear effect generated by collagen at half the wavelength of the incoming laser (860 nm), generated in the purple-blue area of the spectrum; and with Calcein AM green-stained cells appearing in the 481-577 nm region of the spectrum, corresponding to light blue-green region.

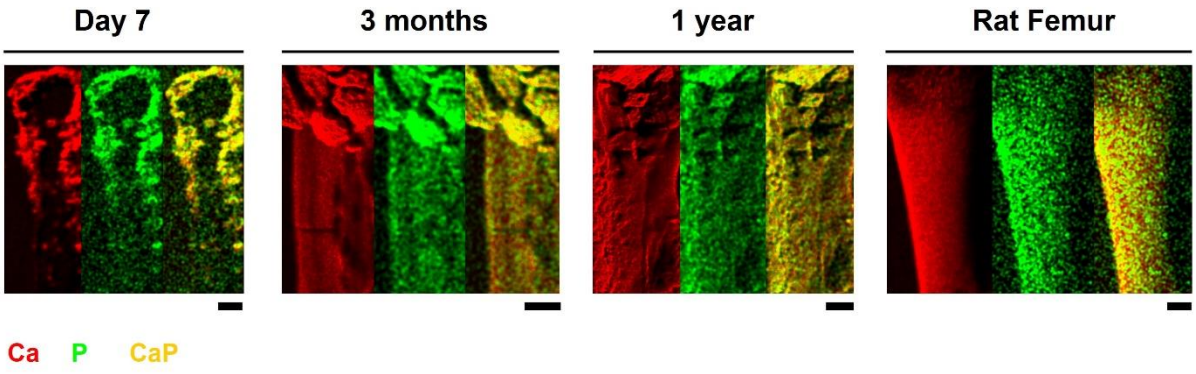

Figure 4.9 | Evolution of the inorganic component over a year in culture, as detected through micro-XRF. Calcium and Phosphorus, main components of the inorganic component of bone, increase with extended culture times until they reach a level similar to that of murine femurs.

CHAPTER V

CELLULAR DEVELOPMENT IN CONSTRUCTS

5.1 INTRODUCTION

During the culture period, the combination of biomechanical and chemical factors (i.e. presence of tensile forces, continuous source of calcium phosphates and osteogenic supplementation) ultimately had an influence on the specialization of the stem cells embedded in the constructs towards an osteoblastic lineage and subsequently recapitulated successive phases of ossification, including cell attachment to scaffold, clot remodelling and matrix production (Franz-Odendaal, Hall et al. 2006, Dallas and Bonewald 2010).

5.2 AIMS AND OBJECTIVES

The aim of this work was to monitor the evolution of the stem cells embedded in the constructs as the matrix changed locally and chemically. Of particular interest was to determine whether embedded cells can terminally differentiate to mature bone cells, osteocytes. The goal was to use a combination of molecular and imaging techniques to

analyse and visualise the maturation of the structures. Lastly, preliminary work was carried out to determine the best type of sample processing for mechanically characterising these 3D, matrix embedded mammalian osteocytes and their environment using atomic force microscopy (AFM) mapping.

5.3 CHARACTERISATION METHODS

5.3.1 REAL-TIME PCR (qPCR)

5 months (n=4) and 12 months (n=2) constructs were removed from culture media and the calcium phosphate anchors were cut out of the tissue and discarded. Tissues were snap frozen by submersion in liquid nitrogen for 1 minute, then rapidly pulverized using a multi-sample biopulverizer (BioSpec Products Inc., OK, USA). mRNA extraction was performed using a Dynabeads® mRNA DirectTM detection kit. The powdered tissue extract was added to 1 ml of a lysis/binding buffer containing 100 mM Tris-HCl, pH 7.5; 500 mM LiCl; 10 mM EDTA, pH 8; 1% LiDS; and 5 mM dithiothreitol (DTT) and was gently vortexed for 2-3 minutes until complete lysis was obtained. The viscosity of the solution was reduced by a DNA-shear step by passing the lysate 3 times through a 21-gauge syringe needle. The fragments of tissue that were not lysed were pelleted by 10 seconds centrifugation and the supernatant was separated.

mRNA isolation was performed by mixing the lysate with 1 mg superparamagnetic beads (Dynabeads®, approx. 2.8 μm diameter) which were covalently coupled to Oligo $(dT)_{25}$ residues, having a capacity of binding a maximum of 2 μg mRNA. Beads were previously removed from the PBS storage suspension (pH 7.4) using a Dynabeads MPC-S magnetic particle concentrator (Dynal AS Oslo, Norway), washed with the lysis/binding buffer and then re-suspended in the crude lysate. Each lysate was incubated with the beads at room temperature for approximately 5 minutes, by continuously mixing on a rotating platform to allow the polyA tail at the 3' end of the mRNA to hybridize to the Oligo $(dT)_{25}$ residues on the beads. The supernatant was then

removed by concentrating the mRNA bound beads at the magnet site and the beads were then washed one time with 500 µl of a buffer solution containing 10 mM Tris-HCl, pH 7.5; 0.15 M LiCl; 1 mM EDTA; 0.1% LiDS; and twice with 500 µl of a buffer solution containing 10 mM Tris-HCl, pH 7.5; 0.15 M LiCl; and 1 mM EDTA. RNA-bound beads were isolated using the magnet, washed in an enzyme-free RT buffer and then re-suspended in a solution containing a reverse transcriptase (RT) polymerase in order to proceed with cDNA synthesis. cDNA synthesis was performed directly on the bead bound mRNA using a SuperScript Reverse Transcriptase kit (Invitrogen, Thermo Fisher Scientific, CA, USA), using 1 µl 10 mM dNTP mix (dATP, dGTP, dCTP, dTTP), 12 µl dH_2O, 4 µl 5X first strand buffer (250 mM Tris-HCl, 375 mM KCl, 15 mM $MgCl_2$), 1 µl 0.1 M DTT, 1 µl RNAse out (40 U/ µl) and 1 µl of the SuperScript RT enzyme (200 U/ µl).

cDNA was synthesized by incubating the 20 µl reaction volume using a Veriti thermal cycler (Applied Biosystems, CA, USA), at 50°C for 5 minutes, 55°C for 20 minutes and 75° for 15 minutes. Amplification of cDNA was performed using a ViiA 7 real-time PCR instrument (Applied Biosystems, CA, USA). The PCR reaction consisted of 2 µl cDNA template, 6 µl dH_2O, 10 µl fast SYBR green master mix (containing a mixture of the SYBR Green I dye, AmpliTaq fast DNA polymerase, Uracil –DNA glycosylase, Rox dye and dNTPs) (Applied Biosystems, CA, USA) and 2 µl rat primer (GAPDH (QT00199633) /SOST (QT00418558) /PDP (QT00174706) (Qiagen, Manchester, UK) and beta-actin (QT00193473) previously reconstituted in Tris –EDTA (TE) buffer, pH 8.1 (Alfa Aesar, MA, USA).

As positive control, cells from an osteosarcoma cell line positive for SOST and PDPN, UMR-106, were used and mRNA was extracted and processed in an identical manner.

These cells were obtained from the American type culture collection (ATCC) and were cloned derivatives of a transplantable rat osteogenic sarcoma.

Data was recorded and analysed using the QuantStudio real-time PCR software, version 1.2 2015 (Applied Biosystems, CA, USA). In addition to no template controls, products were validated using melt point analysis to show a single high temperature melt point.

5.3.2 HISTOLOGICAL PROCESSING

For histology and immunohistochemistry, constructs were fixed in 10% neutral buffered formalin for 3 days, and were then embedded in paraffin wax blocks for sectioning. 4 μm thick paraffin tissue slices were produced using a Leica microtome (Leica Microsystems, Wetzlar, Germany).

Glass slides containing tissue sections were deparaffinised and rehydrated through subsequent washes with Neo-Clear (xylene substitute, Merck Millipore, Massachusetts, USA), twice for 5 minutes, 100% EtOH, 96% EtOH and 70% EtOH twice for 30 seconds each time, followed by a 1 minute wash with dH_2O. Following the application of dyes, slides were prepared for long-term storage by washing with dH_2O followed by dehydration in ascending concentrations of EtOH, as follows: 70%, 96% and 100% EtOH twice for 1 minute, followed by a final wash with Neo-Clear, twice for 5 minutes. Slides were mounted using a water-free agent, Neo-Mount (Merck Millipore, Massachusetts, USA) for long-term storage. Tissue sections were imaged using a Leica DM500 microscope (Leica Microsystems, Wetzlar, Germany).

5.3.3 H&E STAINING

A Haematoxylin and Eosin (H&E) stain was used in order to stain cell nuclei, cytoplasm and the matrix of constructs. Haematoxylin staining solution was applied for 3 minutes and slides were washed under running tap water for 3 minutes. Eosin Y solution 0.5% was applied for 3 minutes. Samples were rinsed under running tap water for 30 seconds.

5.3.4 IMMUNO-HISTOLOGICAL ANALYSIS

Slides containing tissue sections were deparaffinised and rehydrated through subsequent washes with Neo-Clear (xylene substitute, Merck Millipore, Massachusetts, USA) and 100% EtOH twice for 3 minutes; followed by washes in 95% EtOH, 70% EtOH and 50% EtOH for 3 minutes each time, followed by a wash with dH_2O. Antigen retrieval was performed using the water-bath immersion method, where the slides containing tissue sections were immersed in citrate buffer (10 mM sodium citrate in dH_2O, pH 6, Abcam, Cambridge, United Kingdom) for 8 hours at 37°C. Slides were washed twice for 5 min in TBS which contained 0.025% Triton X-100 (Thermo Fisher Scientific, Massachusetts, USA). Tissue sections were blocked in medium containing 1% BSA and 10% normal serum in TBS from either donkey or goat, depending on the species of the secondary antibodies, for 2 hours at room temperature. Primary rabbit antibodies against rat sclerostin (Abcam, Cambridge, United Kingdom), podoplanin (Abcam, Cambridge, United Kingdom) and collagen type I (Thermo Fisher Scientific, Massachusetts, USA) were diluted to a concentration of 10 μg/mL in TBS with 1% BSA. Antibodies were applied to the slides and incubation was performed overnight at 4°C. Samples were rinsed twice with TBS containing 0.025% Triton X-100, with gentle

agitation. Secondary antibodies (donkey anti-rabbit or goat anti-rabbit) conjugated to Alexa Fluor 488 (Figure 5.1) fluorophores, were diluted to 10 μg/mL (donkey) or 5 μg/mL (goat) in 1% BSA in TBS and were incubated with the slides for 1 hour at room temperature. Following incubation, tissue sections were washed three times with TBS for 5 minutes. In order to check for non-specific antibody binding, the steps listed above were performed on additional slides, without the addition of the primary antibodies. Slides were washed with TBS containing 0.1% Triton X-100 for 5 minutes. Phalloidin (Thermo Fisher Scientific, Massachusetts, USA) conjugated to Alexa Flor 594 or 555 (Figure 5.1) was used for cytoskeletal labelling. The lyophilized phallotoxin powder was diluted to a concentration of 200 U/mL using methanol (6.6 μM) and 3U were applied in TBS to each tissue-containing slide. Samples were washed with PBS twice. DAPI (Figure 5.1) was used for nuclear/DNA staining dissolved in mounting agent. Tissue sections were mounted with Pro-Long Diamond anti-fade permanent mountant (Thermo Fisher Scientific, Massachusetts, USA) for fluorescence preservation. Fluorescence images were acquired using an Olympus Fluoview FV1000 confocal laser scanning microscope (Olympus, Tokyo, Japan) equipped with a multi-line argon laser FV5-LAMAR/LAMAR-2 and a Helium-Neon Green Laser FV5-LAHEG-2/FV5-LAHEG. Images acquired from excitation at 405, 488 and 543 nm wavelengths were collected in individual channels and combined using the Fluoview FV10-ASW software, version 4.2 (Olympus, Tokyo, Japan).

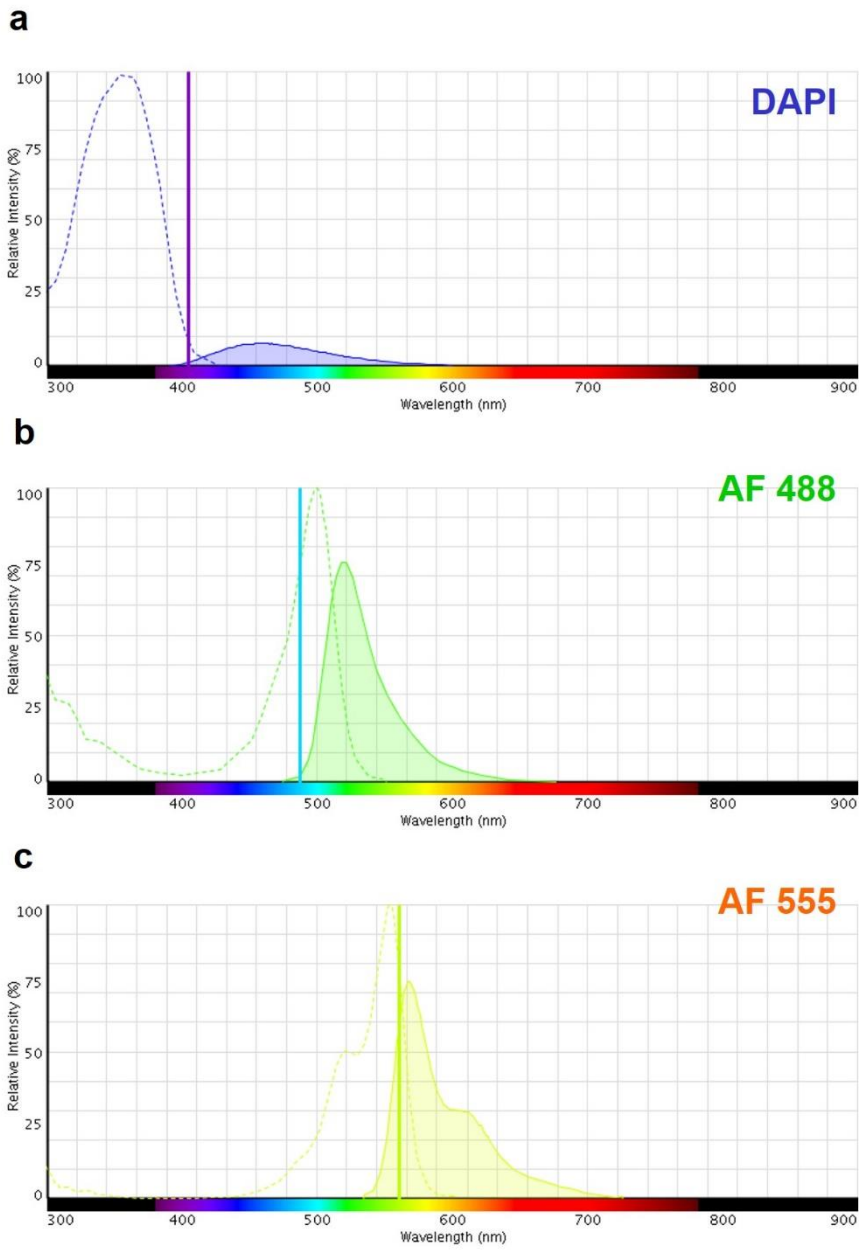

Figure 5.1 | Excitation-Emission Spectra of fluorophores chosen for Immuno-Histochemistry. The Alexa Fluor 488 fluorophore was conjugated to antibodies raised against the molecular markers of interest, Alexa Fluor 555 was conjugated to Phalloidin for detection of cytoskeletal actin and DAPI was applied to detect the presence of DNA/nuclei. Spectra were produced using the Fluorescence SpectraViewer online resource (Thermo Fisher Scientific, MA, USA).

5.3.5 SCANNING ELECTRON MICROSCOPY

12 months-old constructs were fixed with 2.5% glutaraldehyde in phosphate buffered saline and dehydrated over several steps including immersion in ethanol of increasing concentrations and critical point drying using CO_2. Samples were coated with platinum and Scanning Electron Microscope (SEM) images were acquired under vacuum using a Philips xl30 FEG ESEM at a resolution of 3 nm at 15 kV. Various cellular structures were coloured using Adobe Photoshop CC 2015 (Adobe Systems Incorporated, CA, USA) to allow a better visualization.

5.3.6 SYNCHROTRON RADIATION COMPUTED-TOMOGRAPHY

Nano-computed tomography (nanoCT/srCT) represents imaging at resolutions below 1 micron using synchrotron radiation. Synchrotron radiation uses a high-photon flux monochromatic X-Ray beam that is extracted from a synchrotron source, as opposed to microCT, which uses a polychromatic X-Ray source. This prevents beam-hardening artefacts (*described in Chapter 4*), which allows high-resolution, accurate measurements (Martín-Badosa, Amblard et al. 2003). srCT analysis was conducted on the nano-imaging beam line ID16 at the European Synchrotron Radiation Facility (ESRF) in Grenoble, France. Constructs were fixed with 4% formaldehyde and dried for 30 minutes at 50^{o}C. 5 mm samples of constructs were excised and placed on the rotating stage (Figure 5.2). Images were acquired at a resolution of 50 nm or 100 nm and a number of slices of 65-200 was acquired and used for 3D reconstruction.

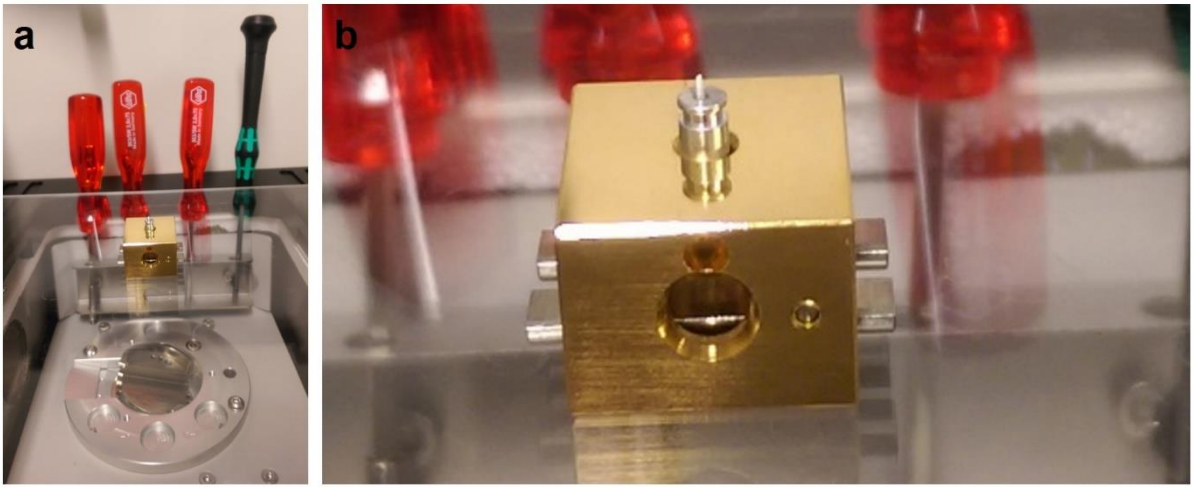

Figure 5.2 | Equipment design for sample scanning using synchrotron-radiation computed tomography. **a**, Stage containing sample is fixed in place. **b**, 5 mm samples were cut from dried constructs and were placed in the centre of the stage used for high-resolution scanning.

5.3.7 THERMAL ISOLATION OF MINERAL

Constructs were removed from culture and their calcium phosphate anchors were excised. Remaining tissues were dried at room temperature overnight and weighed using an Ohaus Pioneer Plus analytical balance (Ohaus, NJ, USA). Tissues were then introduced into a 900°C hot oven for 13 hours to remove organic matter (Carbolite CWF1300, Carbolite Gero, Hope Valley, United Kingdom). Following this period, the inorganic matter isolated was weighed and the percentage mineral content was calculated.

5.3.8 X-RAY DIFFRACTION

X-ray diffraction (XRD) was used to determine the crystalline composition of the samples. The crystals produced from the samples following 13 hours of heating in a furnace were ground into fine powders with a marble mortar and pestle and carefully formed into a 10mm wide thin circular layer on sticky tape. X-Ray diffraction patterns of the mounted powders were then collected using with a Bruker D5000 X-ray diffractometer (Bruker ASX, Karlsruhe, Germany) using the Cu K_{a1} 1.5406Å line, with a 2θ range of 24.6º to 48º, a 0.02º step-size and a step time of 0.05 s/ º leading to a total scan time of approximately 1 hour. Detected peaks were compared to JCPDS reference patterns to identify the crystalline phases in each sample. PDF 00-009-0432 and 00-012-0404 were used as reference patterns for hydroxyapatite and Whitlockite, respectively.

5.3.9 MICRO X-RAY FLUORESCENCE

High-resolution elemental mapping of the lacunar structures and matrix of 1-year constructs was performed on flat, 4 μm thick slices (*see Histoprocessing*) using a spot size of 25 μm, distance of 5 μm, with 10 ms/pixel exposure time and 100 frame counts. Measurements were recorded under vacuum, at approximately 800 mbar.

5.3.10 RAMAN MAPPING OF WHOLE CONSTRUCTS

Large-scale image scans were acquired from fresh constructs using the methodology described in section 5.3.1. Spectral data cubes were pre-processed to remove cosmic rays using the instrument associated software (Witec Project v2.10., Witec, Ulm, Germany). For some experiments (*see Formation of a Periosteal Structure in 1-year-old constructs)* files were exported in .SPC format and imported into MATLAB (MATLAB 2016b. Mathworks, Natick, Massachusetts, USA), baseline corrected using an adaptive iteratively reweighted penalized least squares method and vector normalised. Least squares regression was used for fitting of individual Gaussians to each peak. Octacalcium phosphate was represented by the P–O stretching mode (v_1) of the PO_4 group between 953-956cm^{-1}. Hydroxyapatite was represented by the symmetric stretching mode (v_1) of the PO_4 group (P–O bond) between 958-961cm^{-1}. Collagen was represented across all maps by the amide I peak spanning 1620-1650 cm^{-1}. To best visualise the relative amounts, distribution of, and association between, mineral and collagen throughout the samples RGB image maps were produced by integrating over the sum of peaks of interest. Red represented OCP, Green represented hydroxyapatite and Blue represented collagen. MATLAB was employed in all cases in order to visually represent the co-localisation of the signals for the inorganic-organic components and to be able extract further information regarding the dynamics of ossification. As such, the overlap of different components generated the following colours: yellow when HA (green) and OCP (red) were co-localised, grey when HA (green) and collagen I (blue) were co-localised, and violet/purple when OCP (red) and collagen I (blue) were co-localised.

5.3.11 ATOMIC FORCE MICROSCOPY

5.3.11.1 FRESH SAMPLE PREPARATION FOR AFM

Fort the initial tests, constructs were removed from culture medium following a year in culture and rinsed with PBS for a few seconds. A 1 cm^2 section was cut from the central portion of constructs and positioned flat on a 35 mm x 10 mm polystyrene dish (Corning, New York, USA), which was immersed in 1 ml PBS (Sigma-Aldrich, Germany), a quantity sufficient to maintain the hydration of the tissue section, whilst preventing its movement during testing.

5.3.11.2 FIXED SAMPLE PREPARATION FOR AFM

An alternative type of sample was used to optimise the force measurements, using glass mounted tissue sections of 1 year constructs. These sections were 4 μm thick paraffin and were produced by formalin fixation, followed by paraffin embedding and sectioning using a Leica microtome (Leica Microsystems, Wetzlar, Germany), using the procedures listed previously for histological processing, in *Chapter 5*.

The glass slides containing tissue sections were deparaffinised and rehydrated through subsequent washes with Neo-Clear (xylene substitute, Merck Millipore, Massachusetts, USA), twice for 5 minutes, 100% EtOH, 96% EtOH and 70% EtOH twice for 30 seconds each time, followed by a 1 minute wash with dH_2O. Samples were kept hydrated with PBS prior to and during measurements.

5.3.11.3 MECHANICAL TESTING

Samples were mechanically mapped using a NanoWizard II atomic force microscope (JPK Instruments AG, Berlin, Germany). The NanoWizard II setup consisted of a Carl Zeiss Axiovert 200 microscope, with a joystick controlled motorised stage and ForceWheel device, which allowed navigation across the sample surface; a NanoWizard II head, a manual and automated, and alloy base plate stage providing a travel range of 20 x 20 mm^2 within the field of a 100x objective. The instrument was located inside a closed, acoustic isolated chamber paced on a vibration-isolated table to reduce noise and artefacts.

High-resolution maps were acquired using pyramidal cantilever tips by intermittent contact mode across an X-Y range of 50 x 50 μm, and 100 x 100 μm (512x512 pixels), and across a z range of 15 μm. The acquisition time was approximately one hour for each area scanned. Data was acquired using JPK NanoWizard Control software and measurements for height, slope and adhesion were analyzed and exported using JPK Data Processing software version 4.1.8 (JPK Instruments AG, Berlin, Germany).

5.4 RESULTS AND DISCUSSION

5.4.1 FORMATION OF OSTEOCYTES AND A LACUNO-CANALICULAR SYSTEM

Optical analysis of the cellular morphological features during the months of culture revealed a pronounced restructuring of the cytoskeleton (Figure 5.3), showing the formation of extensive projections characteristic of osteocytes and of long micro-canals as early as 3 months (a). Following 1 year in culture, most of the cells observed displayed an osteocytic morphology (b).

At the molecular level, cells present after a period of 5 months expressed osteocytic marker sclerostin, a negative regulator of bone formation and an inhibitor of osteoblastic activity (Poole, van Bezooijen et al. 2005, Bonewald 2011, Kalajzic, Matthews et al. 2013), on their outer membranes and in their surroundings, which resembled cell networks (Figure 5.4a and 5.5). Further networks rich in sclerostin but also podoplanin, a marker for the embedding osteoid osteocyte (Bonewald 2011), and which is involved in reorganization of the cytoskeleton (Zhang, Barragan-Adjemian et al. 2006), could also be detected following the very extended culture time of 1 year (Figure 5.4a illustrates an example). Sclerostin and podoplanin mRNAs were also detected at these late (5 months) and very late time points (1 year) (Figure 5.4b), suggesting an active role of the cells in building and remodelling the bony matrix.

Interestingly, the mineral to matrix ratio of these constructs at the latter time point reached a value similar to that of bone, with mineral occupying approximately 70% of the total content (Boskey 2013) (Figure 5.4c). Moreover, the mineral was confirmed to be the mature bone hydroxyapatite using X-Ray Diffraction analysis (Bonar, Roufosse et al. 1983) (Figure 5.6).

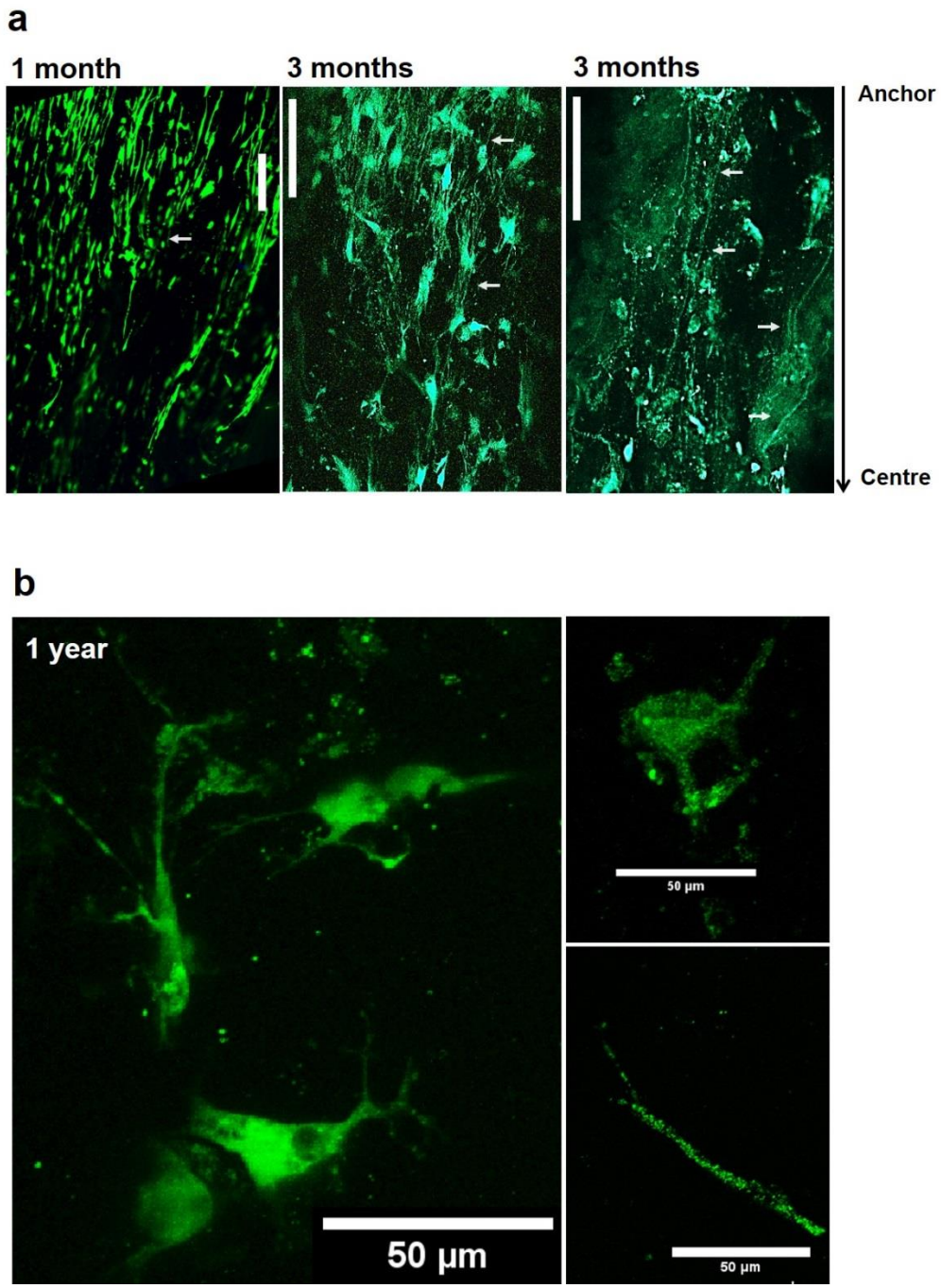

Figure 5.3 | Cellular morphological changes over a year in culture and final differentiation to osteocytes. a, Following a month in culture, morphology of cells in constructs is mainly elongated and resembling osteoblastic cells (**left**). With additional osteogenic supplementation and over the following 2 months, cells develop typical osteocytic characteristics, including numerous interconnected osteocytic networks (**middle**) and canaliculi-like structures containing long cell projections (**right**). **b**, The most mature cells (**1 year**) show a marked re-structuration of the cytoskeleton, displaying osteocytic phenotypes strikingly similar to those encountered in vivo (**left**). The long projections are very well preserved (**right top and bottom**).

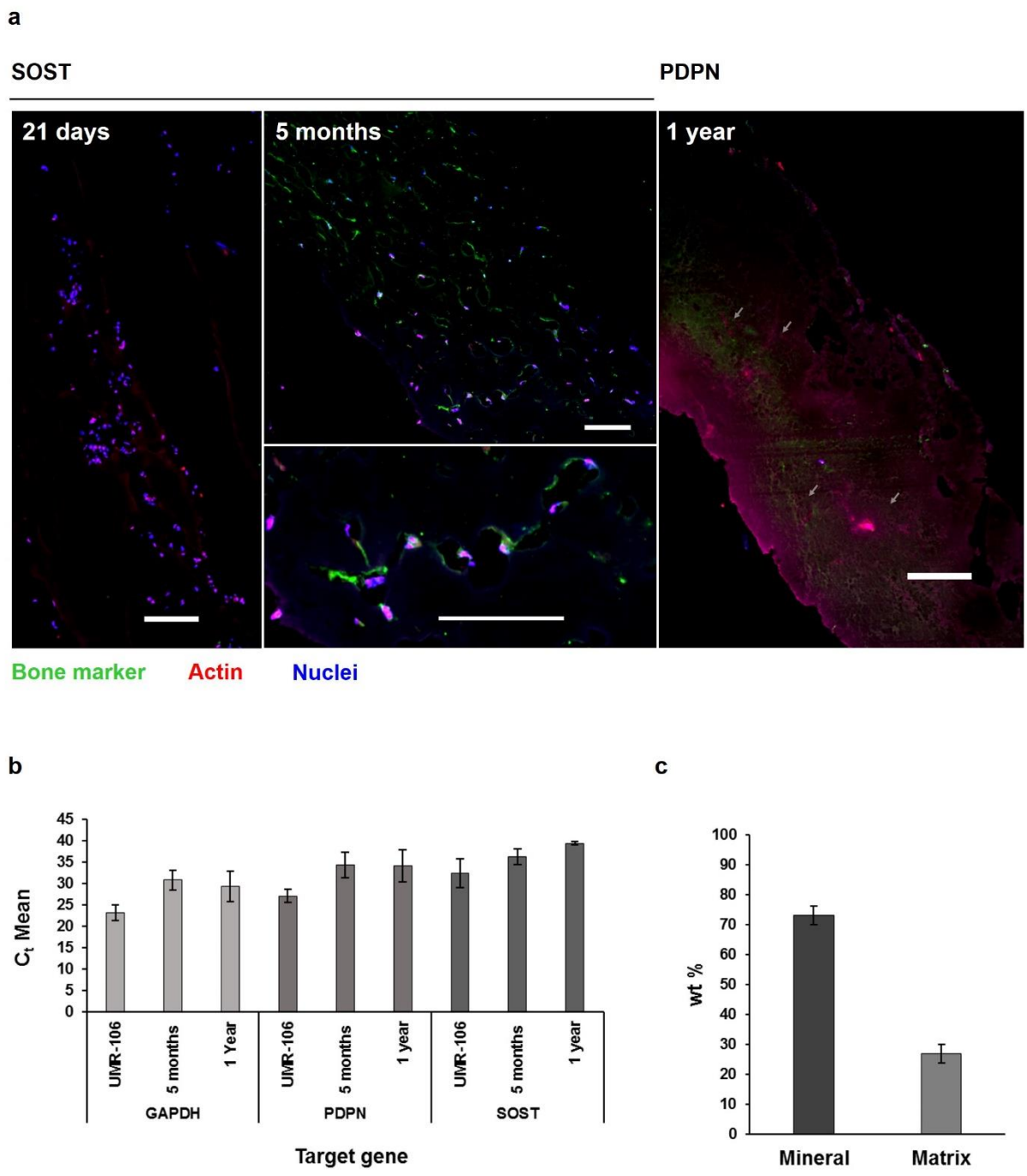

Figure 5.4 | Detection and localisation of bone markers in mature constructs. a, Immunohistochemistry of constructs, showing expression of osteocytic marker sclerostin on the surface of cells and in neighbouring network-like structures at 5 months (**middle**). The matrix of 1 year-old constructs contains long networks, where podoplanin could be detected (**right**). Scale bars = 100 μm. **b**, mRNA for sclerostin and podoplanin was detected at these time points as well. Results are presented compared to a rat osteosarcoma cell line as positive control. UMR-106 produces sclerostin and podoplanin continuously. Please note cycle threshold (C_t) is inversely proportional to the amount of target nucleic acid in the sample. n_{pdpn}= 4 (umr,5 m), 2 (1 yr). n_{sost}= 4 (umr), 2 (5m,1 yr). n_{gapdh}= 4 (umr,5 m), 2 (1 yr). **c**, The inorganic component of constructs following a year in culture equals approximately 70% of the total content. n=3.

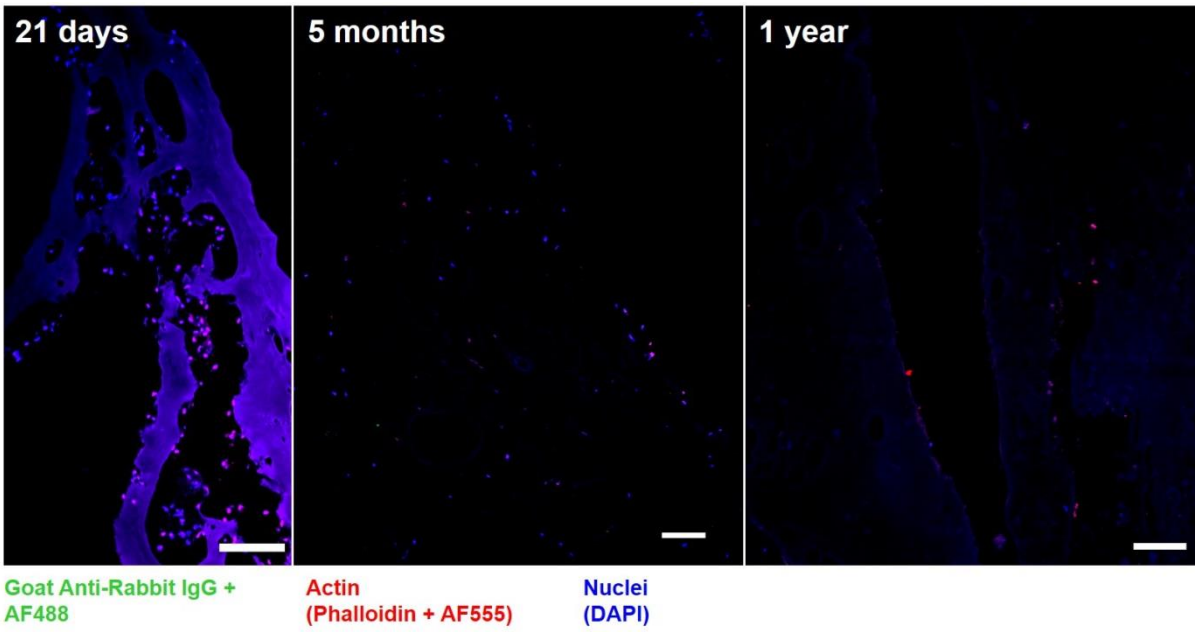

Figure 5.5 | Secondary antibodies are highly specific and do not bind at random locations on constructs during immunohistochemistry. Goat anti-rabbit IgG conjugated to Alexa Fluor 488 (green) were applied to all samples in the same conditions, without the addition of a primary antibody in order to detect non-specific binding. These results that these antibodies were highly specific, showing minimal or non-existent binding to the construct slices, thus reducing the possibility of false positive results.

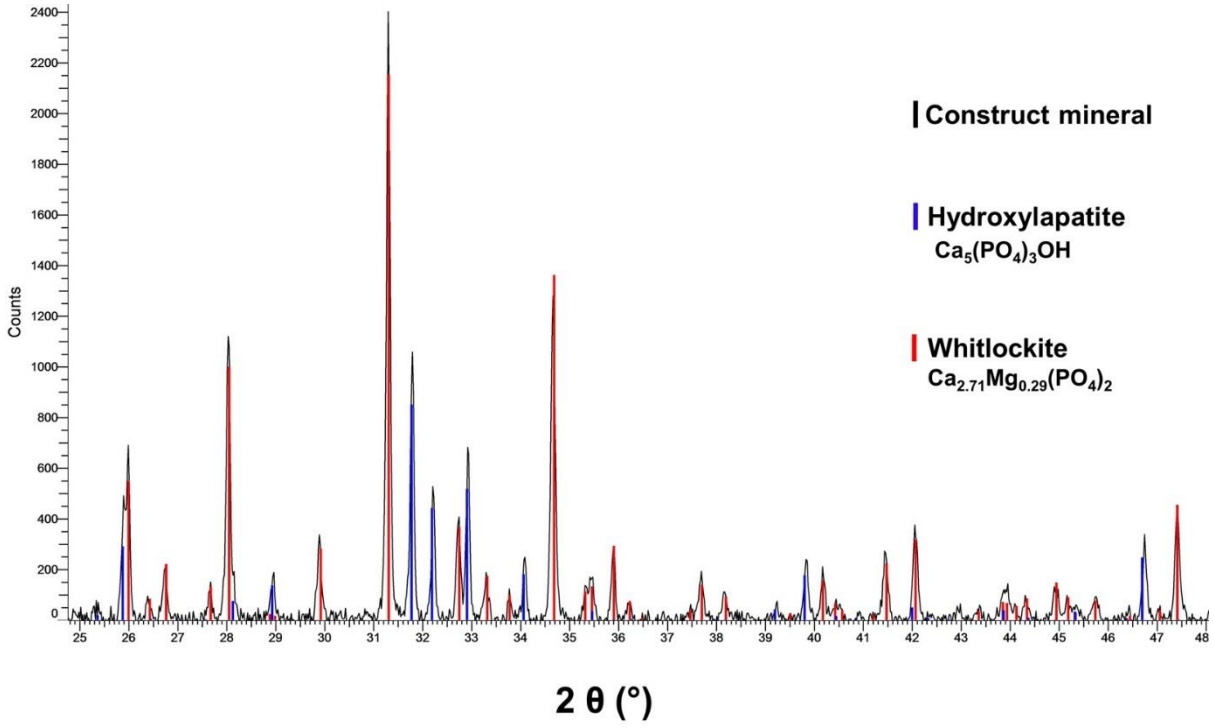

Figure 5.6 | Typical X-Ray Diffraction pattern obtained from mature constructs. The pattern confirms the presence of hydroxyapatite, the mature bone mineral in 1 year samples. Traces of whitlockite, a second type of mineral abundant in bone (Jang, Jin et al. 2014, Jang, Lee et al. 2015), can also be detected.

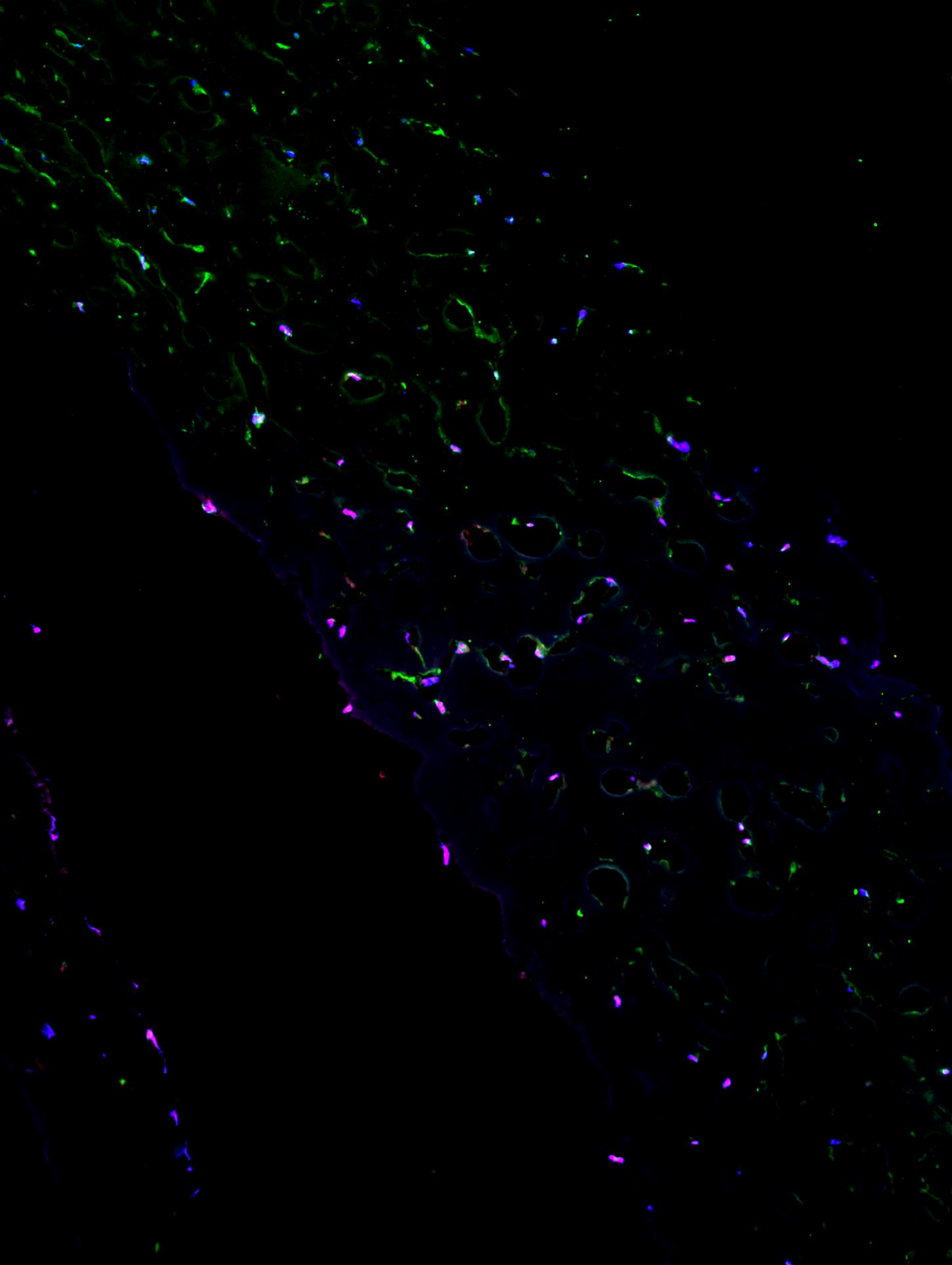

Sclerostin, visualised in a section of a 5 months-old construct using immunohistochemistry.

Blue - Nuclei (DAPI) Red - Actin (Phalloidin conjugated to Alexa Fluor 555), Green - Sclerostin (Goat anti-Rabbit IgG conjugated to Alexa Fluor 488)

High-resolution optical analysis of the cells in the most mature constructs (1 year) demonstrated further osteocytic morphological features. Cells at the surface of constructs, imaged using scanning electron microscopy (Figure 5.7a), appeared embedded in the heavily mineralized matrix. These cells contained a high number of large projections emerging from the cell bodies and reaching adjacent cells, as seen in bone (Gorustovich 2010, Schneider, Meier et al. 2010). Synchrotron radiation computed tomography (srCT), which enabled resolution down to the nanoscale (Langer, Pacureanu et al. 2012, Peyrin, Dong et al. 2014), was used to visualise cells located below the surface, inside the constructs. Figure 5.7b illustrates an example. The tomographic reconstruction further confirmed the presence of a complex canalicular network that linked the embedded cells, the first time that such elaborate structures have been attained using an *in vitro* culture. These channels were visualised using micro-XRF to provide a chemical map of the tissue structures (Figure 5.7c). Lacunae, which were shown to house cells expressing osteocytic markers, were surrounded by a matrix rich in calcium and phosphate salts. The presence of a canalicular network was further supported by this analysis, which showed a sulphur rich network (indicative of the presence of protein) which permeated through and between the lacunar structures (Figure 5.7c). Similar osteocytic structures, containing cellular DNA, were observed at earlier time points as well using histological analysis (Figure 5.8). These lacunar structures were aligned with the mechanical axis of construct and in some cases were connected by microchannels (Figure 5.8c).

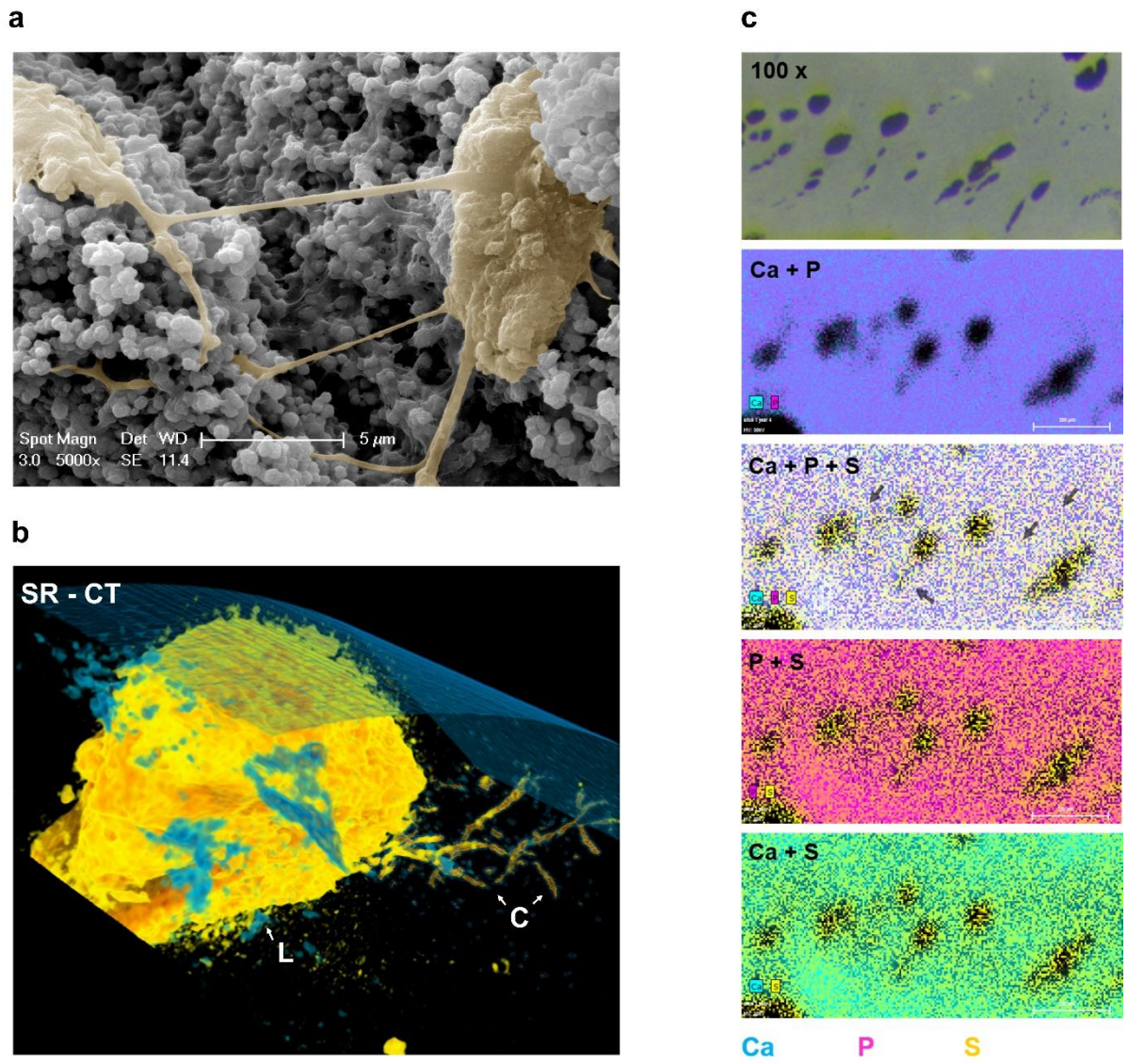

Figure 5.7 | Development of bone cells in constructs. a, SEM images of cells in constructs after 12 months of culture, showing cells embedded in the significantly mineralized matrix. The main cellular structure in **a** has been false-coloured to allow a better visualization. There are many podocytes embedded in the heavily mineralized matrix. Cells communicate through extensive projections. **b**, Synchrotron radiation computed tomography illustrating a typical osteocyte lacuna (**L**) with emerging canaliculi (**C**) that branch into the tissue. **c**, XRF maps based on S, Ca, P showing network-like structures throughout the matrix and connecting adjacent lacunar-like structures (arrows). Scale bars = 200 µm.

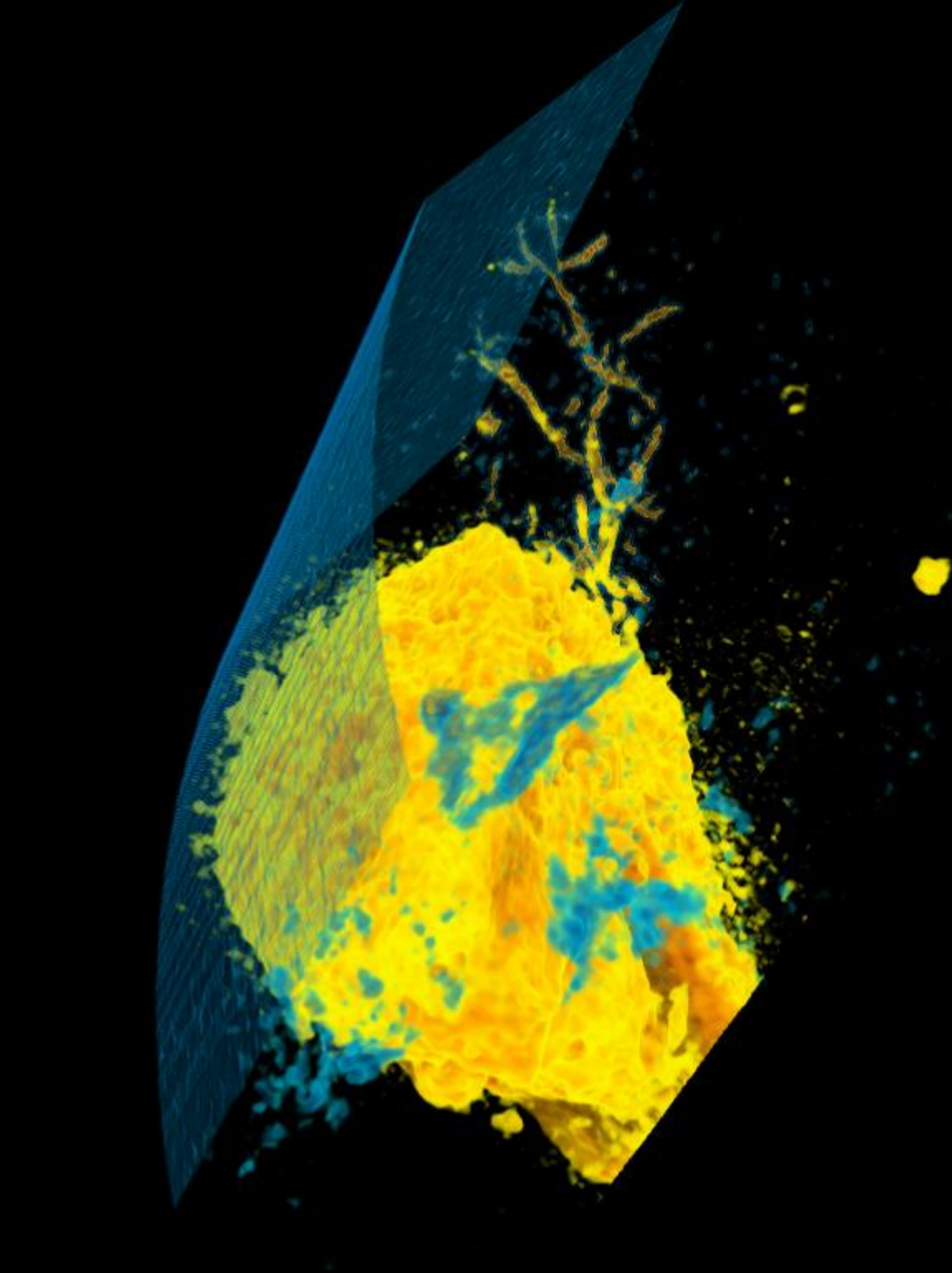

Osteocyte lacunae and canaliculi inside a 1 year-old construct, as seen through synchrotron radiation computed tomography (srCT)

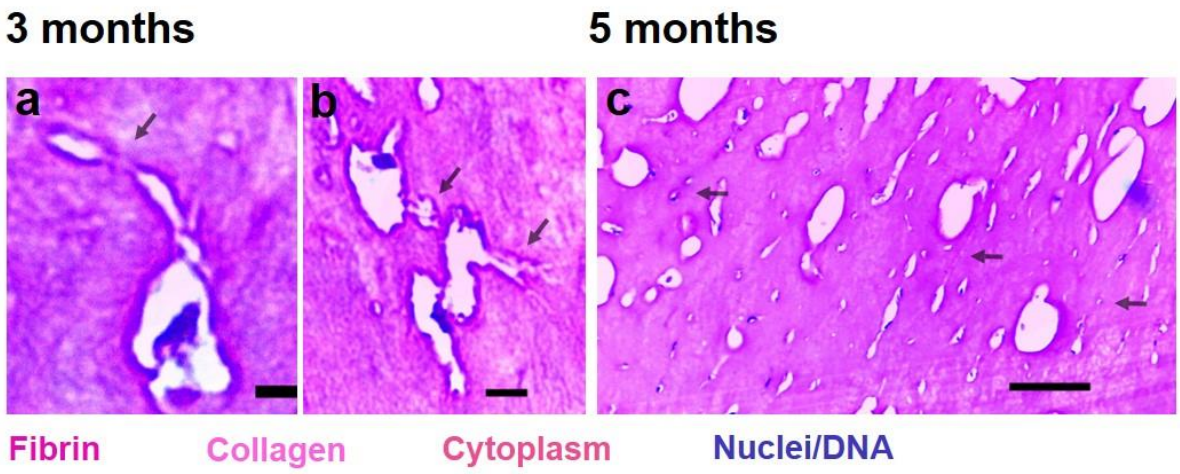

Figure 5.8 | Development of osteocytic features, H&E stain of tissue sections. Canalicular-like structures emerging from lacunar spaces were observed as early as 3 months (**a**, arrows), with some branching into the tissue (**b,** arrows) and connecting adjacent similar structures, which contained cell DNA and remnants of the cytoplasm (**a**, **b**). Networks of DNA containing lacunae (**c**, arrows), could be observed arranged along the length of constructs. Scale bars a, b = 10 µm; c = 100 µm.

Taken together, these results suggest that the microenvironment inside constructs, which developed into mature, mineralized collagen, reached a level of ossification similar to *in vivo* bone following long-term culture, which allowed the differentiation and survival of osteocytic cells over an extended, clinically-useful period of time.

Osteocytes are extremely difficult to differentiate *in-vitro* (Kalajzic, Matthews et al. 2013), as these mature cells form under complex conditions in their environment. They are also very difficult to investigate *in vivo* due to their localization, embedded in lacuno-canalicular networks in hard bone, and their final stage differentiation into mitotically inactive cells (Kalajzic, Matthews et al. 2013). Following isolation, culturing these cells require complex supplementation regimes to prevent a quick de-differentiation into osteoblastic phenotypes. Although standard immortalized osteocyte cell lines (e.g. MLO-Y4) are available, (Kato, Windle et al. 1997) they are not entirely

representative due to reduced marker expression, particularly sclerostin. As a consequence, to this date there are few models available for *ex-vivo* or *in-vitro* study of osteocytes and certainly none that allow for the long-term growth of these cells.

This work demonstrates that it is possible to fine-tune a primary osteoprogenitor cell population towards an osteocytic phenotype in a physiologically-relevant system that develops into bone tissue at most levels, including cellularly (osteoblast and osteocyte development), compositionally and structurally (organised collagenous matrix production and mineralization). Although primary osteoblast to osteocyte cell transition has recently been reported in 3D by a few research groups (Kalajzic, Matthews et al. 2013); this model differs in the close recapitulation of complex *in-vivo* conditions (Boukhechba, Balaguer et al. 2009), and in the self-structuring process as opposed to a pre-formed organic-inorganic matrix template (e.g. collagen scaffold with embedded HA particles) (Sun, Gu et al. 2015). As such, constructs survive over much greater periods of time (i.e. 12 months compared to a few weeks); as well as developing over a real tissue length-scale.

5.4.2 FORMATION OF A 'PERIOSTEAL' STRUCTURE IN 1-YEAR-OLD CONSTRUCTS

Several techniques indicated the formation of a gradient of ossification, not only from the anchors towards the center but also from the midpoint of the constructs towards the edges. These were observed as outer structures which were denser than the remaining construct (Figure 5.9). This process could have been triggered by individual or a combination of factors including the design of the system, mechanical pattern of self-organisation, or local chemical and biological cues. Irrespective of the nature of the underlying mechanisms, the process itself was both fascinating and valuable to this

model, as it brought this system closer to simulating bone by recreating an outer 'periosteal' structure. Figure 5.9 presents the analysis of this aspect. Firstly, the dense outer matrix layer observed with micro-CT (a), when mapped using Raman spectroscopy, it showed an abundance of HA-associated collagen composition, whereas the central portion of constructs contained a mix of mature HA and intermediate phase OCP (b). Interestingly, the abundant collagen content detected at earlier time points using this technique as well as with SHG, was loaded during extended culture periods with further mineral deposits, confirming the high mineral content (70%) detected using other techniques. It cannot be determined soley based on this data whether the formation of this outer structure and the assembly of this highly-mineralised matrix was due to the absence of a marrow-like cavity. Further work involving vascularisation of constructs would be able to shed light on this matter. Sections of these mature tissues were subjected to immunohistological and histological analysis, which revealed some further interesting aspects. The outer, dense layer contained proportonally-high levels of sclerostin, the negative regulator of bone formation, compared to the central portion, where it was encountered in network-like structures (c, left). These outer structures also contained considerable amounts of cellular DNA, suggesting a localisation of the osteocytic cells in this part of the constructs. The presence of cellular DNA was also identified in this region using haematoxylin staining (c, right). It is hard to speculate whether the localisation of cells particularly on the outside layers was a preferential choice due to the heating gradient provided by the well-plate system, but several fine tests could be run in further work to investigate this matter by modifying the culture system, as well as the chemical composition and design of the multi-well plates in order to uniformize the microclimate they provide to the cells.

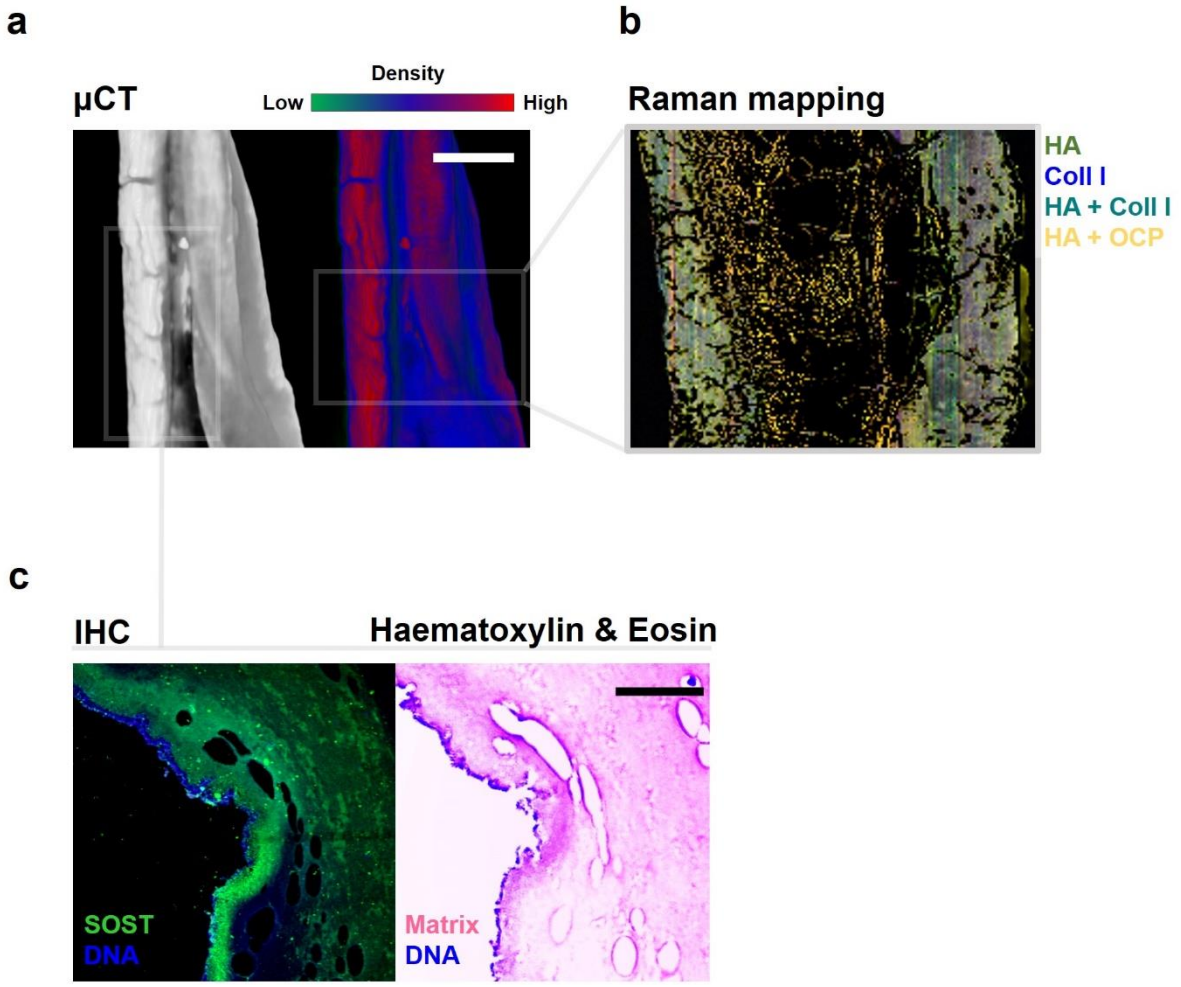

Figure 5.9 | Formation of a 'periosteal' structure in constructs. a, Micro-CT tomographies indicated a density difference between the outer layer of constructs and the central portion in the oldest constructs. **b**, Raman maps of the central area revealed that the outer structure contained collagen type I associated with hydroxyapatite, whereas the central region contained a combination of HA and OCP. **c**, Immunohistochemistry on tissue sections indicated that this region was rich in sclerostin (green) and cellular DNA (blue). The latter was also observed using H&E staining, where DNA was localised to the outer region (blue).

5.4.3 MECHANICAL CHARACTERISATION OF OSTEOCYTES

The ability to differentiate osteoprogenitor cells towards an osteocytic path in this system provides an opportunity to study these cells in a more native environment than previous *in vitro* models. As discussed in Chapter 1, the hierarchical embedding of osteocytes into the bony matrix is essential for their role as mature, mechano-sensing cells. Therefore, preliminary work was performed to determine a suitable method for characterising these cells from a mechanical perspective in order to understand their immediate micro-environment. Atomic force microscopy (AFM) was employed to mechanically map the properties of constructs at high-resolution. Atomic force microscopy is a technique that has been increasingly used in cell biology in the past years for analysing cell features at the nanometre resolution (Lehenkari, Charras et al. 2000, Graham, Hodson et al. 2010) and has been applied for the study of individual osteocytes (Nguyen and Gu 2014).

Whole constructs (1-year-old) were initially subjected to mapping by AFM (Figure 5.10). Maps of 100 μm^2 allowed the identification of cell features, including cellular projections and bodies (top row). Identical features were also observed at a resolution of similar scale using synchrotron radiation computed tomography, where these cell pods appeared to connect to lacunar structures (Figure 5.11). The cell projections showed a high adhesion, indicating the presence of biological material, whilst the matrix surrounding them showed little to no adhesion, suggesting an inorganic, less adhesive component. Smaller areas were then selected (80 and 30 μm^2) to observe further details, however, the procedure generated noisy maps, potentially due to sample movement during investigation (Figure 5.10 Areas 2 and 3).

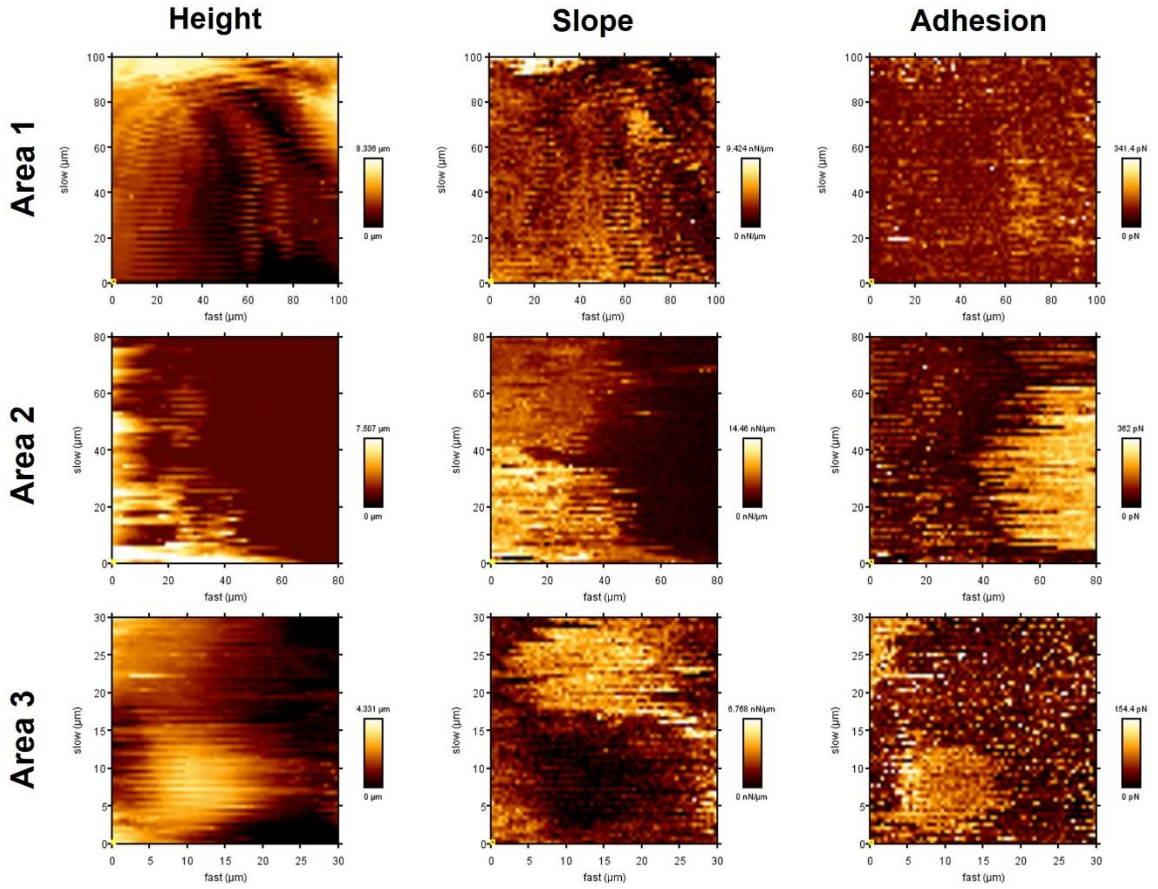

Figure 5.10 | Mechanical characterisation of 3D constructs. Several cellular features can be observed, particularly projections characteristic to osteocytes (Area 1). Pods appear more adhesive compared to the surrounding matrix, suggesting the presence of biological material entrapped within a less adhesive, inorganic component. Areas 2 and 3 appear noisier due to sample movement. These maps appear to show a mixture of structures with different mechanical properties, including round, adhesive structures with a low slope, indicating biological material, and structures which are harder (higher slope) and have less adhesion, indicating inorganic material.

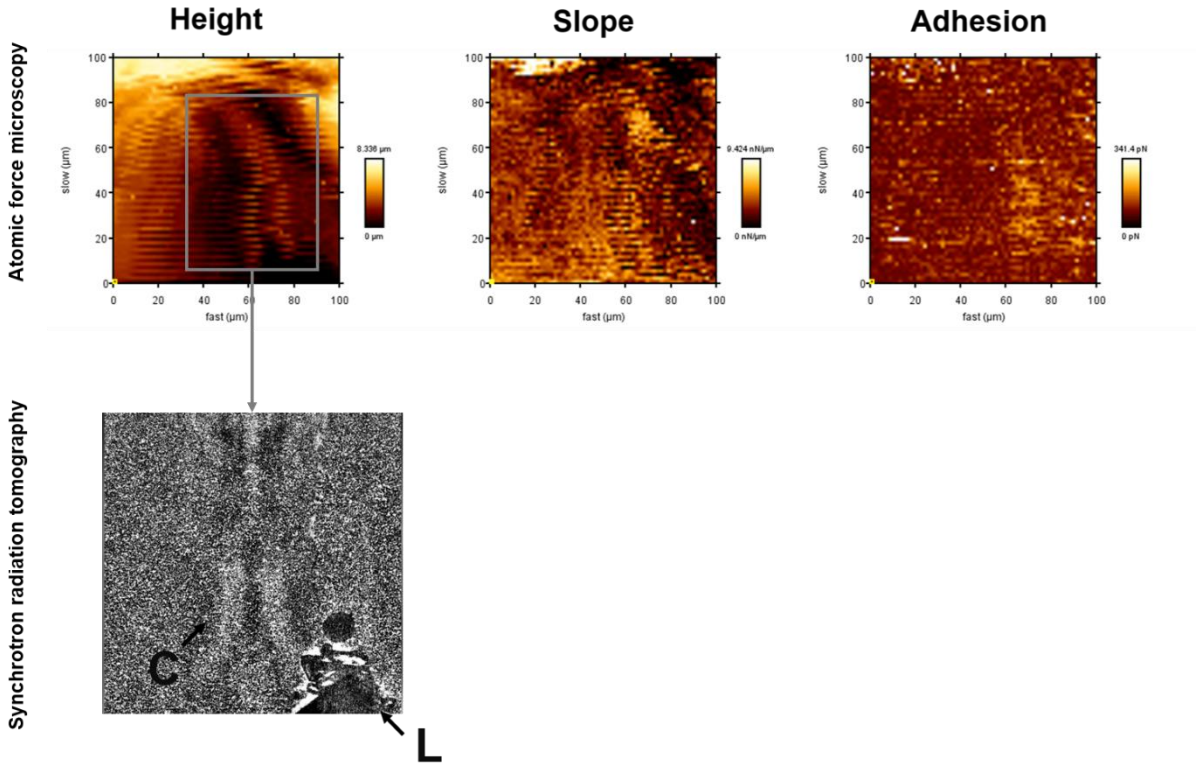

Figure 5.11 | Nano-characterisation of osteocytic features. The cellular projections observed using AFM were also detected using synchrotron radiation tomography, where they appeared as canaliculi (C), connecting lacunar structures (L).

As such, a new type of sample was prepared to remove the issue of movement during measurement, which involved using deparaffinised, re-hydrated 4 µm thick tissue sections fixed onto glass slides. The combination of tissue sectioning and atomic force microscopy has been previously reported as successful for resolving intracellular and extracellular structures in connective tissues (Graham, Hodson et al. 2010).

This method was successful in preventing the sample noise issue and trial 50 μm^2 maps were able to identify osteocytic bodies and projections, with mixed mechanical properties, potentially composed of both organic and inorganic materials (Figure 5.12). Interestingly, the matrix surrounding the osteocytic structures (Figure 5.12 right) showed some degree of consistency, with organic structures alternating inorganic ones.

Although AFM has been increasingly used in biology recently to obtain information at the nanometre resolution scale, many biological features are too unstable or out of the probe's reach (Lehenkari, Charras et al. 2000). In live cells, this is further complicated by the fact that many biological processes take place within seconds as opposed to minutes – hours, which are required for AFM scanning. Further optimisation work in this area is needed to confirm and expand on these results.

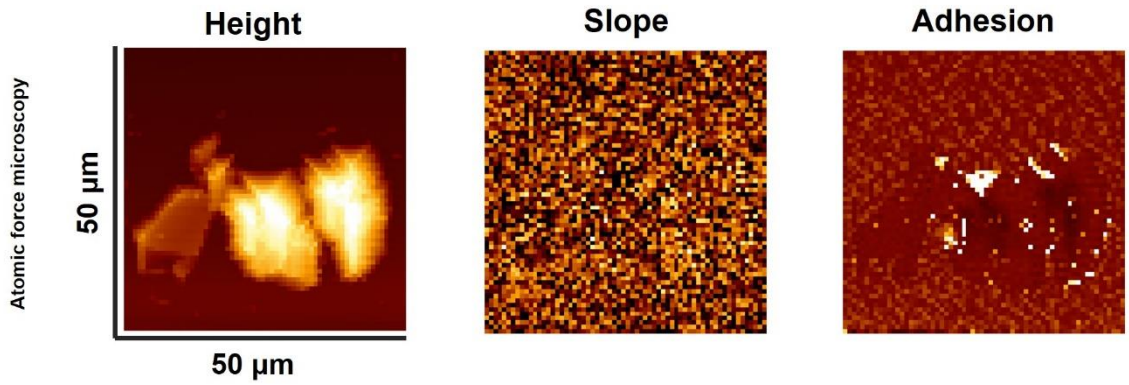

Figure 5.12 | Mechanical characterisation of individual osteocytes in tissue sections. Tissue sectioning allows the detection of clearer osteocytic structures, including cell body and projections. These cells and surrounding matrix showed mixed mechanical properties. The adhesion channel (right) shows a pattern of alternative soft and hard structures.

CHAPTER VI

MATRIX MINERALISATION BY MATRIX VESICLES

6.1 INTRODUCTION

The process of ossification takes places through a cell-mediated route, where cartilaginous and collagenous matrix built by chondrocytic and osteoblastic cells becomes subsequently mineralised in an organised manner, giving rise to the mature bone tissue (Mackie, Ahmed et al. 2008).

It is generally accepted that the process of calcium and phosphate deposition in cartilage, bone and dentin is mediated through exosome/vesicle-like nano-structures, generally referred to as matrix vesicles (MVs) (Anderson 1969, Anderson 2003, Anderson, Sipe et al. 2004). These nanovesicles are thought to bud-off from the plasma membrane of hypertrophic chondrocytes and osteoblasts (Cui, Houston et al. 2016) and contain the optimal conditions for the assembly of Ca and P into Hydroxyapatite, which ultimately becomes precipitated on the surface of collagen fibrils (Anderson 2003, Golub 2009), forming nucleation points (Felix, Herrmann et al. 1978).

The presence of matrix vesicles in the environment of cells embedded in constructs is an indication of the active role played by cells in the ossification process. This has been an area of intense research in the past years and numerous methods have become

available for selecting these nanostructures for further characterisation, each presenting various advantages and disadvantages (Li, Kaslan et al. 2017).

Traditional protocols for selecting these small vesicles involve ultracentrifugation (UC) (Hutcheson, Goettsch et al. 2014), which allows the separation of matrix vesicles on the basis that larger particles sediment faster, while the smaller particles remaining in the supernatant and which can be recovered using further centrifugation steps. In the case of matrix vesicles, it is thought that the mineral phase contained by the vesicles increases their density such that they pellet at a faster rate (Hutcheson, Goettsch et al. 2014). Whilst this method can produce a high yield of nanovesicles, the selection of nanostructures solely on this basis presents significant disadvantages such the inability to remove similar exosomes of equal weight (Safdar, Saleem et al. 2016); deformations and damage associated with the centrifugation process, such as exosomal aggregation (Chiou and Ansel 2016), which can potentially impact proteomic and RNA content analysis (Lamparski, Metha-Damani et al. 2002, Lobb, Becker et al. 2015) as well as inconsistencies related to using the same protocol with different rotors (Livshits, Khomyakova et al. 2015). Moreover, subsequent characterisation techniques used to confirm the nature of exosomes isolated through differential ultracentrifugation, such as optical visualisation using TEM, which has been traditionally used to observe these structures at high resolution, is not always able to confirm the nature of vesicles due to artefacts associated with the sample preparation process for TEM, which causes extreme dehydration and collapse to extracellular vesicles (Lobb, Becker et al. 2015, Li, Kaslan et al. 2017); and the presence of matrix vesicles lacking a mineral phase (Landis, Paine et al. 1977, Landis and Glimcher 1982, Cui, Houston et al. 2016).

Therefore, methods which can select nanovesicles based on previously characterised markers are more reassuring and appropriate to confirm their presence in the mineralising matrix. Markers involved in ossification, abundantly present on the surface of these matrix vesicles, such as tissue non-specific alkaline phosphatase (TNAP)(Hessle, Johnson et al. 2002, Anderson, Sipe et al. 2004, Ciancaglini, Simao et al. 2006, Millán and Whyte 2016) can be targeted and used for immuno-isolation using standard immunoprecipitation protocols (Wittrup, Zhang et al. 2010, Hussain and Davanger 2015). Although a much smaller population can be selected using this procedure, it can provide a confirmation of the presence and involvement of these vesicles in the biomineralization process.

Immuno-isolation of matrix vesicles is a straightforward process *in-vitro*, given the high number of osteoblastic cells that can be cultured in 2D. Extracting these vesicles from more complex structures, such as 3D-engineered bone, can be more challenging due to the smaller number of cells inserted and hence secretome produced. The growth medium of engineered bone tissue such as the one described in this thesis is a useful source of vesicles which can be collected for analysis.

6.2 AIMS AND OBJECTIVES

The goal of this work was to further support the role of embedded cells in constructs in the mineralisation process by attempting to isolate a small sub-population of matrix vesicles from the secretome of cells. The work was based on immunoselection, combined with a panel of characterisation techniques that were used to determine the role of these nanostructures in biological processes taking place in constructs. This chapter presents the results from this work.

6.3 CHARACTERISATION METHODS

6.3.1 IMMUNO-ISOLATION OF VESICLES INVOLVED IN MATRIX MINERALISATION

Matrix vesicles were isolated from the culture medium of constructs by immunoprecipitation using 2.8 μm superparamagnetic Dynabeads (Invitrogen, Thermo Fisher Scientific, CA, USA), covalently coupled to Protein G on their surface (approx. 17 kDa). Rabbit monoclonal antibodies against Rat Alkaline Phosphatase, Tissue Non-Specific (TNAP) were used to isolate the vesicles (Abcam, Cambridge, United Kingdom). Antibodies were attached to the magnetic beads through their Fc region during a 15 minutes incubation with rotation at room temperature, at a ratio of 5 μg of Ab/ 200 μl PBS containing 0.01% Tween-20 and 0.09% sodium azide, in which 1.5 mg magnetic beads were resuspended (Invitrogen, Thermo Fisher Scientific, CA, USA). The complex formed was washed by resuspending in 200 μl buffer and 1000 μl of culture medium containing the matrix vesicles was added to the formed Dynabeads-Ab complex. Samples and complex were incubated for 15 minutes at room temperature, with rotation. Following vesicle binding to the antibody, the beads-Ab-vesicle complex formed was washed four times using PBS washing Buffer (Invitrogen, Thermo Fisher Scientific, CA, USA). The Ab-Vesicle complex was eluted from the beads though the addition of 20 μl elution buffer (Invitrogen, Thermo Fisher Scientific, CA, USA). For gel electrophoresis, vesicles were resuspended in a loading mixture containing 2.5 μl NuPAGE LDS Sample buffer (4X), 1 μl NuPAGE Reducing Agent (10X) (all from Thermo Fisher Scientific, CA, USA) and 6.5 μl dH_2O and were incubated for 10 minutes at 70°C. Samples were loaded onto NuPAGE Novex 4-12% Bis-Tris Protein gels (1 mm thick) and

were run at 160 V for 60 minutes using MOPS buffer. 500 µl NuPage Antioxidant (Thermo Fisher Scientific, CA, USA) was added to the buffer to maintain the reduced state of proteins during protein gel electrophoresis. A Novex Sharp Pre-stained protein standard was used for reference (Thermo Fisher Scientific, CA, USA). For controls, PBS was used instead of culture medium and samples were subjected to the same isolation procedure and steps.

6.3.2 NANOPARTICLE ANALYSIS USING DYNAMIC LIGHT SCATTERING

Dynamic light scattering (DLS) using a Zetasizer Nano ZS Instrument (Malvern Instruments Ltd, Malvern, United Kingdom) was used to characterize the culture medium of young and old constructs at the nano-scale in order to detect the presence of extracellular vesicles. 2.5 ml of supplemented medium for cell culture and culture medium from young and mature constructs were diluted 1:10 in PBS, inserted into 12 mm polystyrene cuvettes (Malvern Instruments Ltd, Malvern, United Kingdom) and size measurements were taken at a 173 degrees scattering angle, using a RI parameter of 1.33, at 22°C. A 4mW, 633 laser was passed through the samples. 3 readings were taken per sample and averaged to obtain the size distribution of nanoparticles based on scattered light intensity.

6.3.3 NANOPARTICLE TRACKYING ANALYSIS

Nanoparticle tracking analysis (NTA) was performed using a NanoSight LM10 instrument (Malvern Instruments Ltd, Malvern, United Kingdom), in order to measure matrix vesicle size and concentration within the culture medium of constructs.

Calibration of the machine was performed using 200 nm polystyrene latex microspheres. Culture medium samples from young (14 days) and old constructs (1 year) were collected and stored at -80°C. Matrix vesicles were isolated using immunoprecipitation and used immediately for NTA.

Approximately 300 µl of nanovesicles suspended in buffer were injected into the NanoSight sample chamber. Control medium samples were diluted 1:10 in PBS prior to injection. In-between recordings, loading chamber was washed with 0.2 µm-filtered PBS and dH_2O for three times.

Particle detection threshold was set to 8 and camera gain was set to a value of 1. For each sample, two NTA videos of 60 seconds duration, containing recordings of the nanovesicles moving under Brownian motion, were collected using the NTA 2.2 software. Nanovesicles were tracked individually by the software based on scattered light when exposed to a 50 µm wide laser. The long-distance scattered light from the vesicles was detected by a 20X magnification microscope, connected to the recording camera. The matrix vesicles hydrodynamic diameters were calculated using the Stokes-Einstein equation and concentration was calculated based on volume. Data generated by the software concerning size and concentration was averaged to produce the final distribution for each sample.

6.3.4 ATP CONTENT

Mineralisation is an ATP-dependent process and staining for ATP was performed directly on the beads to detect its presence using quinacrine dihydrochloride (Orriss, Knight et al. 2009, Akopova, Tatur et al. 2012). Quinacrine dihydrochloride ≥90%, produced by Bayer (Sigma – Aldrich, Germany), was reconstituted using deionised H_2O

(dH_2O) and was used at a concentration of 10 μM, based on previous research (Loncar, Zotz et al. 2007). Following isolation, 750 μl of the bead-antibody-vesicle complexes and controls (beads-antibody complexes, dH_2O was used instead of culture medium) were incubated with the dye for 30 minutes at room temperature. Following incubation, the beads were washed 4 times with dH_2O and samples were imaged using an Olympus Fluoview FV1000 confocal laser scanning microscope (Olympus, Tokyo, Japan) equipped with a multi-line argon laser FV5-LAMAR/LAMAR-2 and a Helium-Neon Green Laser FV5-LAHEG-2/FV5-LAHEG. Images acquired from excitation at a wavelength of 405 nm were collected using the Fluoview FV10-ASW software, version 4.2 (Olympus, Tokyo, Japan) with an exposure time of 20 μs/pixel,

6.3.5 OSTEOCOMPETENCY

An experiment was conducted to determine the ability of these vesicles to interact with a bone-like extracellular matrix composed of collagen I. Matrix vesicles bound to the monoclonal antibody against TNAP were eluted from the beads using the procedures described above using 20 μl elution buffer (Thermo Fisher Scientific, USA) and were added to 300 μl TBS buffer. 100 μl of the re-suspended vesicles were applied in triplicate to 1.9 cm^2 wells in 24 well plates coated with collagen I (Gibco, Life Technologies, Thermo Fisher Scientific, USA) to determine whether the vesicles would be able to bind to collagen type I. Antibody-vesicle complexes were incubated in the plates for 30 minutes at room temperature, followed by a further incubation step at 37^oC for 30 minutes to partially simulate the physiological context. To be able to detect the amount of binding, a secondary antibody against the rabbit monoclonal primary antibody was used. Following incubation, wells were washed three times with TBS to

remove the unbound vesicles. Secondary donkey anti-rabbit antibodies conjugated to Alexa Fluor 488 fluorophores, were diluted to 10 µg/mL in TBS containing 1% BSA and 100 µl were applied in triplicate to the bottom of the wells and left to incubate for 1 hour at room temperature. Following incubation, tissue sections were washed three times with TBS for 1 minute. In order to check for non-specific antibody binding, the steps listed above were performed on additional wells, in triplicate without the addition of the primary antibodies. Samples were imaged using the confocal system described above, using a 10x objective lens. Images acquired from excitation at a wavelength of 488 nm in triplicate for the samples, controls and antibody controls. Data was collected using the Fluoview FV10-ASW software, version 4.2 (Olympus, Tokyo, Japan).

6.4 RESULTS AND DISCUSSION

MV outer membranes have been demonstrated to be rich in tissue non-specific alkaline phosphatase (TNAP), a form of ALP involved in skeletal mineralization and ectopic calcifications (Hessle, Johnson et al. 2002, Ciancaglini, Simao et al. 2006, Golub 2009, Golub 2011, Cui, Houston et al. 2016). Deactivating defects in the TNAP gene have been shown to cause hypophosphatasia (Mornet 2000, Hessle, Johnson et al. 2002, Millán and Whyte 2016), leading to rickets, osteomalacia, spontaneous fractures (*described in Chapter 1*). At a molecular lever, these mutations cause elevated levels of extracellular inorganic pyrophosphate (PPi), a natural substrate of TNAP which is a potent inhibitor of mineral formation (Millán and Whyte 2016). TNAP is present in abundance on the membrane of matrix vesicles (Golub 2011) and as such was targeted for immunoisolation.

Figure 6.1 presents a schematic of the immuno-isolation system used to purify a population of nanostructures with similar characteristics to matrix vesicles. The method involved building an isolation complex by coupling TNAP monoclonal IgG antibodies (Ab) to recombinant protein G (17 kDa) which was covalently bound to the surface of 2.8 μm superparamagnetic beads (MBs). During a 15 minutes incubation at room temperature in PBS-Tween 20, the antibodies became bound via their F_c regions to the beads, leaving the F_{ab} regions on the antibodies available to bind TNAP on the outer surface of vesicles.

As the constructs underwent ossification (Figure 6.2a), secretome analysis was performed on culture medium collected from early (14 days), mature constructs (1 year) and controls to compare the normal distribution of nanoparticles. The medium was subjected to dynamic light scattering analysis (DLS) to obtain an account of the size

distribution of nanoparticles in the growth medium, and compared to cell-free supplemented culture medium (Figure 6.2b-c). Interestingly, both the early and mature culture medium contained nanoparticles in the size range of 50 nm to 300 nm compared to controls (serum supplemented but cell-free medium), which corresponds to the range in which previously described matrix mineralization vesicles were detected (Anderson 1969, Bonucci 2007, Golub 2009). These nanoparticles were particularly abundant in older constructs (1 year). This may be evidence for a sustained population of mineralising osteoblasts during the lengthy culture period, as osteocytes have differentiated away from a primary secretory phenotype and have a more limited ability to mineralise compare to osteoblasts.

To determine whether this set of cell-secreted exosomes contained a sub-population of matrix vesicles involved in skeletal mineralization, the immuno-isolation procedure was used to separate this subset of vesicles from the rest of the exosomes. The isolation procedure involved incubating 1000 µl of culture medium with the Ab-MB complex (Figure 6.2d) for 15 minutes at room temperature, in PBS-Tween-20. During this incubation, the Ab-MB complexes attached to the surface of vesicles via F_{ab}-TNAP binding (e). The remaining debris and unbound vesicles were removed by magnetic separation (f). The Ab-MV complex was subsequently eluted from the beads and used with different analytical techniques.

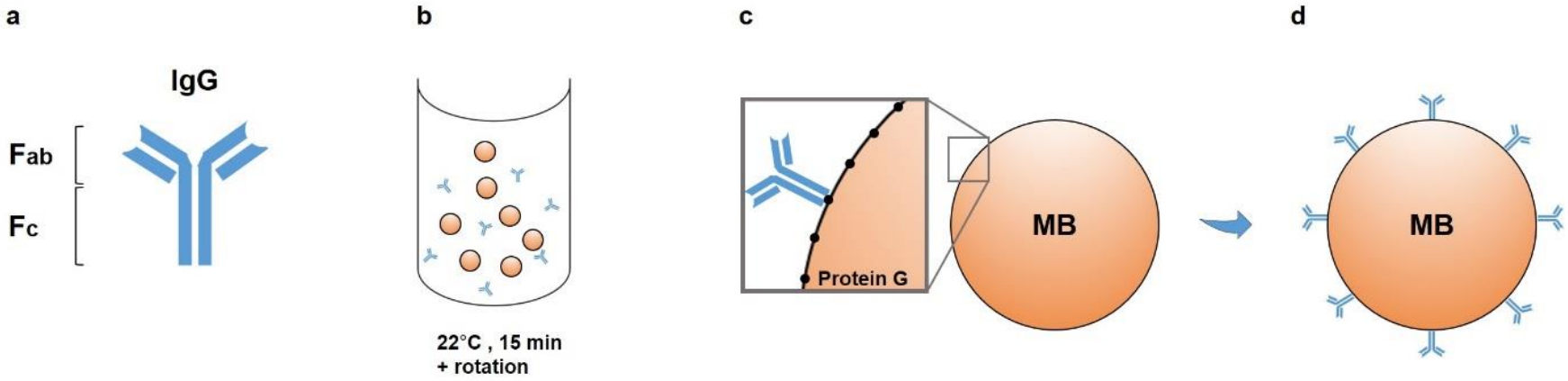

Figure 6.1 | Development of the Immuno-isolation method. Monoclonal IgG antibodies (**a**) were incubated with the magnetic beads for 15 minutes at room temperature with gentle rotation (**b**). During this incubation period, the antibodies bound via their F_c region to protein G, which is covalently coupled to the surface of the beads (**c**). The resulting bead contained multiple antibodies attached to it, which were capable of binding the antigen of interest (TNAP) via their F_{ab} regions (**d**).

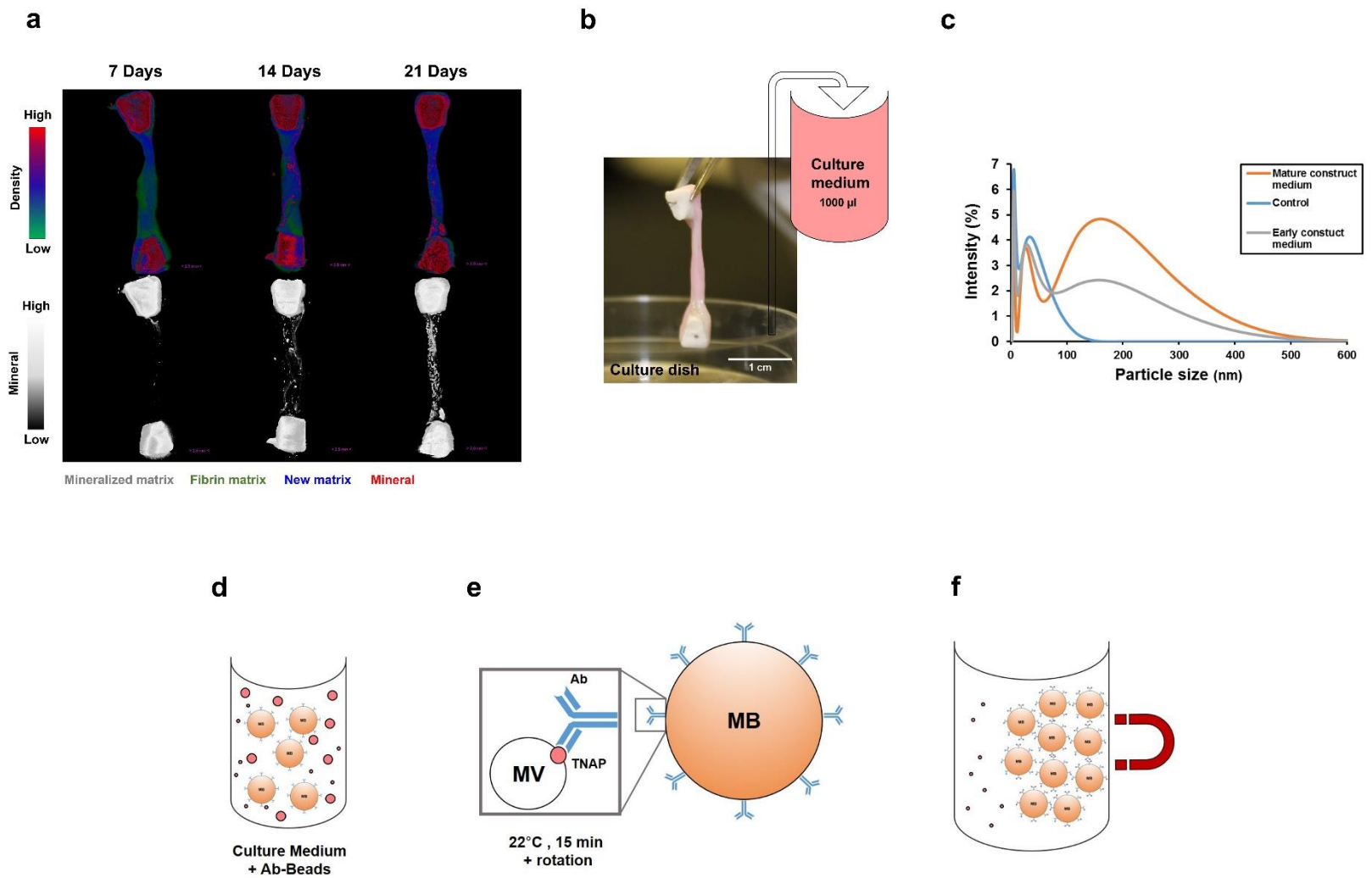

Figure 6.2 | Immuno-isolation of matrix vesicles. a, As mineralisation progresses in constructs with maturation, culture medium is collected from culture dishes (**b**) and subjected to nanoparticle analysis. **c**, Dynamic Light Scattering analysis of samples from control (serum supplemented, cell-free), 14 days and 1 year-old medium samples. Compared to controls, media from both young and mature constructs contained nanoparticles in the size range of 50-300 nm. **d**, Immuno-isolation of matrix vesicles from this population was performed by incubating 1000 µl of culture medium with the Ab-MB complex for 15 minutes at room temperature, in PBS-Tween 20. Monoclonal antibodies bound to the vesicles via their F_{ab} regions by binding to TNAP on the outer membrane of matrix vesicles (**e**). Purification of the Ab-MB-MV complex was performed via magnetic separation (**f**).

Nanoparticle tracking analysis (NTA) performed on isolated matrix vesicles and non-purified construct medium samples (Figure 6.3a-b), indicated that it was possible to isolate a small population of TNAP-containing nanostructures with sizes in a much narrower range than the ones present in the growth medium. The highest concentrations were those of particles which ranged in size from 100-200 nm (Figure 6.3b). This corresponds to the range in which previously described matrix mineralization vesicles were detected by previous authors (Anderson 1969, Golub 2009, Golub 2011, Cui, Houston et al. 2016).

When denatured under SDS-gel electrophoresis, MV-IgG complexes eluted from the beads separated into several fractions (Figure 6.3c). The TNAP band can be observed as a dimer between 80-110 kDa (Ishida, Komaru et al. 2011, Satou, Al-Shawafi et al. 2012), further supporting these results. IgG bands appeared at around 170 kDa, as confirmed by controls, and fractions of other, unidentified proteins belonging to matrix vesicles appeared between 110-160 kDa.

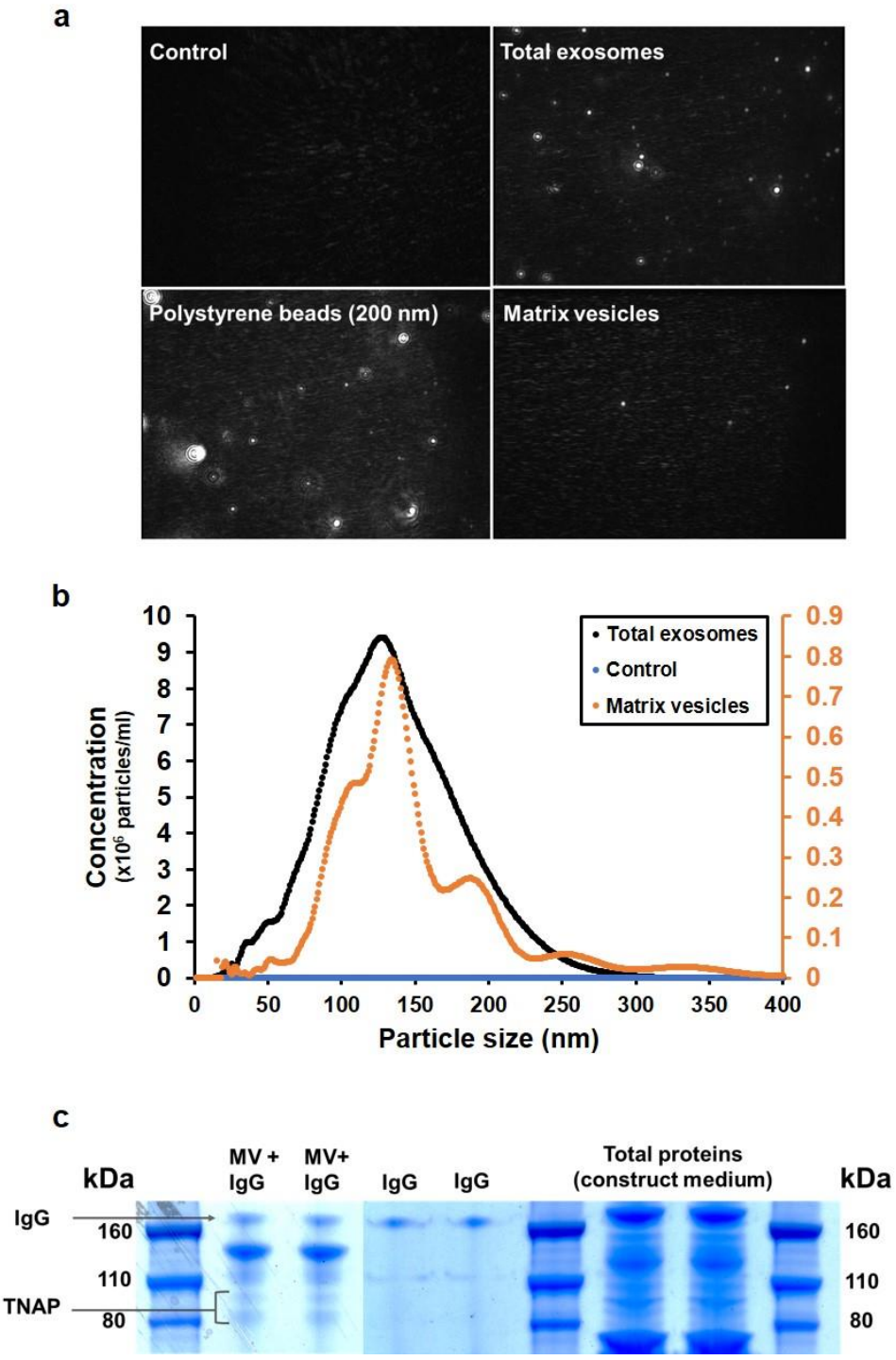

Figure 6.3 | Characterisation of immuno-selected vesicles. **a**, Nanoparticles, visualised in real-time exclusively using NTA. Controls (sterile PBS) do not contain any nano-particles. The growth medium of constructs contains an abundance of nano-particles, whereas the buffer containing the isolated vesicles contains a very small population of particles. Positive controls (200 nm polystyrene beads) are provided for comparison. **b**, The small population of purified vesicles contains particles of sizes in a much more narrow range than total exosomes in construct medium. Vesicles ranging between 100-200 nm are particularly abundant. **c**, When denatured using SDS-PAGE, the Ab-MV complexes separate into several fractions, which include the TNAP protein dimer (80-110 kDa), the IgG antibody (170 kDa) and several unidentified protein fractions belonging to matrix vesicles (110-160 kDa).

TNAP is the major phosphatase of MVs which regulates the generation of extracellular Pi from ATP (Hessle, Johnson et al. 2002, Cui, Houston et al. 2016). These vesicles can maximally initiate the deposition of calcium in the presence of ATP (Hsu and Anderson 1978). Therefore, the potential existence of ATP with the vesicles could be indicative of an active role of these structures in the mineralisation process of constructs. Its presence in matrix vesicles was tested using quinacrine dihydrochloride staining and was imaged indirectly using confocal microscopy of beads (Figure 6.4a). The beads which contained the selected matrix vesicles showed a higher amount of fluorescence compared to controls (beads bound to the antibody-only) (Figure 6.4b).

The role of these vesicles was probed further by assessing their osteogenic potential, or their ability to bind a bone-like extracellular matrix. This was tested by incubating the eluted vesicle-antibody complexes from the beads to collagen I-coated surfaces. Matrix vesicles have been shown to bind to collagen type I, II and X (Wu, Genge et al. 1991) and collagen I has been shown to induce the vesicle-mediated mineralisation of articular cartilage embedded in agarose-collagen hydrogels (Jubeck, Gohr et al. 2008).

The amount of binding of matrix vesicles to collagen was detected by applying a fluorescently-labelled secondary antibody against the primary antibodies. Results are presented in Figure 6.5b and show a striking difference between the MVs-incubated collagen surfaces and controls. The purified vesicles showed a high degree of binding to the collagen matrix, which can be distinguished due to its typical morphology. Eluted antibodies targeted with secondary antibodies and secondary antibodies alone showed a very small degree of non-specific binding.

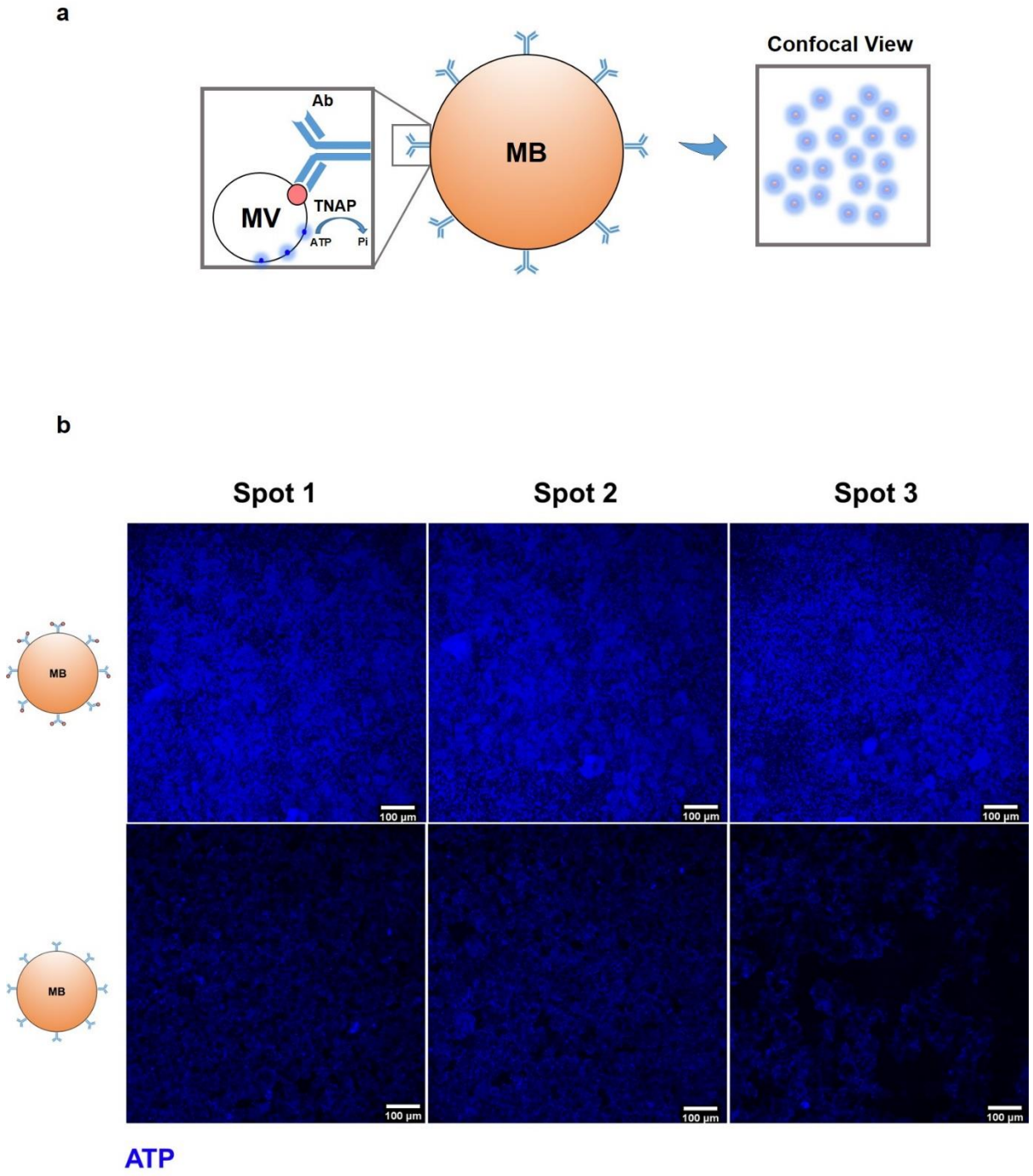

Figure 6.4 | Isolated MVs contain ATP. a, Mineralisation is an ATP-mediated process. ATP is transformed by membrane-bound TNAP on the surface of vesicles into Pi. ATP on vesicles was labelled using quinacrine dihydrochloride and visualised indirectly using confocal microscopy, where it was detected as blue fluorescence from the beads. **b**, Purified MVs and controls were stained directly on the magnetic beads using quinacrine dihydrochloride. Controls contained the bound antibody but were treated with dH_2O as opposed to culture medium. All images were acquired under the same conditions and settings. Some degree of background staining can be observed in control beads. The vesicle-bound beads show a higher amount of fluorescence, indicating the presence of ATP associated with the MVs.

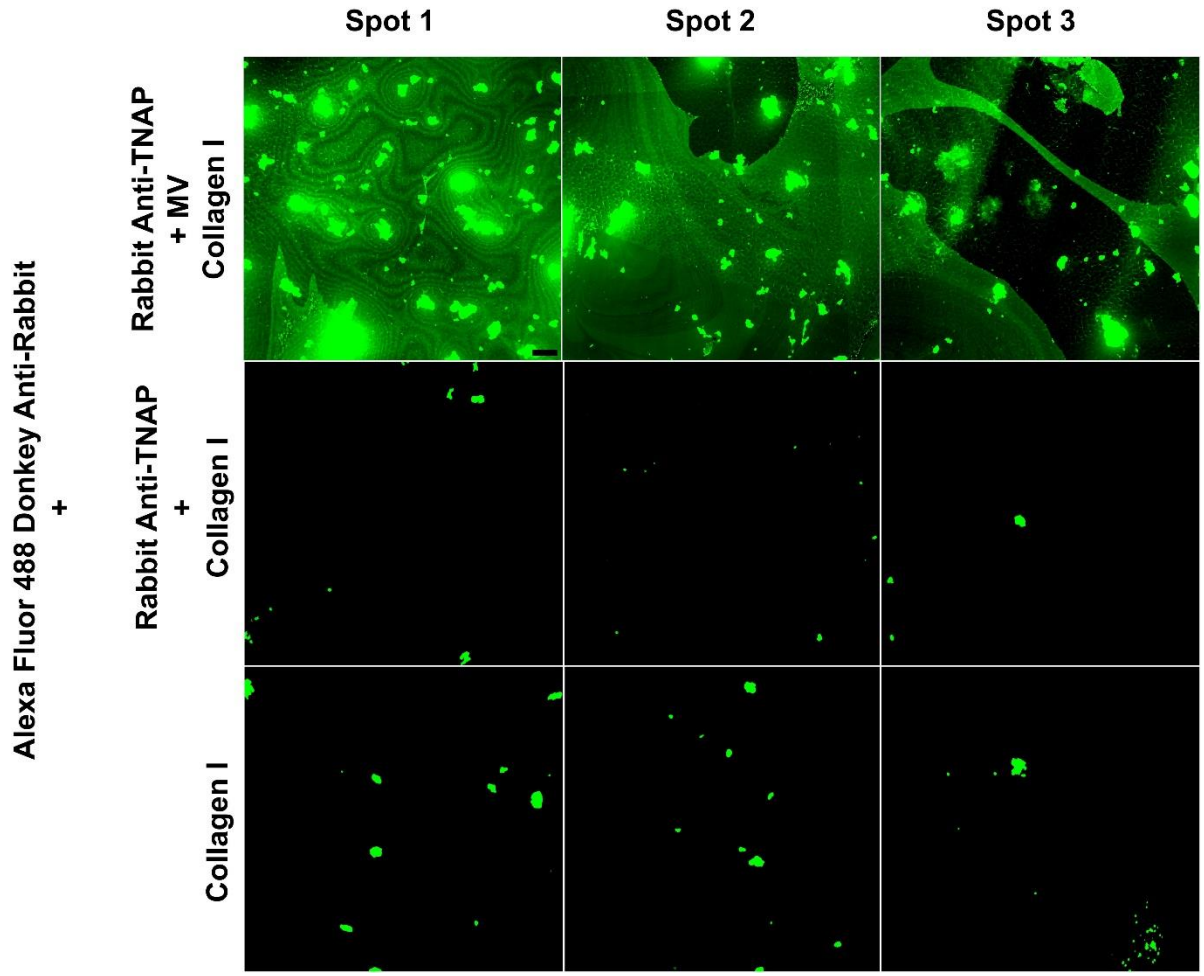

Figure 6.5 | Isolated matrix vesicles show a high degree of osteocompetency. The TNAP-bound vesicles have the ability to bind collagen type I (top row), whereas TNAP antibodies alone (post-elution, centre) show a small degree of non-specific binding. The binding of vesicles and controls to collagen I was detected using secondary antibodies conjugated to Alexa Fluor 488. These secondary antibodies showed a small amount of non-specific binding to the collagen I matrix in the absence of sample/control (bottom). Images were acquired using the same settings and conditions. Scale bar = 100 μm.

CHAPTER VII

ADMINISTRATION OF OSSIFFICATION-INHIBITING COMPOUNDS

7.1 INTRODUCTION

As discussed in previous chapters, the ability to simulate mature bone at multiple levels, including chemical composition, architecture and mature bone cell differentiation, provides the opportunity to apply this system to different research areas where *in vivo* research is in early stages or too complex. Such areas include toxicology and pharmacology and therefore, application of various chemical compounds to this system could provide meaningful results. The interaction between these chemicals and the mature bone tissues was of interest because if successful, this system could provide a screening or testing platform for novel compounds.

Chapter 1, section 1.11.4 describes the current agents used to manage and prevent heterotopic bone formation, as well as their advantages and limitations.

A pilot study over 3 weeks in culture was conducted in order to test novel compounds that can inhibit the ossification process, obtaining promising results. Two promising compounds were selected, CD1530, a nuclear retinoic acid receptor gamma agonist (RAR-γ) that has been increasingly used recently in treating both the acquired and

congenital forms of heterotopic ossification (Kaplan and Shore 2011, Shimono, Tung et al. 2011), and LDN193189, which is a selective inhibitor of the BMP type I activin receptor-like kinase ALK2, ALK3 (Figure 7.1), and a weak inhibitor of ALK 4 and ALK7 and which has been successfully used to reduce heterotopic ossification in transgenic murine models of *Fibrodysplasia ossificans progressiva* (Yu, Deng et al. 2008). RAR-γ agonists like CD1530 are thought to inhibit the formation of ossification in early stages, at the pre-chondrogenic and chondrogenic stages. They also act by blocking BMP-2 signaling, reducing the skeletogenic potential of osteoprogenitor cells and reduce phosphorylation of signaling effectors SMAD 1, SMAD 5 and SMAD 8, thus preventing the subsequent mineralization steps. Similarly, LDN193189 also reduces activation of the BMP signaling effectors, in particular SMAD1, SMAD5 and SMAD8 (Yu, Deng et al. 2008).

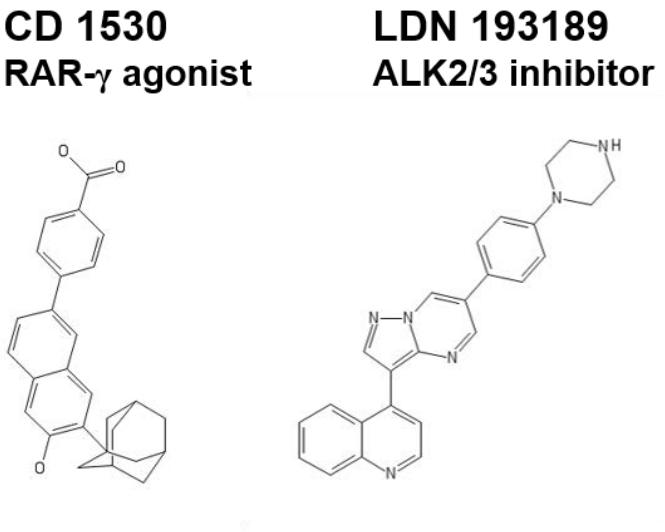

Figure 7.1 | Application of two ossification-inhibiting compounds to constructs. Two novel drugs were selected based on recent advancements. The first compound, CD1530 is a retinoic-acid-γ receptor agonist that has been recently tested with multiple types of heterotopic ossification; while LDN 193189 is an inhibitor of the BMP mineralisation pathway, acting as a selective inhibitor of the BMP type I activin receptor like kinase ALK2 and ALK3.

7.2 AIMS AND OBJECTIVES

The goal of this work was to determine whether heterotopic ossification drugs can prevent the advancement of ossification in constructs. This was performed to demonstrate the system's potential as a drug screening platform and to offer further evidence on the central role of cells in the ossification process.

7.3 CHARACTERISATION METHODS

7.3.1 CONSTRUCT DEVELOPMENT

Constructs were developed using the procedures described in *Chapter 2*, using newly-extracted femoral periosteal cells which were derived from euthanised 3 weeks-old Wistar rats and cultured until confluency. Cells were applied to constructs using the procedures described in *Chapter 2* and allowed to contract for 7 days before supplementation.

7.3.2 CD1530 AND LDN193189 SUPPLEMENTATION

RAR-γ agonist CD15030 and $ALK_{2/3}$ inhibitor LDN193189 were administered in the culture medium of constructs at a concentration of 1 μM and 25 nM, respectively. Starting with day 7 of culture, constructs received one dose every two days (6 doses total) of either CD1530 or LDN193189. Controls received an equivalent amount of DMSO, which was used in drug dissolution. 3 constructs were collected for analysis at each time point from each group (Control, CD1530 and LDN193189). The experiment was terminated at day 22.

7.3.3 VOLUMETRIC ANALYSIS USING MICRO-COMPUTED TOMOGRAPHY

As these constructs were younger (7-21 days) compared to our most mature constructs (3 months-1 year) and hence less ossified and dense, acquisition settings were adjusted for this study to an X-Ray voltage of 50 kV and a tube current of 100 μA; an image pixel

size of 13 μm, with an exposure time of 510 ms, a rotation step of 0.4 degrees and a frame averaging value of 2. Flat field correction was performed for image clarity and no ring artefact correction was applied.

Transfer functions were created in the CTVox software that allowed segmentation of the high-density matrix components, as well as for creating colour-coded versions of the components in the constructs. The same transfer function was used for all constructs in the same group of investigation.

Volumetric quantification of the mineral component was performed using morphometric analysis in the CTAn software (v. 1.13). 200 slices from equivalent regions in the central portions of control and drug treated constructs were isolated and a threshold of 220-255 was applied to segment the high-density mineral component. 3D analysis of the segmented volume was performed and data was averaged to obtain the final volume in mm^3.

7.3.4 STATISTICAL ANALYSIS

Measurements were acquired in triplicate and/or from a sample number of 3 constructs, unless otherwise indicated in the text. Raw data was not pre-processed (normalised/transformed) unless indicated otherwise. All data is presented as mean ± SD. Statistical analysis was performed using a one-tailed distribution t-test, with a heteroscedastic variance assumed. A p value lower than 0.05 was chosen for determining significance (MS Excel, Washington, USA). Percentage difference was calculated using the formula X = (A-B)/A*100.

7.4 RESULTS AND DISCUSSION

Volumetric analysis performed using morphometric CT analysis revealed that treatment with compound CD1530 prevented the advancement of ossification towards the center by 99% compared to controls in the 21 days study (Figures 7.2-7.3). Similarly, the second compound tested, LDN193189, was effective in reducing the mineralized matrix volume centrally by 70% compared to controls, confirming the results seen when RARs were administered (Figures 7.2-7.3).

The fact that CD1530 caused a bigger reduction in the progression of ossification is very interesting, as this drug is thought to prevent bone formation at the chondrogenic stage (Baird and Kang 2009, Shimono, Tung et al. 2011).

The marked reduction in matrix volume following administration of these compounds was further confirmation that mineralization takes place through a cell-mediated route, as encountered during normal long bone formation, fracture repair, and heterotopic ossification (Kaplan and Shore 2011). It also demonstrates the system's potential as a drug screening tool, meaning that it could act as an intermediate between *in vitro* and *in vivo* research and that it could potentially reduce the number of animals used for skeletal research.

In vitro testing is currently used as a first-stage method for assessing the toxicity and compatibility of drugs and implants with different physiological systems, and can avoid the unnecessary use of animals in the testing of cytotoxic or incompatible materials. Whilst this method is the most suitable for standardization and quantification, giving more reproducible results in some cases compared to *in vivo* testing,, there are numerous problems with *in vitro* testing of pharmacological and other compounds (Pearce, Richards et al. 2007).

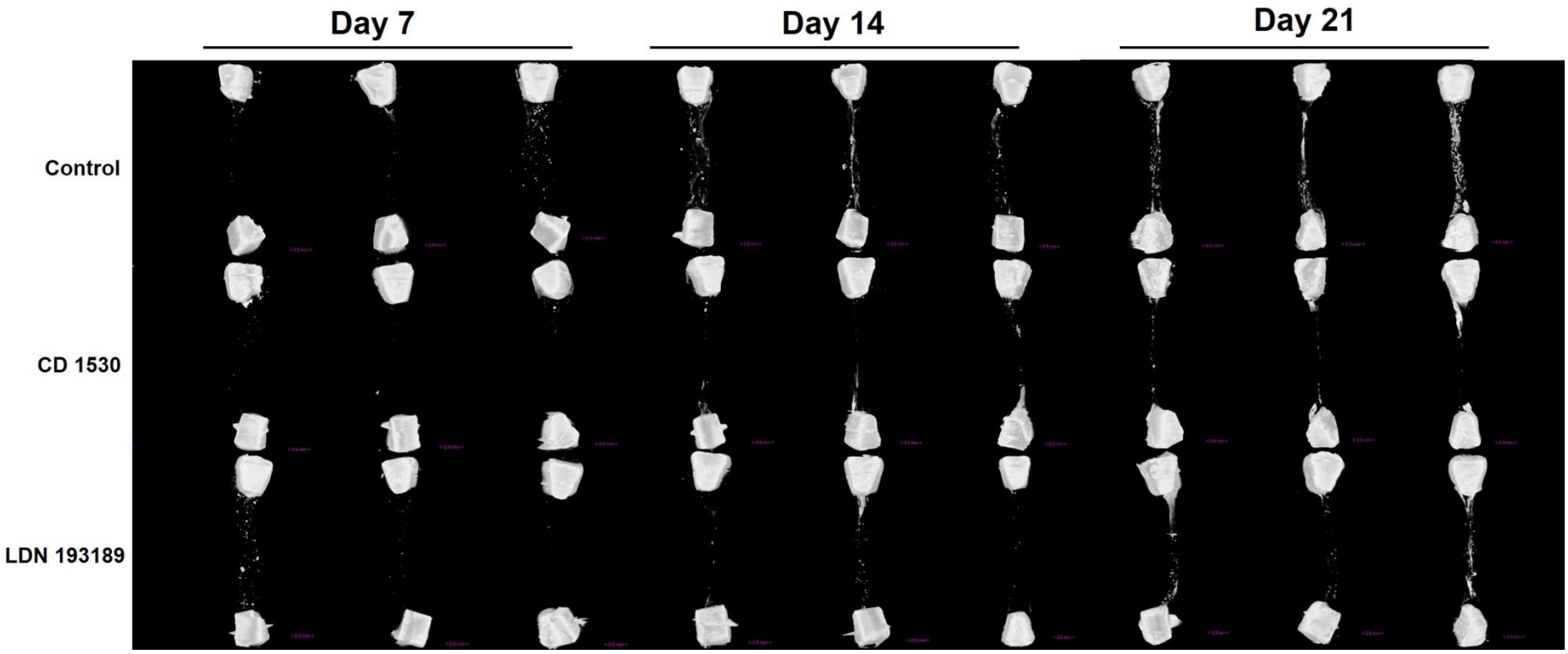

Figure 7.2 | Tomographic analysis of the progression of ossification in constructs. Administration of two inhibiting compounds in a pilot study lasting 21 days appeared to reduce the progression of ossification in treated constructs compared to controls. CD1530 (1 μM) significantly reduced mineralized matrix formation following 21 days of culture compared to equivalent controls. LDN193189 (25 nM) also appeared to be effective.

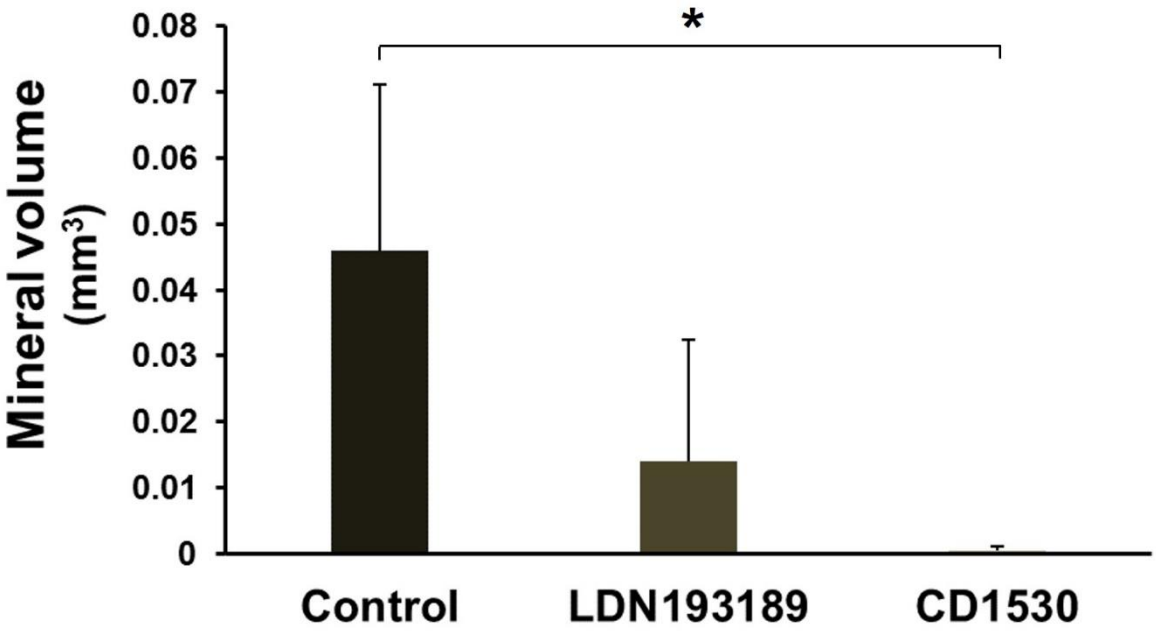

Figure 7.3 | Ossification – inhibiting compounds decrease matrix and mineral formation in constructs. Comparison of the mineral volume located in the central portion of constructs following 21 days of culture, quantified by morphometric CT analysis. Constructs treated with CD1530 showed an average of 99% less mineral in this region compared to controls, which was statistically significant, whereas the group treated with LDN193189 showed 70% less mineral, although not significant. Data is presented as means ± SD. *$p < 0.05$, n=3.

First of all, the cell-response extracted from the results of *in vitro* testing, often referred to as 'biocompatibility' is most of the time incorrect, as this type of cell culture is focused on the behavior of individual cells, which are not organized into complex tissues, and as such, these tests cannot demonstrate whole-tissue response to drugs, biomaterials and implants. In these situations, 'cytotoxic' and 'genotoxic' effects are more suitable terms (Hanks, Wataha et al. 1996, Pearce, Richards et al. 2007, Li, Zhou et al. 2015).

Secondly, the response of isolated cells to drugs and toxic compounds can be much greater than *in vivo*, meaning that the effect of these compounds can be overestimated. This, together with the short lifespan of cells means that the investigations are limited to the acute, short-term effects of these compounds (Hanks, Wataha et al. 1996).

Thirdly, there can be a great variability between cells of different passages and between cells of the same type of cell line, meaning that some cells within an experiment can be less responsive to some compounds, as noted with metal ions from dental materials (Wataha, Hanks et al. 1994).

Lastly, it is difficult to control the behavior of cells *in vitro* and to simulate the organization and cellular interactions found *in vivo*. For this reason, animal models have remained essential for evaluating biocompatibility, whole-tissue and systemic response and mechanical function under chemical and mechanical stress.

The model developed in this thesis provides the advantage of an *in vitro* system in terms of reproducibility and flexibility as well as adaptability, but with a biological complexity more similar to *in vivo* testing. These features are, to the best of my knowledge, unique to date. The system offers a number of additional advantages, such as the ease of

implementation in general cell laboratories and therefore could potentially reduce the unnecessary use of animals for preliminary pharmacological and toxicological research.

CHAPTER VIII

FURTHER APPLICATIONS OF THE SYSTEM AND VASCULARISATION OF CONTRUCTS

8.1 INTRODUCTION

One of the principal advantages of this system compared to previous models is its flexibility and compatibility with cells of different origins, both primary and immortalised lines, derived from different species. Unlike pre-made connective tissue scaffolds which provide temporary structural support to cells when implanted into the affected tissues, this system provides a temporary scaffold which allows cells to produce their endogenous matrices. The versatility of this system makes it possible to develop constructs resembling other tissues of the musculo-skeletal system, including tendons, ligaments and cartilage. Moreover, it would be possible to generate personalised tissues using the patient's own cells and with human-derived components (Meijer, de Bruijn et al. 2007), created using either commercially available fibrinogen and thrombin or extracted from the patient's plasma. The results presented in this chapter represent exploratory work performed to demonstrate these aspects in order

to further support the biological relevance of this model, its potential impact in regenerative medicine and its applicability for the study of different connective tissues.

8.2 AIMS AND OBJECTIVES

Experimental work was undertaken to determine the viability and compatibility of cells from different musculo-skeletal origins with the fibrin constructs. Their development was observed and recorded, including advantages and disadvantages for each system.

The second goal was to develop a 'vascularised bone' model by attempting to form endothelial tubes in constructs and to optimise a culture system for a mixed osteoblastic-vessel construct model.

The final aim of this thesis was to perform a preliminary scoping exercise to create other analogous skeletal structures, such as the vertebral column.

8.3 CHARACTERISATION METHODS

8.3.1 TENDON CONSTRUCTS

Tendon-like constructs were developed using a cell line of avian-derived tendon fibroblasts (CTFs) using the standard methodology described in Chapter 2. Cells had been previously isolated from the flexor tendons of 13 days-old chick embryos using collagenase type-II digestion and recovery using 100 mm cell strainers (BD Biosciences, United Kingdom). They were frozen and thawed using the procedures listed in Chapter 2 and were then cultured in standard DMEM containing 10% FBS and 1% P/S (Thermo Fisher Scientific, USA).

8.3.2 CARTILAGE CONSTRUCTS

Cartilage constructs were developed using the standard procedures described in Chapter 2.

8.3.2.1 CHONDROCYTIC CELLS

Human primary chondrocytes were derived from tissue obtained from the Oxford Musculoskeletal BioBank and was collected with informed donor consent in full compliance with national and institutional ethical requirements, the United Kingdom Human Tissue Act, and the Declaration of Helsinki.

2-5 cm cartilage tissue sections were excised following surgery, minced with a blade prior to overnight digestion in collagenase, followed by plating in sterile, 90 mm

diameter polystyrene petri dishes containing 25 ml DMEM - F12 growth medium, supplemented with 10% FBS and 1% P/S (all from Lonza, Basel, Switzerland).

8.3.2.2 HUMAN FIBRIN SCAFFOLDS

Unlike previous constructs, the fibrin scaffolds developed for use with human-derived chondrocytes were built using human-derived fibrinogen and thrombin (Sigma-Aldrich, Germany).

Following isolation from Petri dishes, cells were seeded into these scaffolds and contraction was monitored over three weeks of culture. At the end of the three weeks, a regime of chondrogenic supplementation was administered to half of the constructs, whereas the remaining half continued to receive the normal DMEM-F12 supplementation.

8.3.2.3 PRO-CHONDROGENIC SUPPLEMENTATION

The supplementation regime consisted of a combination of pro-chondrocytic factors, which were part of a hMSC Chondrogenic SingleQuots Poietics kit (Lonza, Basel, Switzerland). The final supplementation medium consisted of 10% FBS, 0.1% gentamicin sulphate - amphotericin-B, 2.16% L-glutamine, 1.08% proline, 1.08% ascorbate, 1.08% sodium pyruvate, 1.08% insulin-transferrin-selenium supplementation and 0.54% dexamethasone. In addition to these components, TGF-β_3 (Lonza, Basel, Switzerland), was added with each feed. TGF-β_3 was prepared by resuspending the lyophilized powder in sterile 4mM HCl supplemented with 1 mg/ml

BSA to a concentration of 20 μg/ml. TGF-β_3 was added at a ratio of 0.5 μl per ml of chondrogenic feeding medium.

Supplementation was administered for one month, which was the point when visual differences were observed between the groups.

8.3.2.4 WHOLE MOUNT HISTOLOGICAL STAINING FOR CARTILAGE

Whole-mount histological staining for cartilage using Alcian Blue was performed to detect the presence of sulphated proteoglycan-rich matrix in the supplemented and the non-supplemented groups.

Constructs were removed from culture, rinsed with 2 ml PBS twice for 5 seconds and fixed with 2 ml standard Bouin's fluid for 5 hours at room temperature. The fixation fluid was then aspirated and constructs were washed with dH_2O for 15 minutes. Constructs were then stained with Alcian Blue (1%, pH 2.5 in acetic acid) for 1 hour at room temperature. Constructs were gently washed with 70% EtOH to remove excess dye and photographs were taken of constructs in each group.

8.3.3 ANGIOGENESIS IN CONSTRUCTS

Endothelial tubes were formed in constructs using a population of commercial Human Umbilical Vein-derived Endothelial Cells (Cell Applications Inc, San Diego, CA, USA). Cells were cultured using the procedures described in Chapter 2, in Endothelial Basal Medium (EBM-2, Lonza, Basel, Switzerland) containing 10% FBS and 1% P/S. Constructs were developed using the standard procedures described in Chapter 2.

Constructs were allowed to contract for 7 days. A regime of angiogenic supplementation was commenced following contraction in order to initiate blood vessel formation.

Supplementation components were part of a Clonetics EGM-2 SingleQuots kit (Lonza, Basel, Switzerland). The final supplementation medium consisted of 2% FBS, 0.1% Gentamicin Sulfate Amphotericin-B, 0.1% ascorbate, 0.4% pro-angiogenic factor Recombinant Human Fibroblast Growth Factor – B (rhFGF-B), 0.1% pro-angiogenic factors Vascular Endothelial Growth Factor (VEFG), Human Recombinant Epidermal Growth Factor (hrEGF) in buffered BSA saline solution, heparin and recombinant long r insulin- like growth factor-1 (R^3-IGF-1) and 0.04% hydrocortisone.

Images of forming tubes in whole constructs were acquired using a CETI Inverso TC100 brightfield microscope (Medline Scientific, Oxon, United Kingdom).

8.3.4 MIXED ENDOTHELIAL-BONE SYSTEMS

Co-cultures of HUVECS and 2T3 cells were developed using the methodology described previously by encapsulating equal numbers (50.000 cells from each population) in constructs. The culture medium used consisted of equal parts of MEM α and angiogenic EBM-2. Images of viable endothelial tubes were acquired using Two-Photon Excitation Fluorescence using the procedures described in Chapter 5.

8.3.5 VERTEBRAL DISK CONSTRUCTS

To prove this concept, spinal 'discs' were developed by dispersing mouse mesenchymal stem cells in fibrin gels using the procedures described previously. 3D models of human-size vertebra (approximately 65 mm^3) were acquired online and down-scaled to

approximately 15 mm^3 to fit the size requirements for culture into standard 35 mm^2 dishes. For this initial study, the vertebras were 3D printed using standard plastic material from the shape of the ninth thoracic vertebra. Custom moulds were taken of this vertebra and were filled with a liquid brushite-TCP mixture, as described in Chapter 2.

Anchors were placed in the centre of sterilised, Sylgard-coated 6-well dishes and fibrin gels were formed in the dishes using the standard procedures. Stem cells were dispersed into the scaffold and allowed to contract the matrix for a duration of 2 weeks (stem cells contract the matrix slower). During the contraction time, the vertebral 'anchors' served as single retention points around which the cells organised a 'disk-like' structure. Following a month and 5 days of culture, the individual vertebra containing their attached soft tissues were assembled together to form a spinal-like structure. The gels were allowed to fuse with the neighbouring vertebra for a period of approximately one month, during which the matrix also became progressively replaced with mineralised collagen, thus mimicking the ossified spine, or 'bamboo' spine encountered in degenerative conditions such as Ankylosing Spondylitis.

8.4 RESULTS AND DISCUSSION

8.4.1 TENDON CONSTRUCTS

Constructs developed with fibroblastic cells contract very quickly compared to osteoblastic cell constructs and assemble into tendon-like 3D structures as early as 7 days. Figure 8.1a provides an example of a 6 months old, mature construct. Different versions of these constructs have been developed in this research group over the past years, containing modifications such as stainless-steel pin-anchors, titanium anchors and spring reinforcements and chemically adjusted brushite anchors. These constructs were very well characterized biomechanically and biochemically and several papers describe extensive research conducted in this group in this area (Paxton, Donnelly et al. 2010, Paxton, Wudebwe et al. 2012, Lebled, Grover et al. 2014, Wang, Williams et al. 2016).

8.4.2 CARTILAGE CONSTRUCTS

Figure 8.1b-c illustrates examples of constructs developed with chondrocytic cells, which have been stained with Alcian Blue to detect the presence of cartilage. Firstly, this work demonstrates a successful model composed of human-only components. Secondly, the work demonstrates the successful maintenance of the chondrocytic phenotype in constructs after 2 months of culture and following a regime of pro-chondrogenic supplementation. Figure 8.1c illustrates a representative example of a construct which has undergone TGF-β_3 and ITS supplementation (left) compared to a control (right). The amount of cartilage produced in the system is higher in the supplemented

construct. In addition, supplemented constructs appeared to be much stiffer, supporting their own weight and survived the histological processing very well compared to the untreated group, which underwent shrinking. As seen in bone constructs, higher amounts of matrix form around the edges, forming a similar 'periosteal collar' (Mackie, Ahmed et al. 2008).

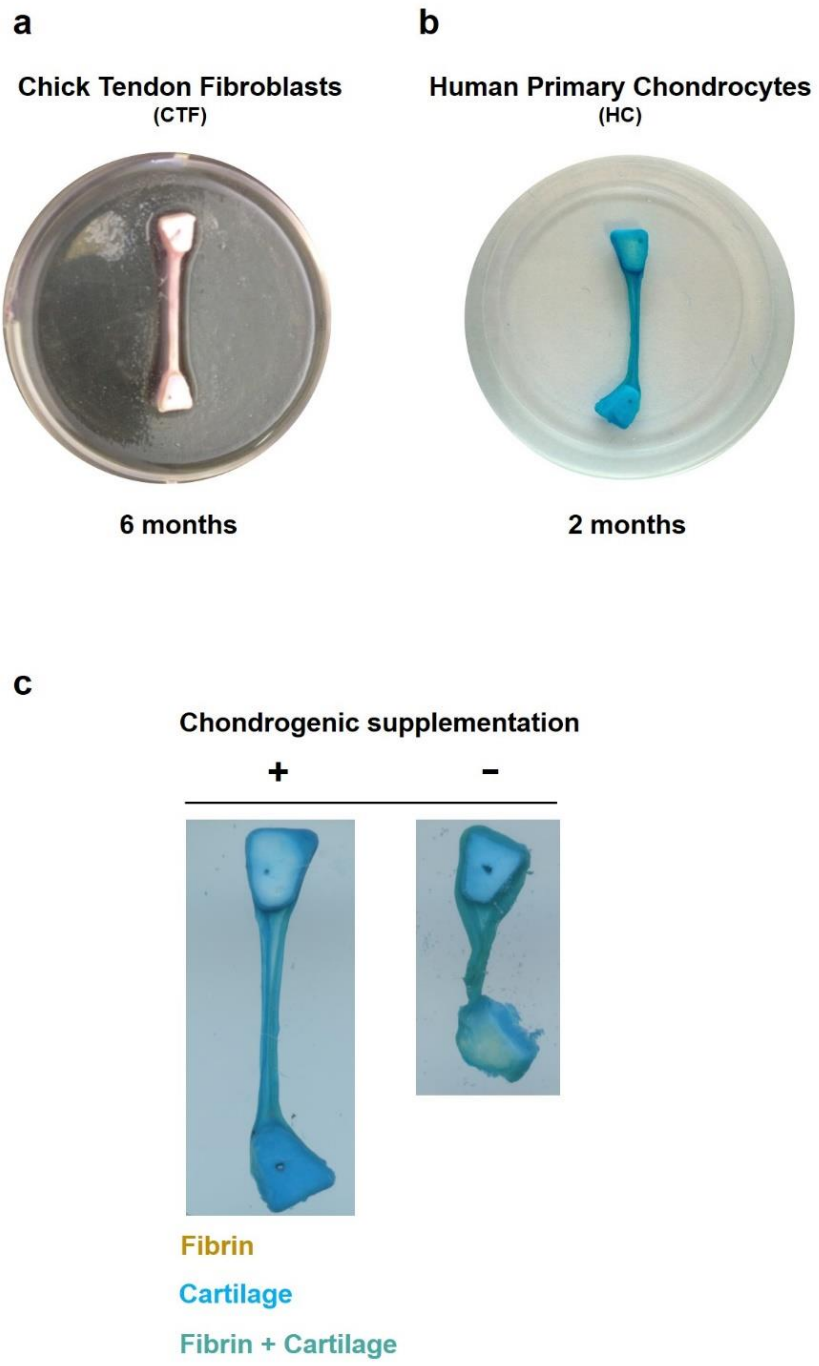

Figure 8.1 | Development of other connective tissues. a, 6-months old construct developed using chick tendon fibroblasts, showing a tendon-like 3D structure. **b**, Example of a construct developed with human chondrocytes and human-derived matrix components, and which has been fixed with Bouin's fluid (yellow, not visible) and stained with Alcian Blue for cartilage detection. **c**, examples of constructs which have undergone pro-chondrogenic treatment (left) vs. control (right). Constructs supplemented with ITS and TGF-β_3 develop more matrix (blue) compared to control (green-blue), are more still and more resilient to histochemical processing compared to controls, which undergo shrinking.

8.4.3 ANGIOGENESIS IN CONSTRUCTS

Endothelial tubes were successfully demonstrated to grow in constructs aligned with the mechanical axis. Figure 8.2 (left) contains an image of a 3 month-old construct, reconstructed from multiple images acquired using a brightfield microscope. Constructs were supplemented with rhFGF-B, VEFG, hrEGF and R^3-IGF-1 for 2 months following contraction to maintain the cellular phenotype and encourage the formation of micro-vessels. The endothelial tube networks were well developed on the surface of constructs (Figure 8.2 middle right) and were part of larger vessel-like structures with diameters ranging from 50 -200 μm (bottom right).

The ability to initiate aligned vascularization in constructs brings the model closer to producing a mature bone system with further similarities to *in vivo* bone (Marenzana and Arnett 2013) and could provide a valuable tool for assessing the role of angiogenesis in traumatic heterotopic ossification (Cocks, Mohan et al. 2017).

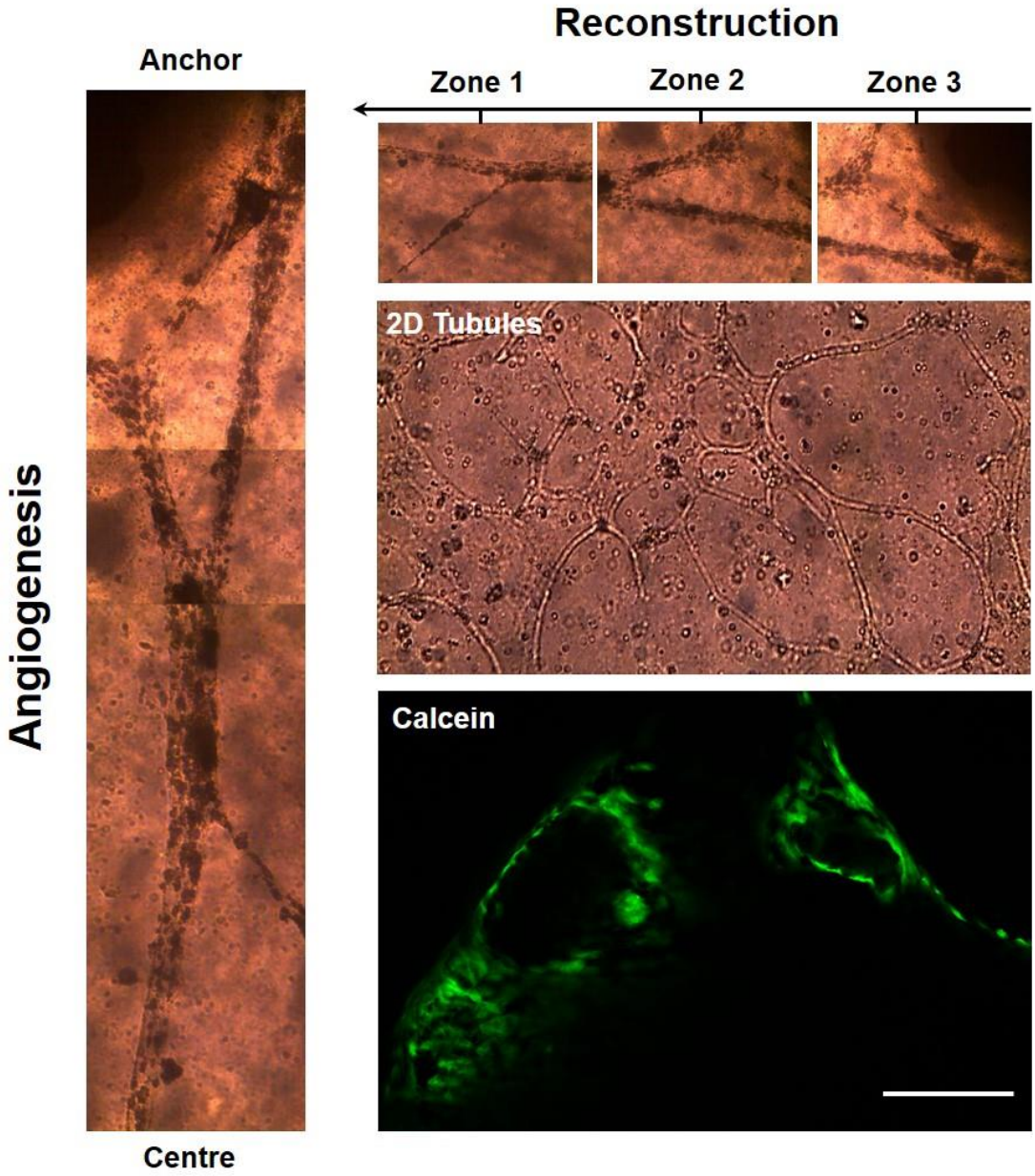

Figure 8.2 | Endothelial tubes resembling microvasculature align with the mechanical axis in constructs. Large image (left) has been reconstructed from multiple brightfield images and shows endothelial tubes branching along the axis of constructs. When observed in a 2D plane (middle right), these cells established complex networks which connect to larger tubes, with diameters ranging between 50-200 μm, as seen through a cross section using TPEF (bottom right). Scale bar = 200 μm.

8.4.4 MIXED ENDOTHELIAL-BONE CONSTRUCTS

A mixed cell system was developed containing co-cultures of osteoblastic cells and endothelial cells to determine whether a vascularised bone model could be produced. Figure 8.3 presents examples a comparison of cellular morphologies in groups of constructs developed with either 2T3 osteoblastic cells, HUVECS or a combination of the two. 2T3 cells in constructs showed an osteoblastic morphology while HUVEC cells, as described above, were able to assemble into micro-vessels as described previously *in vitro* (Naik, Mousa et al. 2003, Chen, Htay et al. 2009). Constructs developed with both types of cells showed tubular structures co-localised with osteoblastic looking cells.

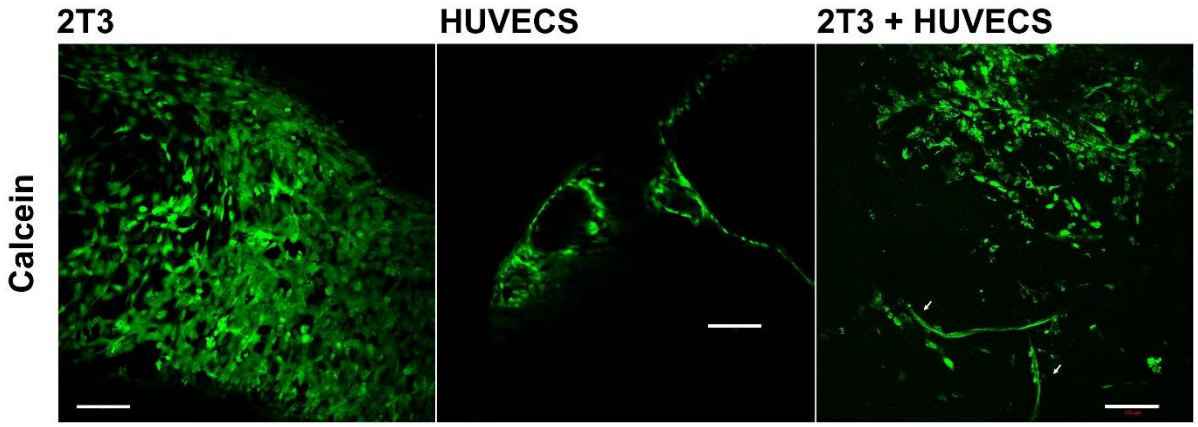

Figure 8.3 | Osteoblastic and vascular cell morphology in individual and mixed-cell constructs. 2T3 cells (left) attached to the matrix and showed a typical osteoblastic morphology, while HUVECS (centre) were able to assemble into tubular structures of 50-200 μm in dimeter. Constructs containing co-cultures of these cell populations showed both types of cell morphology, with endothelial tubes forming adjacent to osteoblastic cells.

8.4.5 VERTEBRAL DISKS CONSTRUCTS

Figure 8.4 shows an example of the assembly process of spinal constructs. Phosphate vertebra are individually placed at the bottom of Sylgard-coated 35 mm^2 wells (Figure 4a). Fibrin gels containing a population of MSCs are formed around the vertebra and allowed to contract fully for 14 days – 1 month. They are assembled together into the spinal structure and discs are allowed to fuse with the neighbouring vertebra over an additional month, until the structure can support its own weight (Figure 8.4b). Over time, the matrix changes in a similar way as observed with regular bone constructs.

This work demonstrated that it is possible to simulate a vertebral-column-like structure and further optimisation work should be carried out to enhance the fusion process and the design.

The spinal model could be further developed by encapsulating a population of intervertebral disk cells (Johnson and Roberts 2003, Erwin and Hood 2014), which are commercially available from a few scientific suppliers, or developing an isolation protocol for extraction from murine spinal discs. Composite hydrogels which can further simulate the biochemical nature (fibrocartilaginous composition) and structure (*annulus fibrosus* and *nucleus pulposus*) of vertebral disks (Mizuno, Roy et al. 2004) could be used instead of fibrin, such as mixed type I-II collagen gels/fibrin (Yang, Seol et al. 2007).

Similar analysis can be undertaken to characterise the ossification process in 'spinal' soft tissue, including micro-CT, and histology-immunohistochemistry of individual discs.

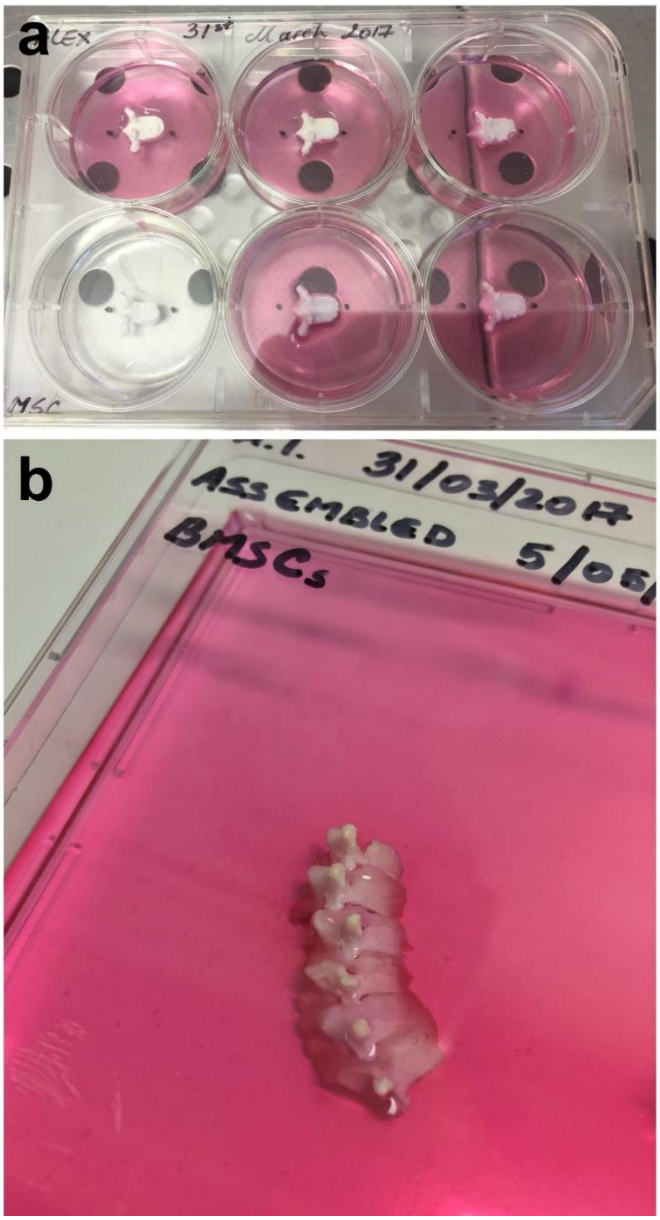

Figure 8.4 | A tissue-engineered model of pathological bone formation in spinal soft tissue where calcium phosphate "vertebrae" are connected with fibrin gels encapsulating a population of stem cells. a, Fibrin gels encapsulating stem cells are formed around phosphate vertebra. Over time, these gels attach strongly to the anchoring material and contract, giving rise to a disk-like structure after approximately 14 days. **b**, The individual 'vertebra' with soft tissue attached to them are assembled together into the spinal structure and gels are allowed to connect to the adjacent vetrebra over the subsequent 3-4 weeks until the structure can support its own weight. Over time, the fibrin is replaced with mineralised collagen and the resulting structures mimic the complex cellular organisation of real bone. These culture systems can be used to study pathological bone formation or to trial new therapies.

A tissue-engineered model of pathological bone formation in spinal soft tissue where calcium phosphate “vertebrae” are connected with fibrin gels encapsulating a population of stem cells.

CHAPTER IX

FINAL CONCLUSIONS

This work demonstrates how simple homogeneous materials (fibrin) may be structured and modified by populations of cells to create complex tissues by making relatively simple geometrical and chemical modifications to the culture system. The composition of the tissues was probed using a suite of chemical analysis techniques that allowed the identification of the distribution and local organisation of matrix components.

After even short periods of culture, the tissues were shown to be heterogeneous in composition and structure, with collagen and mineral distributed in spatially distinct regions. Importantly, the Raman spectral data suggested that the mineral deposited within the tissue was associated with collagen as opposed to precipitated on the surface of the tissue. The mechanism of tissue formation recapitulated several stages of development of a fracture callus and the distribution of collagen and mineral within the tissue was similar to that found in mouse femoral bones.

This model allowed for the production of a complex bone-like tissue *in vitro*, which exhibits features typical of native bone, including a canalicular network populated with mature osteocytes. From longitudinal analysis, it was demonstrated that the tissues form through the differentiation of periosteally-derived stem cells into a heterogeneous population of cells that ultimately lay down a mineralised collagenous matrix with composition similar to native bone. This work is of considerable significance since it was possible to produce mature bone-like tissue and to maintain cultures of osteocytes within it for periods of up to 1 year. This is remarkable since the osteocytic phenotype is extremely hard to maintain in culture for longer than one month. This work demonstrates that by providing cells with the right microenvironment, they can build a complex matrix more representative to the endogenous tissues and as such they can be cultured for significant amounts of time. This work further demonstrated the physiological relevance of this model by blocking the bone formation process using a RAR inhibitor that is known to inhibit bone formation *in vivo* by preventing chondrogenesis as opposed to directly inhibiting mineralisation.

This model will help to fill the gaps between basic research and human applications and will provide insights into bone formation and pathological conditions which may have an influence beyond this field of research. This system can serve as template for further explorations, which could pave the way to organogenesis *in vitro*, reducing the number of animals used in research and screening of drugs prior to *in-vivo* or human studies.

CHAPTER X

FURTHER WORK

10.1 CHOICE OF HYDROGELS

Additional experiments could be performed for comparison by substituting the fibrin matrix with a pre-made collagen scaffold in order to observe the dynamics of collagen remodelling. The first motivation is that collagen matrices have different mechanical properties (Rhee and Grinnell 2007, Grinnell and Petroll 2010, Provenzano, Eliceiri et al. 2010, Song, Olsen et al. 2010) compared to fibrin and that will have an influence on the differentiation and activity of embedded cells. It would be expected that the degree of contraction and modelling seen in this system would be low or absent when using collagen matrices, as they are not as flexible as fibrin (Ngo, Ramalingam et al. 2006). There are additional reasonings for conducting this type of work, including the distinct biochemical characteristics of collagen, which will be discussed in later chapters.

Although less clinically relevant, the use of collagen with cells originating from immortalised cell lines could be attempted. This is because the biodegradability of fibrin can also be disadvantageous (Yang, Seol et al. 2007) when using engineered osteoblastic cell lines such as MC3T3 or 2T3s, which unlike primary cells, were observed to dissolve the fibrin matrix, which then fails to maintain integrity following 14 days of culture. This

is because immortalised cell lines like MC3T3-E1 continuously produce matrix metalloproteinases capable of degrading the extracellular matrix, such as MMP-2 and MMP-13, the later which is up-regulated in the presence of ascorbic acid along with MT1-MMP (Mizutani, Sugiyama et al. 2001). Ascorbic acid is already present in high quantities in the growth medium required for proliferation of these cells (MEM medium containing the alpha modification, approx. 50 mg/L or 0.28 mM) and further ascorbic acid supplementation is added from day 7 in order to induce differentiation (0.25 mM). From that point, the fibrin matrix can only maintain integrity for a maximum of 7 further days. Composite models containing both types of scaffold could be attempted, as described by Yang and colleagues (2007) and could be used for fundamental studies where the requirement for primary cells is not obligatory.

10.2 EARLY EVENTS

In addition, it would be interesting to compare the early events and contraction to a group of constructs treated with pharmacological compounds which inhibit the contractile ability of the cells, such as statins. For this purpose, drugs which can arrest the actin dynamics in living cells could provide further information on the early organisation and matrix re-modelling. Compounds such as Latrunculin (Kopecka, Yamaguchi et al. 2015), which cause G-actin sequestration and prevent F-actin assembly in biological cells, and drugs which can interfere with the rearrangement of the actin network (Blebbistatin) and cytoskeletal structure (Atorvastatin, Simvastatin) and alternatives could be used (Watanabe, Yumoto et al. 2010, Peng, Wilson et al. 2011, Dick, Jonak et al. 2013). Moreover, statins such as Atorvastatin, Simvastatin and Fluvastatin have been shown to inhibit the production of MMPs in certain types of

fibroblasts embedded in 3D collagen cultures, including MMP-1, MMP-3 and MMP-9 (Kamio, Liu et al. 2010), highlighting the important role of these enzymes in the initial matrix building process.

10.3 MONITORING MINERALISATION

The dynamics of mineral deposition could also be temporally and spatially monitored using chromogenic/fluorescently-labelled bisphosphonates (Bae, Sun et al. 2014). Bisphosphonates have been used for many years as the first line therapy for numerous bone myelomas, metastases, Paget's disease, fractures and osteoporosis (McDonald, Schindeler et al. 2007, Drake, Clarke et al. 2008). They have the ability to bind to bone and to remain attached for many years, acting through several mechanisms, including by inhibiting osteoclastic activity (Maraka and Kennel 2015). The wide availability and the numerous types of bisphosphonates available would allow the design of a multi-chromogenic labelling method for spatial localisation of the newly forming bone, which could complement the tomographic data and could provide another method to quantify the newly forming mineral. The same or different type of drug, labelled distinctly, could be applied to forming constructs with every feed, which would be of particular importance especially in the early ossification stages, when different mineral phases are laid down rapidly.

10.4 COLLAGEN ORGANISATION

It would be interesting to analyse constructs using transmission electron microscopy (TEM) at various points during the maturation process, as it would give information on

the organisation and mineralisation of collagen at the nano-scale (Everts, Niehof et al. 2012).

High-resolution Raman maps could be performed for constructs of different ages based on peaks corresponding to different matrix proteins and minerals (amides, phosphate groups, hydroxyproline). These maps can be superimposed and could offer detailed information on regional chemistry and the dynamics of matrix production and ossiffication. These maps can be further supported by histology for collagen using picrosirius red or van Gieson (Segnani, Ippolito et al. 2015) and immunohistochemistry for collagen I.

The presence of other matrix proteins in the newly forming matrix, such as sulfated glycoaminoglycans (GAGs) like chondroitin sulfate, chondroitin 6-sulfate and keratosulfate (Catini and Gheri 1990, Ling, Murali et al. 2006), also involved in ossiffication and bone function, could be evaluated using chemical colorimetric assays. This is particularly important as some types of GAGs have been found in high amounts around osteocytes (Catini and Gheri 1990), the development of which is discussed in the next chapter.

10.5 MECHANICS OF CONTRACTION

The ideal formation of a 'periosteal' structure in constructs could have also occurred due to a preferential migration of cells towards the edges of the culture well walls (and hence fibrin gels) and therefore, a higher number of cells could have given rise to additional bone tissue in this region. This could have been initiated by an 'edge effect' (Lundholt, Scudder et al. 2003), caused by a lack of uniform temperature transfer in the

culture wells (as a result of differences in plastic thickness) in the initial period of incubation.

Viability and morphology analysis on different areas of constructs during the initial 7 days of culture would be able to provide insight into this matter.

To prevent this effect, several commercially available culture plates have been recently designed by many scientific suppliers (e.g. Thermo Fisher, USA; StarLab, UK), which provide a modified design in order to minimise this effect and provide a uniform layer of cells during culture and hydrogel embedding. One example (StarLab) is the chimney well design with 360° open channels around each well, which can be filled with cell growth medium during incubation to prevent the aggregation of cells at the edges.

This type of culture system might also show differences in contraction or matrix production, which would be worth investigating for comparison.

10.6 MECHANICAL PROPERTIES OF CONSTRUCTS

It would be interesting to extend the AFM mechanical characterisation work towards constructing mechanical maps of whole constructs, but at a cellular resolution. High-resolution maps on sections of early, intermediate and mature constructs could be generated using Nano-Indentation mapping (Chen, Lin et al. 2008, Chen, Schirer et al. 2011). Mechanical properties including hardness and reduced modulus could be then compared to cellular distribution in order to obtain further information on the matrix properties around the osteo-canalicular networks. Additional information from this method could support the results seen in micro-tomographies, for example, the regional variation in mechanical properties due to the fracture union-like progress of ossification

and the density gradient from the central portion of constructs to the outer 'periosteal' like structure.

10.7 MOLECULAR MARKERS

Further molecular work should be carried out to detect the presence of other molecular markers involved in the transition of osteoblasts to osteocytes, including PHEX, DMP1, and FGF-23 (Dallas and Bonewald 2010) as well as the starting point of this transition (e.g. low ALPL).

10.8 ENDOCRINE ROLE

Immunocytological and histochemical work should be carried out to test whether the osteocytic cells express features indicating responsiveness to endocrine signalling (Dallas, Prideaux et al. 2013), such as expression of FGF-23 (which acts on the kidneys) or CX-43 gap junctions (Ishihara, Kamioka et al. 2008, Plotkin 2014) which if positive, could make them a potential target for a range of drug investigations.

10.9 VESICLE-MEDIATED MINERALISATION

Additional work should be completed in order to further characterise the matrix vesicles detected in the medium of constructs. Chemical characterisation of protein content should be performed using mass spectrometry, to detect the presence of annexins (5,2,6,11) and peptidases (aminotripeptidase, alanyl beta-naphthylamidase) commonly described as being part of matrix vesicles (Hirschman, Deutsch et al. 1983,

Xiao, Camalier et al. 2007, Xiao, Conrads et al. 2008). Fluorescence imaging using super high-resolution microscopy (SIM, STED, PALM, STORM) (Huang, Bates et al. 2009, Wegel, Göhler et al. 2016) and TEM (Anderson 2003, Anderson, Sipe et al. 2004) would allow visualisation of these nanostructures.

Demonstration of their role in cartilage mineralisation could be attempted using collagen type II – X surfaces (Wu, Genge et al. 1991).

Numerous molecular techniques (qPCR, microarrays, ELISA, Western Blots) that would allow detection and isolation of MMPs, integrins, transport proteins and miRNA species could be used to characterise the role of these structures further (Jiang, Cui et al. 2013, Chaturvedi, Chen et al. 2015, Lin, Rodriguez et al. 2016).

Further analysis of the cellular phenotype at different time points would be useful to reveal the peak of activity and type of cells which secrete the largest amount of vesicles (i.e. osteoblasts vs osteocytes).

10.10 DRUG SCREENING AND ENDOCHONDRAL OSSIFICATION

Further work should be carried out to determine whether the efficacy of CD1530 was due to an inhibition of cartilage formation in constructs. This would be able to confirm whether ossification in this system takes places through a cartilage intermediate as well as through an intramembranous route. This could be accompanied by histological staining with Alcian Blue and Sox-9 and Collagen II Immunohistochemistry. The formation of a cartilage template in some regions is very likely, as the population of stem cells isolated from the periosteum of long bones has a strong chondrogenic potential (*see* Chapter 1).

Investigations using CD1530 should be further expanded to detect the upper and lower limits of efficacy as well as efficiency over longer periods.

The dose-response curves produced for all pharmacological agents investigated will be able to indicate the drug potential and biocompatibility.

10.11 CHONDROCYTE CONSTRUCTS

Chondrocyte constructs could be further exploited to simulate additional steps of the endochondral ossification pathway. With adequate optimization, constructs could be either partially decellularized to remove the chondrocytic cells, and the template could be used as a scaffold for newly-introduced osteoblasts (Thakkar, Fernandes et al. 2015). Alternatively, the population of osteoprogenitor cells could be co-cultured with the chondrocytes from an experimentally-determined time point. Moreover, as demonstrated here, vascularization of these structures can be attempted, creating an alternative route for *in vitro* bone formation and could recreate some additional stages of endochondral ossification, fracture repair and heterotopic ossification. Figure 5 presents a list of all the cell types that have been tested with this system, together with their advantages and disadvantages.

Species	Tissue	Cell Type	Contraction	Mineral
Avian	Tendon	Fibroblasts	+++	-
Human	Cartilage	Chondrocytes	++	-
Human	Blood Vessels	Umbilical Vein Endothelial Cells	+	-
Human	Bone	Osteoblasts	+	+
Human	Skin	Dermal Fibroblasts	++	-
Mouse	Bone	Osteoblasts (MC3T3)	+++	+++
Mouse	Bone	Osteoblasts (2T3)	+++	+++
Mouse	Bone	Marrow Stromal Cells	+	+
Rat	Bone	Marrow Stromal Cells	+	++
Rat	Bone	Periosteal cells	++	+++
Mixed	Bone + Vessels	Osteoblasts + Umbilical Vein Endothelial Cells	++	++

Figure 10.1 | An account of cell types compatible with the present model. Several types of cells, including primary, expanded from tissue and cell lines were encapsulated in constructs. Their characteristics in terms of ability to fully contract the initial fibrin scaffold and their ability to mineralise the tissue were amongst the criteria used for evaluation in developing the final system. Periosteal cells of rat origin were selected due to their enhanced ability to contract the matrix and mineralise it. Cell lines tend to over-contract and detach the constructs from the anchors.

REFERENCES

Abbott, A. (2003). Cell culture: biology's new dimension. Nature. England. **424:** 870-872.

Abzhanov, A. (2010). "Darwin's Galápagos finches in modern biology." Philosophical Transactions of the Royal Society B: Biological Sciences **365**(1543): 1001-1007.

Agarwal, S., S. Loder, C. Brownley, D. Cholok, L. Mangiavini, J. Li, C. Breuler, H. H. Sung, S. Li, K. Ranganathan, J. Peterson, R. Tompkins, D. Herndon, W. Xiao, D. Jumlongras, B. R. Olsen, T. A. Davis, Y. Mishina, E. Schipani and B. Levi (2016). "Inhibition of Hif1α prevents both trauma-induced and genetic heterotopic ossification." Proceedings of the National Academy of Sciences **113**(3): E338-E347.

Ahmed, T., R. Ringuette, V. Wallace and M. Griffith (2015). "Autologous fibrin glue as an encapsulating scaffold for delivery of retinal progenitor cells." Frontiers in Bioengineering and Biotechnology **2**(85).

Ahn, A. C. and A. J. Grodzinsky (2009). "RELEVANCE OF COLLAGEN PIEZOELECTRICITY TO "WOLFF'S LAW": A CRITICAL REVIEW." Medical engineering & physics **31**(7): 733-741.

Ahrengart, L. (1991). "Periarticular heterotopic ossification after total hip arthroplasty. Risk factors and consequences." Clin Orthop Relat Res(263): 49-58.

Akopova, I., S. Tatur, M. Grygorczyk, R. Luchowski, I. Gryczynski, Z. Gryczynski, J. Borejdo and R. Grygorczyk (2012). "Imaging exocytosis of ATP-containing vesicles with TIRF microscopy in lung epithelial A549 cells." Purinergic Signalling **8**(1): 59-70.

Alexander, B., T. L. Daulton, G. M. Genin, J. Lipner, J. D. Pasteris, B. Wopenka and S. Thomopoulos (2012). "The nanometre-scale physiology of bone: steric modelling and scanning transmission electron microscopy of collagen–mineral structure." Journal of The Royal Society Interface **9**(73): 1774.

Alfieri, K. A., J. A. Forsberg and B. K. Potter (2012). "Blast injuries and heterotopic ossification." Bone Joint Res **1**(8): 192-197.

Amar, E., Z. T. Sharfman and E. Rath (2015). "Heterotopic ossification after hip arthroscopy." Journal of Hip Preservation Surgery **2**(4): 355-363.

Amson, E., C. de Muizon, M. Laurin, C. Argot and V. de Buffrénil (2014). "Gradual adaptation of bone structure to aquatic lifestyle in extinct sloths from Peru." Proceedings of the Royal Society B: Biological Sciences **281**(1782).

Anagnostakos, K., E. Schmitt and P. Orth (2014). "A rare case of acetabulum osteomyelitis mimicking bone sarcoma." Orthopedics **37**(8): e750-753.

Anderson, H. C. (1969). "VESICLES ASSOCIATED WITH CALCIFICATION IN THE MATRIX OF EPIPHYSEAL CARTILAGE." The Journal of Cell Biology **41**(1): 59.

Anderson, H. C. (2003). "Matrix vesicles and calcification." Current Rheumatology Reports **5**(3): 222-226.

Anderson, H. C., J. B. Sipe, L. Hessle, R. Dhanyamraju, E. Atti, N. P. Camacho, J. L. Millan and R. Dhamyamraju (2004). "Impaired calcification around matrix vesicles of growth plate and bone in alkaline phosphatase-deficient mice." Am J Pathol **164**(3): 841-847.

Anthonissen, J., C. Ossendorf, J. L. Hock, C. T. Steffen, H. Goetz, A. Hofmann and P. M. Rommens (2016). "The role of muscular trauma in the development of heterotopic ossification after hip surgery: An animal-model study in rats." Injury **47**(3): 613-616.

Ascenzi, A., P. Baschieri and A. Benvenuti (1994). "The torsional properties of single selected osteons." Journal of Biomechanics **27**(7): 875-884.
Atkins, G. J., K. J. Welldon, A. R. Wijenayaka, L. F. Bonewald and D. M. Findlay (2009). "Vitamin K promotes mineralization, osteoblast-to-osteocyte transition, and an anticatabolic phenotype by γ-carboxylation-dependent and -independent mechanisms." American Journal of Physiology - Cell Physiology **297**(6): C1358-C1367.
Atzeni, F., P. Sarzi-Puttini and M. Bevilacqua "Calcium Deposition and Associated Chronic Diseases (Atherosclerosis, Diffuse Idiopathic Skeletal Hyperostosis, and Others)." Rheumatic Disease Clinics **32**(2): 413-426.
Bae, S., S. Sun, T. Aghaloo, J.-E. Oh, C. E. McKenna, M. K. Kang, K.-H. Shin, S. Tetradis, N.-H. Park and R. H. Kim (2014). "Development of oral osteomucosal tissue constructs in vitro and localization of fluorescently-labeled bisphosphonates to hard and soft tissue." International Journal of Molecular Medicine **34**(2): 559-563.
Bagi, C. M., D. Wilkie, K. Georgelos, D. Williams and D. Bertolini (1997). "Morphological and structural characteristics of the proximal femur in human and rat." Bone **21**(3): 261-267.
Baird, E. O. and Q. K. Kang (2009). "Prophylaxis of heterotopic ossification – an updated review." Journal of Orthopaedic Surgery and Research **4**: 12-12.
Balboni, T. A., R. Gobezie and H. J. Mamon (2006). "Heterotopic ossification: Pathophysiology, clinical features, and the role of radiotherapy for prophylaxis." Int J Radiat Oncol Biol Phys **65**(5): 1289-1299.
Ballanti, P., B. M. Wedard and E. Bonucci (1996). "Frequency of adynamic bone disease and aluminum storage in Italian uraemic patients--retrospective analysis of 1429 iliac crest biopsies." Nephrol Dial Transplant **11**(4): 663-667.
Ban, S., T. Jinde and J. Hasegawa (1992). "Phase Transformation of Octacalcium Phosphate in vivo and in vitro." Dental Materials Journal **11**(2): 130-140,217.
Banovac, K. (2000). "The effect of etidronate on late development of heterotopic ossification after spinal cord injury." J Spinal Cord Med **23**(1): 40-44.
Banovac, K., F. Gonzalez and K. J. Renfree (1997). "Treatment of heterotopic ossification after spinal cord injury." J Spinal Cord Med **20**(1): 60-65.
Banovac, K., F. Gonzalez, N. Wade and J. J. Bowker (1993). "Intravenous disodium etidronate therapy in spinal cord injury patients with heterotopic ossification." Paraplegia **31**(10): 660-666.
Barratt, M. R. and S. L. Pool (2008). Principles of Clinical Medicine for Space Flight, Springer New York.
Baschal, E. E., C. I. Wethey, K. Swindle, R. M. Baschal, K. Gowan, N. L. Tang, D. M. Alvarado, G. E. Haller, M. B. Dobbs, M. R. Taylor, C. A. Gurnett, K. L. Jones and N. H. Miller (2014). "Exome sequencing identifies a rare HSPG2 variant associated with familial idiopathic scoliosis." G3 (Bethesda) **5**(2): 167-174.
Bass, S. L., L. Saxon, R. M. Daly, C. H. Turner, A. G. Robling, E. Seeman and S. Stuckey (2002). "The Effect of Mechanical Loading on the Size and Shape of Bone in Pre-, Peri-, and Postpubertal Girls: A Study in Tennis Players." Journal of Bone and Mineral Research **17**(12): 2274-2280.
Bassett, C. A. and R. O. Becker (1962). "Generation of electric potentials by bone in response to mechanical stress." Science **137**(3535): 1063-1064.
Bassett, C. A., R. J. Pawluk and R. O. Becker (1964). "EFFECTS OF ELECTRIC CURRENTS ON BONE IN VIVO." Nature **204**: 652-654.
Baylink, D. J., R. D. Finkelman and S. Mohan (1993). "Growth factors to stimulate bone formation." Journal of Bone and Mineral Research **8**(S2): S565-S572.
Bellows, C. G., J. E. Aubin, J. N. Heersche and M. E. Antosz (1986). "Mineralized bone nodules formed in vitro from enzymatically released rat calvaria cell populations." Calcif Tissue Int **38**(3): 143-154.
Bentov, S., E. D. Aflalo, J. Tynyakov, L. Glazer and A. Sagi (2016). "Calcium phosphate mineralization is widely applied in crustacean mandibles." Scientific Reports **6**: 22118.

Berge, C. (1998). "Heterochronic processes in human evolution: An ontogenetic analysis of the hominid pelvis." American Journal of Physical Anthropology **105**(4): 441-459.
Bigelow, C. L. and M. Tavassoli (1984). "Studies on conversion of yellow marrow to red marrow by using ectopic bone marrow implants." Exp Hematol **12**(7): 581-585.
Blaber, E. A., N. Dvorochkin, C. Lee, J. S. Alwood, R. Yousuf, P. Pianetta, R. K. Globus, B. P. Burns and E. A. C. Almeida (2013). "Microgravity Induces Pelvic Bone Loss through Osteoclastic Activity, Osteocytic Osteolysis, and Osteoblastic Cell Cycle Inhibition by CDKN1a/p21." PLOS ONE **8**(4): e61372.
Board, T. N., A. Karva, R. E. Board, A. K. Gambhir and M. L. Porter (2007). "The prophylaxis and treatment of heterotopic ossification following lower limb arthroplasty." Journal of Bone & Joint Surgery, British Volume **89-B**(4): 434-440.
Boden, S. D. and F. S. Kaplan (1990). "Calcium homeostasis." Orthop Clin North Am **21**(1): 31-42.
Boling, M., D. Padua, S. Marshall, K. Guskiewicz, S. Pyne and A. Beutler (2010). "Gender differences in the incidence and prevalence of patellofemoral pain syndrome." Scandinavian journal of medicine & science in sports **20**(5): 725-730.
Bonar, L. C., A. H. Roufosse, W. K. Sabine, M. D. Grynpas and M. J. Glimcher (1983). "X-ray diffraction studies of the crystallinity of bone mineral in newly synthesized and density fractionated bone." Calcified Tissue International **35**(1): 202-209.
Bonewald, L. F. (2006). "Mechanosensation and Transduction in Osteocytes." BoneKEy osteovision **3**(10): 7-15.
Bonewald, L. F. (2011). "The Amazing Osteocyte." Journal of Bone and Mineral Research **26**(2): 229-238.
Bonewald, L. F. (2013). Osteocytes. Primer on the Metabolic Bone Diseases and Disorders of Mineral Metabolism, John Wiley & Sons, Inc.**:** 34-41.
Bonewald, L. F. and M. L. Johnson (2008). "Osteocytes, mechanosensing and Wnt signaling." Bone **42**(4): 606-615.
Bonewald, L. F. and M. J. Wacker (2013). "FGF23 Production by Osteocytes." Pediatric nephrology (Berlin, Germany) **28**(4): 563-568.
Bonucci, E. (2007). Biological Calcification: Normal and Pathological Processes in the Early Stages, Springer Berlin Heidelberg.
Boskey, A. L. (2013). "Bone composition: relationship to bone fragility and antiosteoporotic drug effects." BoneKEy Rep **2**.
Bouet, G., M. Cruel, C. Laurent, L. Vico, L. Malaval and D. Marchat (2015). "Validation of an in vitro 3D bone culture model with perfused and mechanically stressed ceramic scaffold." Eur Cell Mater **29**: 250-266; discussion 266-257.
Boukhechba, F., T. Balaguer, J.-F. Michiels, K. Ackermann, D. Quincey, J.-M. Bouler, W. Pyerin, G. F. Carle and N. Rochet (2009). "Human Primary Osteocyte Differentiation in a 3D Culture System." Journal of Bone and Mineral Research **24**(11): 1927-1935.
Boyle, W. J., W. S. Simonet and D. L. Lacey (2003). "Osteoclast differentiation and activation." Nature **423**(6937): 337-342.
Braet, K., L. Cabooter, K. Paemeleire and L. Leybaert (2004). "Calcium signal communication in the central nervous system." Biology of the Cell **96**(1): 79-91.
Brown, K. V., S. Dharm-Datta, B. K. Potter, J. Etherington, A. Mistlin, J. R. Hsu and J. C. Clasper (2010). "Comparison of development of heterotopic ossification in injured US and UK Armed Services personnel with combat-related amputations: preliminary findings and hypotheses regarding causality." J Trauma **69 Suppl 1**: S116-122.
Buchan, J. G., D. M. Alvarado, G. E. Haller, C. Cruchaga, M. B. Harms, T. Zhang, M. C. Willing, D. K. Grange, A. C. Braverman, N. H. Miller, J. A. Morcuende, N. L. Tang, T. P. Lam, B. K. Ng, J. C. Cheng, M. B. Dobbs and C. A. Gurnett (2014). "Rare variants in FBN1 and FBN2 are associated with severe adolescent idiopathic scoliosis." Hum Mol Genet **23**(19): 5271-5282.

Buckey, J. C. (2006). Space Physiology, Oxford University Press.
Butler, H. J., L. Ashton, B. Bird, G. Cinque, K. Curtis, J. Dorney, K. Esmonde-White, N. J. Fullwood, B. Gardner, P. L. Martin-Hirsch, M. J. Walsh, M. R. McAinsh, N. Stone and F. L. Martin (2016). "Using Raman spectroscopy to characterize biological materials." Nat Protoc **11**(4): 664-687.
Buttery, L. D., S. Bourne, J. D. Xynos, H. Wood, F. J. Hughes, S. P. Hughes, V. Episkopou and J. M. Polak (2001). "Differentiation of osteoblasts and in vitro bone formation from murine embryonic stem cells." Tissue Eng **7**(1): 89-99.
Calhoun, J. H., M. M. Manring and M. Shirtliff (2009). "Osteomyelitis of the Long Bones." Seminars in Plastic Surgery **23**(2): 59-72.
Campbell, G. M. and A. Sophocleous (2014). "Quantitative analysis of bone and soft tissue by micro-computed tomography: applications to ex vivo and in vivo studies." BoneKEy Reports **3**: 564.
Canalis, E. (2013). "Wnt signalling in osteoporosis: mechanisms and novel therapeutic approaches." Nat Rev Endocrinol **9**(10): 575-583.
Caplan, A. I. (1991). "Mesenchymal stem cells." J Orthop Res **9**(5): 641-650.
Caswell, A., D. F. Guilland-Cumming, P. R. Hearn, M. K. McGuire and R. G. Russell (1983). "Pathogenesis of chondrocalcinosis and pseudogout. Metabolism of inorganic pyrophosphate and production of calcium pyrophosphate dihydrate crystals." Annals of the Rheumatic Diseases **42**(Suppl 1): 27-37.
Catini, C. and G. Gheri (1990). "The GAGs of the bone: a study on human calva." Arch Ital Anat Embriol **95**(3-4): 237-240.
Cavanagh, P. R., A. A. Licata and A. J. Rice (2005). "Exercise and pharmacological countermeasures for bone loss during long-duration space flight." Gravit Space Biol Bull **18**(2): 39-58.
Chakkalakal, S. A., D. Zhang, A. L. Culbert, M. R. Convente, R. J. Caron, A. C. Wright, A. D. Maidment, F. S. Kaplan and E. M. Shore (2012). "An Acvr1 R206H knock-in mouse has fibrodysplasia ossificans progressiva." J Bone Miner Res **27**(8): 1746-1756.
Chalmers, J., D. H. Gray and J. Rush (1975). "Observations on the induction of bone in soft tissues." J Bone Joint Surg Br **57**(1): 36-45.
Champy, M. F., M. Selloum, L. Piard, V. Zeitler, C. Caradec, P. Chambon and J. Auwerx (2004). "Mouse functional genomics requires standardization of mouse handling and housing conditions." Mammalian Genome **15**(10): 768-783.
Chang, H. and M. L. Knothe Tate (2012). "Concise Review: The Periosteum: Tapping into a Reservoir of Clinically Useful Progenitor Cells." Stem Cells Translational Medicine **1**(6): 480-491.
Chaturvedi, P., N. X. Chen, K. O'Neill, J. N. McClintick, S. M. Moe and S. C. Janga (2015). "Differential miRNA Expression in Cells and Matrix Vesicles in Vascular Smooth Muscle Cells from Rats with Kidney Disease." PLoS One **10**(6): e0131589.
Chen, P.-Y., J. Schirer, A. Simpson, R. Nay, Y.-S. Lin, W. Yang, M. I. Lopez, J. Li, E. A. Olevsky and M. A. Meyers (2011). "Predation versus protection: Fish teeth and scales evaluated by nanoindentation." Journal of Materials Research **27**(1): 100-112.
Chen, P. Y., A. Y. M. Lin, Y. S. Lin, Y. Seki, A. G. Stokes, J. Peyras, E. A. Olevsky, M. A. Meyers and J. McKittrick (2008). "Structure and mechanical properties of selected biological materials." Journal of the Mechanical Behavior of Biomedical Materials **1**(3): 208-226.
Chen, X., O. Nadiarynkh, S. Plotnikov and P. J. Campagnola (2012). "Second harmonic generation microscopy for quantitative analysis of collagen fibrillar structure." Nat. Protocols **7**(4): 654-669.
Chen, Z., A. Htay, W. Dos Santos, G. T. Gillies, H. L. Fillmore, M. M. Sholley and W. C. Broaddus (2009). "In vitro angiogenesis by human umbilical vein endothelial cells (HUVEC) induced by three-dimensional co-culture with glioblastoma cells." J Neurooncol **92**(2): 121-128.
Chesnutt, B. M., A. M. Viano, Y. Yuan, Y. Yang, T. Guda, M. R. Appleford, J. L. Ong, W. O. Haggard and J. D. Bumgardner (2009). "Design and characterization of a novel chitosan/nanocrystalline calcium phosphate composite scaffold for bone regeneration." J Biomed Mater Res A **88**(2): 491-502.

Chiou, N.-T. and K. M. Ansel (2016). "Improved exosome isolation by sucrose gradient fractionation of ultracentrifuged crude exosome pellets."
Chirchir, H., T. L. Kivell, C. B. Ruff, J.-J. Hublin, K. J. Carlson, B. Zipfel and B. G. Richmond (2015). "Recent origin of low trabecular bone density in modern humans." Proceedings of the National Academy of Sciences of the United States of America **112**(2): 366-371.
Ciancaglini, P., A. M. Simao, F. L. Camolezi, J. L. Millan and J. M. Pizauro (2006). "Contribution of matrix vesicles and alkaline phosphatase to ectopic bone formation." Braz J Med Biol Res **39**(5): 603-610.
Cipriano, C. A., S. G. Pill and M. A. Keenan (2009). "Heterotopic Ossification Following Traumatic Brain Injury and Spinal Cord Injury." JAAOS - Journal of the American Academy of Orthopaedic Surgeons **17**(11).
Claes, L., S. Recknagel and A. Ignatius (2012). "Fracture healing under healthy and inflammatory conditions." Nat Rev Rheumatol **8**(3): 133-143.
Clément, G. (2007). Fundamentals of Space Medicine, Springer Netherlands.
Cocks, M., A. Mohan, C. A. Meyers, C. Ding, B. Levi, E. McCarthy and A. W. James (2017). "Vascular patterning in human heterotopic ossification." Hum Pathol **63**: 165-170.
Cohen, R. B., G. V. Hahn, J. A. Tabas, J. Peeper, C. L. Levitz, A. Sando, N. Sando, M. Zasloff and F. S. Kaplan (1993). "The natural history of heterotopic ossification in patients who have fibrodysplasia ossificans progressiva. A study of forty-four patients." J Bone Joint Surg Am **75**(2): 215-219.
Collet, P., D. Uebelhart, L. Vico, L. Moro, D. Hartmann, M. Roth and C. Alexandre (1997). "Effects of 1- and 6-month spaceflight on bone mass and biochemistry in two humans." Bone **20**(6): 547-551.
Connor, J. M. and D. A. Evans (1982). "Fibrodysplasia ossificans progressiva. The clinical features and natural history of 34 patients." J Bone Joint Surg Br **64**(1): 76-83.
Cox, G. and E. Kable (2006). Second-Harmonic Imaging of Collagen. Cell Imaging Techniques: Methods and Protocols. D. J. Taatjes and B. T. Mossman. Totowa, NJ, Humana Press**:** 15-35.
Crane, N. J., E. Polfer, E. A. Elster, B. K. Potter and J. A. Forsberg (2013). "Raman spectroscopic analysis of combat-related heterotopic ossification development." Bone **57**(2): 335-342.
Crane, N. J., V. Popescu, M. D. Morris, P. Steenhuis and M. A. Ignelzi Jr (2006). "Raman spectroscopic evidence for octacalcium phosphate and other transient mineral species deposited during intramembranous mineralization." Bone **39**(3): 434-442.
Cui, L., D. A. Houston, C. Farquharson and V. E. MacRae (2016). "Characterisation of matrix vesicles in skeletal and soft tissue mineralisation." Bone **87**: 147-158.
Cullen, N. and J. Perera (2009). "Heterotopic ossification: pharmacologic options." J Head Trauma Rehabil **24**(1): 69-71.
Daeschler, E. B., N. H. Shubin and F. A. Jenkins (2006). "A Devonian tetrapod-like fish and the evolution of the tetrapod body plan." Nature **440**(7085): 757-763.
Dallas, S. L. and L. F. Bonewald (2010). "Dynamics of the Transition from Osteoblast to Osteocyte." Annals of the New York Academy of Sciences **1192**: 437-443.
Dallas, S. L., M. Prideaux and L. F. Bonewald (2013). "The osteocyte: an endocrine cell ... and more." Endocr Rev **34**(5): 658-690.
Day, T. F., X. Guo, L. Garrett-Beal and Y. Yang (2005). "Wnt/beta-catenin signaling in mesenchymal progenitors controls osteoblast and chondrocyte differentiation during vertebrate skeletogenesis." Dev Cell **8**(5): 739-750.
De Buren, N. (1962). "CAUSES AND TREATMENT OF NON-UNION IN FRACTURES OF THE RADIUS AND ULNA." Journal of Bone & Joint Surgery, British Volume **44-B**(3): 614.
de Gorter, D. J. J. and P. ten Dijke (2013). Signal Transduction Cascades Controlling Osteoblast Differentiation. Primer on the Metabolic Bone Diseases and Disorders of Mineral Metabolism, John Wiley & Sons, Inc.**:** 15-24.
de Jong, W. F. (1926). "La Substance Minérale Dans les Os." Recueil des Travaux Chimiques des Pays-Bas **45**(6): 445-448.

de Viguerie, L., V. A. Sole and P. Walter (2009). "Multilayers quantitative X-ray fluorescence analysis applied to easel paintings." Anal Bioanal Chem **395**(7): 2015-2020.
de Viguerie, L., P. Walter, E. Laval, B. Mottin and V. A. Solé (2010). "Revealing the sfumato Technique of Leonardo da Vinci by X-Ray Fluorescence Spectroscopy." Angewandte Chemie International Edition **49**(35): 6125-6128.
del Puente, A., N. Pappone, M. G. Mandes, D. Mantova, R. Scarpa and P. Oriente (1996). "Determinants of bone mineral density in immobilization: A study on hemiplegic patients." Osteoporosis International **6**(1): 50-54.
Demirbag, D., F. Ozdemir, S. Kokino and S. Berkarda (2005). "The relationship between bone mineral density and immobilization duration in hemiplegic limbs." Annals of Nuclear Medicine **19**(8): 695-700.
Denk, W., J. H. Strickler and W. W. Webb (1990). "Two-photon laser scanning fluorescence microscopy." Science **248**(4951): 73-76.
Dick, M., P. Jonak and R. L. Leask (2013). "Statin therapy influences endothelial cell morphology and F-actin cytoskeleton structure when exposed to static and laminar shear stress conditions." Life Sci **92**(14-16): 859-865.
Donaldson, C. L., S. B. Hulley, J. M. Vogel, R. S. Hattner, J. H. Bayers and D. E. McMillan (1970). "Effect of prolonged bed rest on bone mineral." Metabolism **19**(12): 1071-1084.
Drake, M. T., B. L. Clarke and S. Khosla (2008). "Bisphosphonates: Mechanism of Action and Role in Clinical Practice." Mayo Clinic proceedings. Mayo Clinic **83**(9): 1032-1045.
Drury, J. L. and D. J. Mooney (2003). "Hydrogels for tissue engineering: scaffold design variables and applications." Biomaterials **24**(24): 4337-4351.
Dumont, E. R. (2010). "Bone density and the lightweight skeletons of birds." Proceedings of the Royal Society B: Biological Sciences **277**(1691): 2193-2198.
Eanes, E. D., I. H. Gillessen and A. S. Posner (1965). "Intermediate States in the Precipitation of Hydroxyapatite." Nature **208**(5008): 365-367.
Eanes, E. D. and J. L. Meyer (1977). "The maturation of crystalline calcium phosphates in aqueous suspensions at physiologic pH." Calcified Tissue Research **23**(1): 259-269.
Edmondson, R., J. J. Broglie, A. F. Adcock and L. Yang (2014). "Three-Dimensional Cell Culture Systems and Their Applications in Drug Discovery and Cell-Based Biosensors." Assay and Drug Development Technologies **12**(4): 207-218.
Edwards, D. S. and J. C. Clasper (2014). "Heterotopic ossification: a systematic review." Journal of the Royal Army Medical Corps.
Einhorn, T. A. and L. C. Gerstenfeld (2015). "Fracture healing: mechanisms and interventions." Nat Rev Rheumatol **11**(1): 45-54.
Elder, G. A., N. P. Dorr, R. De Gasperi, M. A. Gama Sosa, M. C. Shaughness, E. Maudlin-Jeronimo, A. A. Hall, R. M. McCarron and S. T. Ahlers (2012). "Blast Exposure Induces Post-Traumatic Stress Disorder-Related Traits in a Rat Model of Mild Traumatic Brain Injury." Journal of Neurotrauma **29**(16): 2564-2575.
Elton, S. (2008). "The environmental context of human evolutionary history in Eurasia and Africa." Journal of Anatomy **212**(4): 377-393.
Erwin, W. M. and K. E. Hood (2014). "The cellular and molecular biology of the intervertebral disc: A clinician's primer." The Journal of the Canadian Chiropractic Association **58**(3): 246-257.
Evans, D. M., C. C. A. Spencer, J. J. Pointon, Z. Su, D. Harvey, G. Kochan, U. Oppermann, A. Dilthey, M. Pirinen, M. A. Stone, L. Appleton, L. Moutsianas, S. Leslie, T. Wordsworth, T. J. Kenna, T. Karaderi, G. P. Thomas, M. M. Ward, M. H. Weisman, C. Farrar, L. A. Bradbury, P. Danoy, R. D. Inman, W. Maksymowych, D. Gladman, P. Rahman, C. Spondyloarthritis Research Consortium of, A. Morgan, H. Marzo-Ortega, P. Bowness, K. Gaffney, J. S. H. Gaston, M. Smith, J. Bruges-Armas, A.-R. Couto, R. Sorrentino, F. Paladini, M. A. Ferreira, H. Xu, Y. Liu, L. Jiang, C. Lopez-Larrea, R. Díaz-Peña, A. López-Vázquez, T. Zayats, G. Band, C. Bellenguez, H. Blackburn, J. M. Blackwell, E. Bramon, S. J. Bumpstead,

J. P. Casas, A. Corvin, N. Craddock, P. Deloukas, S. Dronov, A. Duncanson, S. Edkins, C. Freeman, M. Gillman, E. Gray, R. Gwilliam, N. Hammond, S. E. Hunt, J. Jankowski, A. Jayakumar, C. Langford, J. Liddle, H. S. Markus, C. G. Mathew, O. T. McCann, M. I. McCarthy, C. N. A. Palmer, L. Peltonen, R. Plomin, S. C. Potter, A. Rautanen, R. Ravindrarajah, M. Ricketts, N. Samani, S. J. Sawcer, A. Strange, R. C. Trembath, A. C. Viswanathan, M. Waller, P. Weston, P. Whittaker, S. Widaa, N. W. Wood, G. McVean, J. D. Reveille, B. P. Wordsworth, M. A. Brown, P. Donnelly, C. The Australo-Anglo-American Spondyloarthritis and C. the Wellcome Trust Case Control (2011). "Interaction between ERAP1 and HLA-B27 in ankylosing spondylitis implicates peptide handling in the mechanism for HLA-B27 in disease susceptibility." Nature genetics **43**(8): 761-767.

Everts, V., A. Niehof, W. Tigchelaar-Gutter and W. Beertsen (2012). "Transmission electron microscopy of bone." Methods Mol Biol **816**: 351-363.

Eyrich, D., F. Brandl, B. Appel, H. Wiese, G. Maier, M. Wenzel, R. Staudenmaier, A. Goepferich and T. Blunk (2007). "Long-term stable fibrin gels for cartilage engineering." Biomaterials **28**(1): 55-65.

Eyrich, D., A. Göpferich and T. Blunk (2007). Fibrin in Tissue Engineering. Tissue Engineering. J. P. Fisher. Boston, MA, Springer US**:** 379-392.

Fang, J. and B. K. Hall (1996). "In VitroDifferentiation Potential of the Periosteal Cells from a Membrane Bone, the Quadratojugal of the Embryonic Chick." Developmental Biology **180**(2): 701-712.

Fang, M. and M. M. B. Holl (2013). "Variation in type I collagen fibril nanomorphology: the significance and origin." BoneKEy Rep **2**.

Favus, M. J. and D. Goltzman (2013). Regulation of Calcium and Magnesium. Primer on the Metabolic Bone Diseases and Disorders of Mineral Metabolism, John Wiley & Sons, Inc.**:** 171-179.

Felix, R., W. Herrmann and H. Fleisch (1978). "Stimulation of precipitation of calcium phosphate by matrix vesicles." Biochemical Journal **170**(3): 681-691.

Feng, X. H. and R. Derynck (2005). "Specificity and versatility in tgf-beta signaling through Smads." Annu Rev Cell Dev Biol **21**: 659-693.

Filipponi, P., S. Cristallini, G. Policani, C. Casciari and F. Gregorio (1998). "Paget's disease of bone: benefits of neridronate as a first treatment and in cases of relapse after clodronate." Bone **23**(6): 543-548.

Finkelstein, J. S., S. E. Brockwell, V. Mehta, G. A. Greendale, M. R. Sowers, B. Ettinger, J. C. Lo, J. M. Johnston, J. A. Cauley, M. E. Danielson and R. M. Neer (2008). "Bone Mineral Density Changes during the Menopause Transition in a Multiethnic Cohort of Women." The Journal of Clinical Endocrinology and Metabolism **93**(3): 861-868.

Franz-Odendaal, T. A., B. K. Hall and P. E. Witten (2006). "Buried alive: How osteoblasts become osteocytes." Developmental Dynamics **235**(1): 176-190.

Fujiwara, Y., M. Piemontese, Y. Liu, J. D. Thostenson, J. Xiong and C. A. O'Brien (2016). "RANKL (Receptor Activator of NFkappaB Ligand) Produced by Osteocytes Is Required for the Increase in B Cells and Bone Loss Caused by Estrogen Deficiency in Mice." J Biol Chem **291**(48): 24838-24850.

Gannaway, J. N. and C. J. R. Sheppard (1978). "Second-harmonic imaging in the scanning optical microscope." Optical and Quantum Electronics **10**(5): 435-439.

Gauderon, R., P. B. Lukins and C. J. Sheppard (2001). "Simultaneous multichannel nonlinear imaging: combined two-photon excited fluorescence and second-harmonic generation microscopy." Micron **32**(7): 685-689.

Gautschi, O. P., S. P. Frey and R. Zellweger (2007). "Bone morphogenetic proteins in clinical applications." ANZ J Surg **77**(8): 626-631.

Gazzerro, E. and E. Canalis (2006). "Bone morphogenetic proteins and their antagonists." Rev Endocr Metab Disord **7**(1-2): 51-65.

Gerstenfeld, L. C., D. M. Cullinane, G. L. Barnes, D. T. Graves and T. A. Einhorn (2003). "Fracture healing as a post-natal developmental process: Molecular, spatial, and temporal aspects of its regulation." Journal of Cellular Biochemistry **88**(5): 873-884.

Gerstenfeld, L. C. and F. D. Shapiro (1996). "Expression of bone-specific genes by hypertrophic chondrocytes: implication of the complex functions of the hypertrophic chondrocyte during endochondral bone development." J Cell Biochem **62**(1): 1-9.
Glaser, D. L., A. N. Economides, L. Wang, X. Liu, R. D. Kimble, J. P. Fandl, J. M. Wilson, N. Stahl, F. S. Kaplan and E. M. Shore (2003). "In vivo somatic cell gene transfer of an engineered Noggin mutein prevents BMP4-induced heterotopic ossification." J Bone Joint Surg Am **85-a**(12): 2332-2342.
Glaser, D. L., D. M. Rocke and F. S. Kaplan (1998). "Catastrophic falls in patients who have fibrodysplasia ossificans progressiva." Clin Orthop Relat Res(346): 110-116.
Glass, G. E., J. K. Chan, A. Freidin, M. Feldmann, N. J. Horwood and J. Nanchahal (2011). "TNF-α promotes fracture repair by augmenting the recruitment and differentiation of muscle-derived stromal cells." Proceedings of the National Academy of Sciences **108**(4): 1585-1590.
Goldberg, M. and A. L. Boskey (1996). "Lipids and Biomineralizations." Progress in Histochemistry and Cytochemistry **31**(2): III-187.
Golub, E. E. (2009). "Role of Matrix Vesicles in Biomineralization." Biochimica et biophysica acta **1790**(12): 1592-1598.
Golub, E. E. (2011). "Biomineralization and matrix vesicles in biology and pathology." Seminars in immunopathology **33**(5): 409-417.
Gorustovich, A. A. (2010). "Imaging Resin-Cast Osteocyte Lacuno-Canalicular System at Bone-Bioactive Glass Interface by Scanning Electron Microscopy." Microscopy and Microanalysis **16**(02): 132-136.
Graham, H. K., N. W. Hodson, J. A. Hoyland, S. J. Millward-Sadler, D. Garrod, A. Scothern, C. E. M. Griffiths, R. E. B. Watson, T. R. Cox, J. T. Erler, A. W. Trafford and M. J. Sherratt (2010). "Tissue section AFM: In situ ultrastructural imaging of native biomolecules." Matrix Biology **29**(4): 254-260.
Granero-Moltó, F., J. A. Weis, M. I. Miga, B. Landis, T. J. Myers, L. O'Rear, L. Longobardi, E. D. Jansen, D. P. Mortlock and A. Spagnoli (2009). "Regenerative Effects of Transplanted Mesenchymal Stem Cells in Fracture Healing." STEM CELLS **27**(8): 1887-1898.
Grant, P. R. and B. R. Grant (1997). "Genetics and the origin of bird species." Proceedings of the National Academy of Sciences of the United States of America **94**(15): 7768-7775.
Gray, N.-M., K. Kainec, S. Madar, L. Tomko and S. Wolfe (2007). "Sink or swim? Bone density as a mechanism for buoyancy control in early cetaceans." The Anatomical Record: Advances in Integrative Anatomy and Evolutionary Biology **290**(6): 638-653.
Gregory, P., E. Kraemer, G. Zurcher, R. Gentinetta, V. Rohrbach, U. Brodbeck, A. C. Andres, A. Ziemiecki and P. Butikofer (2005). "GPI-specific phospholipase D (GPI-PLD) is expressed during mouse development and is localized to the extracellular matrix of the developing mouse skeleton." Bone **37**(2): 139-147.
Grinnell, F. and W. M. Petroll (2010). "Cell motility and mechanics in three-dimensional collagen matrices." Annu Rev Cell Dev Biol **26**: 335-361.
Guillerman, R. P. (2013). "Marrow: red, yellow and bad." Pediatr Radiol **43 Suppl 1**: S181-192.
Guo, D., A. Keightley, J. Guthrie, P. A. Veno, S. E. Harris and L. F. Bonewald (2010). "Identification of Osteocyte-Selective Proteins." Proteomics **10**(20): 3688-3698.
Gutzwiller, S. C., A. Su and P. M. O'Connor (2013). "Postcranial Pneumaticity and Bone Structure in Two Clades of Neognath Birds." The Anatomical Record **296**(6): 867-876.
Hanks, C. T., J. C. Wataha and Z. Sun (1996). "In vitro models of biocompatibility: a review." Dent Mater **12**(3): 186-193.
Harada, H., S. Tagashira, M. Fujiwara, S. Ogawa, T. Katsumata, A. Yamaguchi, T. Komori and M. Nakatsuka (1999). "Cbfa1 isoforms exert functional differences in osteoblast differentiation." J Biol Chem **274**(11): 6972-6978.
Hardingham, T. E., R. A. Oldershaw and S. R. Tew (2006). "Cartilage, SOX9 and Notch signals in chondrogenesis." Journal of Anatomy **209**(4): 469-480.

Hayden, M. R., S. C. Tyagi, L. Kolb, J. R. Sowers and R. Khanna (2005). "Vascular ossification-calcification in metabolic syndrome, type 2 diabetes mellitus, chronic kidney disease, and calciphylaxis-calcific uremic arteriolopathy: the emerging role of sodium thiosulfate." Cardiovasc Diabetol **4**: 4.
Heino, T. J., T. A. Hentunen and H. K. Vaananen (2002). "Osteocytes inhibit osteoclastic bone resorption through transforming growth factor-beta: enhancement by estrogen." J Cell Biochem **85**(1): 185-197.
Heino, T. J., T. A. Hentunen and H. K. Vaananen (2004). "Conditioned medium from osteocytes stimulates the proliferation of bone marrow mesenchymal stem cells and their differentiation into osteoblasts." Exp Cell Res **294**(2): 458-468.
Henrotin, Y. (2011). "Muscle: a source of progenitor cells for bone fracture healing." BMC Medicine **9**: 136-136.
Hessle, L., K. A. Johnson, H. C. Anderson, S. Narisawa, A. Sali, J. W. Goding, R. Terkeltaub and J. L. Millan (2002). "Tissue-nonspecific alkaline phosphatase and plasma cell membrane glycoprotein-1 are central antagonistic regulators of bone mineralization." Proc Natl Acad Sci U S A **99**(14): 9445-9449.
Hillen, R. J. and D. Eygendaal (2007). "Corrective osteotomy after malunion of mid shaft fractures of the clavicle." Strategies in Trauma and Limb Reconstruction **2**(2): 59-61.
Hirschman, A., D. Deutsch, M. Hirschman, I. A. Bab, J. Sela and A. Muhlrad (1983). "Neutral peptidase activities in matrix vesicles from bovine fetal alveolar bone and dog osteosarcoma." Calcif Tissue Int **35**(6): 791-797.
Holick, M. F. (2006). "Resurrection of vitamin D deficiency and rickets." The Journal of Clinical Investigation **116**(8): 2062-2072.
Holmbeck, K., P. Bianco, I. Pidoux, S. Inoue, R. C. Billinghurst, W. Wu, K. Chrysovergis, S. Yamada, H. Birkedal-Hansen and A. R. Poole (2005). "The metalloproteinase MT1-MMP is required for normal development and maintenance of osteocyte processes in bone." J Cell Sci **118**(Pt 1): 147-156.
Honikel, K. O., U. Schmidt, W. Woltersdorf and L. Leistner (1978). "Effect of storage and processing on tetracycline residues in meat and bones." J Assoc Off Anal Chem **61**(5): 1222-1227.
Houde, J. P., L. A. Schulz, W. J. Morgan, T. Breen, L. Warhold, G. K. Crane and D. T. Baran (1995). "Bone Mineral Density Changes in the Forearm After Immobilization." Clinical Orthopaedics and Related Research **317**.
Hsu, H. H. and H. C. Anderson (1978). "Calcification of isolated matrix vesicles and reconstituted vesicles from fetal bovine cartilage." Proceedings of the National Academy of Sciences **75**(8): 3805-3808.
Huang, B., M. Bates and X. Zhuang (2009). "Super resolution fluorescence microscopy." Annual review of biochemistry **78**: 993-1016.
Huang, C. and R. Ogawa (2010). "Mechanotransduction in bone repair and regeneration." The FASEB Journal **24**(10): 3625-3632.
Huang, P.-Y., P.-K. Wu, C.-F. Chen, F.-T. Lee, H.-T. Wu, C.-L. Liu, T.-H. Chen and W.-M. Chen (2013). "Osteomyelitis of the femur mimicking bone tumors: a review of 10 cases." World Journal of Surgical Oncology **11**: 283-283.
Hughes-Fulford, M. and M. L. Lewis (1996). "Effects of microgravity on osteoblast growth activation." Exp Cell Res **224**(1): 103-109.
Hughes, D. E., D. M. Salter and R. Simpson (1994). "CD44 expression in human bone: a novel marker of osteocytic differentiation." J Bone Miner Res **9**(1): 39-44.
Hulmes, D. J. (2002). "Building collagen molecules, fibrils, and suprafibrillar structures." J Struct Biol **137**(1-2): 2-10.
Hussain, S. and S. Davanger (2015). "Postsynaptic VAMP/Synaptobrevin Facilitates Differential Vesicle Trafficking of GluA1 and GluA2 AMPA Receptor Subunits." PLoS ONE **10**(10): e0140868.

Hutcheson, J. D., C. Goettsch, T. Pham, M. Iwashita, M. Aikawa, S. A. Singh and E. Aikawa (2014). "Enrichment of calcifying extracellular vesicles using density-based ultracentrifugation protocol." Journal of Extracellular Vesicles **3**: 10.3402/jev.v3403.25129.
Iordachescu, A., H. D. Amin, S. M. Rankin, R. L. Williams, C. Yapp, A. Bannerman, A. Pacureanu, O. Addison, P. A. Hulley and L. M. Grover "An In Vitro Model for the Development of Mature Bone Containing an Osteocyte Network." Advanced Biosystems: 1700156-n/a.
Ireland, A., H. Degens, B. Ganse, T. M. Maden-Wilkinson, D. C. Wilks and J. Rittweger (2015). "Greater tibial bone strength in male tennis players than controls in the absence of greater muscle output." Journal of Orthopaedic Translation **3**(3): 142-151.
Ireland, A., T. Maden-Wilkinson, B. Ganse, H. Degens and J. Rittweger (2014). "Effects of age and starting age upon side asymmetry in the arms of veteran tennis players: a cross-sectional study." Osteoporos Int **25**(4): 1389-1400.
Ireland, A., T. Maden-Wilkinson, J. McPhee, K. Cooke, M. Narici, H. Degens and J. Rittweger (2013). "Upper limb muscle-bone asymmetries and bone adaptation in elite youth tennis players." Med Sci Sports Exerc **45**(9): 1749-1758.
Isaacson, B. M., A. A. Brown, L. B. Brunker, T. F. Higgins and R. D. Bloebaum "Clarifying the Structure and Bone Mineral Content of Heterotopic Ossification." Journal of Surgical Research **167**(2): e163-e170.
Isaacson, B. M., J. G. Stinstra, R. S. MacLeod, P. F. Pasquina and R. D. Bloebaum (2010). "Developing a quantitative measurement system for assessing heterotopic ossification and monitoring the bioelectric metrics from electrically induced osseointegration in the residual limb of service members." Ann Biomed Eng **38**(9): 2968-2978.
Ishida, Y., K. Komaru and K. Oda (2011). "Molecular characterization of tissue-nonspecific alkaline phosphatase with an Ala to Thr substitution at position 116 associated with dominantly inherited hypophosphatasia." Biochimica et Biophysica Acta (BBA) - Molecular Basis of Disease **1812**(3): 326-332.
Ishihara, Y., H. Kamioka, T. Honjo, H. Ueda, T. Takano-Yamamoto and T. Yamashiro (2008). "Hormonal, pH, and calcium regulation of connexin 43-mediated dye transfer in osteocytes in chick calvaria." J Bone Miner Res **23**(3): 350-360.
Iwamoto, J., T. Takeda and Y. Sato (2005). "Interventions to prevent bone loss in astronauts during space flight." Keio J Med **54**(2): 55-59.
Jackson, S. F. (1957). "The Fine Structure of Developing Bone in the Embryonic Fowl." Proceedings of the Royal Society of London. Series B - Biological Sciences **146**(923): 270.
Jang, H. L., K. Jin, J. Lee, Y. Kim, S. H. Nahm, K. S. Hong and K. T. Nam (2014). "Revisiting Whitlockite, the Second Most Abundant Biomineral in Bone: Nanocrystal Synthesis in Physiologically Relevant Conditions and Biocompatibility Evaluation." ACS Nano **8**(1): 634-641.
Jang, H. L., H. K. Lee, K. Jin, H.-Y. Ahn, H.-E. Lee and K. T. Nam (2015). "Phase transformation from hydroxyapatite to the secondary bone mineral, whitlockite." Journal of Materials Chemistry B **3**(7): 1342-1349.
Janmey, P. A., J. P. Winer and J. W. Weisel (2009). "Fibrin gels and their clinical and bioengineering applications." J R Soc Interface **6**(30): 1-10.
Jiang, L., Y. Cui, J. Luan, X. Zhou, X. Zhou and J. Han (2013). "A comparative proteomics study on matrix vesicles of osteoblast-like Saos-2 and U2-OS cells." Intractable & Rare Diseases Research **2**(2): 59-62.
Jilka, R. L., R. S. Weinstein, T. Bellido, A. M. Parfitt and S. C. Manolagas (1998). "Osteoblast programmed cell death (apoptosis): modulation by growth factors and cytokines." J Bone Miner Res **13**(5): 793-802.
Johnson, W. E. B. and S. Roberts (2003). "Human intervertebral disc cell morphology and cytoskeletal composition: a preliminary study of regional variations in health and disease." Journal of Anatomy **203**(6): 605-612.

Johnsson, M. S. A. and G. H. Nancollas (1992). "The Role of Brushite and Octacalcium Phosphate in Apatite Formation." Critical Reviews in Oral Biology & Medicine **3**(1): 61-82.
Jubeck, B., C. Gohr, M. Fahey, E. Muth, M. Matthews, E. Mattson, C. Hirschmugl and A. K. Rosenthal (2008). "Promotion of articular cartilage matrix vesicle mineralization by type I collagen." Arthritis Rheum **58**(9): 2809-2817.
Kalajzic, I., B. G. Matthews, E. Torreggiani, M. A. Harris, P. D. Pajevic and S. E. Harris (2013). "In vitro and in vivo approaches to study osteocyte biology." Bone **54**(2): 296-306.
Kamio, K., X. D. Liu, H. Sugiura, S. Togo, S. Kawasaki, X. Wang, Y. Ahn, C. Hogaboam and S. I. Rennard (2010). "Statins inhibit matrix metalloproteinase release from human lung fibroblasts." Eur Respir J **35**(3): 637-646.
Kamioka, H., Y. Ishihara, H. Ris, S. A. Murshid, Y. Sugawara, T. Takano-Yamamoto and S. S. Lim (2007). "Primary cultures of chick osteocytes retain functional gap junctions between osteocytes and between osteocytes and osteoblasts." Microsc Microanal **13**(2): 108-117.
Kan, L. and J. A. Kessler (2011). "Animal Models of Typical Heterotopic Ossification." Journal of Biomedicine and Biotechnology **2011**: 309287.
Kan, L., Y. Liu, T. L. McGuire, D. M. P. Berger, R. B. Awatramani, S. M. Dymecki and J. A. Kessler (2009). "Dysregulation of Local Stem/Progenitor Cells as a Common Cellular Mechanism for Heterotopic Ossification." Stem cells (Dayton, Ohio) **27**(1): 150-156.
Kani, T., M. Kani, Y. Moriwaki and Y. Doi (1983). "Microbeam x-ray diffraction analysis of dental calculus." J Dent Res **62**(2): 92-95.
Kaplan, F. S., R. Craver, G. D. MacEwen, F. H. Gannon, G. Finkel, G. Hahn, J. Tabas, R. J. Gardner and M. A. Zasloff (1994). "Progressive osseous heteroplasia: a distinct developmental disorder of heterotopic ossification. Two new case reports and follow-up of three previously reported cases." J Bone Joint Surg Am **76**(3): 425-436.
Kaplan, F. S., M. Le Merrer, D. L. Glaser, R. J. Pignolo, R. E. Goldsby, J. A. Kitterman, J. Groppe and E. M. Shore (2008). "Fibrodysplasia ossificans progressiva." Best Pract Res Clin Rheumatol **22**(1): 191-205.
Kaplan, F. S. and E. M. Shore (2011). "Derailing heterotopic ossification and RARing to go." Nat Med **17**(4): 420-421.
Kaplan, F. S., E. M. Shore, R. J. Pignolo and D. L. Glaser (2005). "Animal models of fibrodysplasia ossificans progressiva." Clinical Reviews in Bone and Mineral Metabolism **3**(3): 229-234.
Katagiri, T., K. Osawa, S. Tsukamoto, M. Fujimoto, A. Miyamoto and T. Mizuta (2015). "Bone morphogenetic protein-induced heterotopic bone formation: What have we learned from the history of a half century?" Japanese Dental Science Review **51**(2): 42-50.
Kato, Y., J. J. Windle, B. A. Koop, G. R. Mundy and L. F. Bonewald (1997). "Establishment of an Osteocyte-like Cell Line, MLO-Y4." Journal of Bone and Mineral Research **12**(12): 2014-2023.
Kawai, M. and C. J. Rosen (2012). "The Insulin-Like Growth Factor System in Bone: Basic and Clinical Implications." Endocrinology and metabolism clinics of North America **41**(2): 323-vi.
Keller, H. and M. Kneissel (2005). "SOST is a target gene for PTH in bone." Bone **37**(2): 148-158.
Kern, B., J. Shen, M. Starbuck and G. Karsenty (2001). "Cbfa1 contributes to the osteoblast-specific expression of type I collagen genes." J Biol Chem **276**(10): 7101-7107.
Kielty, C. M., A. P. Kwan, D. F. Holmes, S. L. Schor and M. E. Grant (1985). "Type X collagen, a product of hypertrophic chondrocytes." Biochem J **227**(2): 545-554.
Kikuchi, M., S. Itoh, S. Ichinose, K. Shinomiya and J. Tanaka (2001). "Self-organization mechanism in a bone-like hydroxyapatite/collagen nanocomposite synthesized in vitro and its biological reaction in vivo." Biomaterials **22**(13): 1705-1711.
Kim, S. W., P. D. Pajevic, M. Selig, K. J. Barry, J. Y. Yang, C. S. Shin, W. Y. Baek, J. E. Kim and H. M. Kronenberg (2012). "Intermittent parathyroid hormone administration converts quiescent lining cells to active osteoblasts." J Bone Miner Res **27**(10): 2075-2084.

Koczy, B., T. Stoltny, M. Swiderski, M. Pyda, J. Pajak, J. Spindel, W. Wawrzynek, L. Miszczyk, S. Kasperczyk and J. Widuchowski (2009). "Heterotopic ossification in patients with hip osteoarthritis below forty years old after total hip replacement." Ortop Traumatol Rehabil **11**(5): 458-466.
Kon, T., T. J. Cho, T. Aizawa, M. Yamazaki, N. Nooh, D. Graves, L. C. Gerstenfeld and T. A. Einhorn (2001). "Expression of osteoprotegerin, receptor activator of NF-kappaB ligand (osteoprotegerin ligand) and related proinflammatory cytokines during fracture healing." J Bone Miner Res **16**(6): 1004-1014.
Kong, C. and M. F. Hansen (2009). "Biomarkers in Osteosarcoma." Expert opinion on medical diagnostics **3**(1): 13-23.
Kontulainen, S., H. Sievänen, P. Kannus, M. Pasanen and I. Vuori (2003). "Effect of Long-Term Impact-Loading on Mass, Size, and Estimated Strength of Humerus and Radius of Female Racquet-Sports Players: A Peripheral Quantitative Computed Tomography Study Between Young and Old Starters and Controls." Journal of Bone and Mineral Research **18**(2): 352-359.
Kopecka, M., M. Yamaguchi and S. Kawamoto (2015). "Effects of the F-actin inhibitor latrunculin A on the budding yeast Saccharomyces cerevisiae." Microbiology **161**(7): 1348-1355.
Kramer, I., C. Halleux, H. Keller, M. Pegurri, J. H. Gooi, P. B. Weber, J. Q. Feng, L. F. Bonewald and M. Kneissel (2010). "Osteocyte Wnt/beta-catenin signaling is required for normal bone homeostasis." Mol Cell Biol **30**(12): 3071-3085.
Kumar, V. S., N. Barwar and S. A. Khan (2014). "Surface osteosarcomas: Diagnosis, treatment and outcome." Indian Journal of Orthopaedics **48**(3): 255-261.
Kundu, Z. S. (2014). "Classification, imaging, biopsy and staging of osteosarcoma." Indian Journal of Orthopaedics **48**(3): 238-246.
Lafage-Proust, M.-H., B. Roche, M. Langer, D. Cleret, A. Vanden Bossche, T. Olivier and L. Vico (2015). "Assessment of bone vascularization and its role in bone remodeling." BoneKEy Rep **4**.
Lamparski, H. G., A. Metha-Damani, J. Y. Yao, S. Patel, D. H. Hsu, C. Ruegg and J. B. Le Pecq (2002). "Production and characterization of clinical grade exosomes derived from dendritic cells." J Immunol Methods **270**(2): 211-226.
Landis, W. J. and M. J. Glimcher (1982). "Electron optical and analytical observations of rat growth plate cartilage prepared by ultracryomicrotomy: The failure to detect a mineral phase in matrix vesicles and the identification of heterodispersed particles as the initial solid phase of calcium phosphate deposited in the extracellular matrix." Journal of Ultrastructure Research **78**(3): 227-268.
Landis, W. J., K. J. Hodgens, M. J. Song, J. Arena, S. Kiyonaga, M. Marko, C. Owen and B. F. McEwen (1996). "Mineralization of Collagen May Occur on Fibril Surfaces: Evidence from Conventional and High-Voltage Electron Microscopy and Three-Dimensional Imaging." Journal of Structural Biology **117**(1): 24-35.
Landis, W. J., J. Moradian-Oldak and S. Weiner (1991). "Topographic imaging of mineral and collagen in the calcifying turkey tendon." Connect Tissue Res **25**(3-4): 181-196.
Landis, W. J., M. C. Paine and M. J. Glimcher (1977). "Electron microscopic observations of bone tissue prepared anhydrously in organic solvents." Journal of Ultrastructure Research **59**(1): 1-30.
Lane, N. E. (2006). "Epidemiology, etiology, and diagnosis of osteoporosis." American Journal of Obstetrics and Gynecology **194**(2): S3-S11.
Lang, T., A. LeBlanc, H. Evans, Y. Lu, H. Genant and A. Yu (2004). "Cortical and Trabecular Bone Mineral Loss From the Spine and Hip in Long-Duration Spaceflight." Journal of Bone and Mineral Research **19**(6): 1006-1012.
Langer, M., A. Pacureanu, H. Suhonen, Q. Grimal, P. Cloetens and F. Peyrin (2012). "X-Ray Phase Nanotomography Resolves the 3D Human Bone Ultrastructure." PLoS ONE **7**(8): e35691.
Lau, R. Y.-c. and X. Guo (2011). "A Review on Current Osteoporosis Research: With Special Focus on Disuse Bone Loss." Journal of Osteoporosis **2011**: 6.
Le Huec, J. C., R. Saddiki, J. Franke, J. Rigal and S. Aunoble (2011). "Equilibrium of the human body and the gravity line: the basics." European Spine Journal **20**(Suppl 5): 558-563.

Le, V. Q. and K. A. Wharton (2012). "Hyperactive BMP signaling induced by ALK2(R206H) requires type II receptor function in a Drosophila model for classic Fibrodysplasia Ossificans Progressiva." Developmental dynamics : an official publication of the American Association of Anatomists **241**(1): 200-214.
LeBlanc, A., C. Marsh, H. Evans, P. Johnson, V. Schneider and S. Jhingran (1985). "Bone and muscle atrophy with suspension of the rat." Journal of Applied Physiology **58**(5): 1669.
Lebled, C., L. M. Grover and J. Z. Paxton (2014). "Combined decellularisation and dehydration improves the mechanical properties of tissue-engineered sinews." Journal of Tissue Engineering **5**: 2041731414536720.
Lee, K. Y. and D. J. Mooney (2001). "Hydrogels for Tissue Engineering." Chemical Reviews **101**(7): 1869-1880.
Lee, L.-T., P.-C. Kwan, Y.-F. Chen and Y.-K. Wong (2008). "Comparison of the Effectiveness of Autologous Fibrin Glue and Macroporous Biphasic Calcium Phosphate as Carriers in the Osteogenesis Process With or Without Mesenchymal Stem Cells." Journal of the Chinese Medical Association **71**(2): 66-73.
Lehenkari, P. P., G. T. Charras, A. Nykänen and M. A. Horton (2000). "Adapting atomic force microscopy for cell biology." Ultramicroscopy **82**(1): 289-295.
Leung, V. Y., B. Gao, K. K. Leung, I. G. Melhado, S. L. Wynn, T. Y. Au, N. W. Dung, J. Y. Lau, A. C. Mak, D. Chan and K. S. Cheah (2011). "SOX9 governs differentiation stage-specific gene expression in growth plate chondrocytes via direct concomitant transactivation and repression." PLoS Genet **7**(11): e1002356.
Li, J. and S. Dong (2016). "The Signaling Pathways Involved in Chondrocyte Differentiation and Hypertrophic Differentiation." Stem Cells International **2016**: 12.
Li, M., N. Amizuka, K. Oda, K. Tokunaga, T. Ito, K. Takeuchi, R. Takagi and T. Maeda (2004). "Histochemical evidence of the initial chondrogenesis and osteogenesis in the periosteum of a rib fractured model: Implications of osteocyte involvement in periosteal chondrogenesis." Microscopy Research and Technique **64**(4): 330-342.
Li, P., M. Kaslan, S. H. Lee, J. Yao and Z. Gao (2017). "Progress in Exosome Isolation Techniques." Theranostics **7**(3): 789-804.
Li, W., J. Zhou and Y. Xu (2015). "Study of the in vitro cytotoxicity testing of medical devices." Biomedical Reports **3**(5): 617-620.
Lin, L., Q. Shen, T. Xue and C. Yu (2010). "Heterotopic ossification induced by Achilles tenotomy via endochondral bone formation: Expression of bone and cartilage related genes." Bone **46**(2): 425-431.
Lin, Z., N. E. Rodriguez, J. Zhao, A. N. Ramey, S. L. Hyzy, B. D. Boyan and Z. Schwartz (2016). "Selective enrichment of microRNAs in extracellular matrix vesicles produced by growth plate chondrocytes." Bone **88**: 47-55.
Ling, L., S. Murali, C. Dombrowski, L. M. Haupt, G. S. Stein, A. J. van Wijnen, V. Nurcombe and S. M. Cool (2006). "Sulfated glycosaminoglycans mediate the effects of FGF2 on the osteogenic potential of rat calvarial osteoprogenitor cells." J Cell Physiol **209**(3): 811-825.
Liu, D., H. D. Wagner and S. Weiner (2000). "Bending and fracture of compact circumferential and osteonal lamellar bone of the baboon tibia." J Mater Sci Mater Med **11**(1): 49-60.
Liu, M., X. Zeng, C. Ma, H. Yi, Z. Ali, X. Mou, S. Li, Y. Deng and N. He (2017). "Injectable hydrogels for cartilage and bone tissue engineering." **5**: 17014.
Liu, M., C. Zhang, W. Liu, P. Luo, L. Zhang, Y. Wang, Z. Wang and Z. Fei (2015). "A Novel Rat Model of Blast-Induced Traumatic Brain Injury Simulating Different Damage Degree: Implications for Morphological, Neurological, and Biomarker Changes." Frontiers in Cellular Neuroscience **9**: 168.
Liu, X., H. Kang, M. Shahnazari, H. Kim, L. Wang, O. Larm, L. Adolfsson, R. Nissenson and B. Halloran (2014). "A novel mouse model of trauma induced heterotopic ossification." Journal of Orthopaedic Research **32**(2): 183-188.

Livshits, M. A., E. Khomyakova, E. G. Evtushenko, V. N. Lazarev, N. A. Kulemin, S. E. Semina, E. V. Generozov and V. M. Govorun (2015). "Isolation of exosomes by differential centrifugation: Theoretical analysis of a commonly used protocol." **5**: 17319.
Lobb, R. J., M. Becker, S. W. Wen, C. S. Wong, A. P. Wiegmans, A. Leimgruber and A. Moller (2015). "Optimized exosome isolation protocol for cell culture supernatant and human plasma." J Extracell Vesicles **4**: 27031.
Loncar, R., R. B. Zotz, C. Sucker, A. Vodovnik, M. Mihalj and R. E. Scharf (2007). "Platelet adhesion onto immobilized fibrinogen under arterial and venous in-vitro flow conditions does not significantly differ between men and women." Thrombosis Journal **5**: 5-5.
Long, F., X. M. Zhang, S. Karp, Y. Yang and A. P. McMahon (2001). "Genetic manipulation of hedgehog signaling in the endochondral skeleton reveals a direct role in the regulation of chondrocyte proliferation." Development **128**(24): 5099-5108.
Lounev, V. Y., R. Ramachandran, M. N. Wosczyna, M. Yamamoto, A. D. A. Maidment, E. M. Shore, D. L. Glaser, D. J. Goldhamer and F. S. Kaplan (2009). "Identification of Progenitor Cells That Contribute to Heterotopic Skeletogenesis." The Journal of Bone and Joint Surgery. American volume. **91**(3): 652-663.
Lundholt, B. K., K. M. Scudder and L. Pagliaro (2003). "A simple technique for reducing edge effect in cell-based assays." J Biomol Screen **8**(5): 566-570.
M. Lyons, K. (2013). Animal Models: Genetic Manipulation. Primer on the Metabolic Bone Diseases and Disorders of Mineral Metabolism, John Wiley & Sons, Inc.**:** 69-75.
Maas, M., P. Guo, M. Keeney, F. Yang, T. M. Hsu, G. G. Fuller, C. R. Martin and R. N. Zare (2011). "Preparation of mineralized nanofibers: collagen fibrils containing calcium phosphate." Nano Lett **11**(3): 1383-1388.
Mackie, E. J., Y. A. Ahmed, L. Tatarczuch, K. S. Chen and M. Mirams (2008). "Endochondral ossification: how cartilage is converted into bone in the developing skeleton." Int J Biochem Cell Biol **40**(1): 46-62.
Maina, J. N. (2000). "What it takes to fly: the structural and functional respiratory refinements in birds and bats." Journal of Experimental Biology **203**(20): 3045-3064.
Mallarino, R., O. Campàs, J. A. Fritz, K. J. Burns, O. G. Weeks, M. P. Brenner and A. Abzhanov (2012). "Closely related bird species demonstrate flexibility between beak morphology and underlying developmental programs." Proceedings of the National Academy of Sciences of the United States of America **109**(40): 16222-16227.
Malone, A. M., C. T. Anderson, P. Tummala, R. Y. Kwon, T. R. Johnston, T. Stearns and C. R. Jacobs (2007). "Primary cilia mediate mechanosensing in bone cells by a calcium-independent mechanism." Proc Natl Acad Sci U S A **104**(33): 13325-13330.
Maraka, S. and K. A. Kennel (2015). "Bisphosphonates for the prevention and treatment of osteoporosis." BMJ : British Medical Journal **351**.
Marenzana, M. and T. R. Arnett (2013). "The Key Role of the Blood Supply to Bone." Bone Research **1**(3): 203-215.
Marie, P. J. (2015). "Osteoblast dysfunctions in bone diseases: from cellular and molecular mechanisms to therapeutic strategies." Cell Mol Life Sci **72**(7): 1347-1361.
Marieb, E. N. and K. Hoehn (2010). Human Anatomy & Physiology, Benjamin Cummings.
Marsell, R. and T. A. Einhorn (2011). "The biology of fracture healing." Injury **42**(6): 551-555.
Martín-Badosa, E., D. Amblard, S. Nuzzo, A. Elmoutaouakkil, L. Vico and F. Peyrin (2003). "Excised Bone Structures in Mice: Imaging at Three-dimensional Synchrotron Radiation Micro CT." Radiology **229**(3): 921-928.
Martin, G. R., K. A. Piez and M. S. Lewis (1963). "The incorporation of [14C]glycine into the subunits of collagens from normal and lathyritic animals." Biochimica et Biophysica Acta **69**: 472-479.
Martin, J. W., J. A. Squire and M. Zielenska (2012). "The Genetics of Osteosarcoma." Sarcoma **2012**: 11.

Massague, J., J. Seoane and D. Wotton (2005). "Smad transcription factors." Genes Dev **19**(23): 2783-2810.
Matassi, F., L. Nistri, D. Chicon Paez and M. Innocenti (2011). "New biomaterials for bone regeneration." Clinical Cases in Mineral and Bone Metabolism **8**(1): 21-24.
Matsumoto, T., Y. Mifune, A. Kawamoto, R. Kuroda, T. Shoji, H. Iwasaki, T. Suzuki, A. Oyamada, M. Horii, A. Yokoyama, H. Nishimura, S. Y. Lee, M. Miwa, M. Doita, M. Kurosaka and T. Asahara (2008). "Fracture induced mobilization and incorporation of bone marrow-derived endothelial progenitor cells for bone healing." Journal of Cellular Physiology **215**(1): 234-242.
Matthews, B. G., D. Naot, K. E. Callon, D. S. Musson, R. Locklin, P. A. Hulley, A. Grey and J. Cornish (2014). "Enhanced osteoblastogenesis in three-dimensional collagen gels." BoneKEy Rep **3**.
McCarthy, E. F. and M. Sundaram (2005). "Heterotopic ossification: a review." Skeletal Radiology **34**(10): 609-619.
McDonald, M. M., A. Schindeler and D. G. Little (2007). "Bisphosphonate treatment and fracture repair." IBMS BoneKEy **4**(9): 236-251.
McEwen, B. F., M. J. Song and W. J. Landis (1991). "Quantitative determination of the mineral distribution in different collagen zones of calcifying tendon using high voltage electron microscopic tomography." J Comput Assist Microsc **3**(4): 201-210.
McVeigh, C. M. and A. P. Cairns (2006). "Diagnosis and management of ankylosing spondylitis." BMJ : British Medical Journal **333**(7568): 581-585.
Medici, D. and B. R. Olsen (2012). Transformation of Vascular Endothelial Cells into Multipotent Stem-Like Cells: Role of the Activin-Like Kinase 2 Receptor. Stem Cells and Cancer Stem Cells, Volume 8: Therapeutic Applications in Disease and Injury. M. A. Hayat. Dordrecht, Springer Netherlands**:** 207-213.
Medici, D., E. M. Shore, V. Y. Lounev, F. S. Kaplan, R. Kalluri and B. R. Olsen (2010). "Conversion of vascular endothelial cells into multipotent stem-like cells." Nature medicine **16**(12): 1400-1406.
Meijer, G. J., J. D. de Bruijn, R. Koole and C. A. van Blitterswijk (2007). "Cell-Based Bone Tissue Engineering." PLOS Medicine **4**(2): e9.
Merlotti, D., L. Gennari, G. Martini, F. Valleggi, V. De Paola, A. Avanzati and R. Nuti (2007). "Comparison of different intravenous bisphosphonate regimens for Paget's disease of bone." J Bone Miner Res **22**(10): 1510-1517.
Michelsson, J. E., G. Granroth and L. C. Andersson (1980). "Myositis ossificans following forcible manipulation of the leg. A rabbit model for the study of heterotopic bone formation." J Bone Joint Surg Am **62**(5): 811-815.
Millán, J. L. and M. P. Whyte (2016). "Alkaline Phosphatase and Hypophosphatasia." Calcified Tissue International **98**: 398-416.
Miller, C. W., A. Aslo, A. Won, M. Tan, B. Lampkin and H. P. Koeffler (1996). "Alterations of the p53, Rb and MDM2 genes in osteosarcoma." J Cancer Res Clin Oncol **122**(9): 559-565.
Mizuno, H., A. K. Roy, C. A. Vacanti, K. Kojima, M. Ueda and L. J. Bonassar (2004). "Tissue-engineered composites of anulus fibrosus and nucleus pulposus for intervertebral disc replacement." Spine (Phila Pa 1976) **29**(12): 1290-1297; discussion 1297-1298.
Mizutani, A., I. Sugiyama, E. Kuno, S. Matsunaga and N. Tsukagoshi (2001). "Expression of matrix metalloproteinases during ascorbate-induced differentiation of osteoblastic MC3T3-E1 cells." J Bone Miner Res **16**(11): 2043-2049.
Mohan, S. and C. Kesavan (2012). "Role of Insulin-like Growth Factor-1 in the Regulation of Skeletal Growth." Current Osteoporosis Reports **10**(2): 178-186.
Mollon, B., V. da Silva, J. W. Busse, T. A. Einhorn and M. Bhandari (2008). "Electrical stimulation for long-bone fracture-healing: a meta-analysis of randomized controlled trials." J Bone Joint Surg Am **90**(11): 2322-2330.

Moreau, J. L., M. D. Weir and H. H. K. Xu (2009). "Self-setting collagen-calcium phosphate bone cement: Mechanical and cellular properties." Journal of Biomedical Materials Research Part A **91A**(2): 605-613.
Mornet, E. (2000). "Hypophosphatasia: the mutations in the tissue-nonspecific alkaline phosphatase gene." Hum Mutat **15**(4): 309-315.
Morris, M. D. and G. S. Mandair (2011). "Raman Assessment of Bone Quality." Clinical Orthopaedics and Related Research **469**(8): 2160-2169.
Mourad, W. F., S. Packianathan, G. V. Russell, J. K. Ma, R. A. Shourbaji, M. Ryniak, B. M. Rabatic, D. Zaenger, R. He, P. N. Mobit, C. C. Yang, D. Shasha and S. Vijayakumar (2015). "Radiation Prophylaxis of Heterotopic Ossification at the Elbow: Is It Time for XRT Dose-Deescalation?" International Journal of Radiation Oncology*Biology*Physics **93**(3): E465.
Mularchuk, P. and A. Boskey (1990). "Lipids in bone: Optimal conditions for tissue storage prior to lipid analyses." Calcified Tissue International **46**(1): 57-59.
Mullaji, A. B., S. S. Upadhyay, K. D. Luk and J. C. Leong (1994). "Vertebral growth after posterior spinal fusion for idiopathic scoliosis in skeletally immature adolescents. The effect of growth on spinal deformity." J Bone Joint Surg Br **76**(6): 870-876.
Mundlos, S. (1999). "Cleidocranial dysplasia: clinical and molecular genetics." Journal of Medical Genetics **36**(3): 177-182.
Murphy, R. F. and J. F. Mooney (2016). "Complications following spine fusion for adolescent idiopathic scoliosis." Current Reviews in Musculoskeletal Medicine **9**(4): 462-469.
Nabavi, N., A. Khandani, A. Camirand and R. E. Harrison (2011). "Effects of microgravity on osteoclast bone resorption and osteoblast cytoskeletal organization and adhesion." Bone **49**(5): 965-974.
Nagy, T. R., D. Krzywanski, J. Li, S. Meleth and R. Desmond (2002). "Effect of group vs. single housing on phenotypic variance in C57BL/6J mice." Obes Res **10**(5): 412-415.
Naik, M. U., S. A. Mousa, C. A. Parkos and U. P. Naik (2003). "Signaling through JAM-1 and α_vβ₃ is required for the angiogenic action of bFGF: dissociation of the JAM-1 and α_vβ₃ complex." Blood **102**(6): 2108-2114.
Nakashima, T., M. Hayashi, T. Fukunaga, K. Kurata, M. Oh-hora, J. Q. Feng, L. F. Bonewald, T. Kodama, A. Wutz, E. F. Wagner, J. M. Penninger and H. Takayanagi (2011). "Evidence for osteocyte regulation of bone homeostasis through RANKL expression." Nat Med **17**(10): 1231-1234.
Nascimento, F. A., L. A. M. Gatto, R. O. Lages, H. M. Neto, Z. Demartini and G. L. Koppe (2014). "Diffuse idiopathic skeletal hyperostosis: A review." Surgical Neurology International **5**(Suppl 3): S122-S125.
Neer, R. M., C. D. Arnaud, J. R. Zanchetta, R. Prince, G. A. Gaich, J.-Y. Reginster, A. B. Hodsman, E. F. Eriksen, S. Ish-Shalom, H. K. Genant, O. Wang, D. Mellström, E. S. Oefjord, E. Marcinowska-Suchowierska, J. Salmi, H. Mulder, J. Halse, A. Z. Sawicki and B. H. Mitlak (2001). "Effect of Parathyroid Hormone (1-34) on Fractures and Bone Mineral Density in Postmenopausal Women with Osteoporosis." New England Journal of Medicine **344**(19): 1434-1441.
Nefussi, J. R., J. M. Sautier, V. Nicolas and N. Forest (1991). "How osteoblasts become osteocytes: a decreasing matrix forming process." J Biol Buccale **19**(1): 75-82.
Ngo, P., P. Ramalingam, J. A. Phillips and G. T. Furuta (2006). "Collagen gel contraction assay." Methods Mol Biol **341**: 103-109.
Nguyen, T. D. and Y. Gu (2014). "Determination of strain-rate-dependent mechanical behavior of living and fixed osteocytes and chondrocytes using atomic force microscopy and inverse finite element analysis." J Biomech Eng **136**(10): 101004.
Niu, L.-n., S. E. Jee, K. Jiao, L. Tonggu, M. Li, L. Wang, Y.-d. Yang, J.-h. Bian, L. Breschi, S. S. Jang, J.-h. Chen, D. H. Pashley and F. R. Tay (2017). "Collagen intrafibrillar mineralization as a result of the balance between osmotic equilibrium and electroneutrality." Nat Mater **16**(3): 370-378.
Olmsted-Davis, E., F. H. Gannon, M. Ozen, M. M. Ittmann, Z. Gugala, J. A. Hipp, K. M. Moran, C. M. Fouletier-Dilling, S. Schumara-Martin, R. W. Lindsey, M. H. Heggeness, M. K. Brenner and A. R. Davis

(2007). "Hypoxic Adipocytes Pattern Early Heterotopic Bone Formation." The American Journal of Pathology **170**(2): 620-632.
Olsen, B. R. (1964). "Electron microscope studies on collagen." Zeitschrift für Zellforschung und Mikroskopische Anatomie **61**(6): 913-919.
Orgel, J. P. R. O., T. C. Irving, A. Miller and T. J. Wess (2006). "Microfibrillar structure of type I collagen in situ." Proceedings of the National Academy of Sciences **103**(24): 9001-9005.
Orriss, I. R., G. E. Knight, J. C. Utting, S. E. B. Taylor, G. Burnstock and T. R. Arnett (2009). "Hypoxia stimulates vesicular ATP release from rat osteoblasts." Journal of Cellular Physiology **220**(1): 155-162.
Otto, F., A. P. Thornell, T. Crompton, A. Denzel, K. C. Gilmour, I. R. Rosewell, G. W. H. Stamp, R. S. P. Beddington, S. Mundlos, B. R. Olsen, P. B. Selby and M. J. Owen (1997). "Cbfa1, a Candidate Gene for Cleidocranial Dysplasia Syndrome, Is Essential for Osteoblast Differentiation and Bone Development." Cell **89**(5): 765-771.
Palazzini, S., C. Palumbo, M. Ferretti and G. Marotti (1998). "Stromal cell structure and relationships in perimedullary spaces of chick embryo shaft bones." Anat Embryol (Berl) **197**(5): 349-357.
Palmer, L. C., C. J. Newcomb, S. R. Kaltz, E. D. Spoerke and S. I. Stupp (2008). "Biomimetic Systems for Hydroxyapatite Mineralization Inspired By Bone and Enamel." Chemical reviews **108**(11): 4754-4783.
Pan, K. L., W. H. Chan, P. Shanmugam, G. B. Ong, F. Kamaruddin and S. Tan (2014). "Large Volume Osteosarcomas of the Femur Treated with Total Femoral Replacement." Malaysian Orthopaedic Journal **8**(1): 32-36.
Pape, H. C., U. Lehmann, M. van Griensven, A. Gansslen, S. von Glinski and C. Krettek (2001). "Heterotopic ossifications in patients after severe blunt trauma with and without head trauma: incidence and patterns of distribution." J Orthop Trauma **15**(4): 229-237.
Paxton, J. Z., K. Donnelly, R. P. Keatch, K. Baar and L. M. Grover (2010). "Factors Affecting the Longevity and Strength in an In Vitro Model of the Bone–Ligament Interface." Annals of Biomedical Engineering **38**(6): 2155-2166.
Paxton, J. Z., U. N. Wudebwe, A. Wang, D. Woods and L. M. Grover (2012). "Monitoring sinew contraction during formation of tissue-engineered fibrin-based ligament constructs." Tissue Eng Part A **18**(15-16): 1596-1607.
Pearce, A. I., R. G. Richards, S. Milz, E. Schneider and S. G. Pearce (2007). "Animal models for implant biomaterial research in bone: a review." Eur Cell Mater **13**: 1-10.
Peng, G. E., S. R. Wilson and O. D. Weiner (2011). "A pharmacological cocktail for arresting actin dynamics in living cells." Molecular Biology of the Cell **22**(21): 3986-3994.
Perka, C., S. Stern, R.-S. Spitzer and K. Lindenhayn (2003). Chondrocytes and Fibrin Glue. Cartilage Surgery and Future Perspectives. C. Hendrich, U. Nöth and J. Eulert. Berlin, Heidelberg, Springer Berlin Heidelberg**:** 151-155.
Petruska, J. A. and A. J. Hodge (1964). "A SUBUNIT MODEL FOR THE TROPOCOLLAGEN MACROMOLECULE." Proceedings of the National Academy of Sciences of the United States of America **51**(5): 871-876.
Peyrin, F., P. Dong, A. Pacureanu and M. Langer (2014). "Micro- and Nano-CT for the Study of Bone Ultrastructure." Current Osteoporosis Reports **12**(4): 465-474.
Phillips, A. M. (2005). "Overview of the fracture healing cascade." Injury **36**(3, Supplement): S5-S7.
Pidaparti, R. M. and D. B. Burr (1992). "Collagen fiber orientation and geometry effects on the mechanical properties of secondary osteons." J Biomech **25**(8): 869-880.
Pixley, F. J. and E. R. Stanley (2004). "CSF-1 regulation of the wandering macrophage: complexity in action." Trends Cell Biol **14**(11): 628-638.
Plotkin, L. I. (2014). "Connexin 43 hemichannels and intracellular signaling in bone cells." Front Physiol **5**: 131.
Plotkin, L. I. and T. Bellido (2016). "Osteocytic signalling pathways as therapeutic targets for bone fragility." Nat Rev Endocrinol **12**(10): 593-605.

Poole, K. E. S., R. L. van Bezooijen, N. Loveridge, H. Hamersma, S. E. Papapoulos, C. W. Löwik and J. Reeve (2005). "Sclerostin is a delayed secreted product of osteocytes that inhibits bone formation." The FASEB Journal.
Popovic, M., A. Agarwal, L. Zhang, C. Yip, H. J. Kreder, M. T. Nousiainen, R. Jenkinson, M. Tsao, H. Lam, M. Milakovic, E. Wong and E. Chow (2014). "Radiotherapy for the prophylaxis of heterotopic ossification: A systematic review and meta-analysis of published data." Radiotherapy and Oncology **113**(1): 10-17.
Potter, B. K., T. C. Burns, A. P. Lacap, R. R. Granville and D. A. Gajewski (2007). "Heterotopic Ossification Following Traumatic and Combat-Related Amputations." The Journal of Bone & Joint Surgery **89**(3): 476-486.
Potter, M. A. J. B. K., L. J. A. Forsberg, T. A. Davis, C. P. T. K. N. Evans, M. A. J. J. S. Hawksworth, D. Tadaki, T. S. Brown, N. J. Crane, M. A. J. T. C. Burns, C. P. T. F. P. O'Brien and C. D. R. E. A. Elster (2010). "Heterotopic Ossification Following Combat-Related Trauma." The Journal of Bone & Joint Surgery **92**(Supplement 2): 74-89.
Pounds, J. G., G. J. Long and J. F. Rosen (1991). "Cellular and molecular toxicity of lead in bone." Environmental Health Perspectives **91**: 17-32.
Price, C., X. Zhou, W. Li and L. Wang (2011). "Real-time measurement of solute transport within the lacunar-canalicular system of mechanically loaded bone: direct evidence for load-induced fluid flow." J Bone Miner Res **26**(2): 277-285.
Prideaux, M., C. Schutz, A. R. Wijenayaka, D. M. Findlay, D. G. Campbell, L. B. Solomon and G. J. Atkins (2016). "Isolation of osteocytes from human trabecular bone." Bone **88**: 64-72.
Provenzano, P. P., K. W. Eliceiri, D. R. Inman and P. J. Keely (2010). "Engineering three-dimensional collagen matrices to provide contact guidance during 3D cell migration." Curr Protoc Cell Biol **Chapter 10**: Unit 10.17.
Pullig, O., G. Weseloh, S. Gauer and B. Swoboda (2000). "Osteopontin is expressed by adult human osteoarthritic chondrocytes: protein and mRNA analysis of normal and osteoarthritic cartilage." Matrix Biol **19**(3): 245-255.
Rahaman, M. N., D. E. Day, B. S. Bal, Q. Fu, S. B. Jung, L. F. Bonewald and A. P. Tomsia (2011). "Bioactive glass in tissue engineering." Acta Biomater **7**(6): 2355-2373.
Ramachandran, G. N. (1956). "Structure of Collagen." Nature **177**(4511): 710-711.
Ramirez, D. M., M. R. Ramirez, A. M. Reginato and D. Medici (2014). "Molecular and cellular mechanisms of heterotopic ossification." Histology and histopathology **29**(10): 1281-1285.
Rayner, J. M. V., P. W. Viscardi, S. Ward and J. R. Speakman (2001). "Aerodynamics and Energetics of Intermittent Flight in Birds1." American Zoologist **41**(2): 188-204.
Rhee, S. and F. Grinnell (2007). "Fibroblast mechanics in 3D collagen matrices." Adv Drug Deliv Rev **59**(13): 1299-1305.
Robling, A. G., F. M. Hinant, D. B. Burr and C. H. Turner (2002). "Shorter, more frequent mechanical loading sessions enhance bone mass." Med Sci Sports Exerc **34**(2): 196-202.
Roodman, G. D. and J. J. Windle (2005). "Paget disease of bone." Journal of Clinical Investigation **115**(2): 200-208.
Roseberry, H. H., A. B. Hastings and J. K. Morse (1931). "X-RAY ANALYSIS OF BONE AND TEETH." Journal of Biological Chemistry **90**(2): 395-407.
Rosen, C. J., R. Bouillon, J. E. Compston and V. Rosen (2013). Primer on the Metabolic Bone Diseases and Disorders of Mineral Metabolism, Wiley.
Ross, F. P. (2013). Osteoclast Biology and Bone Resorption. Primer on the Metabolic Bone Diseases and Disorders of Mineral Metabolism, John Wiley & Sons, Inc.**:** 25-33.
Rubin, C. T. (1984). "Skeletal strain and the functional significance of bone architecture." Calcif Tissue Int **36 Suppl 1**: S11-18.
Rudman, K. E., R. M. Aspden and J. R. Meakin (2006). "Compression or tension? The stress distribution in the proximal femur." BioMedical Engineering OnLine **5**: 12-12.

Ryan, T. M. and R. A. Ketcham (2005). "Angular orientation of trabecular bone in the femoral head and its relationship to hip joint loads in leaping primates." J Morphol **265**(3): 249-263.
Safdar, A., A. Saleem and M. A. Tarnopolsky (2016). "The potential of endurance exercise-derived exosomes to treat metabolic diseases." Nat Rev Endocrinol **12**(9): 504-517.
Salisbury, E. A., A. R. Dickerson, T. A. Davis, J. A. Forsberg, A. R. Davis and E. A. Olmsted-Davis (2017). "Characterization of Brown Adipose-Like Tissue in Trauma-Induced Heterotopic Ossification in Humans." Am J Pathol **187**(9): 2071-2079.
Sato, K., K. Aoki, Y. Y. Watanabe and P. J. O. Miller (2013). "Neutral buoyancy is optimal to minimize the cost of transport in horizontally swimming seals." **3**: 2205.
Satou, Y., H. A. Al-Shawafi, S. Sultana, S. Makita, M. Sohda and K. Oda (2012). "Disulfide bonds are critical for tissue-nonspecific alkaline phosphatase function revealed by analysis of mutant proteins bearing a C201-Y or C489-S substitution associated with severe hypophosphatasia." Biochimica et Biophysica Acta (BBA) - Molecular Basis of Disease **1822**(4): 581-588.
Schaffler, M. B., W.-Y. Cheung, R. Majeska and O. Kennedy (2014). "Osteocytes: Master Orchestrators of Bone." Calcified tissue international **94**(1): 5-24.
Schipani, E., H. E. Ryan, S. Didrickson, T. Kobayashi, M. Knight and R. S. Johnson (2001). "Hypoxia in cartilage: HIF-1alpha is essential for chondrocyte growth arrest and survival." Genes Dev **15**(21): 2865-2876.
Schmidmaier, G. and B. Wildemann (2009). "The role of BMPs in current orthopedic practice." IBMS BoneKEy **6**(7): 244-253.
Schneider, P., M. Meier, R. Wepf and R. Müller (2010). "Towards quantitative 3D imaging of the osteocyte lacuno-canalicular network." Bone **47**(5): 848-858.
Segnani, C., C. Ippolito, L. Antonioli, C. Pellegrini, C. Blandizzi, A. Dolfi and N. Bernardini (2015). "Histochemical Detection of Collagen Fibers by Sirius Red/Fast Green Is More Sensitive than van Gieson or Sirius Red Alone in Normal and Inflamed Rat Colon." PLoS ONE **10**(12): e0144630.
Semenov, M., K. Tamai and X. He (2005). "SOST is a ligand for LRP5/LRP6 and a Wnt signaling inhibitor." J Biol Chem **280**(29): 26770-26775.
Sessions, N. D., B. P. Halloran, D. D. Bikle, T. J. Wronski, C. M. Cone and E. Morey-Holton (1989). "Bone response to normal weight bearing after a period of skeletal unloading." American Journal of Physiology - Endocrinology And Metabolism **257**(4): E606.
Shackley, M. S. (2014). X-Ray Fluorescence (XRF): Applications in Archaeology. Encyclopedia of Global Archaeology. C. Smith. New York, NY, Springer New York**:** 7933-7938.
Shimono, K., W.-e. Tung, C. Macolino, A. H.-T. Chi, J. H. Didizian, C. Mundy, R. A. Chandraratna, Y. Mishina, M. Enomoto-Iwamoto, M. Pacifici and M. Iwamoto (2011). "Potent inhibition of heterotopic ossification by nuclear retinoic acid receptor-[gamma] agonists." Nat Med **17**(4): 454-460.
Shore, E. M. and F. S. Kaplan (2010). "Inherited human diseases of heterotopic bone formation." Nat Rev Rheumatol **6**(9): 518-527.
Shore, E. M., M. Xu, G. J. Feldman, D. A. Fenstermacher, T. J. Cho, I. H. Choi, J. M. Connor, P. Delai, D. L. Glaser, M. LeMerrer, R. Morhart, J. G. Rogers, R. Smith, J. T. Triffitt, J. A. Urtizberea, M. Zasloff, M. A. Brown and F. S. Kaplan (2006). "A recurrent mutation in the BMP type I receptor ACVR1 causes inherited and sporadic fibrodysplasia ossificans progressiva." Nat Genet **38**(5): 525-527.
Shubin, N. H., E. B. Daeschler and F. A. Jenkins (2006). "The pectoral fin of Tiktaalik roseae and the origin of the tetrapod limb." Nature **440**(7085): 764-771.
Shubin, N. H., E. B. Daeschler and F. A. Jenkins (2014). "Pelvic girdle and fin of Tiktaalik roseae." Proceedings of the National Academy of Sciences **111**(3): 893-899.
Sobacchi, C., A. Schulz, F. P. Coxon, A. Villa and M. H. Helfrich (2013). "Osteopetrosis: genetics, treatment and new insights into osteoclast function." Nat Rev Endocrinol **9**(9): 522-536.
Song, L., R. E. Olsen, J. P. Spalazzi and T. Davisson (2010). "Biomechanical evaluation of acellular collagen matrix augmented Achilles tendon repair in sheep." J Foot Ankle Surg **49**(5): 438-441.

Sowa, H., H. Kaji, T. Yamaguchi, T. Sugimoto and K. Chihara (2002). "Smad3 promotes alkaline phosphatase activity and mineralization of osteoblastic MC3T3-E1 cells." J Bone Miner Res **17**(7): 1190-1199.
Spencer, J. D. and G. A. Missen (1989). "Pseudomalignant heterotopic ossification ("myositis ossificans"). Recurrence after excision with subsequent resorption." J Bone Joint Surg Br **71**(2): 317-319.
St-Jacques, B., M. Hammerschmidt and A. P. McMahon (1999). "Indian hedgehog signaling regulates proliferation and differentiation of chondrocytes and is essential for bone formation." Genes & Development **13**(16): 2072-2086.
St John, H. C., K. A. Bishop, M. B. Meyer, N. A. Benkusky, N. Leng, C. Kendziorski, L. F. Bonewald and J. W. Pike (2014). "The osteoblast to osteocyte transition: epigenetic changes and response to the vitamin D3 hormone." Mol Endocrinol **28**(7): 1150-1165.
Stein, G. S. and J. B. Lian (1993). "Molecular Mechanisms Mediating Proliferation/Differentiation Interrelationships During Progressive Development of the Osteoblast Phenotype." Endocrine Reviews **14**(4): 424-442.
Suda, R. K., P. C. Billings, K. P. Egan, J.-H. Kim, R. McCarrick-Walmsley, D. L. Glaser, D. L. Porter, E. M. Shore and R. J. Pignolo (2009). "Circulating Osteogenic Precursor Cells in Heterotopic Bone Formation." Stem cells (Dayton, Ohio) **27**(9): 2209-2219.
Suda, T., N. Takahashi, N. Udagawa, E. Jimi, M. T. Gillespie and T. J. Martin (1999). "Modulation of osteoclast differentiation and function by the new members of the tumor necrosis factor receptor and ligand families." Endocr Rev **20**(3): 345-357.
Sullivan, M. P., S. J. Torres, S. Mehta and J. Ahn (2013). "Heterotopic ossification after central nervous system trauma: A current review." Bone & Joint Research **2**(3): 51-57.
Sun, Q., Y. Gu, W. Zhang, L. Dziopa, J. Zilberberg and W. Lee (2015). "Ex vivo 3D osteocyte network construction with primary murine bone cells." Bone Research **3**: 15026.
Šupová, M. (2009). "Problem of hydroxyapatite dispersion in polymer matrices: a review." Journal of Materials Science: Materials in Medicine **20**(6): 1201-1213.
Surhone, L. M., M. T. Timpledon and S. F. Marseken (2010). Spaceflight Osteopenia: Osteoporosis, Spaceflight, Astronaut, Calcium, Skeleton, Outer Space, Project Gemini, William E. Thornton, Betascript Publishing.
Swartz, S. M., M. B. Bennett and D. R. Carrier (1992). "Wing bone stresses in free flying bats and the evolution of skeletal design for flight." Nature **359**(6397): 726-729.
Szent-Györgyi, A. G. (1975). "Calcium regulation of muscle contraction." Biophysical Journal **15**(7): 707-723.
Taichman, R. S. (2005). "Blood and bone: two tissues whose fates are intertwined to create the hematopoietic stem-cell niche." Blood **105**(7): 2631.
Takakura, A., R. Takao-Kawabata, Y. Isogai, M. Kajiwara, H. Murayama, S. Ejiri and T. Ishizuya (2016). "Differences in vertebral, tibial, and iliac cancellous bone metabolism in ovariectomized rats." J Bone Miner Metab **34**(3): 291-302.
Takano-Yamamoto, T. (2014). "Osteocyte function under compressive mechanical force." Japanese Dental Science Review **50**(2): 29-39.
Tam, C. S., J. N. Heersche, T. M. Murray and J. A. Parsons (1982). "Parathyroid hormone stimulates the bone apposition rate independently of its resorptive action: differential effects of intermittent and continuous administration." Endocrinology **110**(2): 506-512.
Tamma, R., G. Colaianni, C. Camerino, A. Di Benedetto, G. Greco, M. Strippoli, R. Vergari, A. Grano, L. Mancini, G. Mori, S. Colucci, M. Grano and A. Zallone (2009). "Microgravity during spaceflight directly affects in vitro osteoclastogenesis and bone resorption." The FASEB Journal **23**(8): 2549-2554.

Tannous, O., A. C. Stall, C. Griffith, C. T. Donaldson, R. J. Castellani, Jr. and V. D. Pellegrini, Jr. (2013). "Heterotopic bone formation about the hip undergoes endochondral ossification: a rabbit model." Clin Orthop Relat Res **471**(5): 1584-1592.
Tatsumi, S., K. Ishii, N. Amizuka, M. Li, T. Kobayashi, K. Kohno, M. Ito, S. Takeshita and K. Ikeda (2007). "Targeted ablation of osteocytes induces osteoporosis with defective mechanotransduction." Cell Metab **5**(6): 464-475.
Taylor, M. A. (2000). "Functional significance of bone ballastin in the evolution of buoyancy control strategies by aquatic tetrapods." Historical Biology **14**(1-2): 15-31.
Temiyasathit, S. and C. R. Jacobs (2010). "The osteocyte primary cilium and its role in bone mechanotransduction." Annals of the New York Academy of Sciences **1192**: 422-428.
ten Dijke, P., C. Krause, D. J. de Gorter, C. W. Lowik and R. L. van Bezooijen (2008). "Osteocyte-derived sclerostin inhibits bone formation: its role in bone morphogenetic protein and Wnt signaling." J Bone Joint Surg Am **90 Suppl 1**: 31-35.
Thakkar, S., H. Fernandes and L. Moroni (2015). "Decellularized Extracellular Matrix Scaffolds for Cartilage Regeneration." Methods Mol Biol **1340**: 133-151.
Thein-Han, W., J. Liu and H. H. Xu (2012). "Calcium phosphate cement with biofunctional agents and stem cell seeding for dental and craniofacial bone repair." Dent Mater **28**(10): 1059-1070.
Thilak, J., J. J. Panakkal, T.-Y. Kim, S. M. Goodman, S.-S. Lee and E. A. Salvati "Risk Factors of Heterotopic Ossification Following Total Hip Arthroplasty in Patients With Ankylosing Spondylitis." The Journal of Arthroplasty **30**(12): 2304-2307.
Thompson, Z., T. Miclau, D. Hu and J. A. Helms (2002). "A model for intramembranous ossification during fracture healing." J Orthop Res **20**(5): 1091-1098.
Tong, C., G. Huang, C. Ashton, P. Li and Q.-L. Ying (2011). "Generating gene knockout rats by homologous recombination in embryonic stem cells." Nat. Protocols **6**(6): 827-844.
Toussirot, E. and D. Wendling (2007). "Antiinflammatory treatment with bisphosphonates in ankylosing spondylitis." Curr Opin Rheumatol **19**(4): 340-345.
Toyosawa, S., S. Shintani, T. Fujiwara, T. Ooshima, A. Sato, N. Ijuhin and T. Komori (2001). "Dentin Matrix Protein 1 Is Predominantly Expressed in Chicken and Rat Osteocytes But Not in Osteoblasts." Journal of Bone and Mineral Research **16**(11): 2017-2026.
Ueno, M., K. Uchida, M. Takaso, H. Minehara, K. Suto, N. Takahira, R. Steck, M. A. Schuetz and M. Itoman (2011). "Distribution of Bone Marrow-Derived Cells in the Fracture Callus during Plate Fixation in a Green Fluorescent Protein-Chimeric Mouse Model." Experimental Animals **60**(5): 455-462.
Ueno, T., T. Kagawa, M. Kanou, T. Fujii, J. Fukunaga, N. Mizukawa, T. Sugahara and T. Yamamoto (2003). "Immunohistochemical observations of cellular differentiation and proliferation in endochondral bone formation from grafted periosteum:: expression and localization of BMP-2 and -4 in the grafted periosteum." Journal of Cranio-Maxillofacial Surgery **31**(6): 356-361.
Urist, M. R. (1965). "Bone: formation by autoinduction." Science **150**(3698): 893-899.
Ushiku, C., D. J. Adams, X. Jiang, L. Wang and D. W. Rowe (2010). "Long bone fracture repair in mice harboring GFP reporters for cells within the osteoblastic lineage." Journal of Orthopaedic Research **28**(10): 1338-1347.
van Kuijk, A. A., A. C. Geurts and H. J. van Kuppevelt (2002). "Neurogenic heterotopic ossification in spinal cord injury." Spinal Cord **40**(7): 313-326.
Vanden Bossche, L. and G. Vanderstraeten (2005). "Heterotopic ossification: a review." J Rehabil Med **37**(3): 129-136.
Vazquez, M., B. A. J. Evans, D. Riccardi, S. L. Evans, J. R. Ralphs, C. M. Dillingham and D. J. Mason (2014). "A New Method to Investigate How Mechanical Loading of Osteocytes Controls Osteoblasts." Frontiers in Endocrinology **5**: 208.
Viapiana, O., D. Gatti, L. Idolazzi, E. Fracassi, S. Adami, S. Troplini, M. R. Povino and M. Rossini (2014). "Bisphosphonates vs infliximab in ankylosing spondylitis treatment." Rheumatology **53**(1): 90-94.

Vico, L., M. Hinsenkamp, D. Jones, P. J. Marie, A. Zallone and R. Cancedda (2001). "Osteobiology, strain, and microgravity. Part II: Studies at the tissue level." Calcified Tissue International **68**(1): 1-10.
von der Mark, K., P. Wendt, F. Rexrodt and K. Kühn (1970). "Direct evidence for a correlation between amino acid sequence and cross striation pattern of collagen." FEBS Letters **11**(2): 105-108.
Wahl, D. A. and J. T. Czernuszka (2006). "Collagen-hydroxyapatite composites for hard tissue repair." Eur Cell Mater **11**: 43-56.
Wang, A., R. L. Williams, N. Jumbu, J. Z. Paxton, E. T. Davis, M. A. Snow, A. Campbell Ritchie, C. B. Johansson, R. L. Sammons and L. M. Grover (2016). "Development of tissue engineered ligaments with titanium spring reinforcement." RSC Advances **6**(100): 98536-98544.
Wang, H., M. Bongio, K. Farbod, A. W. Nijhuis, J. van den Beucken, O. C. Boerman, J. C. van Hest, Y. Li, J. A. Jansen and S. C. Leeuwenburgh (2014). "Development of injectable organic/inorganic colloidal composite gels made of self-assembling gelatin nanospheres and calcium phosphate nanocrystals." Acta Biomater **10**(1): 508-519.
Wang, H., C. Lindborg, V. Lounev, J.-H. Kim, R. McCarrick-Walmsley, M. Xu, L. Mangiavini, J. C. Groppe, E. M. Shore, E. Schipani, F. S. Kaplan and R. J. Pignolo (2016). "Cellular Hypoxia Promotes Heterotopic Ossification by Amplifying BMP Signaling." Journal of Bone and Mineral Research **31**(9): 1652-1665.
Wang, P., L. Zhao, J. Liu, M. D. Weir, X. Zhou and H. H. K. Xu (2014). "Bone tissue engineering via nanostructured calcium phosphate biomaterials and stem cells." **2**: 14017.
Wang, R. N., J. Green, Z. Wang, Y. Deng, M. Qiao, M. Peabody, Q. Zhang, J. Ye, Z. Yan, S. Denduluri, O. Idowu, M. Li, C. Shen, A. Hu, R. C. Haydon, R. Kang, J. Mok, M. J. Lee, H. L. Luu and L. L. Shi (2014). "Bone Morphogenetic Protein (BMP) signaling in development and human diseases." Genes & Diseases **1**(1): 87-105.
Wang, Y.-H., Y. Liu, P. Maye and D. W. Rowe (2006). "Examination of Mineralized Nodule Formation in Living Osteoblastic Cultures Using Fluorescent Dyes." Biotechnology progress **22**(6): 1697-1701.
Wang, Y., T. Azaïs, M. Robin, A. Vallée, C. Catania, P. Legriel, G. Pehau-Arnaudet, F. Babonneau, M.-M. Giraud-Guille and N. Nassif (2012). "The predominant role of collagen in the nucleation, growth, structure and orientation of bone apatite." Nat Mater **11**(8): 724-733.
Wang, Y., Y.-P. Li, C. Paulson, J.-Z. Shao, X. Zhang, M. Wu and W. Chen (2014). "Wnt and the Wnt signaling pathway in bone development and disease." Frontiers in bioscience (Landmark edition) **19**: 379-407.
Wataha, J. C., C. T. Hanks and Z. Sun (1994). "Effect of cell line on in vitro metal ion cytotoxicity." Dent Mater **10**(3): 156-161.
Watanabe, M., M. Yumoto, H. Tanaka, H. H. Wang, T. Katayama, S. Yoshiyama, J. Black, S. E. Thatcher and K. Kohama (2010). "Blebbistatin, a myosin II inhibitor, suppresses contraction and disrupts contractile filaments organization of skinned taenia cecum from guinea pig." Am J Physiol Cell Physiol **298**(5): C1118-1126.
Wegel, E., A. Göhler, B. C. Lagerholm, A. Wainman, S. Uphoff, R. Kaufmann and I. M. Dobbie (2016). "Imaging cellular structures in super-resolution with SIM, STED and Localisation Microscopy: A practical comparison." **6**: 27290.
Weinbaum, S., S. C. Cowin and Y. Zeng (1994). "A model for the excitation of osteocytes by mechanical loading-induced bone fluid shear stresses." J Biomech **27**(3): 339-360.
Weiner, S. and L. Hood (1975). "Soluble protein of the organic matrix of mollusk shells: a potential template for shell formation." Science **190**(4218): 987.
Weiner, S. and W. Traub (1986). "Organization of hydroxyapatite crystals within collagen fibrils." FEBS Letters **206**(2): 262-266.
Westbroek, I., K. E. De Rooij and P. J. Nijweide (2002). "Osteocyte-specific monoclonal antibody MAb OB7.3 is directed against Phex protein." J Bone Miner Res **17**(5): 845-853.

Williams, J. T., S. S. Southerland, J. Souza, A. F. Calcutt and R. G. Cartledge (1999). "Cells isolated from adult human skeletal muscle capable of differentiating into multiple mesodermal phenotypes." Am Surg **65**(1): 22-26.
Wittenberg, R. H., U. Peschke and U. Botel (1992). "Heterotopic ossification after spinal cord injury. Epidemiology and risk factors." Journal of Bone & Joint Surgery, British Volume **74-B**(2): 215-218.
Wittkowske, C., G. C. Reilly, D. Lacroix and C. M. Perrault (2016). "In Vitro Bone Cell Models: Impact of Fluid Shear Stress on Bone Formation." Frontiers in Bioengineering and Biotechnology **4**: 87.
Wittrant, Y., S. Théoleyre, C. Chipoy, M. Padrines, F. Blanchard, D. Heymann and F. Rédini (2004). "RANKL/RANK/OPG: new therapeutic targets in bone tumours and associated osteolysis." Biochimica et Biophysica Acta (BBA) - Reviews on Cancer **1704**(2): 49-57.
Wittrup, A., S.-H. Zhang, K. J. Svensson, P. Kucharzewska, M. C. Johansson, M. Mörgelin and M. Belting (2010). "Magnetic nanoparticle-based isolation of endocytic vesicles reveals a role of the heat shock protein GRP75 in macromolecular delivery." Proceedings of the National Academy of Sciences **107**(30): 13342-13347.
Wolff, J., P. Maquet and R. Furlong (1986). The law of bone remodelling, Springer-Verlag.
Wu, L. N., B. R. Genge, G. C. Lloyd and R. E. Wuthier (1991). "Collagen-binding proteins in collagenase-released matrix vesicles from cartilage. Interaction between matrix vesicle proteins and different types of collagen." J Biol Chem **266**(2): 1195-1203.
Wudebwe, U. N. G., A. Bannerman, P. Goldberg-Oppenheimer, J. Z. Paxton, R. L. Williams and L. M. Grover (2015). "Exploiting cell-mediated contraction and adhesion to structure tissues in vitro." Philosophical Transactions of the Royal Society B: Biological Sciences **370**.
Xiao, Z., C. E. Camalier, K. Nagashima, K. C. Chan, D. A. Lucas, M. J. de la Cruz, M. Gignac, S. Lockett, H. J. Issaq, T. D. Veenstra, T. P. Conrads and G. R. Beck, Jr. (2007). "Analysis of the extracellular matrix vesicle proteome in mineralizing osteoblasts." J Cell Physiol **210**(2): 325-335.
Xiao, Z., T. P. Conrads, G. R. Beck and T. D. Veenstra (2008). "Analysis of the extracellular matrix and secreted vesicle proteomes by mass spectrometry." Methods Mol Biol **428**: 231-244.
Yamazaki, M., H. Fukushima, M. Shin, T. Katagiri, T. Doi, T. Takahashi and E. Jimi (2009). "Tumor necrosis factor alpha represses bone morphogenetic protein (BMP) signaling by interfering with the DNA binding of Smads through the activation of NF-kappaB." J Biol Chem **284**(51): 35987-35995.
Yang, Y. (2013). Skeletal Morphogenesis and Embryonic Development. Primer on the Metabolic Bone Diseases and Disorders of Mineral Metabolism, John Wiley & Sons, Inc.**:** 1-14.
Yang, Y. I., D. L. Seol, H. I. Kim, M. H. Cho and S. J. Lee (2007). "Composite fibrin and collagen scaffold to enhance tissue regeneration and angiogenesis." Current Applied Physics **7**: e103-e107.
Ye, Q., G. Zund, P. Benedikt, S. Jockenhoevel, S. P. Hoerstrup, S. Sakyama, J. A. Hubbell and M. Turina (2000). "Fibrin gel as a three dimensional matrix in cardiovascular tissue engineering." Eur J Cardiothorac Surg **17**(5): 587-591.
Yu, P. B., D. Y. Deng, C. S. Lai, C. C. Hong, G. D. Cuny, M. L. Bouxsein, D. W. Hong, P. M. McManus, T. Katagiri, C. Sachidanandan, N. Kamiya, T. Fukuda, Y. Mishina, R. T. Peterson and K. D. Bloch (2008). "BMP type I receptor inhibition reduces heterotopic ossification." Nat Med **14**(12): 1363-1369.
Zelzer, E., R. Mamluk, N. Ferrara, R. S. Johnson, E. Schipani and B. R. Olsen (2004). "VEGFA is necessary for chondrocyte survival during bone development." Development **131**(9): 2161-2171.
Zhang, K., C. Barragan-Adjemian, L. Ye, S. Kotha, M. Dallas, Y. Lu, S. Zhao, M. Harris, S. E. Harris, J. Q. Feng and L. F. Bonewald (2006). "E11/gp38 Selective Expression in Osteocytes: Regulation by Mechanical Strain and Role in Dendrite Elongation." Molecular and Cellular Biology **26**(12): 4539-4552.
Zhang, P., A. S. Jobert, A. Couvineau and C. Silve (1998). "A homozygous inactivating mutation in the parathyroid hormone/parathyroid hormone-related peptide receptor causing Blomstrand chondrodysplasia." J Clin Endocrinol Metab **83**(9): 3365-3368.
Zhang, X., C. Naik A Fau - Xie, D. Xie C Fau - Reynolds, J. Reynolds D Fau - Palmer, A. Palmer J Fau - Lin, H. Lin A Fau - Awad, R. Awad H Fau - Guldberg, E. Guldberg R Fau - Schwarz, R. Schwarz E Fau -

O'Keefe and R. O'Keefe (2005). "Periosteal stem cells are essential for bone revitalization and repair." (1108-7161 (Print)).
Zhao, G. Q. (2003). "Consequences of knocking out BMP signaling in the mouse." Genesis **35**(1): 43-56.
Zhao, S., Y. K. Zhang, S. Harris, S. S. Ahuja and L. F. Bonewald (2002). "MLO-Y4 osteocyte-like cells support osteoclast formation and activation." J Bone Miner Res **17**(11): 2068-2079.
Zhao, W., M. H. Byrne, Y. Wang and S. M. Krane (2000). "Osteocyte and osteoblast apoptosis and excessive bone deposition accompany failure of collagenase cleavage of collagen." J Clin Invest **106**(8): 941-949.
Zimmermann, S. M., L. W. Schwitter, M. J. Scheyerer, T. Jentzsch, H.-P. Simmen and C. M. L. Werner (2016). "Prevention of heterotopic ossification: an experimental study using a plasma expander in a murine model." BMC Surgery **16**: 29.
Zuscik, M. J. (2013). Skeletal Healing. Primer on the Metabolic Bone Diseases and Disorders of Mineral Metabolism, John Wiley & Sons, Inc.**:** 90-98.

ACHIEVEMENTS

AWARDS

Young Scientist Award 2016

World Biomaterials Congress, Montreal, Canada

Was offered this prestigious Merit award for the present work, titled: *A new method for developing bone tissue, using a tissue-engineered fracture repair model.*

PUBLICATIONS

Iordachescu A, Amin HD, Rankin SM, Williams RL, Yapp C, Bannerman A, Pacureanu A, Addison O, Bullock AN, Hulley PA and Grover LM. *An in-vitro model for the development of mature bone containing an osteocyte network.* **Advanced Biosystems (2017).**

Iordachescu A, Hulley PA and Grover LM (2017). *A novel method for the collection of nanoscopic vesicles from an organotypic culture model.* **Royal Society of Chemistry Advances (2018).**

CONFERENCE PAPERS

ORAL PRESENTATIONS

Iordachescu A, Hulley PA, Amin H., Rankin S and Grover LM **(2015)**. Heterotopic Ossification: Investigating the cellular effects of blast overpressure using a tissue-engineered 3D model. *Oral presentation at the* NC3Rs Summer School, June 2015, Oxford, United Kingdom

Iordachescu A, Hulley PA, Amin H., Rankin S and Grover LM **(2015)**. Heterotopic Ossification: Investigating the cellular effects of blast overpressure using a tissue-engineered 3D model. *Oral presentation at the 6th Elsevier International Conference on Mechanics of Biomaterials and Tissues (ICMoBT).* December 2015, Waikoloa, USA.

Iordachescu A, Hulley PA, Bannerman A and Grover LM **(2016)**. A new method for developing bone tissue, using a tissue-engineered fracture repair model. *Front. Bioeng. Biotechnol. Conference Abstract: 10th World Biomaterials Congress.* doi:

10.3389/conf.FBIOE.2016.01.02436. *Oral presentation at the 10th World Biomaterials Congress.* May 2016, Montreal, Canada.

Iordachescu A, Hulley PA, Bannerman A and Grover LM **(2017*).*** Development of a biologically self-assembling bone tissue model. *3rd BioNano Symposium*. 12th December 2016, Chemical Engineering, University of Birmingham.

Iordachescu A, Amin HD, Rankin SM, Williams RL, Yapp C, Bannerman A, Pacureanu A, Addison O, Bullock AN, Hulley PA and Grover LM **(2017)**. Development of a self-structuring bone system. *Oral presentation at the 6th Elsevier International Conference on Mechanics of Biomaterials and Tissues (ICMoBT).* December 2017, Waikoloa, USA.

INVITED PRESENTATIONS

Iordachescu A, Grover LM **(2017)**. Regenerative medicine and Vascularised Composite Allotransplantation. Competitors or the perfect couple? *18th Congress of the European Society for Organ Transplantation*. September 2017, Barcelona, Spain.